

UC San Diego

UC San Diego Electronic Theses and Dissertations

Title

Improving management of exploited species with knowledge of life history and spatial processes

Permalink

<https://escholarship.org/uc/item/8zb9k9j2>

Author

Stock, Brian

Publication Date

2019

Peer reviewed|Thesis/dissertation

UNIVERSITY OF CALIFORNIA SAN DIEGO

Improving management of exploited species with knowledge of life history and spatial processes

A dissertation submitted in partial satisfaction of the
requirements for the degree
Doctor of Philosophy

in

Marine Biology

by

Brian Curtis Stock

Committee in charge:

Professor Brice X. Semmens, Chair
Professor Lisa T. Ballance
Professor David M. Checkley
Professor Stuart A. Sandin
Professor Jonathan B. Shurin

2019

Copyright
Brian Curtis Stock, 2019
All rights reserved.

The dissertation of Brian Curtis Stock is approved, and it is acceptable in quality and form for publication on microfilm and electronically:

Chair

University of California San Diego

2019

TABLE OF CONTENTS

Signature Page	iii
Table of Contents	iv
List of Figures	v
List of Tables	viii
Acknowledgements	ix
Vita	xii
Abstract of the Dissertation	xiii
Chapter 1	Unifying error structures in commonly used biotracer mixing models	1
Chapter 2	Comparing predictions of fisheries bycatch using multiple spatiotemporal species distribution model frameworks	11
	2.1 Introduction	13
	2.2 Methods	18
	2.3 Results	30
	2.4 Discussion	39
Chapter 3	Assessing the response of Cayman Islands Nassau Grouper (<i>Epinephelus striatus</i>) spawning aggregations to spatial protections using <i>in situ</i> length data	80
	3.1 Introduction	83
	3.2 Methods	90
	3.3 Results	99
	3.4 Discussion	110
Chapter 4	3-dimensional advection, diffusion, and mortality of eggs and larvae dispersing from a Nassau Grouper (<i>Epinephelus striatus</i>) spawning aggregation observed with a novel plankton imaging system	129
	4.1 Introduction	131
	4.2 Methods	134
	4.3 Results	147
	4.4 Discussion	164

LIST OF FIGURES

Figure 1.1:	Mixing model error terms	3
Figure 1.2:	1-tracer distributions of different consumer variances, demonstrating the difference between Model 1 (process error only, MixSIR), Model 3 (process + residual error, SIAR), and Model 4 (process \times residual error)	4
Figure 1.3:	Simulation results as functions of consumer variance: (a) mean Δ DIC, (b) percent of true proportions captured by 95% credible intervals, (c) mean 95% credible interval widths, and (d) mean absolute percent error (MAPE)	6
Figure 1.4:	Differences in DIC from the model with lowest DIC for each literature dataset	7
Figure 2.1:	Effort and target species catch density in the West Coast groundfish trawl fishery from 2003 to 2012	20
Figure 2.2:	Effort and target species catch density in the shallow-set Hawaii longline swordfish fishery from 1994 to 2014	22
Figure 2.3:	Predictive performance of the a) binomial and b) positive components of the delta-model on test data from 5-fold cross-validation repeated 10 times	32
Figure 2.4:	Bycatch-to-target species catch ratio achieved by using the binomial component of the delta-model to predict and remove fishing sets in the test data, relative to the bycatch-to-target ratio with no fishing sets removed	33
Figure 2.5:	Maps of blue shark bycatch predictions with uncertainty for the Hawaii longline swordfish fishery in 2014 from the GMRF and random forest (RF) models (binomial \times positive = expected)	35
Figure 2.6:	Predictive performance of the a) binomial and b) positive components of the GMRF-CONSTANT and RF delta-models at test locations beyond the geographic data range (i.e. spatial extrapolation)	36
Figure 2.7:	Covariate effects estimated by the GMRF and random forest (RF) models for darkblotched rockfish	38
Figure 2.8:	GMRF-YEAR random field for bycatch probability of darkblotched rockfish from 2008 to 2012	43
Figure 3.1:	Map showing the location of historic and current Nassau Grouper spawning aggregations in the Cayman Islands	89
Figure 3.2:	Laser caliper system used to measure fish lengths <i>in situ</i>	91
Figure 3.3:	Measurement error of the laser caliper system as a function of distance-to-camera and angle offset from perpendicular	92
Figure 3.4:	Length distributions for major versus minor spawning months	93
Figure 3.5:	Length distributions measured from the stereo camera and laser calipers	94
Figure 3.6:	Range of growth parameters used to fit the length-based assessment model	97
Figure 3.7:	Nassau Grouper catch length distributions from four FSA fisheries in the Cayman Islands before protections	100
Figure 3.8:	Length distributions from the west and east end Little Cayman Nassau Grouper FSAs	101

Figure 3.9:	Estimated spawning potential ratio (SPR) for Cayman Islands Nassau Grouper spawning aggregations before and after protections implemented in 2003 . . .	103
Figure 3.10:	Range of von Bertalanffy growth curve parameters, k (growth rate, yr^{-1}) and L_{∞} (asymptotic size, cm), used to fit the length-based assessment model	104
Figure 3.11:	Fits to <i>in situ</i> Little Cayman length-frequency data from the LIME model with lowest AIC	105
Figure 3.12:	Length-based assessment model output for the Nassau Grouper spawning aggregation on Little Cayman Island	106
Figure 3.13:	Bimodal length distributions from Little Cayman and Cayman Brac in 2017 and 2018	108
Figure 3.14:	Bootstrap distribution of the growth increment of modes from 2017 to 2018 . .	108
Figure 3.15:	Habitat area available to Nassau Grouper on Little Cayman and Cayman Brac .	109
Figure 3.16:	Bootstrap distribution of the difference in modes between Little Cayman and Cayman Brac in 2017 and 2018	110
Figure 3.17:	Sea surface temperature surrounding Little Cayman after spawning events from 2004–2018	113
Figure 4.1:	Satellite-tracked drifters released from the Little Cayman FSA on nights of spawning in 2016 and 2017	137
Figure 4.2:	20-hour drifter tracks from sampled spawning nights in 2016 and 2017	138
Figure 4.3:	In situ plankton imaging systems used to measure Nassau Grouper egg concentration	140
Figure 4.4:	Ord plots of egg count data from cohorts 1 and 2	145
Figure 4.5:	Hatching time of lab-reared Nassau Grouper eggs collected from spawning on Feb 14–15, 2017	148
Figure 4.6:	Diameters of fish eggs sampled near drifters using different methods	149
Figure 4.7:	Image sequences showing Nassau Grouper egg and larvae development over 1–37 hours post fertilization	151
Figure 4.8:	In situ microscope images of possible predation on Nassau Grouper eggs by invertebrate zooplankton	152
Figure 4.9:	Vertical density profile and distribution of Nassau Grouper eggs along the track of the drifter centroid following spawning for cohort 1 (Feb 14, 2017)	154
Figure 4.10:	Best fit vertical diffusion model for Nassau Grouper eggs following spawning for cohort 1 (Feb 14, 2017)	154
Figure 4.11:	Horizontal diffusion of Nassau Grouper eggs in the 15 hours following cohort 1 spawning (Feb 14, 2017)	155
Figure 4.12:	Predicted egg concentrations from the best fit 3D diffusion-mortality model versus observed Nassau Grouper egg counts (s^{-1} for cohort 1 (Feb 14, 2017) .	157
Figure 4.13:	Drifter grounding locations and horizontal distribution of Nassau Grouper eggs and yolk-sac larvae following cohort 2 spawning (Feb 15, 2017)	159
Figure 4.14:	Vertical salinity profile around drifters released during spawning of cohort 2 (Feb 15, 2017)	160
Figure 4.15:	Horizontal diffusion of Nassau Grouper eggs in the 20 hours following spawning on Feb 15, 2017 (cohort 2)	160

Figure 4.16: Best fit vertical diffusion model for Nassau Grouper eggs following spawning on Feb 15, 2017 (cohort 2) 161

Figure 4.17: Predicted egg concentrations from the best fit diffusion-mortality model versus observed Nassau Grouper egg counts (s^{-1}) for cohort 2 (Feb 15, 2017) 163

Figure 4.18: Estimated dispersal of larvae from the Little Cayman FSA on Feb 29, 2011 around drifters released during spawning on Feb 24 and Feb 25 168

LIST OF TABLES

Table 2.1:	Properties of the considered statistical models and how each model incorporates spatial fishing locations	26
Table 3.1:	Parameters used to fit the LBSPR model	96
Table 3.2:	Parameters used to fit the LIME model	96
Table 4.1:	AIC table for considered distributions for the egg count data	145
Table 4.2:	3D diffusion-mortality model results for cohort 1 (Feb 14, 2017)	156
Table 4.3:	3D diffusion-mortality model results for cohort 2 (Feb 15, 2017)	162

ACKNOWLEDGEMENTS

The work in this dissertation is the result of many, many people contributing a tremendous amount of time, money, and energy.

Brice Semmens has been an amazing adviser, providing abundant opportunities to learn and grow as a marine scientist. I am incredibly grateful for his strong example, mentorship, and support developing a wide range of skills: statistical modeling, presentation as story-telling, executing boat- and dive-based work, crafting and writing articles, and establishing collaborations. He and Christy Pattengill-Semmens have nurtured a wonderful lab and family that is such a joy to be a part of.

My committee of Lisa Ballance, Dave Checkley, Jon Shurin, and Stuart Sandin have been very supportive, motivating, and a valued sounding board. SIO has been a great place for graduate school in part because of the breadth and expertise of the faculty, and I owe thanks to many professors for guidance and advice on my final chapter in particular: Dave Checkley for ichthyoplankton sampling, Jules Jaffe for the original idea—and much subsequent encouragement—to use his SPC microscopes, Peter Franks for teaching me about advection and diffusion, Ron Burton for holding my hand through DNA barcoding, and Mark Ohman for the lessons on zooplankton. SIO has excellent scientific diver and small boat training and support—thanks to Christian, Rich, Phil, and Brett. Thanks to the SIO graduate department staff for helping navigate the logistics.

Eric Ward and Tomo Eguchi secured me one year of funding through the NMFS Protected Species Toolbox program, which led to fun and productive collaborations on spatial bycatch modeling that also included Jim Thorson and Jason Jannot. Eric effectively served as a co-adviser for much of my time as a student, and I am thankful for how generous he has been with his time and expertise. I am still dumbfounded at how quickly Eric and Jim respond to my emails asking for help—thank you! Thanks also to Eric, Don Kobayashi, Summer Martin, and T Todd Jones for mentoring me via a NSF GRIP internship. I learned a lot about bycatch management issues from my stays at the NWFSC and PIFSC, and I appreciate the time it took to get me access to NMFS facilities, show me around, and make me feel welcome.

The two chapters on Nassau Grouper were made possible by the Grouper Moon Project, a collaboration between the Cayman Islands Department of the Environment (DOE) and Reef Environmental Education Foundation (REEF). Participating in Grouper Moon has been a blast and allowed me to grow immensely as a diver and scientist—thanks especially to Christy Pattengill-Semmens, Scott Heppell, Steve Gittings, Lynn Waterhouse, Hal Peterson, Todd Bohannon, and Peter Hillenbrand. Thanks to the dedicated DOE team that makes it happen on and off the water: Croy McCoy, Bradley Johnson, Keith Neale, Robert Walton, Ivan Montieth, Cody Pantan, Tammi Warrender, Chris, Kevin Jackson, Tim Austin, and Gina Ebanks-Petrie.

My graduate education was enhanced by generously offered remote courses from the University of Washington (thanks to Andre Punt, Jim Thorson, Eric Ward, Eli Holmes, and Mark Scheuerell), as well as workshops hosted by the Center for the Advancement of Population Assessment Methodology (CAPAM). I was fortunate to have steady funding through several programs: a NSF Graduate Research Fellowship, NMFS Protected Species Toolbox funds, and the NMFS QUEST/CIMEC funds that support the Semmens Lab. It was very nice to have a reliable source of conference travel funding from the SIO department. The fieldwork for my final chapter chasing Nassau Grouper eggs was largely funded by the UCSD Frontiers of Innovation Scholarship Program (FISP).

To all my Semmens Lab-mates, thanks for all the help and good times—Josh Stewart, Lynn Waterhouse, Lyall Bellquist, Noah Ben-Aderet, Peter Kuriyama, Kayla Blincow, Jordan DiNardo, Erica Mason, and India Dove.

Finally, I am thankful for the love and support of my family and friends. To my parents, Donna and Curt Stock, thank you for your steadfast encouragement and being such good role models. To Elizabeth, thank you for your generosity and openness with your home—I never would have moved to San Diego without you. Jake and Jon, I have cherished all the rock slapping and tickling. You all enrich my life in so many ways.

To Sarah, the woman of my dreams, thank you for everything.

Chapter 1, in full, is a reprint of material as it appears in *Ecology*: Stock, B. C. and B. X. Semmens, 2016, volume 97, pages 2562-2569. The dissertation author was the primary investigator and author of this paper.

Chapter 2, in full, has been submitted for publication and is printed here with the permission of co-authors Eric J. Ward, Tomoharu Eguchi, Jason E. Jannot, James T. Thorson, Blake E. Feist, and Brice X. Semmens. The dissertation author was the primary investigator and author of this paper.

Chapter 3, in part, is currently in preparation for submission for publication and is printed here with the permission of co-authors Scott A. Heppell, Lynn Waterhouse, India C. Dove, Christy V. Pattengill-Semmens, Croy M. McCoy, Phillippe G. Bush, Gina Ebanks-Petrie, and Brice X. Semmens. The dissertation author was the primary investigator and author of this paper.

Chapter 4, in part, is currently in preparation for submission for publication and is printed here with the permission of co-authors Andrew D. Mullen, Jules S. Jaffe, Allison Candelmo, Scott A. Heppell, Christy V. Pattengill-Semmens, Croy M. McCoy, Bradley Johnson, and Brice X. Semmens. The dissertation author was the primary investigator and author of this paper.

VITA

- 2009 B. S. in Mathematical Biology, Harvey Mudd College, Claremont, CA
- 2013 - 2018 Graduate Student Researcher, Scripps Institution of Oceanography, University of California, San Diego, CA
- 2019 Ph. D. in Marine Biology, Scripps Institution of Oceanography, University of California, San Diego, CA

PUBLICATIONS

- Stock, B. C.** and Semmens, B. X. 2016. MixSIAR GUI User Manual. Version 3.1. <https://github.com/brianstock/MixSIAR>. DOI: 10.5281/zenodo.1209993.
- deVries, M. S., **Stock, B. C.**, Christy, J. H., Goldsmith, G. R., and Dawson, T. E. 2016. Specialized morphology corresponds to a generalist diet: linking form and function in smashing mantis shrimp crustaceans. *Oecologia* 128(2):429–442. DOI: 10.1007/s00442-016-3667-5.
- Stock, B. C.** and Semmens, B. X. 2016. Unifying error structures in commonly used biotracer mixing models. *Ecology* 97:2562–2569. DOI: 10.1002/ecy.1517
- Upadhayay, H. R., Bodé, S., Griepentrog, M., Huygens, D., Bajracharya, R. M., Blake, W. H., Dercon, G., Mabit, L., Gibbs, M., Semmens, B. X., **Stock, B. C.**, Cornelis, W., and Boeckx, P. 2017. *Journal of Soils and Sediments* 17(6):1537-1553. DOI: 10.1007/s11368-017-1706-4.
- Stock, B. C.**, Jackson, A. L., Ward, E. J., Parnell, A. C., Phillips, D. L., and Semmens, B. X. 2018. Analyzing mixing systems using a new generation of Bayesian tracer mixing models. *PeerJ* 6:e5096. DOI: 10.7717/peerj.5096.
- Blake, W. H., Boeckx, P., **Stock, B. C.**, Smith, H. G., Bodé, S., and others. 2018. A deconvolutional Bayesian mixing model approach for river basin sediment source apportionment. *Scientific Reports* 8(1):13073. DOI: 10.1038/s41598-018-30905-9.
- Stock, B. C.**, Ward, E. J., Thorson, J. T., Jannot, J. E. and Semmens, B. X. 2018. The utility of spatial model-based estimators of unobserved bycatch. *ICES Journal of Marine Science*. DOI: 10.1093/icesjms/fsy153.
- Stock, B. C.**, Ward, E. J., Eguchi, T., Jannot, J. E., Thorson, J. T., Feist, B. E., and Semmens, B. X. Semmens. *In Review*. Comparing predictions of fisheries bycatch using multiple spatiotemporal species distribution model frameworks.

ABSTRACT OF THE DISSERTATION

Improving management of exploited species with knowledge of life history and spatial processes

by

Brian Curtis Stock

Doctor of Philosophy in Marine Biology

University of California San Diego, 2019

Professor Brice X. Semmens, Chair

My dissertation is motivated by the desire to achieve balance between conservation and exploitation of marine populations (i.e., sustainable harvest). Navigating between the extremes of preservationism and extinction with any confidence requires that we assess the status of exploited populations and the ecosystems that support them. Single-species, equilibrium-based fisheries management has been somewhat divisive, with proponents giving it credit for largely ending overfishing and critics citing spectacular examples of failing to prevent fisheries collapses. One of the primary critiques of traditional fisheries assessments is that they ignore important ecological realities, such as variability in vital population rates stemming from: 1) environmental variability, 2)

spatial population structure and movement, and 3) species interactions.

My dissertation focuses on improving management of exploited species by adapting models to species' life history, with particular emphasis on the effect of spatial structure. Chapter 1 improves stable isotope mixing models, used to estimate animal diets, by introducing a new statistical structure makes more ecologically-realistic assumptions about the relationship between predator and prey isotope signatures. We demonstrate that this new parameterization implicitly estimates predators' consumption rate and outperforms existing models. Chapter 2 considers how fisheries bycatch species' life history traits, use of space, and catch rates affect models used to predict spatiotemporal bycatch risk. We find that machine learning approaches (e.g. random forests) outperform recently developed semiparametric spatial models for the purpose of generating fisheries bycatch predictions to be used in dynamic management tools. Chapter 3 develops assessment methodology for protected fish species that form spawning aggregations, a life history strategy particularly vulnerable to overexploitation. While no catch or effort data can be collected from the protected population, we demonstrate the efficacy of length-frequency time-series collected in situ to detect recruitment spikes and population recovery. Chapter 4 investigates the mortality and 3-dimensional dispersal of eggs and larvae from a Nassau Grouper (*Epinephelus striatus*) spawning aggregation, and discusses the likelihood of large self-recruitment events.

Chapter 1

Unifying error structures in commonly used biotracer mixing models

Unifying error structures in commonly used biotracer mixing models

BRIAN C. STOCK¹ AND BRICE X. SEMMENS

Scripps Institution of Oceanography, University of California, San Diego, La Jolla, California 92093 USA

Abstract. Mixing models are statistical tools that use biotracers to probabilistically estimate the contribution of multiple sources to a mixture. These biotracers may include contaminants, fatty acids, or stable isotopes, the latter of which are widely used in trophic ecology to estimate the mixed diet of consumers. Bayesian implementations of mixing models using stable isotopes (e.g., MixSIR, SIAR) are regularly used by ecologists for this purpose, but basic questions remain about when each is most appropriate. In this study, we describe the structural differences between common mixing model error formulations in terms of their assumptions about the predation process. We then introduce a new parameterization that unifies these mixing model error structures, as well as implicitly estimates the rate at which consumers sample from source populations (i.e., consumption rate). Using simulations and previously published mixing model datasets, we demonstrate that the new error parameterization outperforms existing models and provides an estimate of consumption. Our results suggest that the error structure introduced here will improve future mixing model estimates of animal diet.

Key words: Bayesian; biotracers; fatty acid; mixing model; MixSIR; SIAR; stable isotope.

INTRODUCTION

Studies in trophic ecology often require estimates of consumer diets. Typically, the diets of consumers are difficult to quantify because direct in situ observations are challenging. When direct observation is not possible, researchers have relied on a raft of techniques, including experimentation, fecal analysis, and gut content analysis (Paine 1966, Root 1967, Hyslop 1980). In recent decades, ecologists have increasingly leveraged biological tracers (“biotracers”) in order to estimate consumer diet. Common biotracers include bulk stable isotopes (SI) as well as compound-specific SI and fatty acids (Boecklen et al. 2011).

Mixing models use biotracers to quantify diet by calculating source (prey) proportions to a mixture (consumer), using the principle, “you are what you eat.” While they are commonly applied to diet analyses, mixing models also inform such basic ecological inquiries as animal movement, nutrient cycling, and interspecific interactions (Caut et al. 2006, Granek et al. 2009, Carlisle et al. 2012). More broadly, mixing models are employed across the natural sciences to elucidate source contributions to

a mixture; for instance, to identify sediment sourcing in river systems using trace element fingerprinting (Dutton et al. 2013, Nosrati et al. 2014). Herein, we use the terms “source” proportions to a “consumer” using “tracer” data, although a given application may use fatty acids to estimate prey proportions of an animal’s diet (Iverson et al. 2004, Galloway et al. 2014*a, b*), or use compound-specific SI to estimate sediment sources of a soil sample (Gibbs 2008, Blake et al. 2012).

Recent Bayesian approaches to mixing models (Moore and Semmens 2008, Semmens et al. 2009*b*, Parnell et al. 2010) have addressed many of the criticisms leveled at simpler linear mixing models (e.g., IsoSource; Phillips and Gregg 2003), such as the inability to incorporate prior information, the failure to encapsulate uncertainty in tracer data, and the assumption that all consumers in a population share the same diet proportions. For ecologists, a main advantage of Bayesian mixing models is that their flexible likelihood-based structure allows them to account for variability in consumer tracer data (hereafter, consumer variability) due to known biological processes (Appendix S1: Table S1).

The most widely used Bayesian mixing model software packages are MixSIR (Moore and Semmens 2008) and SIAR (Parnell et al. 2010), which differ in their assumptions about consumer variability (i.e., their error structures). This difference has been debated in the literature

Manuscript received 26 July 2015; revised 9 December 2015; accepted 25 May 2016; final version received 27 June 2016.
Corresponding Editor: D. E. Schindler.

¹E-mail: b1stock@ucsd.edu

(Jackson et al. 2009, Semmens et al. 2009a), but has not been resolved, with model choice likely based on software platform and familiarity rather than statistical philosophy. Since the difference between MixSIR and SIAR is subtle, the biological assumptions of these mixing models may be unclear to many ecologists. The objectives of our analysis are to unify and improve the MixSIR/SIAR framework by introducing a more process-based formulation of uncertainty in mixing models (Stock and Semmens 2013), and to evaluate how this new formulation compares to the existing models. Herein, we introduce a set of ecological process-based scenarios in order to understand the assumptions behind each error structure. We then explicitly define the model error structure equations, and finally, we evaluate model performance.

Model descriptions

Thinking of a simple hypothetical consumer-source interaction will help illustrate two ways variability in source tracer values propagates into consumer variability. Imagine a consumer population feeding exclusively on one source. After subtracting the trophic discrimination factor (TDF, difference between tracer values in consumer and source tissues), we expect the consumer tracer values to directly match those of the source. However, if we think of predation events as individual consumers sampling the source population tracer distribution, there are two reasons consumer tracer values can differ from the source mean due to the process of sampling alone:

1. Sampling error: Consumer tracer values are an average of a finite number of samples, and there will be some variability in these sample means due to chance.
2. Specialization: Individual consumers may preferentially sample above or below the source mean, resulting in some consumers enriched or depleted. For instance, larger shrimp can have higher $\delta^{13}\text{C}$ values (Fry and Arnold 1982), so larger fish preferentially eating larger shrimp would be enriched in ^{13}C relative to smaller fish.

We refer to these as “process error”: variation in consumer tracer values due to the sampling process. Researchers also can include “residual error” terms in mixing models to account for other agents of consumer variability, such as individual differences in digestibility, assimilation efficiency, and metabolic rates (see Table 1 in Boecklen et al. 2011). Importantly, note one conspicuously absent driver of consumer variability—diet. If we do not include hierarchical model structures (as in Semmens et al. 2009b), all consumers are assumed to have the same diet. Researchers assume that deviations among consumers are due to some combination of these process and residual errors to derive mixing model error structures, which we introduce below:

Model 1: consumers as perfect specialists (MixSIR)

Consumers sample at exactly one location from each source distribution. All variability in consumer tracer values results from individual specialization and sampling error as described previously (process error, Fig. 1a). Model 1 assumes the consumer tracer values, X_{ij} , follow Eq. 1:

$$X_{ij} \sim N \left(\sum_k p_k (\mu_{jk} + \lambda_{jk}), \sum_k p_k^2 (\omega_{jk}^2 + \tau_{jk}^2) \right) \quad (1)$$

where:

- X_{ij} = tracer value j of mixture (consumer) i ,
- p_k = (diet) proportion of source k (estimated by model),
- μ_{jk} = source k mean for tracer j ,
- λ_{jk} = mean trophic discrimination factor (TDF) for tracer j on source k ,
- ω_{jk}^2 = source k variance for tracer j , and
- τ_{jk}^2 = discrimination factor variance for tracer j on source k .

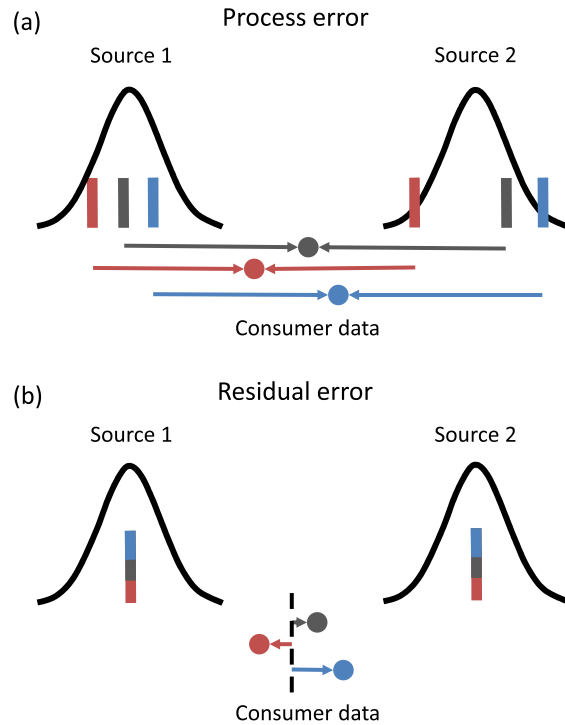


FIG. 1. Mixing model error terms. (a) Process error: consumers sample in different locations from each source distribution, and the variation in consumer tracer values is due to this sampling process. For example, the blue consumer has a higher tracer value (blue circle) than the red and grey consumers (red, grey circles) because it samples sources with higher tracer values (blue lines). (b) Residual error: all consumers sample from the source means (colored lines), and variation in consumer tracer data (circles) is due to unexplained deviations from the consumer mean (black dashed line). Potential sources of residual error include individual differences in digestibility, assimilation efficiency, and metabolic rates (see Table 1 in Boecklen et al. 2011).

The variance term in Model 1 (MixSIR, Eq. 4 in Moore and Semmens 2008) is the mathematical result obtained by adding k independent normal random variables, and defines the consumer variance as a function of the source variances (Fig. 1a). Importantly, note that no distinction is made between source variance, ω_{jk}^2 , and TDF variance, τ_{jk}^2 . Researchers often do not directly measure TDF means or variances for their system, yet accurate estimates of these quantities are important to mixing model results (Bond and Diamond 2011).

Model 2: consumers as perfect integrators, but with residual error

Consumers randomly sample the source distributions many times, effectively sampling the mean. The observed spread in consumer tracer values is entirely due to unexplained deviations from the mean (residual error, Fig. 1b). While this “residual error only” model appears simpler, it introduces j new parameters by adding one σ_j^2 residual error term per tracer, seen in Eq. 2:

$$X_{ij} \sim N\left(\sum_k p_k (\mu_{jk} + \lambda_{jk}), \sigma_j^2\right). \quad (2)$$

Model 3: consumers as perfect specialists, but with residual error (SIAR)

Consumers sample at exactly one location from each source distribution, which results in some consumer variability as in Model 1. Then we assume the consumer variability is higher than expected under Model 1, so we add residual error as in Model 2. This is how SIAR-based models are structured (Parnell et al. 2010). Model 3 (SIAR, Eq. 9 in Parnell et al. 2010) adds the variance terms in Models 1 and 2:

$$X_{ij} \sim N\left(\sum_k p_k (\mu_{jk} + \lambda_{jk}), \sum_k p_k^2 (\omega_{jk}^2 + \tau_{jk}^2) + \sigma_j^2\right). \quad (3)$$

The advantage of Model 3 is that it can fit “wide” consumer data, with more variability than that of the sources, unlike Model 1 (Fig. 2a). On the other hand, Model 3 must fit j additional parameters. Both Models 1 and 3 are unable to fit “narrow” consumer data, where the consumer variance is less than that of the sources (Fig. 2c). Yet, one may expect this to be the case in natural predator-prey systems, as each consumer repeatedly samples the prey population.

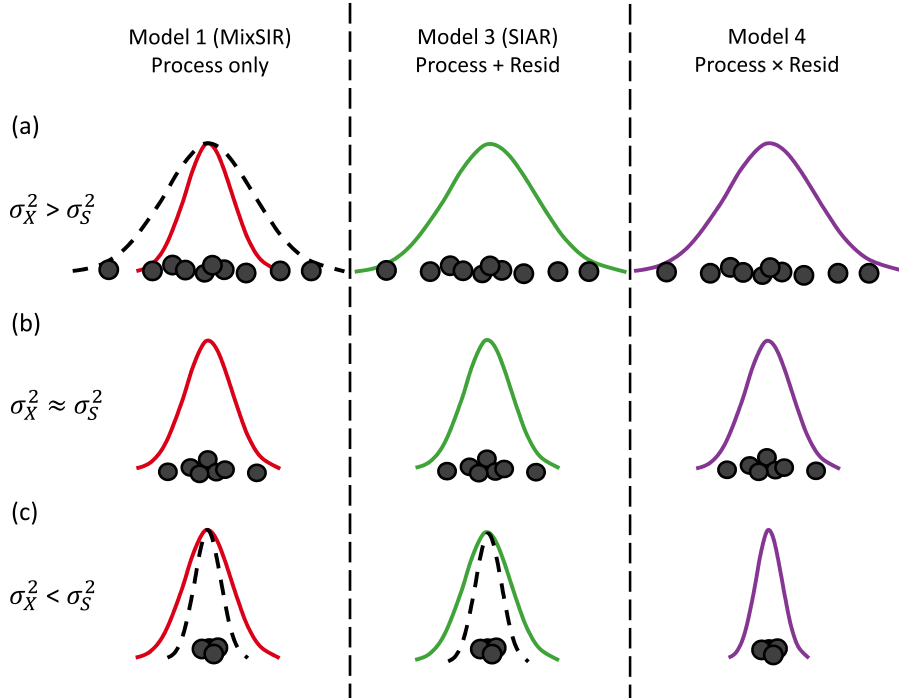


FIG. 2. 1-tracer distributions of different consumer variances, demonstrating the difference between Model 1 (process error only, MixSIR), Model 3 (process + residual error, SIAR), and Model 4 (process \times residual error). Solid colored lines show each model fit to the consumer data (black points), and black dashed lines show the true consumer distribution. (a) Model 1 cannot fit wide consumer data, $\sigma_X^2 > \sigma_S^2$, because it does not have a residual error term. (b) When the consumer and source variances are roughly equal, $\sigma_X^2 \approx \sigma_S^2$, all models fit well. (c) Models 1 and 3 cannot fit narrow consumer data, $\sigma_X^2 < \sigma_S^2$, where the consumer variance is much less than the source variances. Note that all models fit the same mean.

Model 4: consumers between perfect specialists and perfect integrators

Considering these existing frameworks, it becomes clear that the ecologically most realistic scenario is missing; namely, Model 4, in which consumer populations fall somewhere between perfect specialists and perfect integrators. Model 4 multiplies the process error by a multiplicative error term, ε_j , as in Eq. 4:

$$X_{ij} \sim N\left(\sum_k p_k (\mu_{jk} + \lambda_{jk}), \sum_k p_k^2 (\omega_{jk}^2 + \tau_{jk}^2) \times \varepsilon_j\right). \quad (4)$$

The multiplicative error term, ε_j , allows the model to switch consumers from perfect integrators ($\varepsilon_j=0$) to perfect specialists ($\varepsilon_j=1$) to fit narrow consumer data, as well as fit wide consumer data with more variability than expected under Model 1 ($\varepsilon_j > 1$; Fig. 2a–c). A $U(0,20)$ prior was chosen for the ε_j term because models with this prior outperformed others considered in simulation tests (Appendix S2: Figs. S1 and S2).

Model 4 has the same number of parameters as Models 2 and 3. However, in contrast to the ecologically meaningless σ_j^2 residual terms in Models 2 and 3, the ε_j term is related to the consumer consumption rate (biomass consumed per tissue turnover period). The underlying idea is that the ratio of consumer tracer variance to source variance contains information about how frequently consumers sample sources—more frequent sampling reduces consumer variance. If we assume that all consumer variability is either due to process error (Fig. 1a) or accounted for by covariates (i.e., there is no residual error), then we can solve for consumption, C , in terms of the variance, biomass, and diet proportion of the sources (for derivation see Appendix S3). The consumption of each source, C_k , is then $C_k = Cp_k$.

We hypothesize that Model 4 is generally a more appropriate model than Models 1 and 3, especially for systems with narrow consumer data ($\varepsilon_j < 1$). We used simulated and published datasets to test the performance of all four models, calculating model selection criteria such as relative error, DIC, and credible interval width.

METHODS

Simulations

We first tested the models using simulated data where the “true” diet proportions were known, across a range of consumer variability—generated by allowing consumers to sample the source distributions a variable number of times ($C = 320, 160, 80, 40, 20, 10, 5$) and adding residual error. We carried out all simulations for a simple case of three sources, two tracers, 10 consumer data points, and each source biomass = 1. Since mixing models assume that the correct sources have been identified a priori, we did not allow any source to contribute <5% to the true diet.

We simulated 1,000 datasets for each level of consumer variability, according to the following pseudo-code (see Appendix S9 for code):

1. Generate true proportions, p_k , for each source k (\mathbf{p} is a K -vector, the number of sources):

$$\mathbf{p} \sim \text{Dirichlet}(\boldsymbol{\alpha}), \alpha_k = 1$$

2. Generate source means, μ_{jk} , and standard deviations, ω_{jk} , for each tracer j :

$$\mu_{jk} \sim \mathcal{N}(0, 5)$$

$$\omega_{jk} \sim \mathcal{U}(0.5, 1.5)$$

3. Each consumer i takes a sample of size Z_{ik} from source k (\mathbf{Z}_i is a K -vector):

$$\mathbf{Z}_i \sim \text{Multinomial}(C, \mathbf{p})$$

4. Consumer i draws Z_{ik} samples from source k , resulting in sample means Y_{ijk} for each tracer j :

$$Y_{ijk} = \frac{\sum_{z=1}^{Z_{ik}} \mathcal{N}(\mu_{jk}, \omega_{jk}^2)}{Z_{ik}}$$

5. Each consumer i 's tracer values, X_{ij} , are means of all source samples:

$$X_{ij} = \frac{\sum_k Y_{ijk} Z_{ik}}{C}$$

6. Add residual error from $\mathcal{N}(0, 0.1)$.

Representative simulated datasets across the range of consumer variability are shown in Appendix S4: Fig. S1.

For each dataset, we fit all four models via Markov Chain Monte Carlo (MCMC) using JAGS and R software (Plummer 2003, R Core Team 2015). We assessed model convergence with the Gelman-Rubin diagnostic, not allowing more than 50 values above 1.1 across all variables and datasets for each level of mixture variability (Gelman et al. 2004). Finally, we used the following metrics to gauge model performance (for details see Appendix S5):

1. Proportion of true p_k captured within 95% credible intervals.
2. Mean difference in DIC (Δ DIC).
3. Mean 95% credible interval width.
4. Mean absolute percent error.

Published datasets

Simulations are useful in model assessment because knowing the truth allows us to evaluate model accuracy and precision. However, simulated data may not adequately describe variation found in natural systems.

While we hypothesize that Model 4 will perform well in situations with narrow consumer data, how often is this the case?

We surveyed the recent ecological literature for published datasets from studies employing mixing models. Searching in ISI Web of Science for terms “stable isotope*” AND “mixing model*” returned 387 articles for years 2012–2014, of which thirteen had complete data—raw consumer tracer values (not means and standard deviations), source tracer values (raw, or means, standard deviations, and sample size), and discrimination values (Appendix S6). Three additional SI datasets were available online and opportunistically included (Stock and Semmens 2013). As in the simulation study, we fit the models via MCMC using JAGS and R, remaining faithful to the original mixing model analysis as performed by the authors. We included multiple mixture groups analyzed separately by the authors as one model with fixed effects

in order to avoid one study dominating the results (see Appendix S10 for code). We compared models solely using ΔDIC , since estimating model accuracy without knowing the true diet is not possible.

RESULTS

Simulations

Models 2 and 4 outperformed Models 1 and 3 (MixSIR and SIAR) across all measures of model selection for low consumer variability: lower ΔDIC (Fig. 3a), more accurate point estimates (Fig. 3b), tighter credible intervals (Fig. 3c), and lower absolute percent error (Fig. 3d). Model 4 performed similarly to Model 2 (residual error only) except a slight tradeoff between accuracy and precision for datasets with higher consumer variability (Fig. 3). As expected, Model 1 (MixSIR) was clearly the worst model for datasets

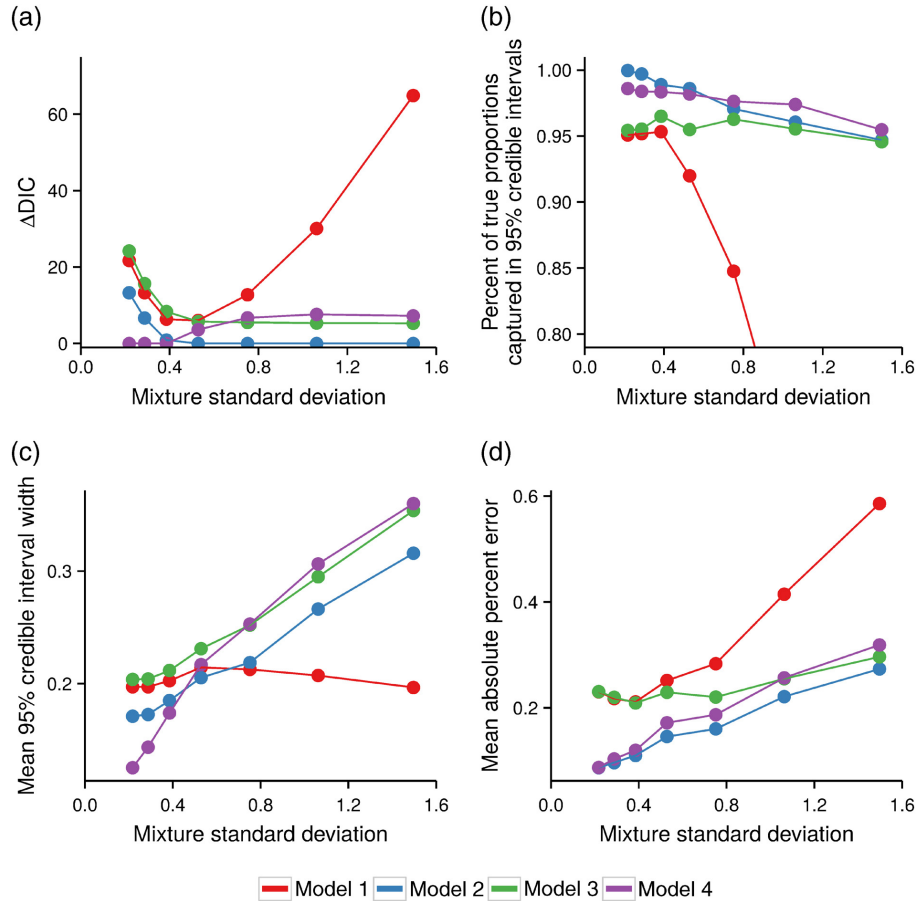


FIG. 3. Simulation results as functions of consumer variance: (a) mean ΔDIC , (b) percent of true proportions captured by 95% credible intervals, (c) mean 95% credible interval widths, and (d) mean absolute percent error (MAPE). Model 1 = process error only (MixSIR), Model 2 = residual error only, Model 3 = process + residual error (SIAR), and Model 4 = process \times residual error. MAPE is calculated as $\sum \left| \frac{\text{est}.p - \text{true}.p}{\text{true}.p} \right| / 1,000$, where *est.p* is the proportion point estimate (median posterior density) and *true.p* is the simulated “true” proportion. Error bars (SE) are smaller than the size of points ($n = 1,000$ simulations).

with higher consumer variability, while the other three models performed adequately.

Published datasets

Without knowing the true proportions of the published datasets, we cannot evaluate the models' accuracy or bias directly. However, Models 2 and 4 fit the published datasets better than Models 1 and 3 overall, as evidenced by lower median Δ DIC values (Model 2 = 1.5, Model 4 = 2.7, Model 1 = 8.1, Model 3 = 9.2, Fig. 4). Model 2 had strong support for most datasets (11 out of 16 Δ DIC ≤ 3.2), but performed poorly in the others (five out of 16 Δ DIC ≥ 40). Just under half (46%) of the estimated ϵ_j terms in Model 4 were less than one, indicative of narrow consumer data (Appendix S7: Fig. S1). Based on the simulation results, we would expect Model 4 to outperform Models 1 and 3 for these datasets with $\epsilon_j < 1$ (more accurate point estimates and tighter intervals). Model 4 diet estimates were quite different than those of Models 1 and 3 for some—but not all—datasets (for a typical example, Appendix S7: Fig. S2).

Consumption rate calculation

We calculated consumption rates from ϵ_j terms estimated by Model 4 fit to data simulated without residual error, and these agreed with the true simulated consumption rates (Appendix S3: Fig. S1). We then tested the practicality of using ϵ_j to estimate consumption rates using a familiar SI mixing model application to coastal wolf diet (Semmens et al. 2009b). Inserting the fitted ϵ_j values (maximum posterior densities, 0.90 and 0.38) into Eq. 4 yielded consumption rates between 3.8 and 0.3 kg per wolf per day (see Appendix S3 for calculations), which straddle other estimates of consumption for wolves primarily relying on deer (Kolenosky 1972, Person et al. 1996).

DISCUSSION

The error structures in two commonly used Bayesian mixing models, MixSIR (Model 1) and SIAR (Model 3), were clearly outperformed by Models 2 (residual error only) and 4 (multiplicative error) in both simulations and published datasets. This is likely due to inaccurate underlying assumptions about the biological process of predation, where it is helpful to think of predation events as individual consumers sampling the source population biotracer distributions.

Models 2 and 4 performed similarly in simulation tests (Fig. 3), but Model 4 rests on more ecologically realistic assumptions. Model 2 assumes the observed variation in consumer tracer values is completely due to unexplained deviations from the mean (Fig. 1b). In contrast, Model 4 is founded on a basic biological process—consumers sample sources through predation events—linked to the consumption rate. Thus, we advise implementing

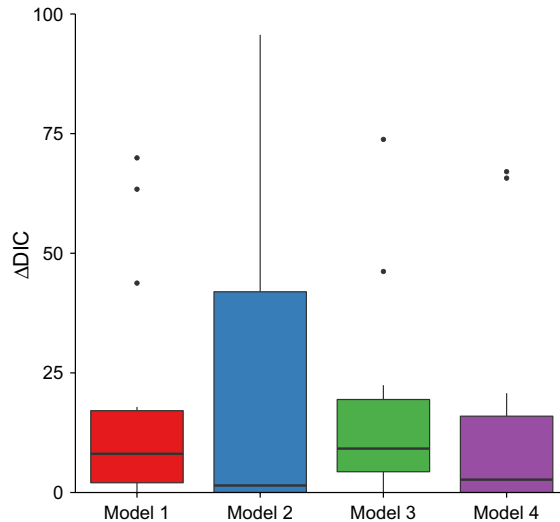


FIG. 4. Differences in DIC from the model with lowest DIC for each literature dataset. Model 2 had the lowest DIC (Δ DIC = 0) for six of the 16 datasets and lowest median Δ DIC, 1.5. Model 4 had the lowest DIC for five of the 16 datasets and next lowest median Δ DIC, 2.7. Models 1 and 3 had higher median Δ DIC: 8.1 and 9.2, respectively. DIC differences of 3–7 are significant.

multiplicative error (Model 4) as the default option in mixing models, although Models 1 and 2 are useful in some cases. For instance, Model 1 is the only option for fitting single mixture data points and may make sense when including hierarchical structures. Model 2 could be preferred in applications other than diet estimation (e.g., sediment sourcing), or where consumers essentially feed infinitely many times (e.g., filter feeders such as oysters).

If predation cannot be envisioned as occurring in discrete events, as with oysters filter feeding, the quantitative estimates of consumption from Model 4 may not make sense. In such cases, the ϵ_j terms should still qualitatively agree with our biological knowledge of the consumption rate (see Appendix S7: Table S1 for all ϵ_j estimates). For example, it is unclear what the biomass of POM that an oyster consumes in a “predation event” is, or even if it makes sense to think of “predation events” for oysters. Model 2 is probably more appropriate for oysters: assume they integrate so many source particles that they effectively “feed at the mean” of each source. Still, Model 4 estimates low ϵ_j (0.13 and 0.32, Appendix S7: Table S1), which is consistent with our conceptualization of how consumer sampling affects biotracer variance—oysters consume many individual particles per tissue turnover period, thus we expect their biotracer values to vary less than that of their sources.

Importantly, the relative support for Model 4 increases as biotracer variability from ecological processes is accounted for in the mixing model (Appendix S1: Table S1). As an example, consider the wolf SI dataset of Semmens et al. (2009b). Adding region and pack as random effects in the model explains much of the

variation in wolf isotope values. As a result, the consumer variance becomes less than the source variance, ϵ_j estimates decrease, and Model 4 gains more support (Appendix S8: Table S1). Researchers are increasingly building such processes into mixing models, and Model 4 should perform well in these process-based mixing models (Parnell et al. 2013, Ogle et al. 2014).

Relative support for Model 4 also depends on researchers faithfully incorporating uncertainty in trophic discrimination factor (TDF) values. Recall that mixing models do not distinguish source variance from TDF variance (ω_{jk}^2 and τ_{jk}^2 in Eqs. 1–4). Including unrealistically low estimates of τ_{jk}^2 , or worse, assuming a single fixed TDF ($\tau_{jk}^2=0$), artificially reduces $\sum p_k^2 (\omega_{jk}^2 + \tau_{jk}^2)$ and increases ϵ_j in Eq. 4, weakening relative support for Model 4 over Models 1 and 3. Along with others, we consider the inclusion of uncertainty in TDFs into Bayesian mixing models a significant advance (Bond and Diamond 2011), especially given the wide range of calculated TDFs and the prevalence of borrowing literature values from different species and tissues (Caut et al. 2009). Calculating TDF variance via feeding experiments is clearly preferable, and we suspect mixing model users tend to underestimate TDF variance when using borrowed values. In such cases, including appropriate τ_{jk}^2 values would strengthen relative support for Model 4.

Including ecological processes and realistic TDF variance in mixing models not only determines relative model support, it also strongly affects the consumption rate calculation. The idea that there is information about consumption rate in the ratio of consumer to source biotracer variance is intriguing and merits further study, since consumption is fundamental to population dynamics but difficult to measure (Lotka 1925, Holling 1959). The primary limitation is that ϵ_j is confounded with unexplained, residual error. Thus, consumption estimates depend on accurate measures of the variability in consumer and source tracer values, as well as accounting for consumer variability from ecological processes and trophic discrimination. Additionally, the method derived here should underestimate consumption, since it assumes all of the consumer variance is due to the sampling process, when in reality some is due to residual error (i.e., ϵ_j are too high). Despite these limitations, this work provides a basis upon which to improve estimates of consumption via source apportionment, especially as including more (and better conserved) biotracers becomes common in ecology (e.g., fatty acids, compound-specific SI).

Finally, there has been confusion whether the models considered here—simply by virtue of being Bayesian—can solve the problem of underdetermined systems (number of sources > number of tracers + 1, Boecklen et al. 2011). We simulated determined systems (three sources, two tracers), but six of the sixteen published datasets analyzed were underdetermined (Appendix S6: Table S1). While Bayesian mixing models can fit any number of sources, they are not a panacea for underdetermined systems—as Brett (2014)

demonstrates, the “uninformative” prior has more weight the less information (more uncertainty) the data contain. Including biotracers beyond bulk SI offers the opportunity to increase the number of sources while avoiding underdetermined systems. We caution, however, that the effect of an “uninformative” prior increases with the number of sources and is not only an issue in underdetermined systems—this is true even with more tracers than sources.

ACKNOWLEDGMENTS

We thank Eric Ward, Charlotte Boyd, Aaron Galloway, and one anonymous reviewer for helpful comments. Funding was provided in part by the Cooperative Institute for Marine Ecosystems and Climate (CIMEC) and the Center for the Advancement of Population Assessment Methodology (CAPAM). BCS received support from the National Science Foundation Graduate Research Fellowship under Grant No. DGE-1144086. This work used the Extreme Science and Engineering Discovery Environment (XSEDE), supported by National Science Foundation grant number ACI-1053575.

LITERATURE CITED

- Blake, W. H., K. J. Ficken, P. Taylor, M. A. Russell, and D. E. Walling. 2012. Tracing crop-specific sediment sources in agricultural catchments. *Geomorphology* 139:322–329.
- Boecklen, W. J., C. T. Yarnes, B. A. Cook, and A. C. James. 2011. On the use of stable isotopes in trophic ecology. *Annual Review of Ecology, Evolution, and Systematics* 42: 411–440.
- Bond, A. L., and A. W. Diamond. 2011. Recent Bayesian stable-isotope mixing models are highly sensitive to variation in discrimination factors. *Ecological Applications* 21:1017–1023.
- Brett, M. T. 2014. Resource polygon geometry predicts Bayesian stable isotope mixing model bias. *Marine Ecology Progress Series* 514:1–12.
- Carlisle, A. B., S. L. Kim, B. X. Semmens, D. J. Madigan, S. J. Jorgensen, C. R. Perle, S. D. Anderson, T. K. Chapple, P. E. Kanive, and B. A. Block. 2012. Using stable isotope analysis to understand the migration and trophic ecology of north-eastern Pacific white sharks (*Carcharodon carcharias*). *PLoS ONE* 7: e30492.
- Caut, S., G. W. Roemer, C. J. Donlan, and F. Courchamp. 2006. Coupling stable isotopes with bioenergetics to estimate interspecific interactions. *Ecological Applications* 16:1893–1900.
- Caut, S., E. Angulo, and F. Courchamp. 2009. Variation in discrimination factors ($\Delta^{15}\text{N}$ and $\Delta^{13}\text{C}$): the effect of diet isotopic values and applications for diet reconstruction. *Journal of Applied Ecology* 46:443–453.
- Dutton, C., S. C. Anisfeld, and H. Ernstberger. 2013. A novel sediment fingerprinting method using filtration: application to the Mara River, East Africa. *Journal of Soils and Sediments* 13:1708–1723.
- Fry, B., and C. Arnold. 1982. Rapid $^{13}\text{C}/^{12}\text{C}$ turnover during growth of brown shrimp (*Penaeus aztecus*). *Oecologia* 54:200–204.
- Galloway, A., M. Eisenlord, M. Dethier, G. Holtgrieve, and M. Brett. 2014a. Quantitative estimates of isopod resource utilization using a bayesian fatty acid mixing model. *Marine Ecology Progress Series* 507:219–232.
- Galloway, A. W., S. J. Taipale, M. Hiltunen, E. Peltomaa, U. Strandberg, M. T. Brett, and P. Kankaala. 2014b. Diet-specific biomarkers show that high-quality phytoplankton fuels herbivorous zooplankton in large boreal lakes. *Freshwater Biology* 59:1902–1915.

- Gelman, A., J. B. Carlin, H. S. Stern, and D. B. Rubin. 2004. Bayesian data analysis. Chapman and Hall/CRC Press, Boca Raton, Florida, USA.
- Gibbs, M. 2008. Identifying source soils in contemporary estuarine sediments: a new compound-specific isotope method. *Estuaries and Coasts* 31:344–359.
- Granek, E. F., J. E. Compton, and D. L. Phillips. 2009. Mangrove-exported nutrient incorporation by sessile coral reef invertebrates. *Ecosystems* 12:462–472.
- Holling, C. S. 1959. The components of predation as revealed by a study of small-mammal predation of the European pine sawfly. *The Canadian Entomologist* 91:293–320.
- Hyslop, E. J. 1980. Stomach contents analysis—a review of methods and their application. *Journal of Fish Biology* 17:411–429.
- Iverson, S. J., C. Field, W. Don Bowen, and W. Blanchard. 2004. Quantitative fatty acid signature analysis: a new method of estimating predator diets. *Ecological Monographs* 74:211–235.
- Jackson, A. L., R. Inger, S. Bearhop, and A. Parnell. 2009. Erroneous behaviour of MixSIR, a recently published Bayesian isotope mixing model: a discussion of Moore and Semmens (2008). *Ecology Letters* 12:E1–E5.
- Kolenosky, G. B. 1972. Wolf predation on wintering deer in east-central Ontario. *The Journal of Wildlife Management* 36:357–369.
- Lotka, A. J. 1925. *Elements of physical biology*. Williams & Wilkins, Baltimore, Maryland, USA.
- Moore, J. W., and B. X. Semmens. 2008. Incorporating uncertainty and prior information into stable isotope mixing models. *Ecology Letters* 11:470–480.
- Nosrati, K., G. Govers, B. X. Semmens, and E. J. Ward. 2014. A mixing model to incorporate uncertainty in sediment fingerprinting. *Geoderma* 217:173–180.
- Ogle, K., C. Tucker, and J. M. Cable. 2014. Beyond simple linear mixing models: process-based isotope partitioning of ecological processes. *Ecological Applications* 24:181–195.
- Paine, R. T. 1966. Food web complexity and species diversity. *American Naturalist* 100:65–75.
- Parnell, A. C., R. Inger, S. Bearhop, and A. L. Jackson. 2010. Source partitioning using stable isotopes: coping with too much variation. *PLoS ONE* 5:e9672.
- Parnell, A. C., D. L. Phillips, S. Bearhop, B. X. Semmens, E. J. Ward, J. W. Moore, A. L. Jackson, J. Grey, D. J. Kelly, and R. Inger. 2013. Bayesian stable isotope mixing models. *Environmetrics* 24:387–399.
- Person, D. K., M. Kirchhoff, V. Van Ballenberghe, G. C. Iverson, and E. Grossman. 1996. The Alexander Archipelago wolf: a conservation assessment. Technical report, U.S. Department of Agriculture, Forest Service, Pacific Northwest Research Station, Portland, Oregon, USA.
- Phillips, D. L., and J. W. Gregg. 2003. Source partitioning using stable isotopes: coping with too many sources. *Oecologia* 136:261–269.
- Plummer, M. 2003. JAGS: a program for analysis of Bayesian graphical models using Gibbs sampling. Proceedings of the 3rd international workshop on distributed statistical computing Vienna, Austria.
- R Core Team. 2015. R: a language and environment for statistical computing. R Foundation for Statistical Computing, Vienna, Austria. <http://www.R-project.org/>
- Root, R. B. 1967. The niche exploitation pattern of the blue-gray gnatcatcher. *Ecological Monographs* 37:317–350.
- Semmens, B. X., J. W. Moore, and E. J. Ward. 2009a. Improving Bayesian isotope mixing models: a response to Jackson et al. (2009). *Ecology Letters* 12:E6–E8.
- Semmens, B. X., E. J. Ward, J. W. Moore, and C. T. Darimont. 2009b. Quantifying interand intra-population niche variability using hierarchical Bayesian stable isotope mixing models. *PLoS ONE* 4:e6187.
- Stock, B. C., and B. X. Semmens. 2013. MixSIAR User Manual. Version 3.1. <https://github.com/brianstock/MixSIAR>

SUPPORTING INFORMATION

Additional supporting information may be found in the online version of this article at <http://onlinelibrary.wiley.com/doi/10.1002/ecy.1517/supinfo>

Chapter 1, in full, is a reprint of material as it appears in *Ecology*: Stock, B. C., and B. X. Semmens, 2016, volume 97, pages 2562–2569. The dissertation author was the primary investigator and author of this paper.

Chapter 2

Comparing predictions of fisheries bycatch using multiple spatiotemporal species distribution model frameworks

Abstract

Spatiotemporal predictions of bycatch (i.e. catch of non-targeted species) have shown promise as dynamic ocean management tools for reducing bycatch. However, which spatiotemporal model framework to use for generating these predictions is unclear. We evaluated a relatively new method, Gaussian Markov random fields (GMRFs), with two other frameworks, generalized additive models (GAMs) and random forests. We fit geostatistical delta-models to fisheries observer bycatch data for six species with a broad range of movement patterns (e.g. highly migratory sea turtles vs. sedentary rockfish) and bycatch rates (percent of observations with non-zero catch, 0.3-96.2%). Random forests had better interpolation performance than the GMRF and GAM models for all six species, but random forests performance was more sensitive when predicting data at the edge of the fishery (i.e. spatial extrapolation). Using random forests to identify and remove the 5% highest bycatch risk fishing events reduced the bycatch-to-target species catch ratio by 34% on average. All models considerably reduced the bycatch-to-target ratio, demonstrating the clear potential of species distribution models to support spatial fishery management.

2.1 Introduction

Bycatch—catch of non-targeted species—occurs in nearly every commercial and recreational fishery, and in many cases is a serious environmental and economic problem (Alverson et al., 1994; Davies et al., 2009; NMFS, 2016). For high-profile protected species such as loggerhead sea turtles (*Caretta caretta*), even extremely low bycatch rates can result in population impacts and fisheries closures (Howell et al., 2015). Some species sustain highly valuable targeted fisheries but are considered bycatch in others, resulting in litigation and economic losses (e.g. chinook salmon bycatch in the Alaska pollock fishery; Ianelli and Stram, 2015). Bycatch of undesired and unprotected species is also concerning because it reduces fishing efficiency and threatens ecosystem biodiversity (Boyce, 1996; FAO, 1995; Kelleher, 2005). Thus, for a variety of reasons, the fishing community is interested in using species distribution models (SDMs) to understand spatiotemporal patterns of bycatch, with the hope that SDM-based tools could predict—and thus help avoid—bycatch.

Maps of relative bycatch risk (e.g. probability or density) updated in near real-time have already shown promise as dynamic ocean management tools, both complementing and contrasting traditional static time and area closures (Breivik et al., 2016; Dunn et al., 2016; Eguchi et al., 2017; Hazen et al., 2017; Howell et al., 2008, 2015; Lewison et al., 2015). It is not clear, however, what SDM is most appropriate to use as the framework supporting such tools. Further, because bycatch species vary from commonly to rarely caught, bycatch datasets offer a wide range of occurrence rates and densities. Thus, in addition to providing guidance for spatial bycatch management, large bycatch datasets are excellent testbeds for evaluating SDM performance more generally.

Understanding how species distributions change in time and space is critical for conservation planning and natural resource management (Parmesan and Yohe, 2003; Sumaila et al., 2011; Pinsky et al., 2013), and this has motivated rapid development of SDMs in the last decade. There is now a wide range of statistical tools available to ecologists and fisheries scientists for fitting data on species presence/absence and abundance (Phillips et al., 2006; Illian et al., 2013; Conn et al., 2015;

Golding and Purse, 2016).

SDMs can be coarsely divided into parametric, semiparametric, and nonparametric approaches. Generalized linear models (GLMs) are one of the simplest parametric approaches used to understand species distributions and their relationships with biotic and abiotic covariates (Venables and Ripley, 2002). GLMs predict the response variable, Y_i (species presence/absence or abundance at location i), by specifying a probability distribution and link function:

$$\begin{aligned}
 Y_i &\sim \text{distribution with mean } \mu_i, \\
 g(\mu_i) &= \eta_i, \\
 \eta_i &= \mathbf{X}_i \boldsymbol{\beta}
 \end{aligned}
 \tag{2.1}$$

where \mathbf{X}_i is a vector of covariate values for location i , and $\boldsymbol{\beta}$ is a vector of coefficients to be estimated. GLMs can permit nonlinear relationships between the covariates and response by including transformations of the covariates, e.g. polynomial terms $\eta_i = \beta_0 + \beta_1 X_{1i} + \beta_2 X_{1i}^2 + \beta_3 X_{1i}^3 + \dots$, or by discretizing continuous covariates and treating them as categorical variables.

Generalized additive models (GAMs) extend the GLM framework by allowing the linear predictor to include smooth functions of the covariates (Guisan and Thuiller, 2005; Wood, 2017). GAMs are often referred to as semiparametric, since the smoothers do not have a specified functional form but do have associated parameters that are estimated using penalized likelihood (Wood, 2011; Guélat and Kéry, 2018). The ability of GAMs to incorporate complex, non-linear covariate effects, as well as improvements to computing power and software, has led to their wide adoption in fisheries and ecology in the last decade (Becker et al., 2014; Leathwick et al., 2006; Li and Pan, 2011; Watson et al., 2009). Extending the linear predictor in Equation 2.1 to include a 2-dimensional spline, $f(\cdot)$, on the geographical coordinates of location i , \mathbf{s}_i , specifies a GAM:

$$\eta_i = \mathbf{X}_i \boldsymbol{\beta} + f(\mathbf{s}_i).
 \tag{2.2}$$

Equation 2.2 is estimated by penalized likelihood maximization, which balances smoothness and fit to the data by penalizing the curvature (i.e. integral of the squared second derivative) of $f(\mathbf{s}_i)$ (Wood, 2017). Kammann and Wand (2003) refer to Equation 2.2 as a ‘geoaddivitive’ model, and have shown that this is mathematically equivalent to explicitly modeling spatial correlation with random effects, \mathbf{u} :

$$\eta_i = (\mathbf{X}\boldsymbol{\beta} + \mathbf{Z}\mathbf{u})_i \quad (2.3)$$

(Diggle et al., 1998; Kneib et al., 2008; Péron et al., 2011; Fahrmeir et al., 2013; Guélat and Kéry, 2018). When the spatial random effects are assumed to follow a zero-mean multivariate normal distribution, Equation 2.3 can be written as:

$$\begin{aligned} \eta_i &= \mathbf{X}_i\boldsymbol{\beta} + \varepsilon(\mathbf{s}_i), \\ \varepsilon(\mathbf{s}) &\sim MVN(0, \boldsymbol{\Sigma}), \end{aligned} \quad (2.4)$$

where ε is a Gaussian field (Kneib et al., 2008). Analogous to how the curvature of the spline is penalized when estimating the GAM, the correlation function that defines $\boldsymbol{\Sigma}$ acts as a penalized spatial smoother in the Gaussian field model—nearby locations are more highly correlated, and thus more smoothed, than distant locations (Fahrmeir et al., 2013). Gaussian fields are attractive because they directly model spatial correlation, but applications have historically been limited to smaller datasets because inverting the covariance matrix, $\boldsymbol{\Sigma}$, makes them computationally intense (Lindgren et al., 2011). In summary, both the GAM and Gaussian field model account for spatial autocorrelation not explained by environmental covariates, are semiparametric, mathematically equivalent, and typically fit using penalized likelihood that optimizes spatial smoothing.

Modeling species distributions using Gaussian Markov random fields (GMRFs) has become increasingly common as advances in computing power and software implementation have allowed ecologists to apply them to large datasets. Lindgren et al. (2011) demonstrated that a Gaussian field, which is defined in continuous space, can be approximated by a discrete GMRF that arises as the solution to a stochastic partial differential equation. Among other advantages, the GMRF

approach can be implemented by integrated nested Laplace approximation, which is faster than other methods of Bayesian inference (i.e. Markov chain Monte Carlo) and allow GMRF approximations of Gaussian fields to be computationally feasible (Rue et al., 2009). GMRF models have shown promise in assessing relationships between habitat and distribution (Illian et al., 2013), the effects of interspecific relationships such as density dependence (Thorson et al., 2015c), as well as the relationships between multiple co-occurring taxa (Ward et al., 2015). From a quantitative standpoint, GMRF models have been shown to estimate population abundance trends with greater precision and accuracy compared to non-spatial models (Thorson et al., 2015b).

Clearly, GMRFs are intimately related to GAMs, since GMRFs approximate the Gaussian field model (Eqn. 2.4), which is an alternative parameterization of the GAM in Equation 2.2. The spatial smoothing terms for both GAMs and GMRFs can be defined on a sphere or differ according to spatial direction (anisotropy can be included in GAMs by using tensor product smooths, and Σ can be both non-stationary and anisotropic in GMRFs). GAMs and GMRFs differ, however, in two regards. First, the spatial smoothing term appears as a mean trend for GAMs and as a covariance matrix for GMRFs. This distinction may not be important for modelling species distributions, and researchers may prefer the method that reflects their view of how spatial autocorrelation arises in the problem at hand. For instance, GMRFs would be the more natural framework if the spatial variation remaining after including environmental covariates is considered random. Second, and more importantly, the different parameterizations lead to different estimation methods and software implementations. Since spatial models for large datasets contain many parameters, numerically efficient implementations are crucial (Fahrmeir et al., 2013). Several R packages fit GAMs, the most popular being ‘mgcv,’ which uses generalized cross-validation to estimate smooth terms by default (Wood, 2017). GMRFs can be fit via ‘INLA,’ which uses a Bayesian framework and estimates models by integrated nested Laplace approximation (Lindgren and Rue, 2015). In theory, ‘mgcv’ and ‘INLA’ should be quite similar. In practice, however, differences in approximation methods, runtime, convergence criteria, ease of use, and default settings may impact model predictions.

Most nonparametric approaches ecologists use to model species distributions have evolved from machine learning algorithms (Hastie et al., 2009; Olden et al., 2008). These data-driven approaches include random forests (RF; Breiman, 2001; Cutler et al., 2007), MaxEnt (Phillips et al., 2006; Phillips and Dudík, 2008), and support vector machines (Drake et al., 2006). In this analysis we highlight RF because 1) data in our application—fisheries bycatch—contain true absences, whereas MaxEnt is designed for presence-only data, and 2) RF is widely used and has shown good predictive performance in SDM testing (Prasad et al., 2006; Marmion et al., 2009; Scales et al., 2016). The RF algorithm predicts the response by constructing m regression (or classification) trees and averaging their predictions (Breiman, 2001). Each individual tree begins with all observations and then iteratively partitions the data by splitting along one covariate (e.g. depth > 100 m versus depth ≤ 100 m), choosing the covariate and split point that minimizes the sums of squares error at each node (where the predicted response at each node is the mean of observations within the node; Breiman et al., 1984). The process continues until each terminal node contains less than a specified number of observations. Individual trees are simple and computationally cheap but are also unstable (i.e. sensitive to slight alterations in the data) and sub-optimal at prediction (i.e. they are “weak learners”), because they only allow rectangular partitions of covariate space. The RF algorithm increases predictive performance by reducing the correlation between trees, which is accomplished via two processes: 1) fitting each tree to a bootstrap sample of the original data, and 2) at each split, randomly selecting a subset of covariates to consider (Kuhn and Johnson, 2013). This works because reducing the correlation between individual trees reduces the correlation of their errors, which therefore reduces the predictive error of their average, the RF estimate.

Random forests are popular because they are simple to use (few parameters to tune and the default values work well in most cases), generate accurate predictions, designed to not overfit, seamlessly accommodate missing data, and are robust to the inclusion of many non-informative covariates (Biau and Scornet, 2016). Compared to parametric and semiparametric models, RF will often have better out-of-sample (i.e. cross-validated) prediction performance due to their ability to

estimate more complex patterns, as non-linearity and interactions are inherent in their construction (Elith and Leathwick, 2009). However, this data-driven complexity does come at the cost of model interpretability, and this is one of the main factors limiting the adoption of RF—and machine learning methods more generally—by ecologists (Olden et al., 2008). Three other disadvantages of RF are the difficulty of generating uncertainty estimates with well-understood properties, analyzing model diagnostics, and specifying constraints on model fit (e.g., we may wish yearly estimates to be independent, which can be specified in parametric models).

The primary objective of this paper is to compare the performance of GAMs, GMRFs and RF in a predictive framework. There has been an increased emphasis on predictive metrics in ecology (Hooten and Hobbs, 2015), and one of the advantages of this approach is that nonparametric and parametric models can be compared (Ward et al., 2014). While each of these methods have individually been applied to understand spatiotemporal trends in fisheries bycatch (Becker et al., 2014; Hazen et al., 2017; McCracken, 2004; Watson et al., 2009; Breivik et al., 2016, 2017; Cosandey-Godin et al., 2015; Carretta et al., 2017; Eguchi et al., 2017; Pons et al., 2009), their predictive performance has not been tested in a comparative study. A secondary objective of our analysis is to evaluate whether any of these models offer consistent advantages across a wide range of bycatch rates (% fishing events with non-zero catch) and life history characteristics (such as movement or habitat preference). Our final objective is to evaluate the utility of using SDM predictions of bycatch risk as a tool to reduce bycatch in fisheries.

2.2 Methods

Fisheries observer data

Collecting reliable bycatch data depends on fisheries observer programs, where on-board observers enumerate and record the species caught (as well as fishing location, gear type, time, and other relevant information). To explore the performance of species distribution models across taxa, we used two datasets from United States fisheries observer programs in the Pacific Ocean

with high observer coverage. The first dataset was from the West Coast Groundfish Observer Program (WCGOP) at the Northwest Fisheries Science Center (NWFSC; Bellman et al., 2010). The WCGOP dataset contained records of 42 786 commercial bottom trawls from 2003-2012 off the west coast of the USA, primarily targeting groundfish such as Dover sole (*Microstomus pacificus*), thornyheads (*Sebastolobus* spp.), sablefish (*Anoplopoma fimbria*), and rockfish (*Sebastes* spp., Fig. 2.1). Observers recorded haul duration, location, date, time, depth, gear type, and catch (which includes at-sea discarded bycatch; for details see NWFSC, 2016). Observer coverage was approximately 20% from 2003-2010 under limited access management, with 100% coverage starting in 2011 with the transition to an individual fishing quota (IFQ) system. In the pre-IFQ era, fishermen were not permitted to land rebuilding species (i.e. populations declared overfished with management plans to rebuild to sustainable levels), so we defined bycatch as only at-sea discards. Under the IFQ system fishermen can land a low quota of rebuilding species, so we considered bycatch to be the sum of discarded and retained catch for non-target species.

The second dataset was from the Hawaii longline (HILL) fishery, monitored by the Pacific Islands Regional Observer Program (PIROP, 2014), which has recorded fishing location, date, time, sea surface temperature (SST), gear characteristics, and catch of longline sets from 1994-2014. The Hawaii longline fleet is divided into two sectors, one targeting tuna (*Thunnus* spp.) and the other swordfish (*Xiphias gladius*), with distinct gear configurations and spatiotemporal effort patterns, both of which affect interaction rates with bycatch species (Li and Pan, 2011). We modeled 16 714 observations from the shallow-set swordfish fishery in 1994-2001 and 2005-2014 (Fig. 2.2), distinguishing between sets targeting swordfish and tuna by the number of hooks between surface floats (following Li and Pan, 2011). Concerns over bycatch of protected species, particularly of loggerhead (*Caretta caretta*) and leatherback sea turtles (*Dermochelys coriacea*), motivated the closure of the swordfish fishery from 2001 to 2004. This led to two important differences between the data from 1994-2001 and 2005-2014. First, sea turtle bycatch rates have been an order of magnitude lower in the later period, the result of stricter regulations and modifying hooks (J to circle

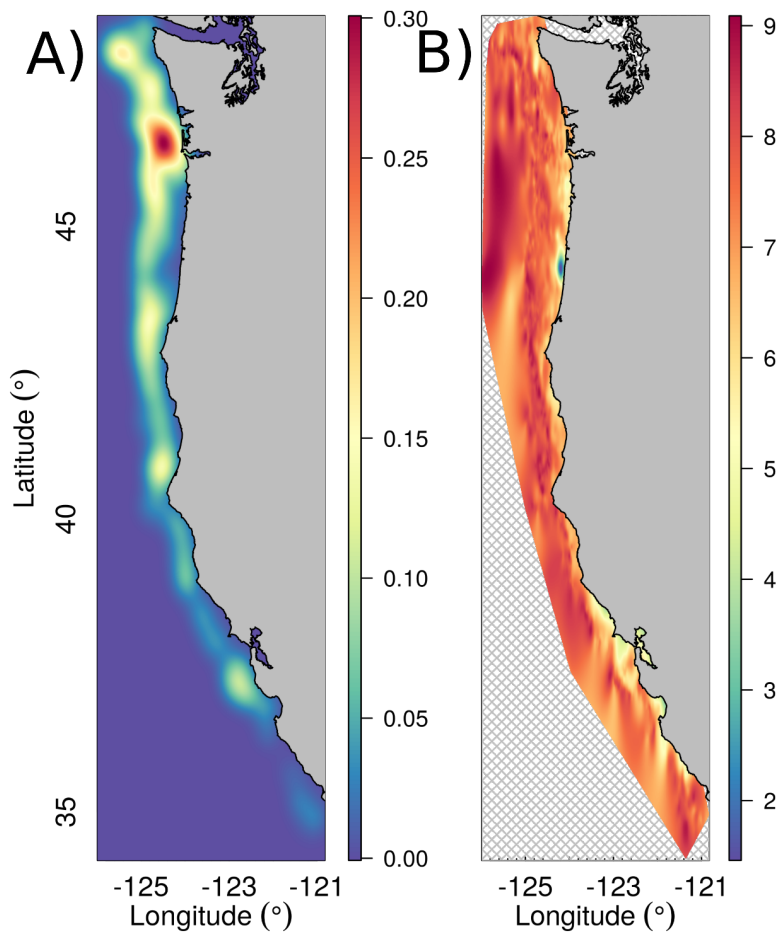


Figure 2.1: Effort and target species catch density in the West Coast groundfish trawl fishery from 2003 to 2012. a) Bivariate kernel density estimate showing smoothed density of fishing effort (42,786 haul locations, ‘bkde2D’ function in R package ‘KernSmooth’). b) Thin plate spline surface estimating the average *density* of target species catch at a given location, log(pounds groundfish) per haul, fit using the ‘Tps’ function from the R package ‘fields’. Note that the map of total catch would be produced by multiplying a) effort and b) target catch density, just as the binomial and positive components are multiplied in the delta-model.

hooks) and bait types (squid to fish; Gilman et al., 2007). Second, observer coverage increased from roughly 5% to 100% (Howell et al., 2008).

Model performance may be linked to species' movement patterns, because species that move less (or whose movement patterns do not change in time) may not need a spatiotemporal model. Instead, a time-constant spatial model may be adequate. To ascertain whether differences in SDM performance were related to movement pattern or bycatch rate (i.e. % observations with non-zero catch), we selected three bycatch species from each dataset: blue shark (*Prionace glauca*), Pacific halibut (*Hippoglossus stenolepis*), darkblotched rockfish (*Sebastes crameri*), yelloweye rockfish (*Sebastes ruberrimus*), loggerhead sea turtle, and leatherback sea turtle. These species widely differ in their bycatch rates (96.2%, 28.9%, 17.9%, 1.4%, 0.7%, and 0.3%, respectively), habitat preferences, and movement patterns. For instance, rockfish are relatively sedentary and closely associated with rocky bottom habitat, whereas halibut exhibit seasonal and long-distance migrations (Skud, 1977; Gunderson, 1997). In contrast to the groundfish, blue sharks and sea turtles inhabit the open ocean and range much more widely (Benson et al., 2011; Kobayashi et al., 2008; Nichols et al., 2000).

While both datasets include periods with 100% observer coverage, they also span periods with partial coverage. This is relevant since the models assume that the data represent a random sample of the studied fishery, i.e. each fishing event has an equal probability of being observed. For several reasons, it is difficult for observer programs to achieve random sampling: a list of trips and their departures often does not exist far in advance, certain vessels may not be able to accommodate observers, observers may not always be available, and fisher behavior can change when observers are on board (Hall, 1999; Liggins et al., 1997; McCracken, 2004). The WCGOP data from years with 20% coverage are likely to be representative of the fishery, because the WCGOP stratified sampling by port group, vessel, and 2-month blocks with the goals of sampling all vessels for two months in each year and discouraging changes to fishing behavior when observers were on-board (NWFSC, 2006). It is less likely that this was true for the 1994-2001 HILL data. Nevertheless,

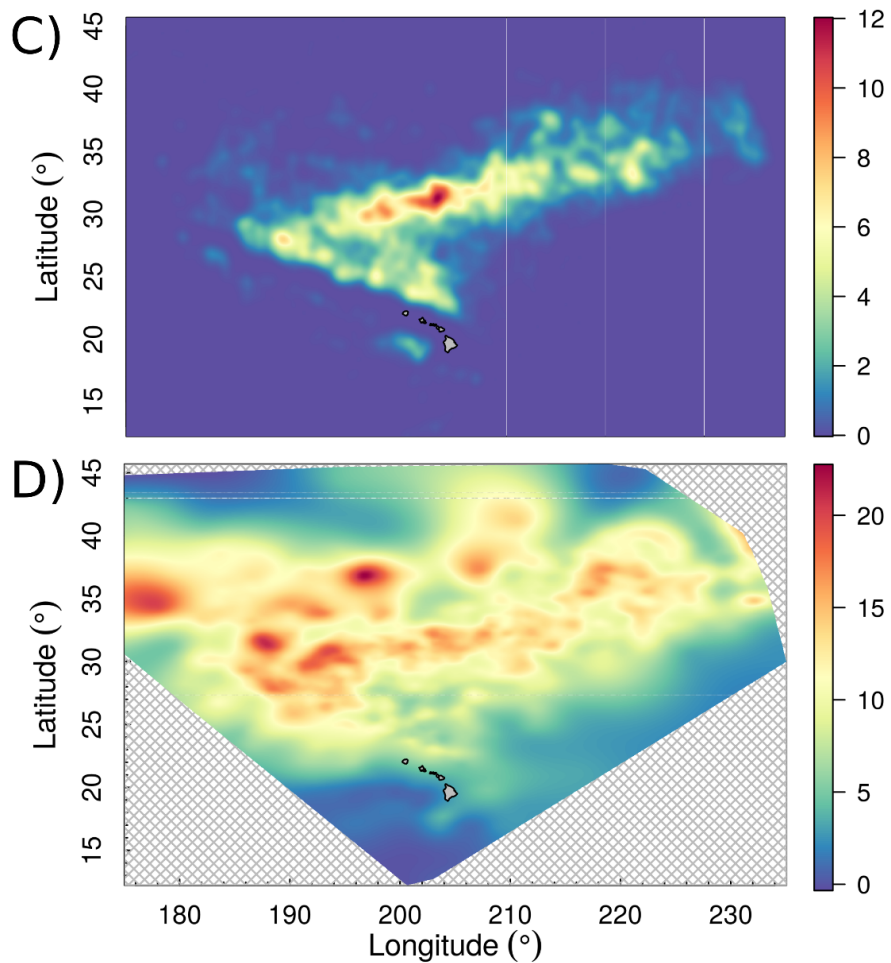


Figure 2.2: Effort and target species catch density in the shallow-set Hawaii longline swordfish fishery from 1994 to 2014. c) Bivariate kernel density estimate showing smoothed density of fishing effort (16,714 set locations, ‘bkde2D’ function in R package ‘KernSmooth’). d) Thin plate spline surface estimating the average *density* of target species catch at a given location, number of swordfish per set, fit using the ‘Tps’ function from the R package ‘fields’.

we included data from periods with partial coverage because there were very few observations of non-zero catch for rarely encountered species in the years with full coverage (yelloweye rockfish: 38, loggerhead turtle: 89, leatherback turtle: 82), and in many cases, bycatch of these ‘rare-event’ species are often of highest management concern (Martin et al., 2015).

Environmental covariates

In addition to the locations of observed fishing, we considered several spatially referenced covariates that may help explain the likelihood of bycatch events. For the WCGOP dataset, we included fishing depth, day of year, sea surface temperature (SST), distance to rocky habitat, size of nearest rocky patch, predicted occurrence from survey data, and whether the trawl occurred in or near a Rockfish Conservation Area (RCA). RCAs are large areas along the U.S. West Coast closed to fishing designed primarily to reduce bycatch of overfished rockfish, such as two of the species we considered. RCA boundaries have changed by and within years, and are defined by latitude, date, and depth (NOAA Fisheries West Coast Region, 2015). Trawls were determined to be inside or outside of an RCA based on the trawl date, average position of trawl start and end, and bottom depth (calculated via bathymetry from NOAA National Centers for Environmental Information, 2015). We included linear and quadratic terms for fishing depth and SST following Shelton et al. (2014). Depth was recorded by on-board observers, while SST anomalies were measured via satellite. For each trawl, we collected daily SST anomalies on a 0.25° grid and used bilinear interpolation to create SST values corresponding to each trawl location (<http://www.esrl.noaa.gov/psd/>, Reynolds et al., 2007). Rocky habitat data were from NMFS (2013), calculated as per Shelton et al. (2014). Finally, we used the above covariates to fit a geostatistical delta-GLMM to fisheries-independent trawl survey data (Bradburn et al. 2011, modeled as in Shelton et al. 2014), and applied this model to predict bycatch occurrence at the fishing times and locations in the observer dataset. These survey-predicted occurrence probabilities were included as another linear covariate. All environmental covariates were standardized and centered before model estimation.

The only available environmental covariate for the HILL dataset was observer-recorded SST, and therefore we fit the HILL models with covariates of standardized SST, SST^2 , and day of year.

Statistical models

As is common for species distribution data, five of the six species exhibited large proportions of zero catches. We followed the hurdle- or delta-model approach to this complication, which is commonly applied in ecology and fisheries (Pennington, 1983; Maunder and Punt, 2004). Delta-models separate the observed catches, Y_i , into two processes: a ‘binomial’ component for the probability of non-zero catch, π_i , and a ‘positive’ component for the mean catch density given the catch is non-zero, μ_i :

$$\begin{aligned} Z_i &\sim \text{Bernoulli}(\pi_i), \\ Y_i &\sim Z_i h(\mu_i), \end{aligned} \tag{2.5}$$

where Z_i is a binary variable that equals 1 if the species was caught and 0 if it was not, and $h()$ is a distribution to be specified (e.g. lognormal, gamma). Splitting the modeling into these two components can be advantageous because different mechanisms may affect one component but not the other (e.g. a habitat quality covariate may be a significant predictor of catch rate, but not occurrence).

We applied a total of eight delta-models with varying spatial structure to each of the six species included in our analysis (Table 2.1). Bycatch of yelloweye rockfish, loggerhead turtles, and leatherback turtles were extremely rare events (0.3-1.4% non-zero observations) with too few multiple-individual catches to meaningfully fit the positive component. All analyses were conducted using R v3.4.1 (R Core Team, 2017), with the following libraries: ‘mgcv’ was used to implement GLMs and GAMs (v1.8-17, Wood, 2017); ‘randomForest’ (v4.6-12, Liaw and Wiener, 2002), ‘DMwR’ (v0.4.1, Torgo, 2010), and ‘forestFloor’ (v1.9.5, Welling et al., 2016) were used to fit RFs; and ‘INLA’ was used to fit the GMRF models (v0.0-1485844051, Lindgren and Rue, 2015). We assessed model fit with plots of covariate-response relationships, predicted versus

observed response in out-of-sample data, spatial residual maps, and spatial correlograms (Moran’s I, package ‘ncf’ v1.2-5, Bjørnstad and Falck, 2001). Code to fit each of the models is provided at <https://github.com/brianstock/spatial-bycatch>.

Our first model was a delta-GLM with linear and quadratic effects of the environmental covariates (which are intrinsically spatially correlated), but without any spatial terms—neither geographic coordinates nor spatial autocorrelation for residual errors. As in Guélat and Kéry (2018), the delta-GLM served as a baseline that allowed us to evaluate the value of adding spatial terms in the subsequent models, which were fit using the same covariates and only differ in how they include spatial information. The delta-GLM fits the observed bycatch in fishing event i , Y_i , as in Eqns. 2.1 and 2.5, with binomial component determining the probability of non-zero bycatch, π_i :

$$\begin{aligned} Z_i &\sim \text{Bernoulli}(\pi_i), \\ \text{logit}(\pi_i) &= \mathbf{X}_i\boldsymbol{\alpha}, \end{aligned} \tag{2.6}$$

and positive component for the mean catch density given the catch is non-zero, μ_i :

$$\begin{aligned} Y_i &\sim Z_i\text{Gamma}(\mu_i, k), \\ \log(\mu_i) &= \mathbf{X}_i\boldsymbol{\beta}. \end{aligned} \tag{2.7}$$

where \mathbf{X}_i is a vector of covariate values for location i , $\boldsymbol{\alpha}$ and $\boldsymbol{\beta}$ are vectors of coefficients to be estimated, and k is the shape parameter of the gamma distribution. The gamma distribution is appropriate for positive, right-skewed data, and therefore is commonly used in the positive component of delta-models for fisheries catch (Lecomte et al., 2013; Stefansson, 1996). While we would not expect the GLM to outperform the models with explicit spatial terms, it is possible that the (spatially-structured) environmental covariates could explain most of spatial structure in the response. In that case, including spatial terms in the model (i.e. a 2-d spline as in Eqn. 2.2 or covariance matrix as in Eqn. 2.4) would be unnecessary.

We fit two delta-GAM models that extend Eqns. 2.6 and 2.7 by adding a 2-dimensional

Table 2.1: Properties of the considered statistical models and how each model incorporates spatial fishing locations. The GLM model serves as the baseline model—no spatial data included. GAM models fit 2-d splines on geographical coordinates (i.e. latitude and longitude), either constant across years (GAM-CONSTANT) or estimating a different spline for each year (GAM-YEAR). Gaussian Markov random field (GMRF) models incorporate spatial locations by estimating the covariance between locations as a random field (with stationary Matern covariance function). As for GAMs, we fit GMRFs that estimate one random field kept constant across years (GMRF-CONSTANT) or estimate a random field for each year (GMRF-YEAR). RF is nonparametric and thus only incorporates spatial locations by including covariates of latitude and longitude. All models for a given species were fit using the same non-spatial covariates (habitat, depth, SST, etc.). We used the R packages ‘mgcv’ (GLM and GAM), ‘INLA’ (GMRF), ‘randomForest’ (RF), and ‘caret’ (RF-SMOTE).

Model	Parametric?	Computational intensity	R package	Inclusion of spatial locations
Generalized linear model	Parametric			
GLM		Low	mgcv	None
Generalized additive model	Semiparametric			
GAM-CONSTANT		Low	mgcv	+ s(Lat, Lon, k=100)
GAM-YEAR		Medium	mgcv	+ s(Lat, Lon, k=100, by=year)
Gaussian Markov random field	Semiparametric			
GMRF-CONSTANT		High	INLA	+ f(i, model=spde)
GMRF-YEAR		Very high	INLA	+ f(i, model=spde, group=year, control.group=list(model='exchangeable'))
Random forests	Nonparametric			
RF-BASE		Low	randomForest	+ Lat + Lon
RF-DOWN		Low	randomForest	+ Lat + Lon
RF-SMOTE		Low	caret	+ Lat + Lon

spline, $f()$, on the geographical coordinates of location i , \mathbf{s}_i , to both the binomial and positive components, as in Eqn. 2.2:

$$\begin{aligned}
Z_i &\sim \text{Bernoulli}(\pi_i), \\
\text{logit}(\pi_i) &= \mathbf{X}_i\boldsymbol{\alpha} + f_Z(\mathbf{s}_i), \\
Y_i &\sim \text{Gamma}(\mu_i, k), \\
\log(\mu_i) &= \mathbf{X}_i\boldsymbol{\beta} + f_Y(\mathbf{s}_i).
\end{aligned} \tag{2.8}$$

The first, ‘‘GAM-CONSTANT,’’ includes one 2-d spline constant across years, with an offset (fixed effect) for each year. This allows the mean bycatch probability and density to vary temporally and spatially, but in the same pattern each year. The second, ‘‘GAM-YEAR,’’ fits an independent 2-d spline for each year, which allows the spatial pattern to vary between years (Table 2.1).

As for the GAMs, we fit two delta-GMRF models which extend Eqns. 2.6 and 2.7 by estimating the covariance between observed locations, \mathbf{s}_i , as in Eqn. 2.4:

$$\begin{aligned}
Z_i &\sim \text{Bernoulli}(\pi_i), \\
\text{logit}(\pi_i) &= \mathbf{X}_i\boldsymbol{\alpha} + \boldsymbol{\varepsilon}_Z(\mathbf{s}_i), \\
\boldsymbol{\varepsilon}_Z(\mathbf{s}) &\sim \text{MVN}(0, \mathbf{Q}_Z^{-1}), \\
Y_i &\sim \text{Gamma}(\mu_i, k), \\
\log(\mu_i) &= \mathbf{X}_i\boldsymbol{\beta} + \boldsymbol{\varepsilon}_Y(\mathbf{s}_i), \\
\boldsymbol{\varepsilon}_Y(\mathbf{s}) &\sim \text{MVN}(0, \mathbf{Q}_Y^{-1}),
\end{aligned} \tag{2.9}$$

where both \mathbf{Q}_Z^{-1} and \mathbf{Q}_Y^{-1} are defined to approximate stationary, isotropic Matérn covariances:

$$\text{Cov}(s_1, s_2) = \frac{\sigma^2}{2^{\nu-1}\Gamma(\nu)} (\kappa\|s_1 - s_2\|)^\nu K_\nu(\kappa\|s_1 - s_2\|), \tag{2.10}$$

and $\boldsymbol{\varepsilon}_Z()$ and $\boldsymbol{\varepsilon}_Y()$ represent the estimated spatial fields using random effects. We used the default Matérn smoothness, $\nu = 1$, and priors on parameters as implemented in R-INLA (Lindgren and

Rue, 2015). Analogous to the GAM-CONSTANT and GAM-YEAR models, we fit a “GMRF-CONSTANT” model with one random field constant across all years, and a “GMRF-YEAR” model with a random field estimated for each year (Table 2.1). As for GAM-CONSTANT, the GMRF-CONSTANT model includes fixed effect terms for each year, which allow for an increase or decrease in the mean bycatch probability and density for each year while assuming the spatial pattern is constant across years. The GMRF-YEAR model uses the simplest spatiotemporal option in R-INLA, ‘exchangeable,’ which refers to the spatiotemporal structure—the random fields in all years are uniformly correlated (as opposed to an autoregressive spatiotemporal structure where nearby years are more correlated than distant years).

To include spatiotemporal effects in RFs, we added year (treated as a factor), latitude, and longitude as covariates. For the positive component of the delta-model, we fit only one RF model: “RF-BASE,” following the original RF algorithm as described by Breiman (2001) and implemented in the ‘randomForest’ R package (Liaw and Wiener, 2002). For the binomial component, we also fit two modifications to the original RF algorithm designed to improve performance on imbalanced class data (i.e. proportions of 0s and 1s very unequal), because several species showed strong class imbalance (e.g., yelloweye rockfish had 99.7% tows with zero catch and only 0.3% tows with non-zero catch). Training a RF on such severely imbalanced class data tends to produce models that predict the majority class well but performs poorly on the minority class (Kuhn and Johnson, 2013). The first approach was to *down-sample* the majority class observations (e.g. 0s, tows with zero catch for yelloweye rockfish) when training the RF such that each tree used a stratified bootstrap sample of the data with equal numbers of majority and minority (e.g. 1s, tows with non-zero catch for yelloweye rockfish) class observations. We implemented down-sampling in the “RF-DOWN” model, setting the sample size equal to one-sixth the number of minority class observations. The second approach, “RF-SMOTE” (Synthetic Minority Over-sampling Technique, Chawla et al., 2002), combined down-sampling of the majority class with over-sampling of the minority class. Simply over-sampling the minority class with replacement overfits the RF to the specific observed

minority data and typically does not significantly improve prediction of the minority class. Instead, SMOTE creates synthetic minority class samples by generating random linear combinations of nearby observed minority samples, i.e. if \mathbf{X}_1 and \mathbf{X}_2 are nearest neighbors with $\mathbf{X}_1 = \{\text{SST}_1, \text{Lat}_1, \text{Lon}_1\}$ and $\mathbf{X}_2 = \{\text{SST}_2, \text{Lat}_2, \text{Lon}_2\}$, draw p from $\text{Uniform}(0,1)$ and create $\mathbf{X}_{\text{syn}} = \{p(\text{SST}_1 - \text{SST}_2) + \text{SST}_2, p(\text{Lat}_1 - \text{Lat}_2) + \text{Lat}_2, p(\text{Lon}_1 - \text{Lon}_2) + \text{Lon}_2\}$.

Model performance comparison

We performed 5-fold cross-validation repeated 10 times, which allowed us to evaluate semiparametric and nonparametric SDMs' predictive error on new data (Shmueli, 2010; Kuhn and Johnson, 2013). We blocked by year (rather than systematically excluding a given year) to account for temporal structure and mimic predictive performance for cases where a random subset of samples in a given year are not observed (Roberts et al., 2017). Thus, we generated 50 test/train splits, where each selects 20% of the data from each year to reserve for testing, and fits the models on the remaining 80% training data. After fitting the models to training data, we used the fitted models to predict bycatch probability (binomial component of the delta-model) and density (positive component of the delta-model) at the test locations. This gave us predicted and observed values to compare parametric and nonparametric model performance: area under the receiver operating characteristic curve (AUC) scores for the binomial component, and root-mean-square error (RMSE) for the positive component. AUC can be interpreted as the expectation that a model ranks a uniformly drawn random positive (bycatch event) as more likely than a uniformly drawn random negative (non-bycatch event, Hand, 2009).

Since AUC and RMSE are abstract metrics of model performance, we calculated a more tangible measure: how much each of the models could possibly reduce the bycatch-to-target species catch ratio if it were used to identify and remove high bycatch risk fishing events. In other words, what does an AUC performance gap of 0.03 mean in terms of bycatch reduction (keeping catch of the target species constant)? For each species and model fit, we rank-ordered the bycatch probabilities

predicted by the binomial component, identified the X% of fishing events with the highest bycatch probabilities (X% = 1%, 2%, 5%, and 10%), removed both bycatch and target catch from those events, and calculated the resultant change in bycatch-to-target species catch ratio.

Finally, we evaluated the transferability, i.e. spatial extrapolation performance, of the GMRF and RF models by conducting a second cross-validation blocking on spatial data density. Predictions in areas of covariate-space with few data are more sensitive to model misspecification and overfitting, and therefore caution is especially warranted for complex, nonparametric approaches such as RF (Merow et al., 2014). In addition, SDMs that are more data-driven and complex have been shown to have better interpolation performance but be worse at spatial extrapolation (Araujo and Rahbek, 2006; Heikkinen et al., 2012; Randin et al., 2006). Since we wished to evaluate using SDM predictions of bycatch risk as a spatial management tool, it was important to assess how sensitive the predictions were to spatial location. For example, one model may have higher predictive performance in the core fishing area with high data density but underperform other models in areas with sparse sampling coverage. Whereas our previous cross-validation procedure partitioned the data into training and testing sets *randomly*, here we constructed test/train splits by ordering fishing locations relative to data density. We calculated a bivariate kernel density estimate at each of the observed fishing locations ('bkde2D' function in 'KernSmooth' R package) and sequentially used the lowest 0.5%, 1%, 2%, 5%, 10%, and 20% density locations as test datasets.

2.3 Results

For all species, residuals were more variable between cross-validation fits as model complexity increased (RF > GMRF > GAM > GLM, Figs. S1-S18). Most models did not exhibit spatial patterns in residuals, although residuals in the positive component of the delta-model were larger and more variable for blue shark and Pacific halibut north of 40°N and 47°N, respectively (Figs. S1-S2, S11-S12). GMRFs and GAMs had similarly lower residual spatial autocorrelation compared to the baseline GLMs, with one exception where the GMRF reduced spatial autocorrelation more

than the GAM (blue shark positive model, Fig. A1). RF generally had the lowest spatial autocorrelation, and it was negative instead of positive at short distances. The Hawaii longline species had greater decorrelation distances than the West Coast groundfish species (distance at which spatial autocorrelation goes to zero, 40 km vs. 5 km, Fig. A1).

RF provided better bycatch predictions than both GAMs and GMRFs for all six species in both the binomial (higher AUC, Fig. 2.3a) and positive (lower RMSE, Fig. 2.3b) components of the delta-model, although the magnitude of this performance advantage varied by species. RF modifications designed for data with imbalanced classes, down-sampling and SMOTE, outperformed the original RF algorithm for the four species with high or low bycatch rates (Fig. A2). Of the semiparametric models, GMRF-YEAR that allowed for time-varying spatial effects performed the best (Figs. 2.3 and A3), whereas the binomial GAM-YEAR that estimated 2-d splines by year failed to converge. For rare bycatch species with few positive occurrences, GMRF models that allowed for time-varying spatial effects offered no improvement over the time-constant spatial models (Fig. A3); in such cases, this time-constant GMRF spatial model would only be marginally different from a GLM including latitude and longitude (Fig. A4). The variability in model performance among cross-validation runs was similar within a given species but varied greatly between species; variability in the binomial component was lowest for species with moderate bycatch rates (darkblotched rockfish and Pacific halibut in Fig. 2.3a), and in the positive component it was lowest for species with high bycatch rates (blue shark in Fig. 2.3b).

When using the models to identify and remove high bycatch risk fishing events, RF also performed best. Averaged across the six species, RF reduced the bycatch-to-target species catch ratio by 8% when removing 1% of fishing effort, 34% when removing 5% of fishing effort, and 50% when removing 10% of fishing effort (Fig. 2.4). Bycatch predictability as measured by bycatch-to-target ratio reduction generally agreed with the traditional performance metrics (AUC and RMSE) and varied substantially among the six species (Fig. A5). As GMRF and RF outperformed GLM and GAM, we only considered these two models in further comparisons.

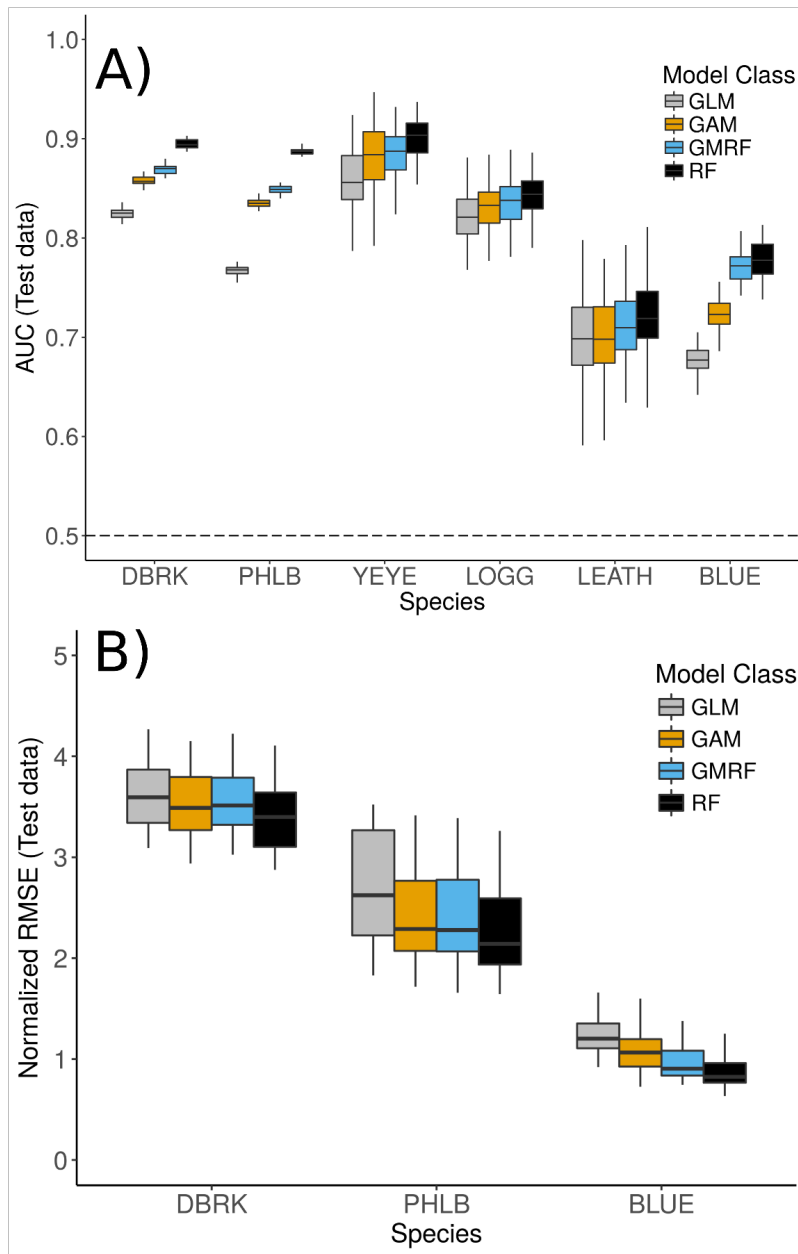


Figure 2.3: Predictive performance of the a) binomial and b) positive components of the delta-model on test data from 5-fold cross-validation repeated 10 times: a) AUC for the binomial component, and b) normalized RMSE for the positive component. Random forests (RFs) outperformed GAMs and GMRFs for all species (highest AUC, lowest RMSE). Binomial component results were more variable for species with extremely low or high bycatch rates (YEYE, LOGG, LEATH, and BLUE). Species abbreviations: DBRK = darkblotched rockfish, PHLB = Pacific halibut, YEYE = yelloweye rockfish, LOGG = loggerhead turtle, LEATH = leatherback turtle, BLUE = blue shark. Only the best submodel, e.g. CONSTANT or YEAR, within each model class for each species is shown here (see Supplement).

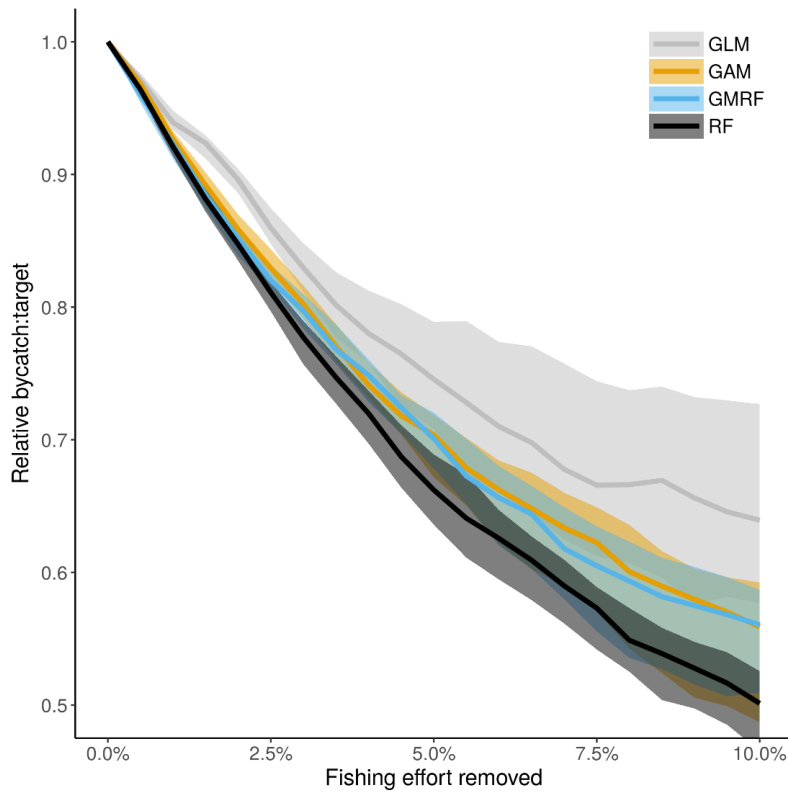


Figure 2.4: Bycatch-to-target species catch ratio achieved by using the binomial component of the delta-model to predict and remove fishing sets in the test data, relative to the bycatch-to-target ratio with no fishing sets removed. Lines show median of 50 cross-validation runs for each model class (5-fold CV repeated 10 times), averaged across the six species. Shaded areas are bootstrapped 95% confidence intervals for the median. Random forest (RF) performed the best, reducing the bycatch-to-target ratio by 34% when removing 5% of fishing, and by 50% when removing 10% of fishing. As in Figure 2.3, only the best submodel within each model class (e.g. CONSTANT or YEAR) for each species is shown here.

Predictions from the GMRF and RF models were highly correlated for all species ($r = 0.69-0.91$, Fig. A6) and therefore produced roughly similar bycatch risk maps. Taking blue sharks as an example, both models predicted higher bycatch in the north and moderate bycatch west of 195°E (Fig. 2.5a,c). We calculated the variance at each grid point for both GMRF (using the posterior standard deviation) and RF (using the infinitesimal jackknife estimator, Wager et al. 2014) predictions to produce maps of prediction uncertainty (Fig. 2.5b,d). Bycatch risk maps from both models revealed artifacts of their construction: the mesh triangulation is evident in the GMRF variance map (Fig. 2.5b), and the sharp gradients in the RF mean (Fig. 2.5c) and variance (Fig. 2.5d) maps are a consequence of RF trees splitting on latitude and longitude. As expected, the uncertainty of GMRF predictions was lower in areas of high data density (compare Figs. 2.2c and 2.5b). Uncertainty in RF predictions did not follow this trend—RF variance was relatively low and constant below 41.5°N latitude, and much higher above 41.5°N latitude (Fig. 2.5d). However, this was consistent with the data, as there were few observed sets north of 41.5°N and these had higher and more variable bycatch (Fig. A7).

To investigate this difference, we tested the models' ability to extrapolate in space, i.e. to predict at locations outside the core area of the fishery when trained using observations in areas of highest data density. In this test, GMRFs and RFs performed equal to or worse than when test-train splits were random (Fig. 2.6). GMRFs had lower RMSE than RFs in the positive component of the delta-model but there was no difference in AUC in the binomial component (Wilcoxon signed-rank test, $p = 0.91$ for $\text{AUC}_{\text{GMRF}} \neq \text{F}$, AUC_{RF} , $p = 0.003$ for $\text{RMSE}_{\text{GMRF}} \neq \text{RMSE}_{\text{RF}}$). Compared to GMRFs, RF performance was also more sensitive to withholding data at the edge of the fishery (Fig. 2.6). The degree to which this was true, however, differed widely between species. For instance, the performance of both models was stable for some species (e.g. darkblotched rockfish in binomial component, blue shark in positive component), indicating that both models captured relevant spatial environment-bycatch relationships in the core area of the fishery and that these relationships remained valid at the edge of the fishery.

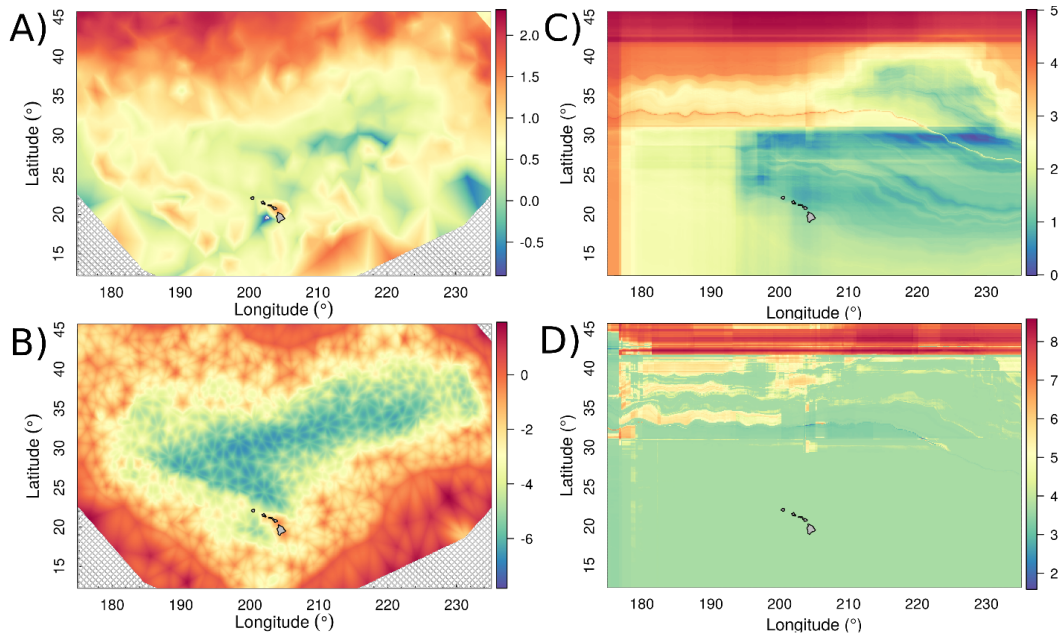


Figure 2.5: Maps of blue shark bycatch predictions with uncertainty for the Hawaii longline swordfish fishery in 2014 from the GMRF and random forest (RF) models (binomial \times positive = expected). a) Log mean expected bycatch from the GMRF-CONSTANT model. b) Log variance of expected bycatch from the GMRF-CONSTANT model. c) Log mean expected bycatch from the RF-BASE model. d) Log variance of expected bycatch from the RF-BASE model. Maps created by both models show artifacts of their construction: the mesh triangulation is evident in the GMRF variance map (b), and the sharp gradients in the RF mean (c) and variance (d) maps are a consequence of RF trees splitting on latitude and longitude.

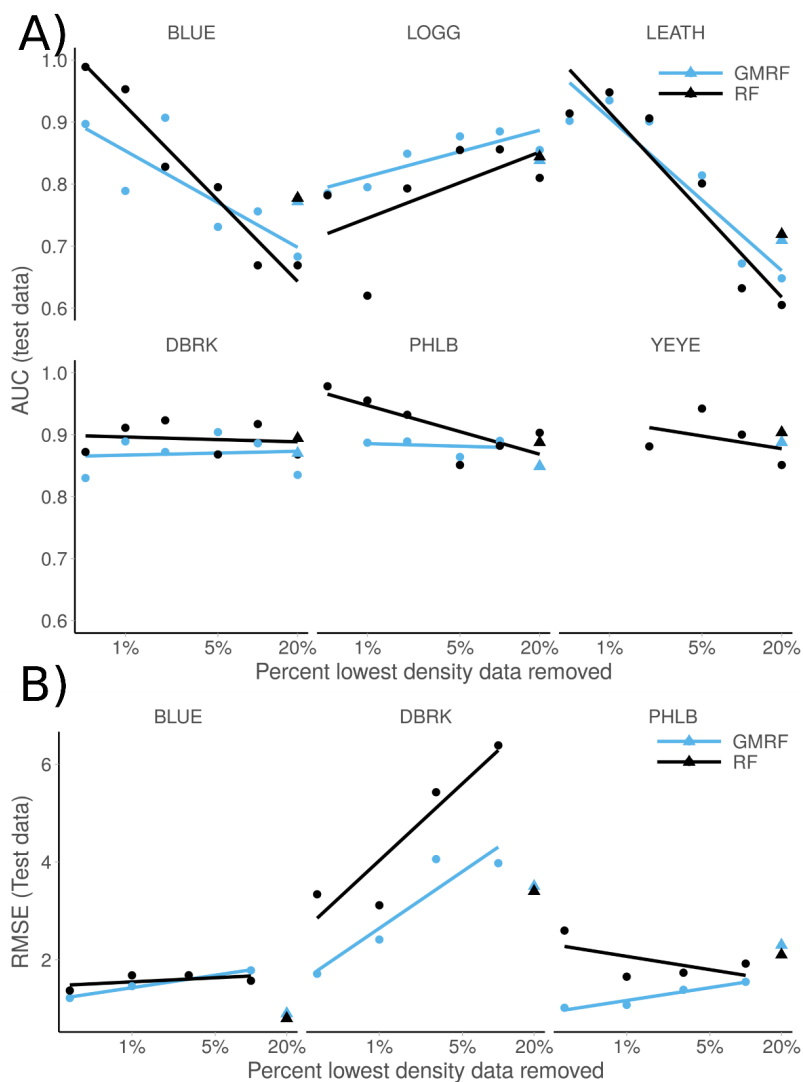


Figure 2.6: Predictive performance of the a) binomial and b) positive components of the GMRF-CONSTANT and RF delta-models at test locations beyond the geographic data range (i.e. spatial extrapolation). We fit a 2d kernel density estimate at each observed fishing location ('bkde2D' function in 'KernSmooth' R package), then sequentially used the lowest 0.5%, 1%, 2%, 5%, 10%, and 20% density locations as test datasets. Triangles show median model performance from 5-fold cross-validation runs with random test/train splits. When extrapolating spatially, GMRF and RF performed equal to or worse than when interpolating (i.e. points are lower AUC and higher RMSE than triangles). GMRF had lower RMSE than RF in the positive component of the delta-model but there was no difference in AUC in the binomial component (Wilcoxon signed-rank test, $p = 0.91$ for $AUC_{\text{GMRF}} \neq AUC_{\text{RF}}$, $p = 0.003$ for $RMSE_{\text{GMRF}} \neq RMSE_{\text{RF}}$). Compared to GMRF, RF performance was more sensitive to withholding data at the edge of the fishery (i.e. regression lines have steeper slopes). Species abbreviations: DBRK = darkblotched rockfish, PHLB = Pacific halibut, YEYE = yelloweye rockfish, LOGG = loggerhead turtle, LEATH = leatherback turtle, BLUE = blue shark.

GMRF and RF models estimated similar covariate effects, as demonstrated for darkblotched rockfish (Fig. 2.7). The main covariate effects were as expected: both probability and amount of bycatch increased with higher survey-predicted occurrence, increased for tows inside or near RCAs, and showed an optimal depth range of 100-300 fathoms.

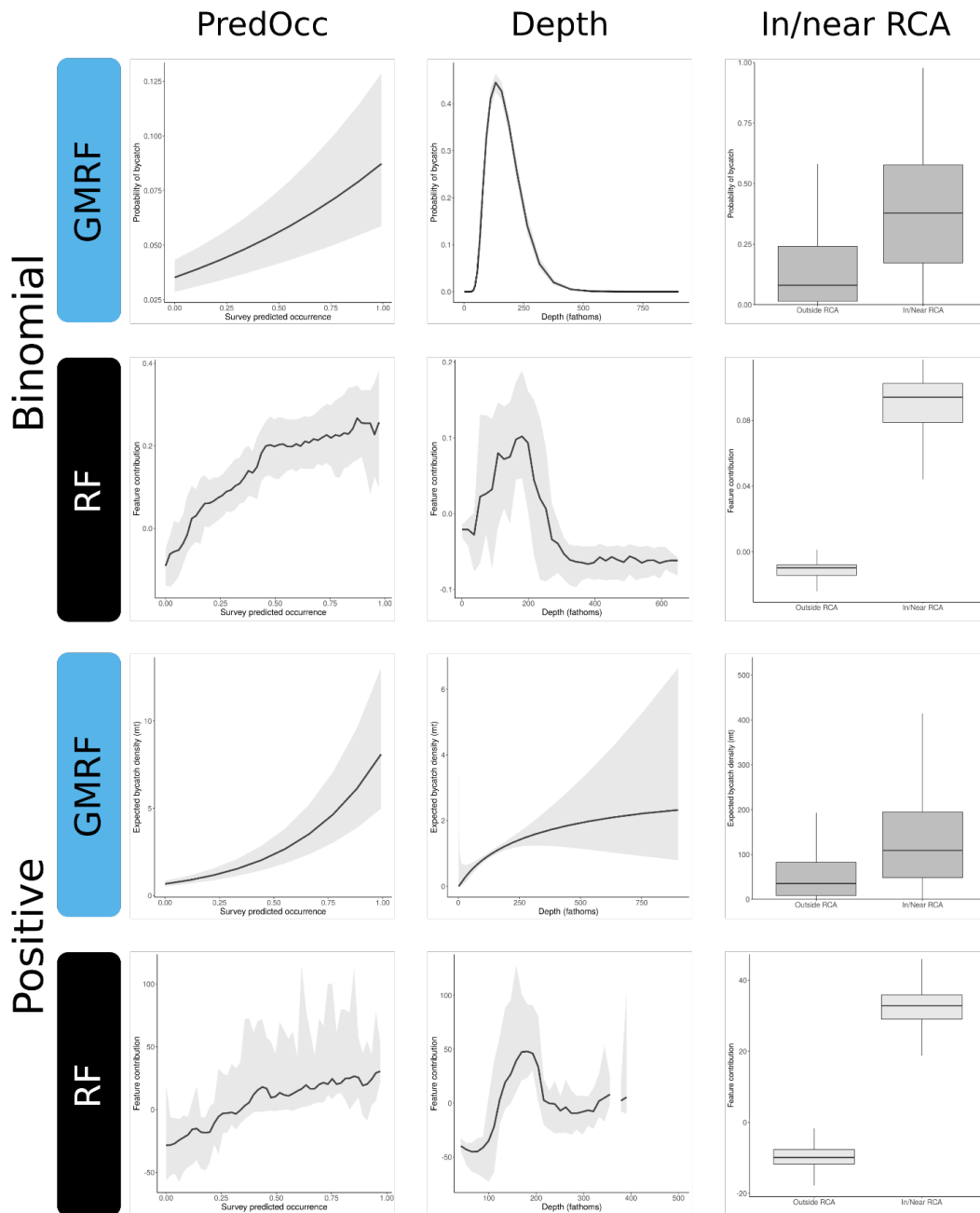


Figure 2.7: Covariate effects estimated by the GMRF and random forest (RF) models for darkblotched rockfish. GMRF and RF estimate a positive effect of PredOcc (predicted occurrence from survey data, left column), quadratic effect of Depth, and positive effect of In/near RCA (haul location inside or near rockfish conservation area boundary) for both the binomial and positive components of the delta-model. GMRF covariate effects are marginal posterior distributions ('INLA' package in R), and RF covariate effects are feature contributions ('forestFloor' package in R).

2.4 Discussion

The interpolation performance of the four models was consistent across a wide range of bycatch rates and life histories: RFs performed best, followed by GMRFs, GAMs, and the baseline GLM (Fig. 2.3). When extrapolating beyond the geographic range of the data, however, RFs were more sensitive to which data were withheld and performed similar to, or worse than, GMRFs (Fig. 2.6b). This is consistent with previous work documenting that more data-driven, complex SDMs can have better interpolation performance but be worse at spatial extrapolation (Heikkinen et al., 2012; Randin et al., 2006).

Our results beg the question: if RFs are expected to have higher interpolation accuracy, why ever use GMRFs or GAMs? This is a decidedly relevant concern given the significant research investment in these modeling approaches (Becker et al., 2014; Thorson and Barnett, 2017). RF will generally have better out-of-sample prediction, largely due to its ability to incorporate nonlinear and interaction effects of covariates inherently (i.e., without user specification). In addition, RF models are much simpler and quicker to both write code for and run. Contrary to references describing RFs as “black boxes” (Prasad et al., 2006; Cutler et al., 2007; Elith and Leathwick, 2009; Evans and Cushman, 2009; Kuhn and Johnson, 2013), there are methods for investigating RF model structure, including covariate effects and interactions (Fig. 6, Welling et al., 2016). In a similar vein, it is possible to calculate prediction variance and confidence intervals for RF (Meinshausen, 2006; Wager et al., 2014), despite older ecological literature stating otherwise (Cutler et al., 2007; Olden et al., 2008), or using ad-hoc substitutes such as the standard deviation of individual tree predictions (Smoliński and Radtke, 2017). Additionally, promising theoretical work may soon widen the ability to use RFs for statistical inference by developing asymptotically normal, unbiased point estimates with valid confidence intervals (Mentch and Hooker, 2017; Wager and Athey, 2017). In many cases, RF’s performance advantage is probably sufficient to warrant its use over other semiparametric methods. Yet, there may be several cases where semiparametric methods are preferred.

Semiparametric frameworks like GMRFs and GAMs have clear advantages over machine

learning algorithms such as RF. First, they can be derived from probability theory and therefore allow for traditional statistical inference on their mean response predictions. GMRF estimates full posterior distributions for the response variable (in this study, probability and/or expected amount of bycatch) everywhere in the spatial domain. This enables us, for instance, to use a GMRF model to identify regions that are above/below a threshold probability (i.e. risk level) of a defined bycatch quantity. By contrast, basic statistical properties of RF remain unknown (Biau and Scornet, 2016). Thus, GMRF models may be preferred for applications where estimates of model uncertainty are decidedly important, such as using models to produce annual estimates of bycatch (expanded from the observed to unobserved fleet). Second, GMRFs and GAMs explicitly estimate covariate effects with uncertainty intervals, facilitating ecological interpretation of factors significantly affecting the response (Fig. 2.7). This is especially important when the primary goal of ecological modeling is parameter estimation, as in fisheries stock assessments. Third, GMRF models are particularly well-suited to incorporate spatial ecological processes, such as movement, spatial variation in fishing mortality or observation error. RFs, on the other hand, are based solely on observations without taking into consideration the data generating process. Fourth, GAMs and GMRFs produce smoothed spatial predictions that are more likely ecologically plausible, whereas RF spatial predictions appear rectangular by default due to splits on the geographical coordinates. This can be mediated, however, by including transformations of the coordinates, fitting a linear model within each node instead of taking the mean (Quinlan, 1992, 1993), or including buffer distances as covariates (Hengl et al., 2018). Fifth, RFs can simultaneously have high interpolation accuracy and lower extrapolation accuracy (Fig. 5b). This matters if SDM predictions of bycatch risk are to be used as a spatial management tool, where predictions in areas with sparse or no sampling coverage may be most important. Finally, GMRFs can be easily specified to produce independent or exchangeable estimates of a given quantity (e.g., total predicted bycatch in different years), while it is unclear how to assign a specific dependence-structure on factors in a RF model. This is important when using estimates from a spatial model as input in a secondary model, for

example, where the secondary model assumes that estimates are independent among years. In situations where these concerns are inconsequential, however, RFs may be the better method for spatial bycatch prediction—they are faster and have better predictive performance than the alternatives.

On a more detailed level, the six species differed widely in their predictability. The West Coast groundfish species were more predictable than the Hawaii longline species, likely because we included several more relevant environmental covariates (WCGOP: sea surface temperature, depth, rocky habitat, in/near RCA, and survey-predicted occurrence; HILL: sea surface temperature) and the WCGOP dataset had 2.5 times the number of observations (WCGOP: 42 786; HILL: 16 714). The HILL models' performance could presumably be improved by incorporating more satellite-based environmental covariates capable of explaining the species' distributions, such as chlorophyll and SST-derived frontal indices (Nieto et al., 2017). Among the West Coast species, Pacific halibut was more difficult to predict than the two rockfish species, despite having more positive bycatch occurrences for the models to fit. One possible explanation is that adult halibut move more and have less strict habitat associations than rockfish, decreasing their predictability (Skud, 1977; Gunderson, 1997). Among the Hawaii longline species, loggerhead turtles were much easier to predict than leatherback turtles and blue sharks, perhaps because they have stronger SST-based habitat preferences where the fishing occurs (Howell et al., 2015). Indeed, the loggerhead-temperature association is the basis for TurtleWatch, a decade-long effort to reduce turtle bycatch by providing fishermen with dynamic recommendations of high bycatch risk areas to avoid in the Central Pacific (Howell et al., 2008). Despite plausible life history explanations for some among-species differences in predictability, however, the advantage of fitting time-varying vs. time-constant models appeared to be primarily driven by the species' bycatch rates. In other words, there was little difference in model performance for rare bycatch species (yelloweye rockfish, loggerhead turtle, and leatherback turtle) and greater differences between models for common bycatch species (darkblotched rockfish, Pacific halibut, and blue shark, Figs. 2.3a and A3).

Our results demonstrate the clear potential of SDMs to predict fishing activity with higher bycatch risk. Importantly, predicting and removing high bycatch risk fishing lowered the bycatch-to-target ratio because target catch and bycatch were generally not correlated. In other words, removing 5% of fishing effort typically only removed 5% of target catch, but much more than 5% of the total bycatch. While the models varied considerably in their ability to predict bycatch, even the worst performer (baseline GLM without latitude and longitude) achieved AUC from 0.68–0.86 and reduced bycatch-to-target ratios on average by 25% for a 5% reduction in fishing effort. RF performed the best, achieving cross-validated AUC above 0.89 for all three West Coast groundfish species and reducing bycatch-to-target ratios by 34% for a 5% reduction in fishing effort averaged across the six species.

Given their good predictive performance overall, SDMs could be used to support spatial bycatch management, whether static (e.g. design habitat closures to be semi-permanent, such as the Pacific Leatherback Conservation Area along the U.S. West Coast; 50 CFR Part 660) or dynamic in time (e.g. closures change every year, month, week, etc., such as the Loggerhead Turtle Conservation Area along the Southern California Bight, 72FR 31756; Fig. 2.8, as in Dunn et al. 2016). If so, they should be compared to and integrated with existing tools that aim to reduce bycatch by producing risk maps; examples include Eguchi et al. (2017), TurtleWatch (Howell et al., 2008, 2015), and WhaleWatch (Hazen et al., 2017). Both TurtleWatch and WhaleWatch are based on satellite telemetry observations and known habitat preferences of sea turtles and blue whales, in contrast to the models developed here that rely exclusively on fisheries observer data. Since fisheries observer datasets cover many more bycatch species than those with satellite tagging programs, SDMs based on fisheries observer data are more widely applicable than those based solely on satellite telemetry. Bycatch occurs when non-target species and fishing gear co-occur, both of which are affected by various factors, such as environmental conditions, economics, and behavior (Soykan et al., 2014). Consequently, using fishery observer data combined with animal movements data would provide a comprehensive dataset to develop predictive models of bycatch.

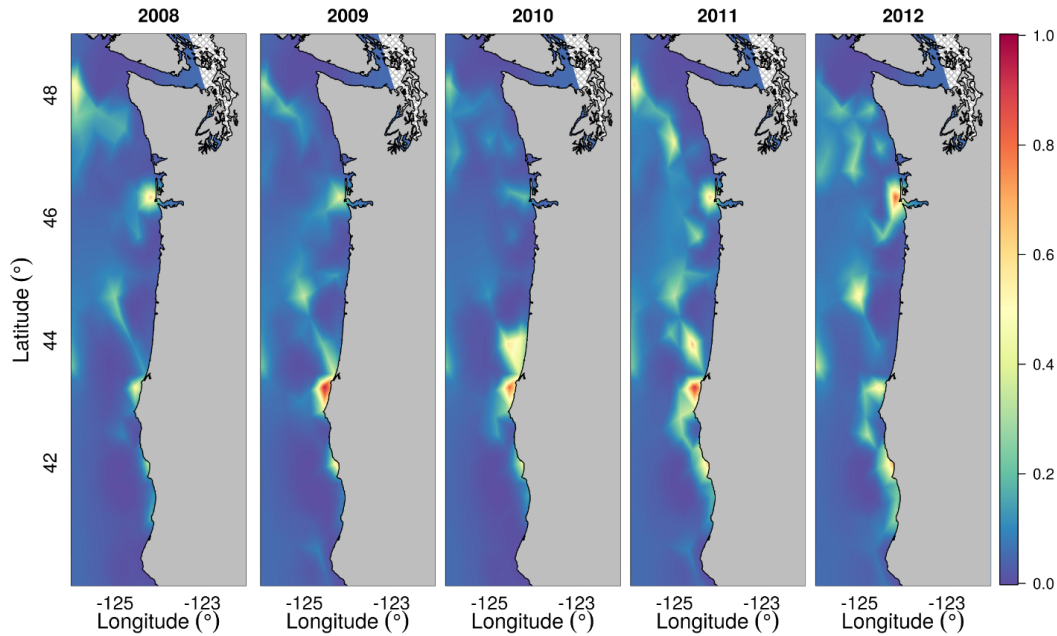


Figure 2.8: GMRF-YEAR random field for bycatch probability of darkblotched rockfish from 2008 to 2012.

Future efforts to use spatial models to predict fisheries bycatch risk should carefully consider the hierarchical structure common to observer datasets with less than 100% coverage. In the typical case where observers are placed on vessels on a trip-by-trip basis and then observe all sets within a trip, the sets are likely not independent (e.g. sets within the same trip, and trips on the same vessel may be correlated). As done in this study, including spatiotemporal correlation structure will account for some of the correlation between sets within a trip because they are presumably closer together in time and space. One approach is to include the nested data structure in the model as random effects (Candy, 2004; Thorson et al., 2015b), although this can be more complicated than it first appears (e.g. captains and crew transfer between vessels in the Hawaii longline fishery, making it unclear whether including a vessel effect is appropriate). Roberts et al. (2017) make an excellent case for an alternative approach, using block cross-validation to account for spatial, temporal, and group dependence structure when validating and selecting models. A related issue with the delta-models used here is that they assume two independent processes determine the probability

and amount of bycatch (i.e., the binomial and positive components of the delta-model). Thorson (2017) and Cantoni et al. (2017) both recently demonstrated that this is unlikely to be true, and their proposed solutions should improve spatial bycatch analyses in the future.

Finally, just as single-species fisheries management paints a rosier picture than can truly be implemented, the results presented here are unrealistic in their treatment of multispecies fisheries because bycatch prediction cannot be optimized for each individual species simultaneously. These results are still useful if fisheries managers are particularly concerned about a single species, but less so if reducing bycatch of multiple species is the objective. Both RF and GMRF models have multivariate extensions that could fruitfully be applied to multispecies spatial bycatch prediction, and future work should investigate this possibility (Thorson et al., 2015a; Thorson and Barnett, 2017; Ishwaran and Kogalur, 2017).

Data Accessibility

Unsummarized fisheries observer data are deemed confidential. Code to download and process publicly available fisheries survey data, run each of the models, and replicate figures is provided at <https://github.com/brianstock/spatial-bycatch>. Summarized reports of the fisheries observer program data are available at: https://www.nwfsc.noaa.gov/research/divisions/fram/observation/data_products/data_library.cfm (U.S. West Coast groundfish) and http://www.fpir.noaa.gov/OBS/obs_hi_ll_ss_rprts.html (Hawaii longline).

Acknowledgements

T. Todd Jones, Summer Martin, Don Kobayashi, Eric Forney, and Marti McCracken shared valuable knowledge of the Hawaii longline fishery and observer program. BCS received support from the National Science Foundation Graduate Research Fellowship under Grant No. DGE-1144086. BCS also received support from the NMFS Protected Species Toolbox and benefited from discussions at two NMFS Protected Species Assessment Workshops. This work used the

Extreme Science and Engineering Discovery Environment (XSEDE), supported by National Science Foundation grant number ACI-1053575.

This chapter, in full, has been submitted for publication and is printed here with the permission of co-authors Eric J. Ward, Tomoharu Eguchi, Jason E. Jannot, James T. Thorson, Blake E. Feist, and Brice X. Semmens. The dissertation author was the primary investigator and author of this paper.

References

- Alverson, D. L., M. H. Freeberg, S. A. Murawski, and J. G. Pope. 1994. A global assessment of fisheries bycatch and discards. Technical Report FAO Fisheries Technical Paper. No. 339., FAO, Rome.
- Araujo, M. B. and C. Rahbek. 2006. How Does Climate Change Affect Biodiversity? *Science*, **313**:1396–1397.
- Becker, E., K. Forney, D. Foley, R. Smith, T. Moore, and J. Barlow. 2014. Predicting seasonal density patterns of California cetaceans based on habitat models. *Endangered Species Research*, **23**:1–22.
- Bellman, M. A., E. Heery, and J. Majewski. 2010. Observed and Estimated Total Bycatch of Green Sturgeon in the 2002-2008 U.S. West Coast Groundfish Fisheries. Technical report, NWFSC, West Coast Groundfish Observer Program, 2725 Montlake Blvd E., Seattle, WA 98112.
- Benson, S. R., T. Eguchi, D. G. Foley, K. A. Forney, H. Bailey, C. Hitipeuw, B. P. Samber, R. F. Tapilatu, V. Rei, P. Ramohia, J. Pita, and P. H. Dutton. 2011. Large-scale movements and high-use areas of western Pacific leatherback turtles, *Dermochelys coriacea*. *Ecosphere*, **2**:art84.
- Biau, G. and E. Scornet. 2016. A random forest guided tour. *TEST*, **25**:197–227.
- Bjørnstad, O. N. and W. Falck. 2001. Nonparametric spatial covariance functions: estimation and testing. *Environmental and Ecological Statistics*, **8**:53–70.
- Boyce, J. R. 1996. An Economic Analysis of the Fisheries Bycatch Problem. *Journal of Environmental Economics and Management*, **31**:314–336.
- Bradburn, M., A. Keller, and B. Horness. 2011. The 2003 to 2008 U.S. West Coast bottom trawl surveys of groundfish resources off Washington, Oregon, and California: Estimates of distribution, abundance, length, and age composition. Technical Report NOAA Technical Memorandum NMFS-NWFSC-114, NOAA, NFMS, NWFSC.

- Breiman, L. 2001. Random forests. *Machine Learning*, **45**:5–32.
- Breiman, L., J. Friedman, R. A. Olshen, and C. J. Stone. 1984. *Classification And Regression Trees*. Chapman & Hall/CRC, Boca Raton, FL.
- Breivik, O. N., G. Storvik, and K. Nedreaas. 2016. Latent Gaussian models to decide on spatial closures for bycatch management in the Barents Sea shrimp fishery. *Canadian Journal of Fisheries and Aquatic Sciences*, **73**:1271–1280.
- Breivik, O. N., G. Storvik, and K. Nedreaas. 2017. Latent Gaussian models to predict historical bycatch in commercial fishery. *Fisheries Research*, **185**:62–72.
- Candy, S. G. 2004. Modelling catch and effort data using generalised linear models, the Tweedie distribution, random vessel effects, and random stratum-by-year effects. *CCAMLR Science*, **11**:59–80.
- Cantoni, E., J. Mills Flemming, and A. H. Welsh. 2017. A random-effects hurdle model for predicting bycatch of endangered marine species. *The Annals of Applied Statistics*, **11**:2178–2199.
- Carretta, J. V., J. E. Moor, and K. A. Forney. 2017. Regression tree and ratio estimates of marine mammal, sea turtle, and seabird bycatch in the California drift gillnet fishery, 1990-2015. Technical Report NOAA Tech. Memo., NOAA-TM-NMFS-SWFSC-568.
- Chawla, N. V., K. W. Bowyer, L. O. Hall, and W. P. Kegelmeyer. 2002. SMOTE: Synthetic Minority Over-sampling Technique. *Journal of Artificial Intelligence Research*, **16**:321–357.
- Conn, P. B., D. S. Johnson, J. M. V. Hoef, M. B. Hooten, J. M. London, and P. L. Boveng. 2015. Using spatiotemporal statistical models to estimate animal abundance and infer ecological dynamics from survey counts. *Ecological Monographs*, **85**:235–252.
- Cosandey-Godin, A., E. T. Krainski, B. Worm, and J. M. Flemming. 2015. Applying Bayesian spatiotemporal models to fisheries bycatch in the Canadian Arctic. *Canadian Journal of Fisheries and Aquatic Sciences*, **72**:186–197.
- Cutler, D. R., T. C. Edwards, K. H. Beard, A. Cutler, K. T. Hess, J. Gibson, and J. J. Lawler. 2007. Random forests for classification in ecology. *Ecology*, **88**:2783–2792.
- Davies, R., S. Cripps, A. Nickson, and G. Porter. 2009. Defining and estimating global marine fisheries bycatch. *Marine Policy*, **33**:661–672.
- Diggle, P. J., J. A. Tawn, and R. A. Moyeed. 1998. Model-based geostatistics. *Journal of the Royal Statistical Society: Series C (Applied Statistics)*, **47**:299–350.
- Drake, J. M., C. Randin, and A. Guisan. 2006. Modelling ecological niches with support vector machines. *Journal of Applied Ecology*, **43**:424–432.

- Dunn, D. C., S. M. Maxwell, A. M. Boustany, and P. N. Halpin. 2016. Dynamic ocean management increases the efficiency and efficacy of fisheries management. *Proceedings of the National Academy of Sciences*, **113**:668–673.
- Eguchi, T., S. R. Benson, D. G. Foley, and K. A. Forney. 2017. Predicting overlap between drift gillnet fishing and leatherback turtle habitat in the California Current Ecosystem. *Fisheries Oceanography*, **26**:17–33.
- Elith, J. and J. R. Leathwick. 2009. Species Distribution Models: Ecological Explanation and Prediction Across Space and Time. *Annual Review of Ecology, Evolution, and Systematics*, **40**:677–697.
- Evans, J. S. and S. A. Cushman. 2009. Gradient modeling of conifer species using random forests. *Landscape Ecology*, **24**:673–683.
- Fahrmeir, L., T. Kneib, S. Lang, and B. Marx. 2013. Nonparametric regression. In *Regression: models, methods and applications*, pages 413–533. Springer-Verlag Berlin Heidelberg.
- FAO. 1995. Code of Conduct for Responsible Fisheries. Technical report, Rome, FAO.
- Gilman, E., D. Kobayashi, T. Swenarton, N. Brothers, P. Dalzell, and I. Kinan-Kelly. 2007. Reducing sea turtle interactions in the Hawaii-based longline swordfish fishery. *Biological Conservation*, **139**:19–28.
- Golding, N. and B. V. Purse. 2016. Fast and flexible Bayesian species distribution modelling using Gaussian processes. *Methods in Ecology and Evolution*, **7**:598–608.
- Guisan, A. and W. Thuiller. 2005. Predicting species distribution: offering more than simple habitat models. *Ecology Letters*, **8**:993–1009.
- Gunderson, D. R. 1997. Spatial patterns in the dynamics of slope rockfish stocks and their implications for management. *Fishery Bulletin*, **95**:219–230.
- Guélat, J. and M. Kéry. 2018. Effects of spatial autocorrelation and imperfect detection on species distribution models. *Methods in Ecology and Evolution*, **9**:1614–1625.
- Hall, M. A. 1999. Estimating the ecological impacts of fisheries: What data are needed to estimate bycatches? In C. P. Nolan, editor, *Proceedings of the International Conference on Integrated Fisheries Monitoring*, pages 175–184. Rome: FAO, Sydney, Australia.
- Hand, D. J. 2009. Measuring classifier performance: a coherent alternative to the area under the ROC curve. *Machine Learning*, **77**:103–123.
- Hastie, T., R. Tibshirani, and J. Friedman. 2009. *The elements of statistical learning*. Springer New York, 2nd ed edition.

- Hazen, E. L., D. M. Palacios, K. A. Forney, E. A. Howell, E. Becker, A. L. Hoover, L. Irvine, M. DeAngelis, S. J. Bograd, B. R. Mate, and H. Bailey. 2017. WhaleWatch: a dynamic management tool for predicting blue whale density in the California Current. *Journal of Applied Ecology*, **54**:1415–1428.
- Heikkinen, R. K., M. Marmion, and M. Luoto. 2012. Does the interpolation accuracy of species distribution models come at the expense of transferability? *Ecography*, **35**:276–288.
- Hengl, T., M. Nussbaum, M. N. Wright, G. B. Heuvelink, and B. Gräler. 2018. Random Forest as a generic framework for predictive modeling of spatial and spatio-temporal variables. *PeerJ Preprints*, page e26693v1.
- Hooten, M. B. and N. T. Hobbs. 2015. A guide to Bayesian model selection for ecologists. *Ecological Monographs*, **85**:3–28.
- Howell, E., D. Kobayashi, D. Parker, G. Balazs, and a. Polovina. 2008. TurtleWatch: a tool to aid in the bycatch reduction of loggerhead turtles *Caretta caretta* in the Hawaii-based pelagic longline fishery. *Endangered Species Research*, **5**:267–278.
- Howell, E. A., A. Hoover, S. R. Benson, H. Bailey, J. J. Polovina, J. A. Seminoff, and P. H. Dutton. 2015. Enhancing the TurtleWatch product for leatherback sea turtles, a dynamic habitat model for ecosystem-based management. *Fisheries Oceanography*, **24**:57–68.
- Ianelli, J. N. and D. L. Stram. 2015. Estimating impacts of the pollock fishery bycatch on western Alaska Chinook salmon. *ICES Journal of Marine Science*, **72**:1159–1172.
- Illian, J. B., S. Martino, S. H. Sørbye, J. B. Gallego-Fernández, M. Zunzunegui, M. P. Esquivias, and J. M. J. Travis. 2013. Fitting complex ecological point process models with integrated nested Laplace approximation. *Methods in Ecology and Evolution*, **4**:305–315.
- Ishwaran, H. and U. B. Kogalur. 2017. Random forests for survival, regression and classification (RF-SRC).
- Kammann, E. E. and M. P. Wand. 2003. Geoadaptive models. *Journal of the Royal Statistical Society: Series C (Applied Statistics)*, **52**:1–18.
- Kelleher, K. 2005. Discards in the world's marine fisheries: an update. Technical report, Food and Agriculture Organization of the United Nations, Rome. OCLC: 254906620.
- Kneib, T., J. Müller, and T. Hothorn. 2008. Spatial smoothing techniques for the assessment of habitat suitability. *Environmental and Ecological Statistics*, **15**:343–364.
- Kobayashi, D. R., J. J. Polovina, D. M. Parker, N. Kamezaki, I.-J. Cheng, I. Uchida, P. H. Dutton, and G. H. Balazs. 2008. Pelagic habitat characterization of loggerhead sea turtles, *Caretta caretta*, in the North Pacific Ocean (1997–2006): Insights from satellite tag tracking and remotely sensed data. *Journal of Experimental Marine Biology and Ecology*, **356**:96–114.
- Kuhn, M. and K. Johnson. 2013. *Applied Predictive Modeling*. Springer New York, New York, NY.

- Leathwick, J., J. Elith, and T. Hastie. 2006. Comparative performance of generalized additive models and multivariate adaptive regression splines for statistical modelling of species distributions. *Ecological Modelling*, **199**:188–196.
- Lecomte, J.-B., H. P. Benoît, S. Ancelet, M.-P. Etienne, L. Bel, and E. Parent. 2013. Compound Poisson-gamma vs. delta-gamma to handle zero-inflated continuous data under a variable sampling volume. *Methods in Ecology and Evolution*, **4**:1159–1166.
- Lewison, R., A. J. Hobday, S. Maxwell, E. Hazen, J. R. Hartog, D. C. Dunn, D. Briscoe, S. Fossette, C. E. O’Keefe, M. Barnes, M. Abecassis, S. Bograd, N. D. Bethoney, H. Bailey, D. Wiley, S. Andrews, L. Hazen, and L. B. Crowder. 2015. Dynamic Ocean Management: Identifying the Critical Ingredients of Dynamic Approaches to Ocean Resource Management. *BioScience*, **65**:486–498.
- Li, S. and M. Pan. 2011. Fishing Opportunities under the Sea Turtle Interaction Caps—A Spatial Bio-economic Model for the Hawaii-based Longline Swordfish. Technical Report SOEST 11-02, JIMAR Contribution 11-378, Joint Institute for Marine and Atmospheric Research, University of Hawaii, 910 A Pueo Street, Honolulu, HI.
- Liaw, A. and M. Wiener. 2002. Classification and Regression by randomForest. **2**:5.
- Liggins, G. W., M. J. Bradley, and S. J. Kennelly. 1997. Detection of bias in observer-based estimates of retained and discarded catches from a multi species trawl fishery. *Fisheries Research*, **32**:133–147.
- Lindgren, F. and H. Rue. 2015. Bayesian Spatial Modelling with *R* - **INLA**. *Journal of Statistical Software*, **63**.
- Lindgren, F., H. Rue, and J. Lindström. 2011. An explicit link between Gaussian fields and Gaussian Markov random fields: the stochastic partial differential equation approach: Link between Gaussian Fields and Gaussian Markov Random Fields. *Journal of the Royal Statistical Society: Series B (Statistical Methodology)*, **73**:423–498.
- Marmion, M., M. Parviainen, M. Luoto, R. K. Heikkinen, and W. Thuiller. 2009. Evaluation of consensus methods in predictive species distribution modelling. *Diversity and Distributions*, **15**:59–69.
- Martin, S. L., S. M. Stohs, and J. E. Moore. 2015. Bayesian inference and assessment for rare-event bycatch in marine fisheries: a drift gillnet fishery case study. *Ecological Applications*, **25**:416–429.
- Maunder, M. N. and A. E. Punt. 2004. Standardizing catch and effort data: a review of recent approaches. *Fisheries Research*, **70**:141–159.
- McCracken, M. L. 2004. Modeling a very rare event to estimate sea turtle bycatch: Lessons learned. Technical report, U.S. Dep. Commer., NOAA Tech. Memo., NOAA-TM-NMFS-PIFSC-3.

- Meinshausen, N. 2006. Quantile regression forests. *Journal of Machine Learning Research*, **7**:983–999.
- Mentch, L. and G. Hooker. 2017. Formal Hypothesis Tests for Additive Structure in Random Forests. *Journal of Computational and Graphical Statistics*, **26**:589–597.
- Merow, C., M. J. Smith, T. C. Edwards, A. Guisan, S. M. McMahon, S. Normand, W. Thuiller, R. O. Wüest, N. E. Zimmermann, and J. Elith. 2014. What do we gain from simplicity versus complexity in species distribution models? *Ecography*, **37**:1267–1281.
- Nichols, W. J., A. Resendiz, J. A. Seminoff, and B. Resendiz. 2000. Transpacific migration of a loggerhead turtle monitored by satellite telemetry. *Bulletin of Marine Science*, **67**:11.
- Nieto, K., Y. Xu, S. L. Teo, S. McClatchie, and J. Holmes. 2017. How important are coastal fronts to albacore tuna (*Thunnus alalunga*) habitat in the Northeast Pacific Ocean? *Progress in Oceanography*, **150**:62–71.
- NMFS. 2013. Groundfish essential fish habitat synthesis: a report to the Pacific Fishery Management Council. Technical report, National Marine Fisheries Service, Seattle, WA.
- NMFS. 2016. U.S. National Bycatch Report First Edition Update 2. Technical report, U.S. Dep. Commer., National Marine Fisheries Service.
- NOAA Fisheries West Coast Region. 2015. Rockfish conservation areas. http://www.westcoast.fisheries.noaa.gov/fisheries/management/groundfish_closures/rockfish_areas.html.
- NOAA National Centers for Environmental Information. 2015. U.S. Coastal Relief Model. <https://www.ngdc.noaa.gov/mgg/coastal/crm.html>.
- NWFSC. 2006. Observer Coverage Plan: Sampling Plan and Logistics for West Coast Groundfish Observer Program. Technical report, NOAA, West Coast Groundfish Observer Program, 2725 Montlake Blvd E, Seattle, WA.
- NWFSC. 2016. West Coast Groundfish Observer Program 2016 catch share training manual. Technical report, Northwest Fisheries Science Center, Seattle, WA.
- Olden, J., J. Lawler, and N. Poff. 2008. Machine Learning Methods Without Tears: A Primer for Ecologists. *The Quarterly Review of Biology*, **83**:171–193.
- Parmesan, C. and G. Yohe. 2003. A globally coherent fingerprint of climate change impacts across natural systems. *Nature*, **421**:37–42.
- Pennington, M. 1983. Efficient Estimators of Abundance, for Fish and Plankton Surveys. *Biometrics*, **39**:281.
- Phillips, S. J., R. P. Anderson, and R. E. Schapire. 2006. Maximum entropy modeling of species geographic distributions. *Ecological Modelling*, **190**:231–259.

- Phillips, S. J. and M. Dudík. 2008. Modeling of species distributions with Maxent: new extensions and a comprehensive evaluation. *Ecography*, **31**:161–175.
- Pinsky, M. L., B. Worm, M. J. Fogarty, J. L. Sarmiento, and S. A. Levin. 2013. Marine Taxa Track Local Climate Velocities. *Science*, **341**:1239–1242.
- PIROP. 2014. Hawaii longline observer program observer field manual. Technical Report Version LM.14.04, Pacific Islands Regional Observer Program, NOAA/IRC 1, 1845 Wasp Blvd. Bldg. 176, Honolulu, Hawaii 96818.
- Pons, M., S. Marroni, I. Machado, B. Ghattas, and A. Domingo. 2009. Machine learning procedures: An application to by-catch data of the the marine turtles *Caretta caretta* in the southwestern Atlantic Ocean. *Collect. Vol. Sci. Pap. ICCAT*, **64**:2443–2454.
- Prasad, A. M., L. R. Iverson, and A. Liaw. 2006. Newer Classification and Regression Tree Techniques: Bagging and Random Forests for Ecological Prediction. *Ecosystems*, **9**:181–199.
- Péron, G., Y. Ferrand, F. Gossmann, C. Bastat, M. Guenezan, and O. Gimenez. 2011. Nonparametric spatial regression of survival probability: visualization of population sinks in Eurasian Woodcock. *Ecology*, **92**:1672–1679.
- Quinlan, J. 1992. Learning with continuous classes. In 5th Australian Joint Conference on Artificial Intelligence, pages 343–348.
- Quinlan, J. 1993. Combining instance-based and model-based learning. In Proceedings of the Tenth International Conference on Machine Learning., pages 236–243. Elsevier.
- R Core Team. 2017. R: a language and environment for statistical computing.
- Randin, C. F., T. Dirnböck, S. Dullinger, N. E. Zimmermann, M. Zappa, and A. Guisan. 2006. Are niche-based species distribution models transferable in space? *Journal of Biogeography*, **33**:1689–1703.
- Reynolds, R. W., T. M. Smith, C. Liu, D. B. Chelton, K. S. Casey, and M. G. Schlax. 2007. Daily High-Resolution-Blended Analyses for Sea Surface Temperature. *Journal of Climate*, **20**:5473–5496.
- Roberts, D. R., V. Bahn, S. Ciuti, M. S. Boyce, J. Elith, G. Guillera-Arroita, S. Hauenstein, J. J. Lahoz-Monfort, B. Schröder, W. Thuiller, D. I. Warton, B. A. Wintle, F. Hartig, and C. F. Dormann. 2017. Cross-validation strategies for data with temporal, spatial, hierarchical, or phylogenetic structure. *Ecography*, **40**:913–929.
- Rue, H., S. Martino, and N. Chopin. 2009. Approximate Bayesian inference for latent Gaussian models by using integrated nested Laplace approximations. *Journal of the Royal Statistical Society: Series B (Statistical Methodology)*, **71**:319–392.

- Scales, K. L., P. I. Miller, S. N. Ingram, E. L. Hazen, S. J. Bograd, and R. A. Phillips. 2016. Identifying predictable foraging habitats for a wide-ranging marine predator using ensemble ecological niche models. *Diversity and Distributions*, **22**:212–224.
- Shelton, A. O., J. T. Thorson, E. J. Ward, and B. E. Feist. 2014. Spatial semiparametric models improve estimates of species abundance and distribution. *Canadian Journal of Fisheries and Aquatic Sciences*, **71**:1655–1666.
- Shmueli, G. 2010. To Explain or to Predict? *Statistical Science*, **25**:289–310.
- Skud, B. E. 1977. Drift, migration, and intermingling Of Pacific Halibut stocks. Technical Report Scientific Report No. 63, International Pacific Halibut Commission, Seattle, WA.
- Smoliński, S. and K. Radtke. 2017. Spatial prediction of demersal fish diversity in the Baltic Sea: comparison of machine learning and regression-based techniques. *ICES Journal of Marine Science: Journal du Conseil*, **74**:102–111.
- Soykan, C. U., T. Eguchi, S. Kohin, and H. Dewar. 2014. Prediction of fishing effort distributions using boosted regression trees. *Ecological Applications*, **24**:71–83.
- Stefansson, G. 1996. Analysis of groundfish survey abundance data: combining the GLM and delta approaches. *ICES Journal of Marine Science*, **53**:577–588.
- Sumaila, U. R., W. W. L. Cheung, V. W. Y. Lam, D. Pauly, and S. Herrick. 2011. Climate change impacts on the biophysics and economics of world fisheries. *Nature Climate Change*, **1**:449–456.
- Thorson, J. T. 2017. Three problems with the conventional delta-model for biomass sampling data, and a computationally efficient alternative. *Canadian Journal of Fisheries and Aquatic Sciences*, pages 1–14.
- Thorson, J. T. and L. A. K. Barnett. 2017. Comparing estimates of abundance trends and distribution shifts using single- and multispecies models of fishes and biogenic habitat. *ICES Journal of Marine Science: Journal du Conseil*, **74**:1311–1321.
- Thorson, J. T., M. D. Scheuerell, A. O. Shelton, K. E. See, H. J. Skaug, and K. Kristensen. 2015*a*. Spatial factor analysis: a new tool for estimating joint species distributions and correlations in species range. *Methods in Ecology and Evolution*, **6**:627–637.
- Thorson, J. T., A. O. Shelton, E. J. Ward, and H. J. Skaug. 2015*b*. Geostatistical delta-generalized linear mixed models improve precision for estimated abundance indices for West Coast groundfishes. *ICES Journal of Marine Science*, **72**:1297–1310.
- Thorson, J. T., H. J. Skaug, K. Kristensen, A. O. Shelton, E. J. Ward, J. H. Harms, and J. A. Benante. 2015*c*. The importance of spatial models for estimating the strength of density dependence. *Ecology*, **96**:1202–1212.
- Torgo, L. 2010. *Data Mining with R: Learning with Case Studies*, volume 20105341 of *Chapman & Hall/CRC Data Mining and Knowledge Discovery Series*. Chapman and Hall/CRC.

- Venables, W. and C. Dichmont. 2004. GLMs, GAMs and GLMMs: an overview of theory for applications in fisheries research. *Fisheries Research*, **70**:319–337.
- Wager, S. and S. Athey. 2017. Estimation and inference of heterogeneous treatment effects using random forests. *Journal of the American Statistical Association*, pages 1–15.
- Wager, S., T. Hastie, and B. Efron. 2014. Confidence intervals for random forests: The jackknife and the infinitesimal jackknife. *Journal of Machine Learning Research*, **15**:1625–1651.
- Ward, E. J., E. E. Holmes, J. T. Thorson, and B. Collen. 2014. Complexity is costly: a meta-analysis of parametric and non-parametric methods for short-term population forecasting. *Oikos*, **123**:652–661.
- Ward, E. J., J. E. Jannot, Y.-W. Lee, K. Ono, A. O. Shelton, and J. T. Thorson. 2015. Using spatiotemporal species distribution models to identify temporally evolving hotspots of species co-occurrence. *Ecological Applications*, **25**:2198–2209.
- Watson, J. T., T. E. Essington, C. E. Lennert-Cody, and M. A. Hall. 2009. Trade-Offs in the Design of Fishery Closures: Management of Silky Shark Bycatch in the Eastern Pacific Ocean Tuna Fishery. *Conservation Biology*, **23**:626–635.
- Welling, S. H., H. H. F. Refsgaard, P. B. Brockhoff, and L. H. Clemmensen. 2016. Forest Floor Visualizations of Random Forests. arXiv:1605.09196 [cs, stat]. ArXiv: 1605.09196.
- Wood, S. N. 2011. Fast stable restricted maximum likelihood and marginal likelihood estimation of semiparametric generalized linear models: Estimation of Semiparametric Generalized Linear Models. *Journal of the Royal Statistical Society: Series B (Statistical Methodology)*, **73**:3–36.
- Wood, S. N. 2017. *Generalized additive models: An introduction with R* (2nd ed.). Chapman & Hall/CRC, Boca Raton, FL.

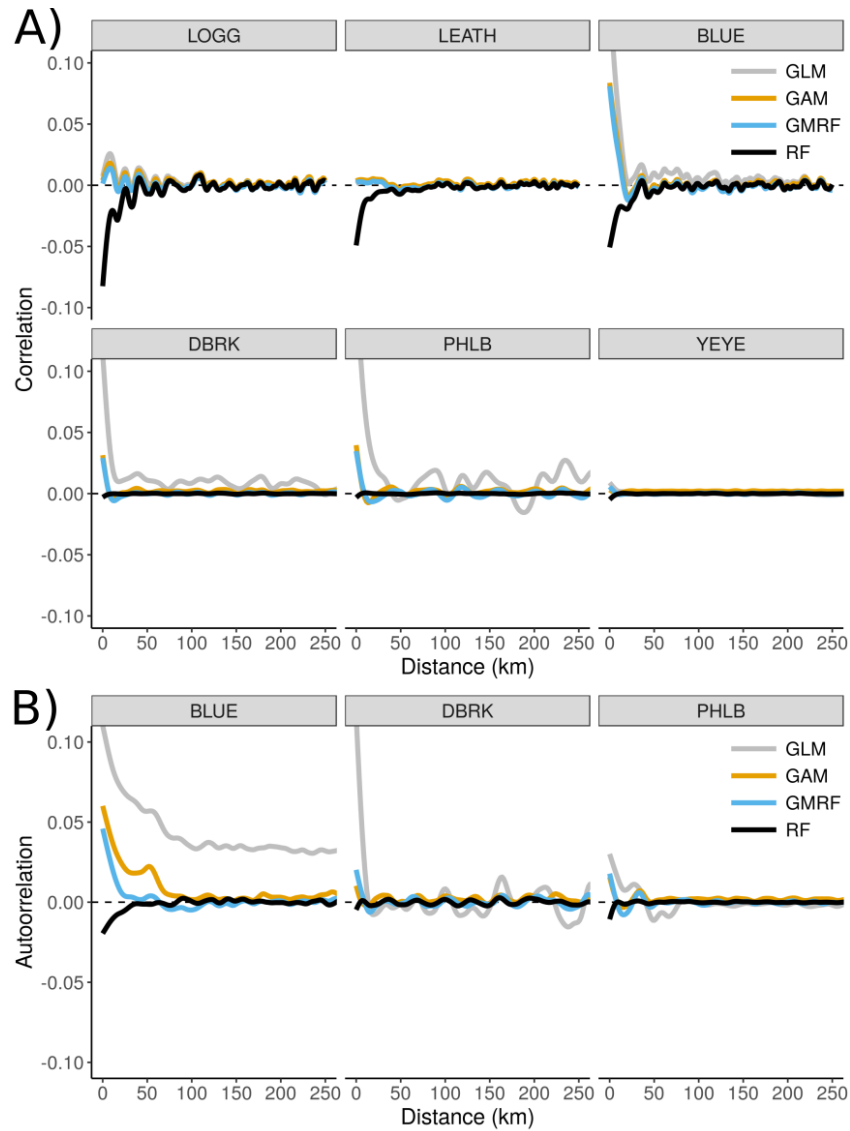


Figure A1. Spatial spline correlograms of residuals from the A) binomial and B) positive components of the delta-models. Positive and negative values indicate positive and negative spatial autocorrelation (Moran's I), and $y = 0$ is the expected value under the null hypothesis of no spatial autocorrelation. The distance where the autocorrelation intersects $y = 0$ is the decorrelation distance, which is roughly 40 km for the Hawaii longline species (blue shark = BLUE, loggerhead turtle = LOGG, and leatherback turtle = LEATH) and 5 km for the West Coast groundfish species (darkblotched rockfish = DBRK, Pacific halibut = PHLB, yelloweye rockfish = YEYE). Calculations were made by package 'ncf' v1.2-5 (Bjornstad and Falck 2001).

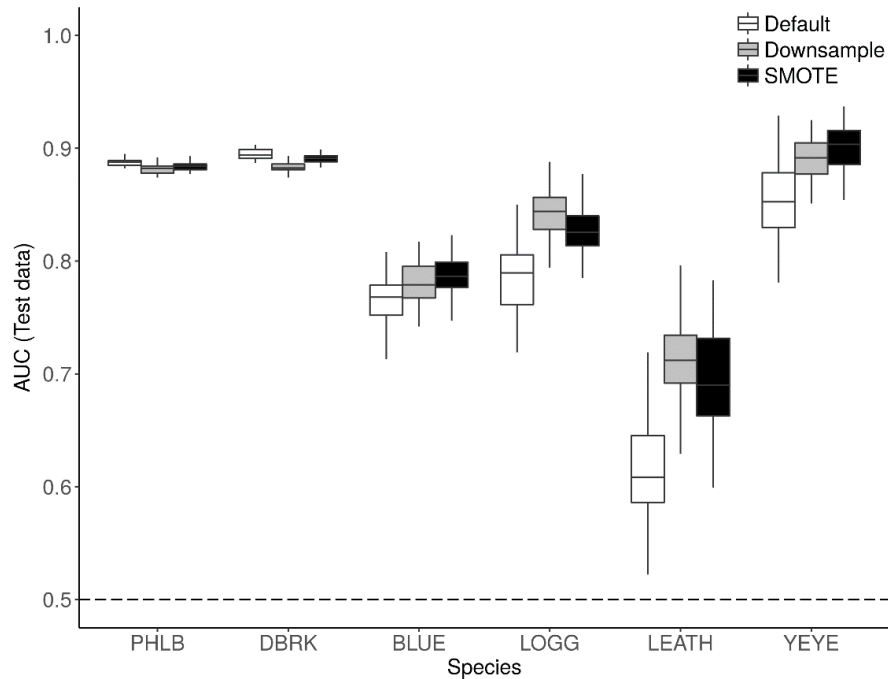


Figure A2. Binomial model predictive performance (AUC) for the three random forest (RF) algorithms for all six species. Modifications designed for data with severely imbalanced classes, downsampling and SMOTE, outperformed the default algorithm for the four species with high or low bycatch rates (BLUE, LOGG, LEATH, and YEYE). Species are sorted on the x-axis by class imbalance, i.e. PHLB has the most moderate bycatch rate (29%), and YEYE has the most extreme bycatch rate (0.3%). For blue sharks the minority class is negative (sets with zero bycatch, 3.8%). Species abbreviations: DBRK = darkblotched rockfish, PHLB = Pacific halibut, YEYE = yelloweye rockfish, LOGG = loggerhead turtle, LEATH = leatherback turtle, BLUE = blue shark.

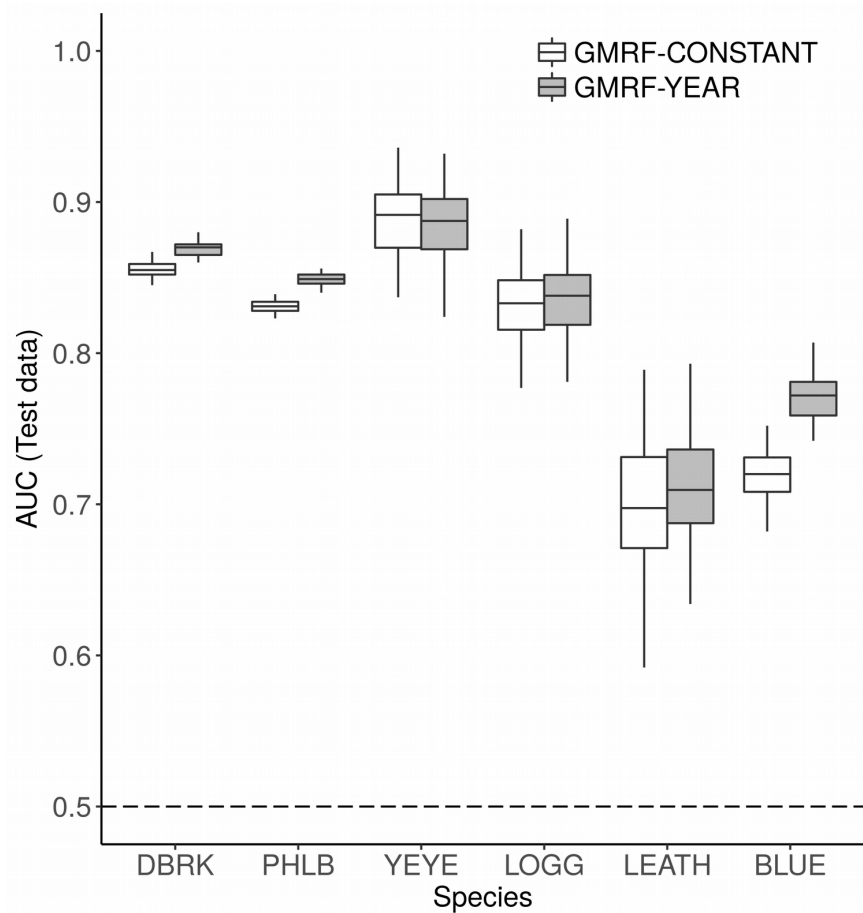


Figure A3. Binomial model predictive performance (AUC) for the two GMRF models: CONSTANT (white, one random field constant across years) and YEAR (grey, random field fit for each year). Fitting random fields for each year (GMRF-YEAR) resulted in better model performance (higher AUC) for species with moderate to high bycatch rates (DBRK, PHLB, BLUE), but nearly identical performance for species with few bycatch occurrences (YEYE, LOGG, LEATH). Species abbreviations: DBRK = darkblotched rockfish, PHLB = Pacific halibut, YEYE = yelloweye rockfish, LOGG = loggerhead turtle, LEATH = leatherback turtle, BLUE = blue shark.

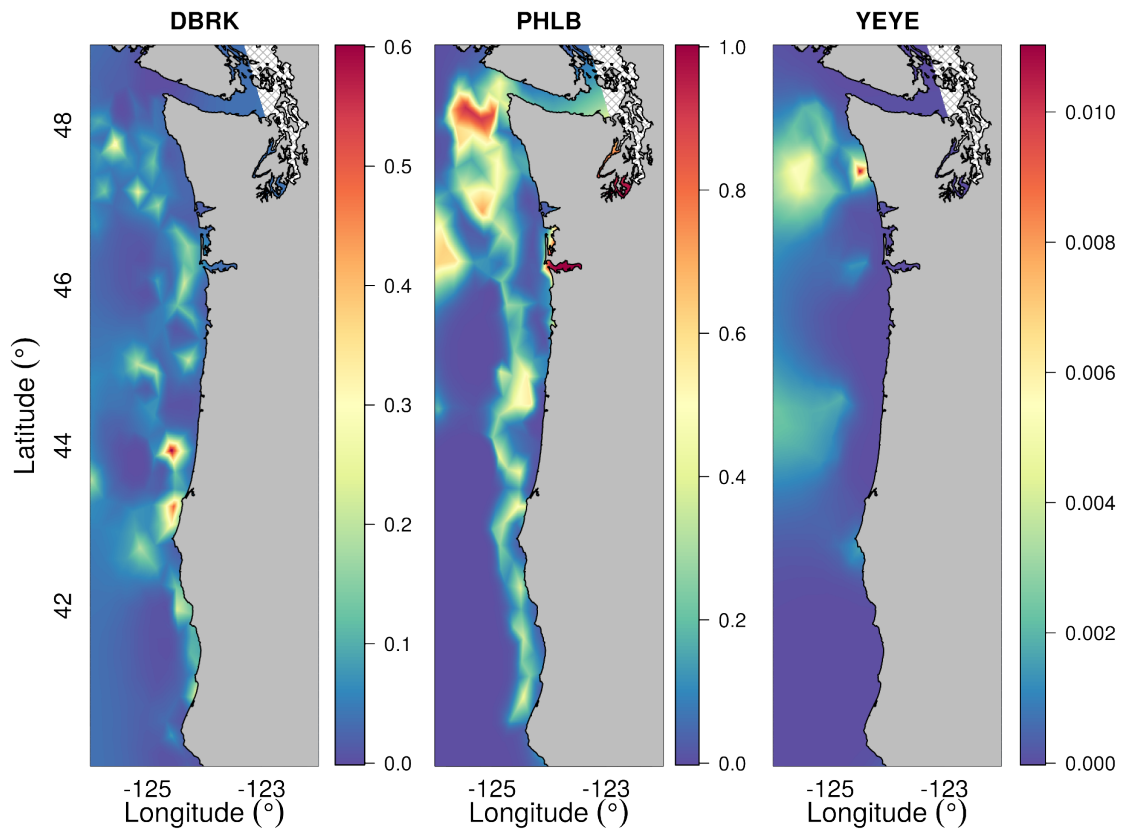


Figure A4. GMRF-CONSTANT spatial random field for bycatch probability of the three West Coast groundfish species (DBRK = darkblotched rockfish, PHLB = Pacific halibut, and YEYE = yelloweye rockfish). The GMRF-CONSTANT model estimates one spatial field constant across years from 2003-2012. Fitting a complex spatial field is less useful for species with very low bycatch rates (e.g. yelloweye rockfish, right panel, non-zero bycatch in 143 out of 42,787 tows). In these cases, simply including linear and quadratic effects of latitude and longitude could achieve nearly the same result.

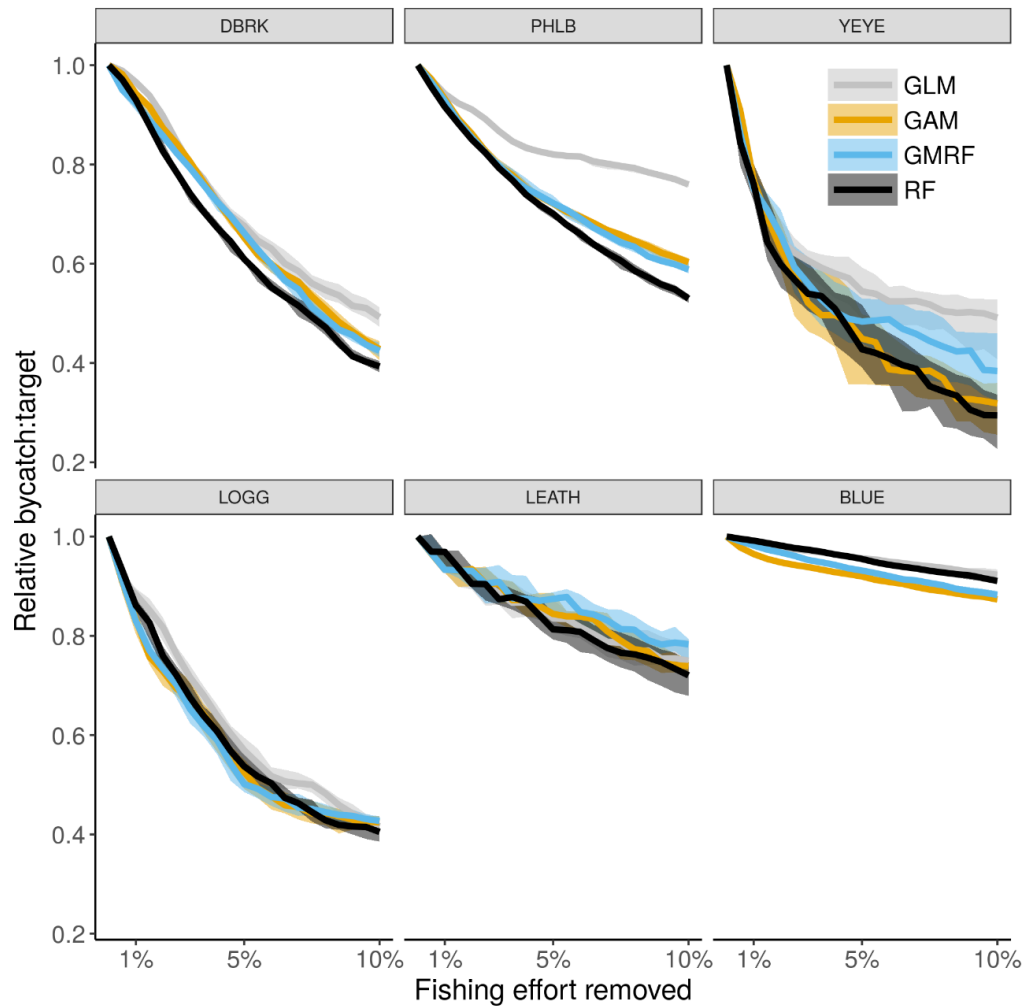


Figure A5. Bycatch-to-target ratio achieved for each species by using the binomial component of the delta model to predict fishing sets to remove in the test data, relative to 0% fishing removed. Lines show median of 50 cross-validation runs for each model class (5-fold CV repeated 10 times). Lines are noisier for species with few bycatch events (e.g. YEYE, LOGG, and LEATH). Species abbreviations: DBRK = darkblotched rockfish, PHLB = Pacific halibut, YEYE = yelloweye rockfish, LOGG = loggerhead turtle, LEATH = leatherback turtle, BLUE = blue shark.

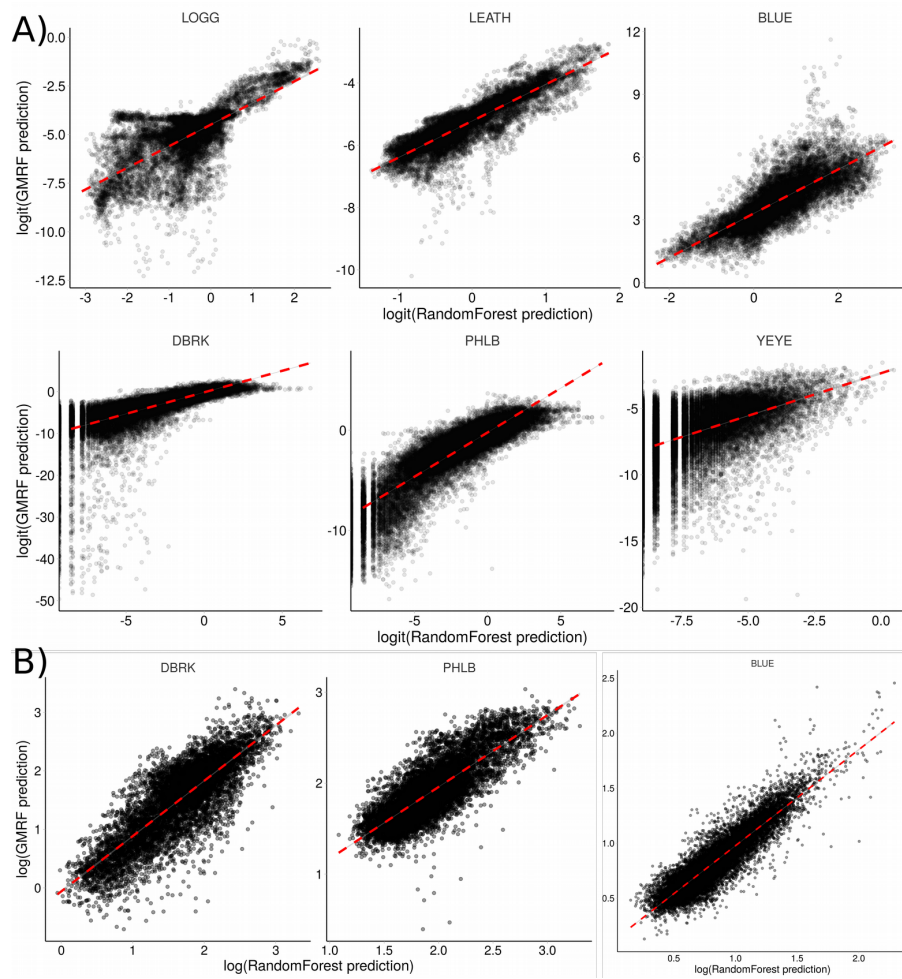


Figure A6. Correlations between predictions from GMRF and RF for the A) binomial and B) positive components of the delta-model. Each point depicts the mean out-of-sample prediction for each observation, i.e. averaged across cross-validation runs when it was in the test data. Correlations were high for all species, $r = 0.69-0.91$.

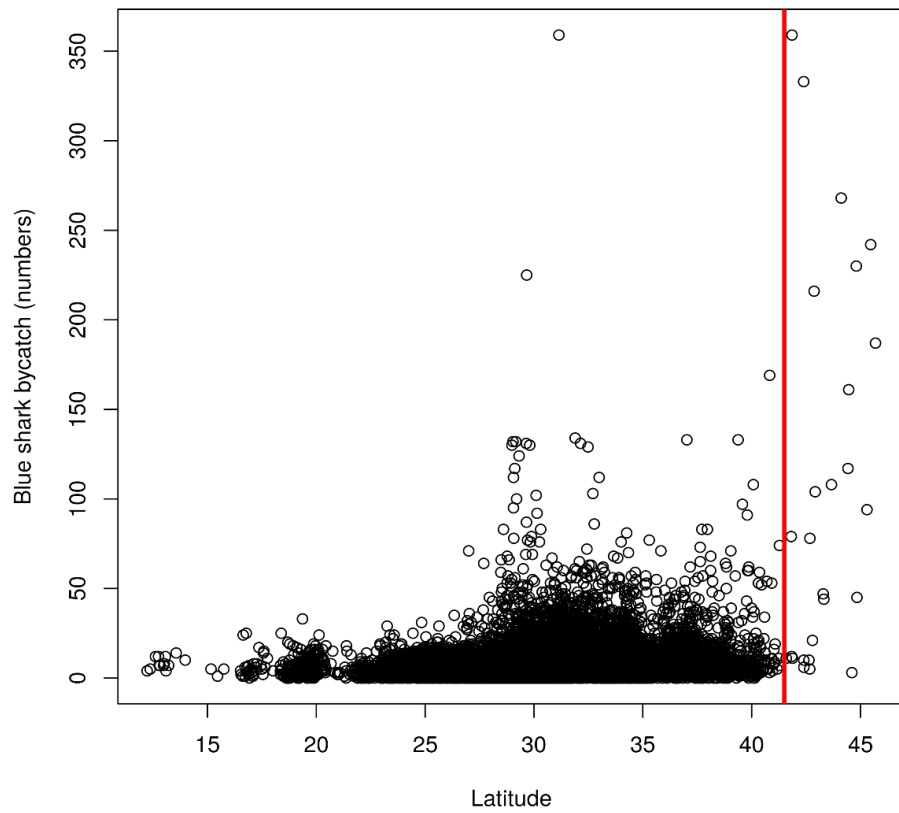


Figure A7. Distribution of blue shark bycatch by latitude. Above 41.5°N (red line), there were few observed fishing sets (26 out of 16,714 total), and these resulted in higher and more variable bycatch.

Comparing predictions of fisheries bycatch using multiple spatiotemporal species distribution model frameworks

Brian C. Stock*, Eric J. Ward, Tomoharu Eguchi, Jason E. Jannot, James T. Thorson, Blake E. Feist, and Brice X. Semmens

*b1stock@ucsd.edu

Supplementary Figures S1-S18. Maps of model residuals for all species for the binomial and positive components of the delta-model. For each species and model, means and variances of raw residuals were calculated for each data point in out-of-sample cross-validation runs (i.e. when each data point was in the test dataset). These means and variances were then averaged within spatial bins on a hexagonal grid to protect confidentiality of fisheries observer data while still displaying spatial patterns of the residuals and their variance. Residuals were calculated as predicted – observed in order to better visualize where models were over- and under-predicting observed bycatch.

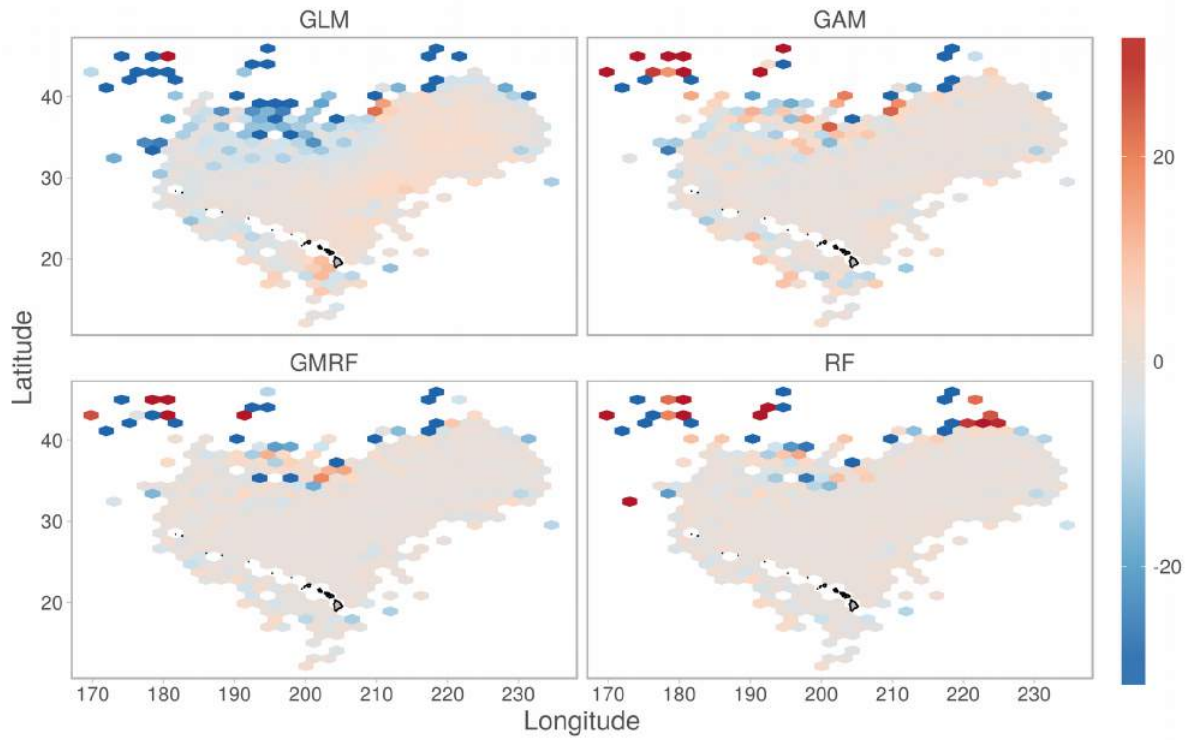


Figure S1. Blue shark positive mean. GLM exhibits significant large-scale spatial autocorrelation (negative residuals to NW, positive to SE). Residuals from all models were quite variable north of 35°N, and especially north of 40°N.

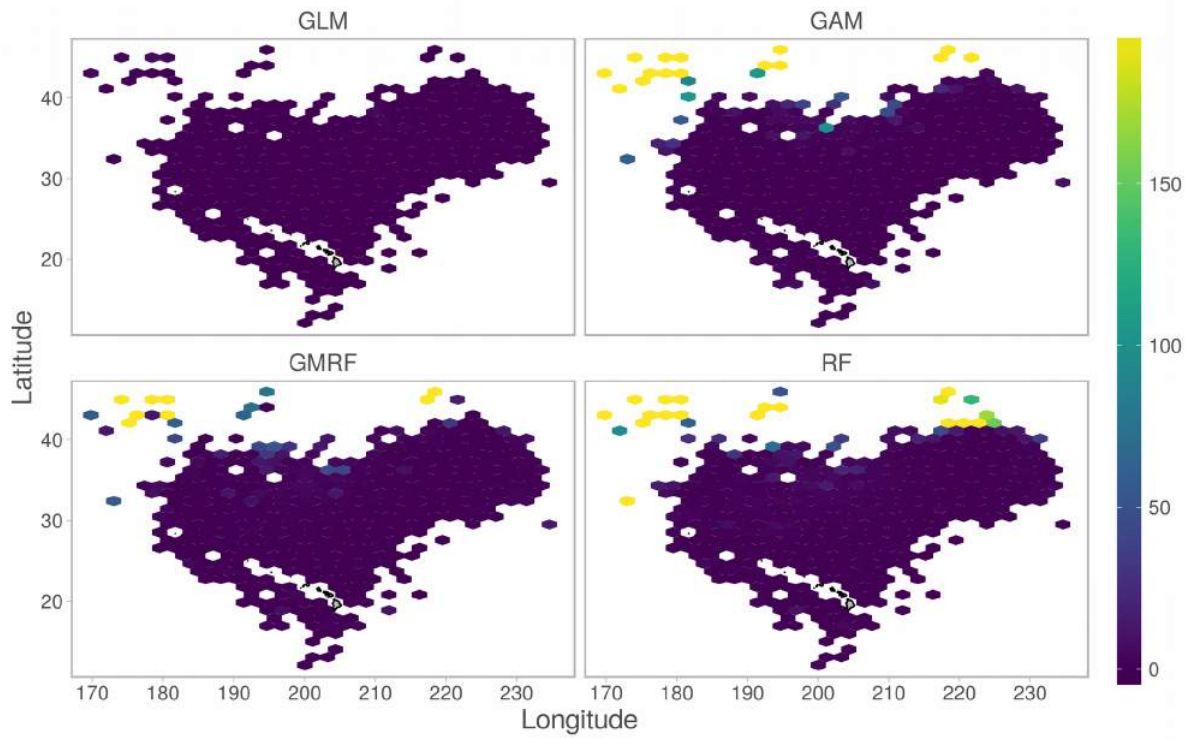


Figure S2. Blue shark positive variance. Predictions of the three spatial models (GAM, GMRF, and RF) were more variable than for the GLM north of 40°N.

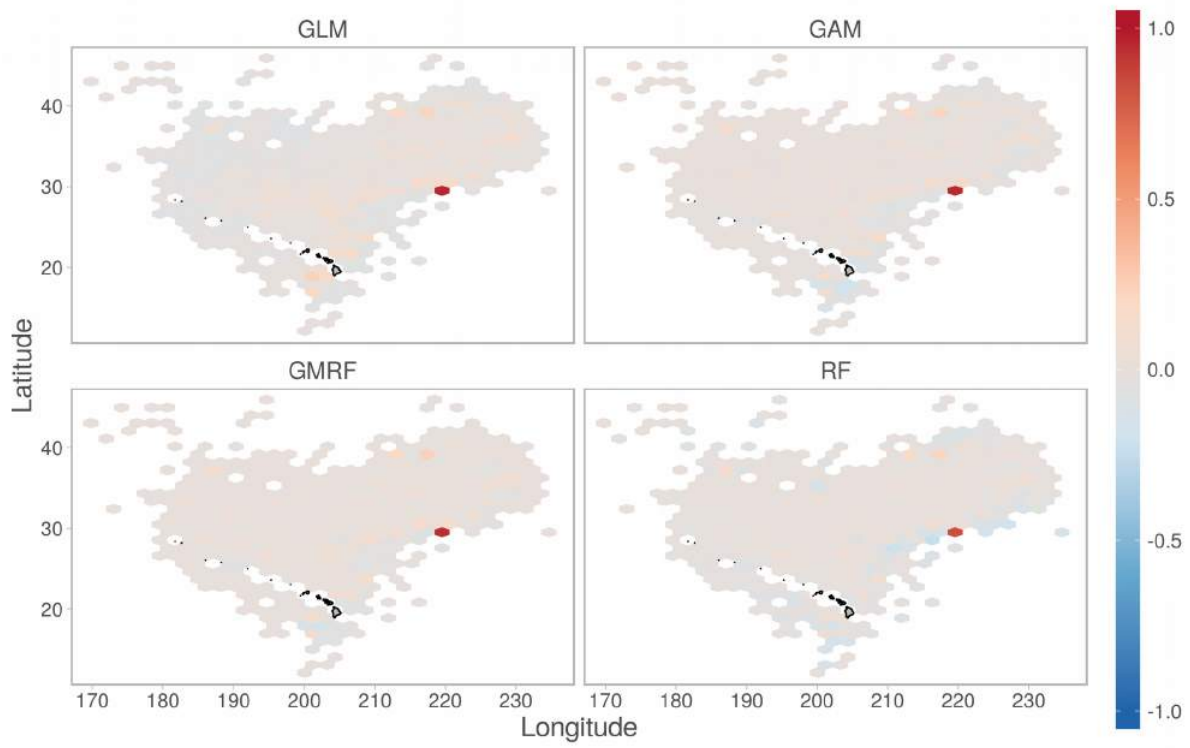


Figure S3. Blue shark binomial mean.

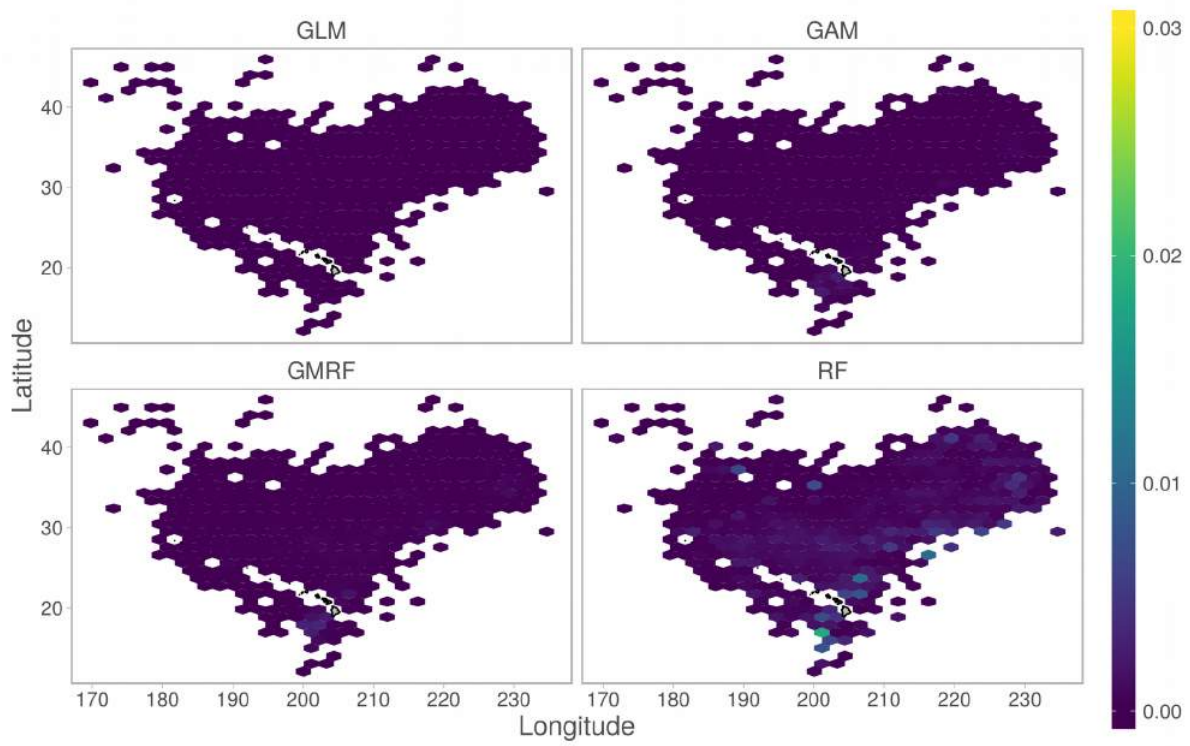


Figure S4. Blue shark binomial variance. RF predictions were more variable than the other three models throughout the fishery region.

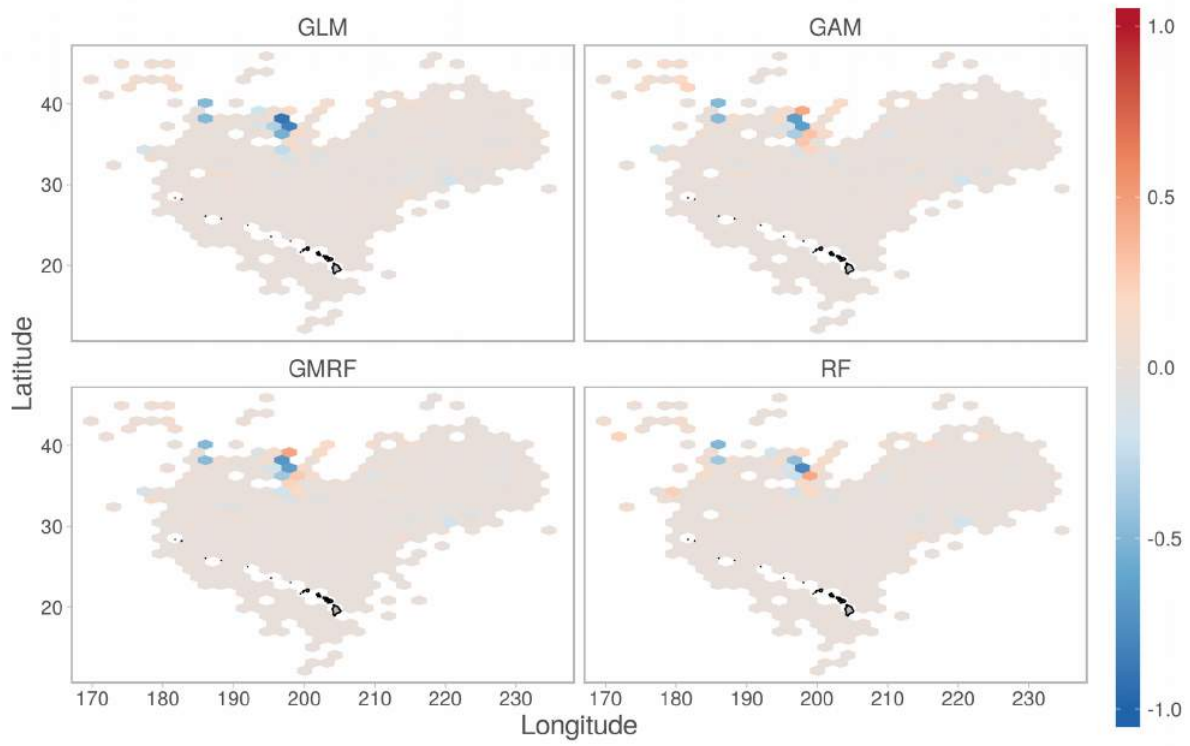


Figure S5. Loggerhead sea turtle binomial mean.

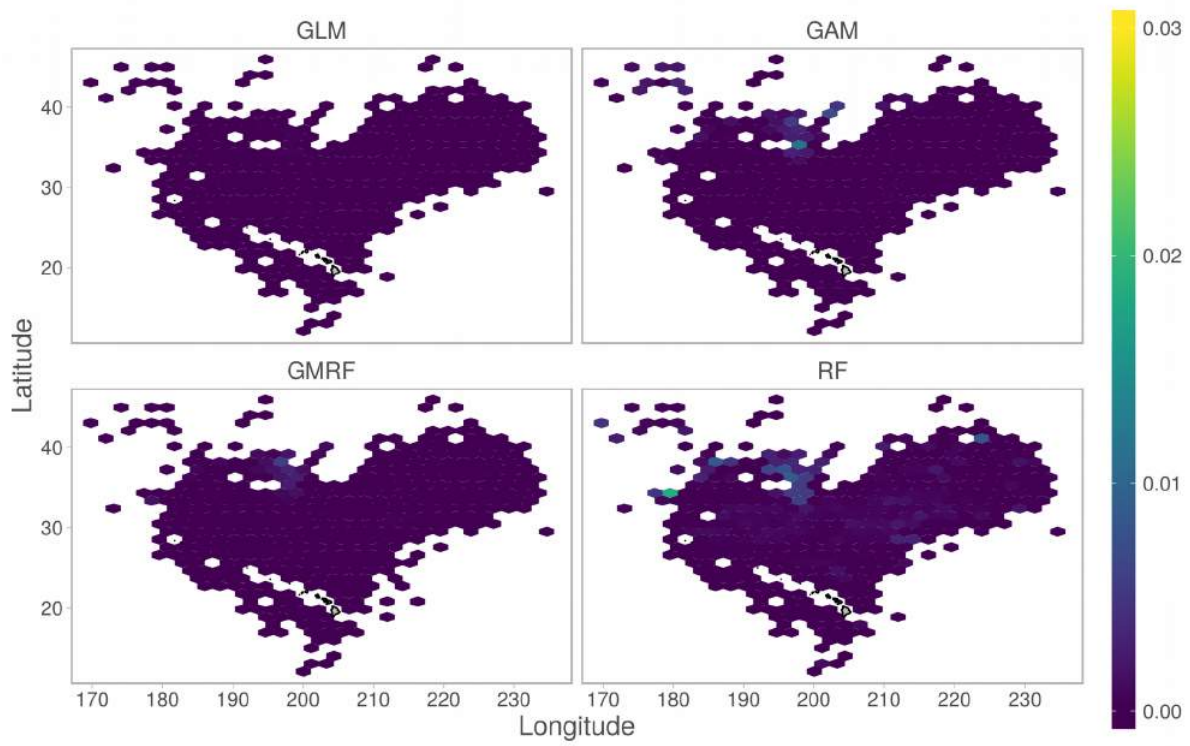


Figure S6. Loggerhead sea turtle binomial variance. RF predictions were more variable than the other three models throughout the fishery region.

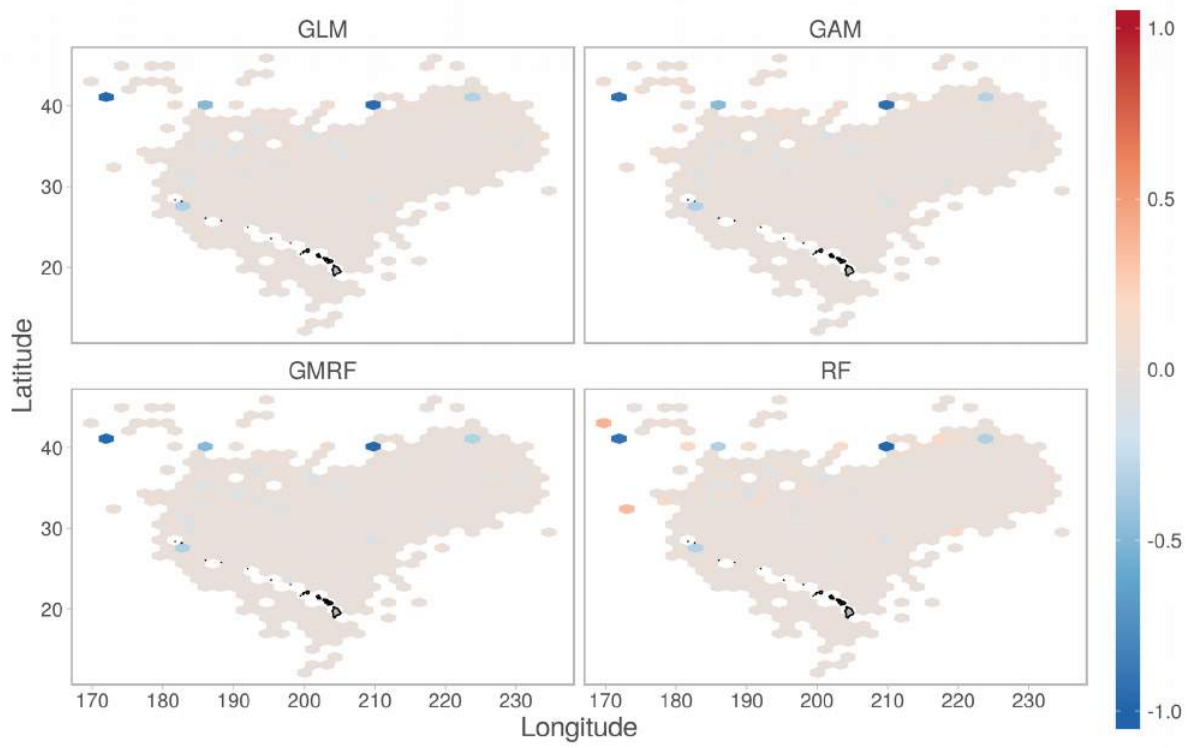


Figure S7. Leatherback sea turtle binomial mean.

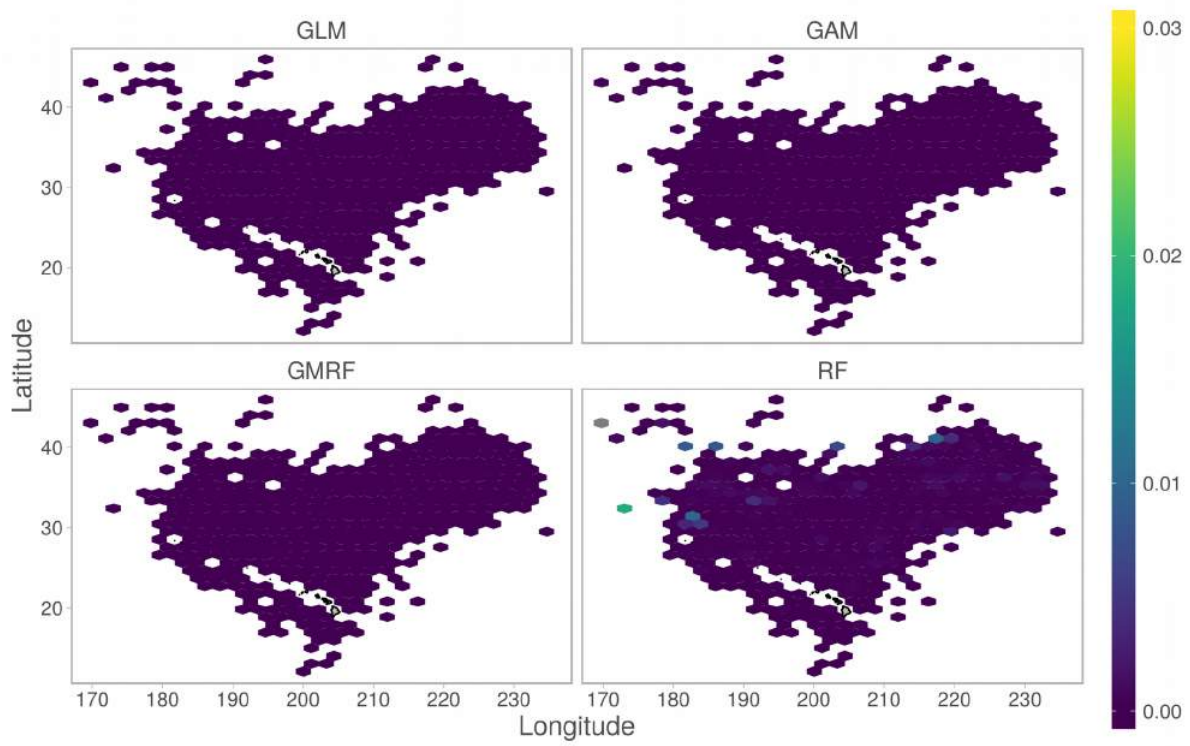


Figure S8. Leatherback sea turtle binomial variance.

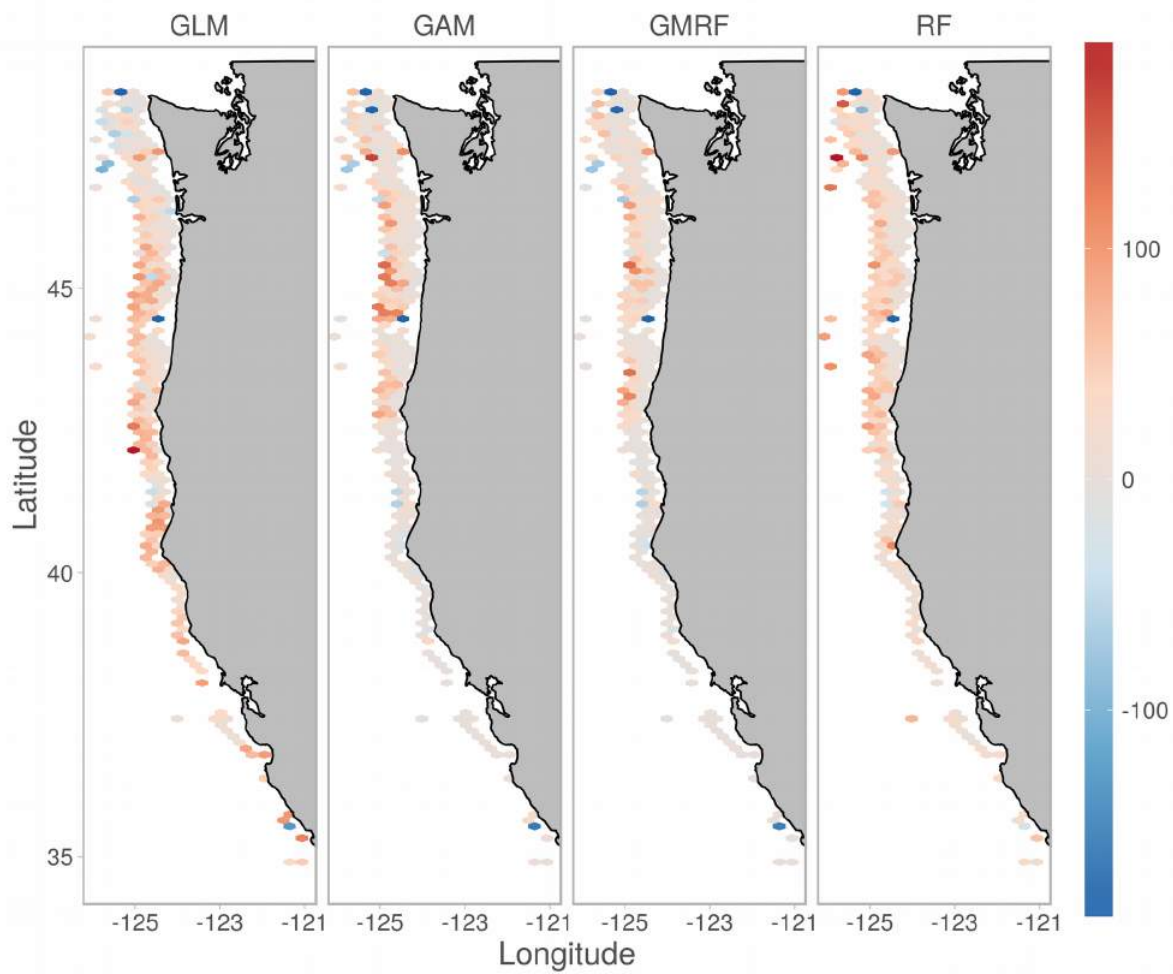


Figure S9. Darkblotched rockfish positive mean.

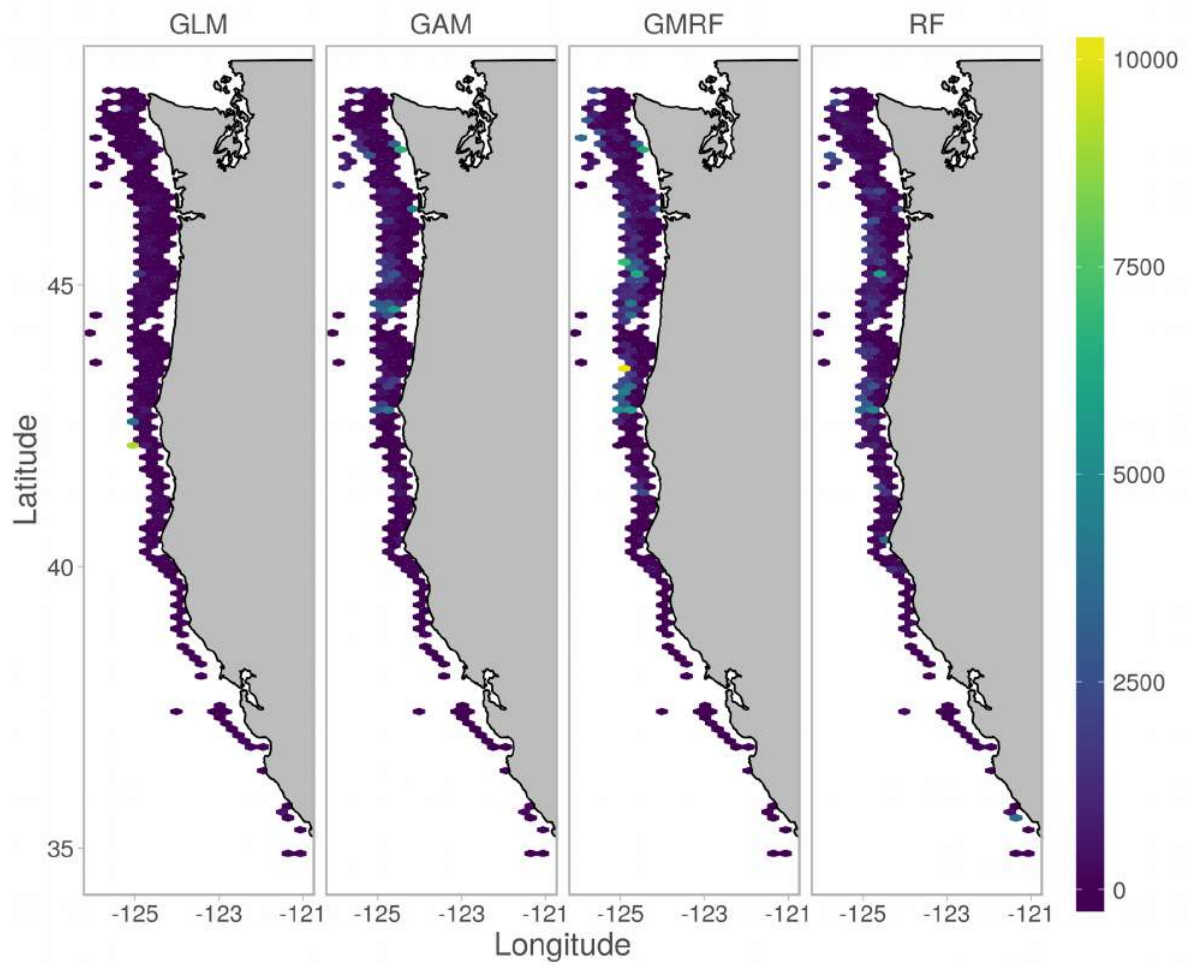


Figure S10. Darkblotched rockfish positive variance. Predictions from GAM and GMRF were more variable than from GLM and RF.

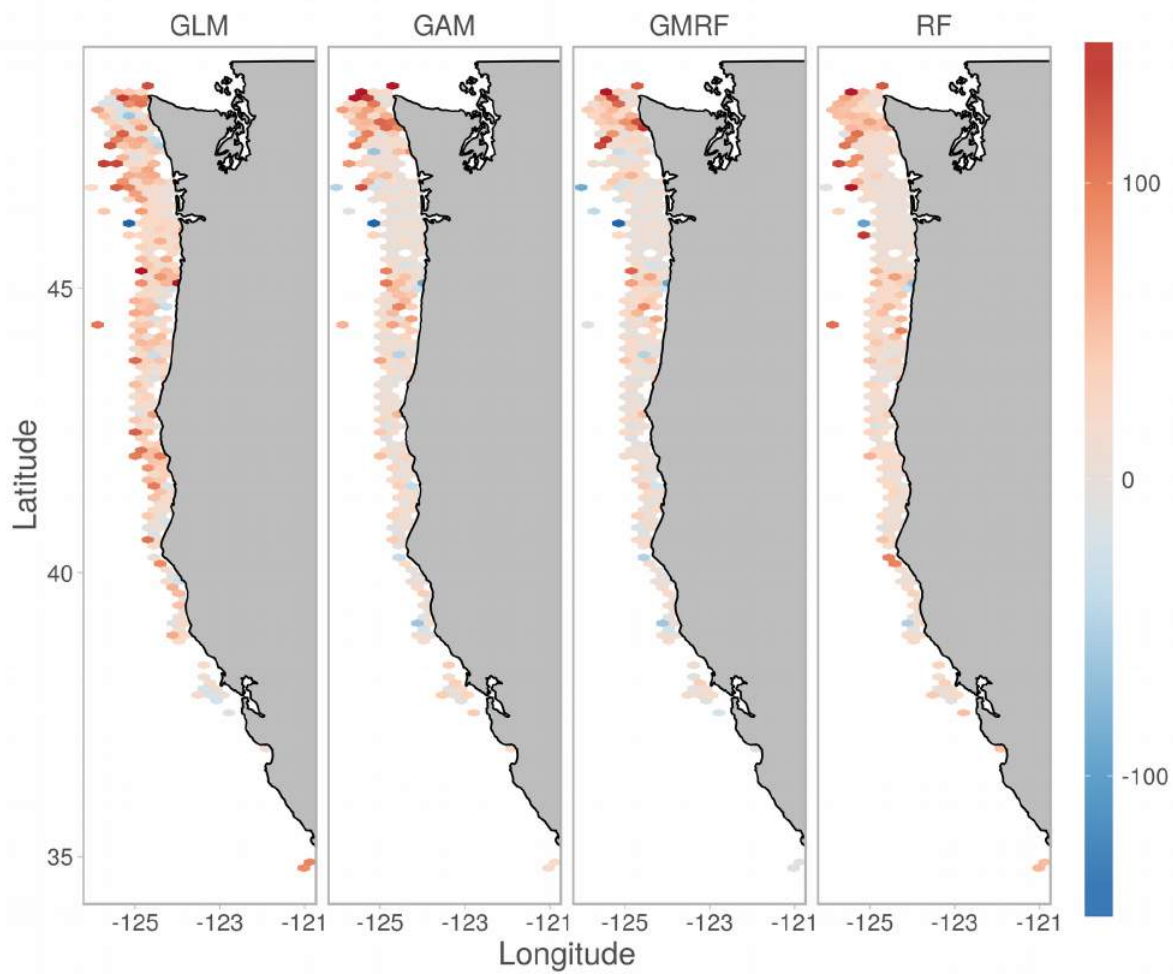


Figure S11. Pacific halibut positive mean. Residuals were highest for the GLM, followed by GAM, GMRF, and RF.

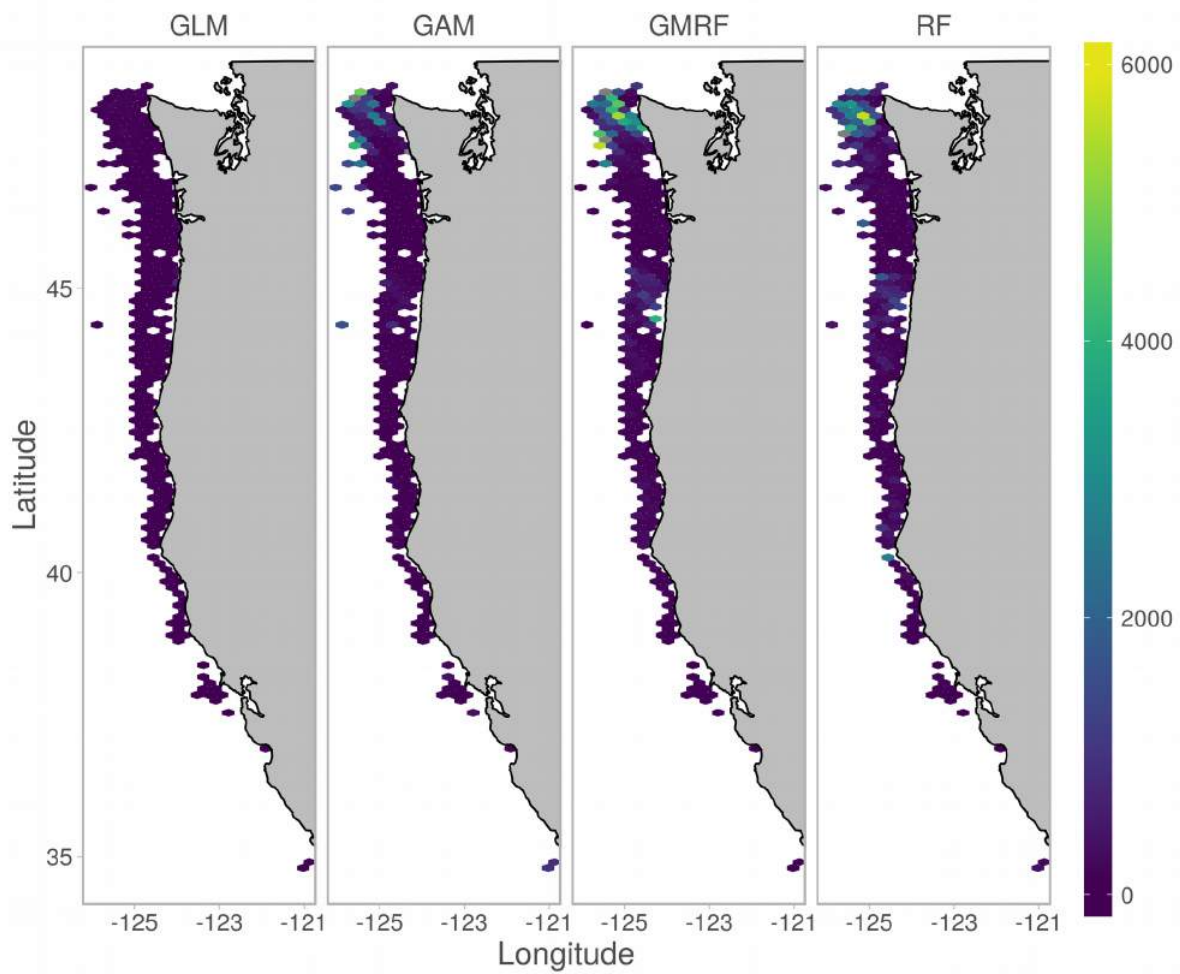


Figure S12. Pacific halibut positive variance. Predictions from GMRF and RF were more variable than for GLM and GAM. Predictions were more variable north of 47°N for all models.

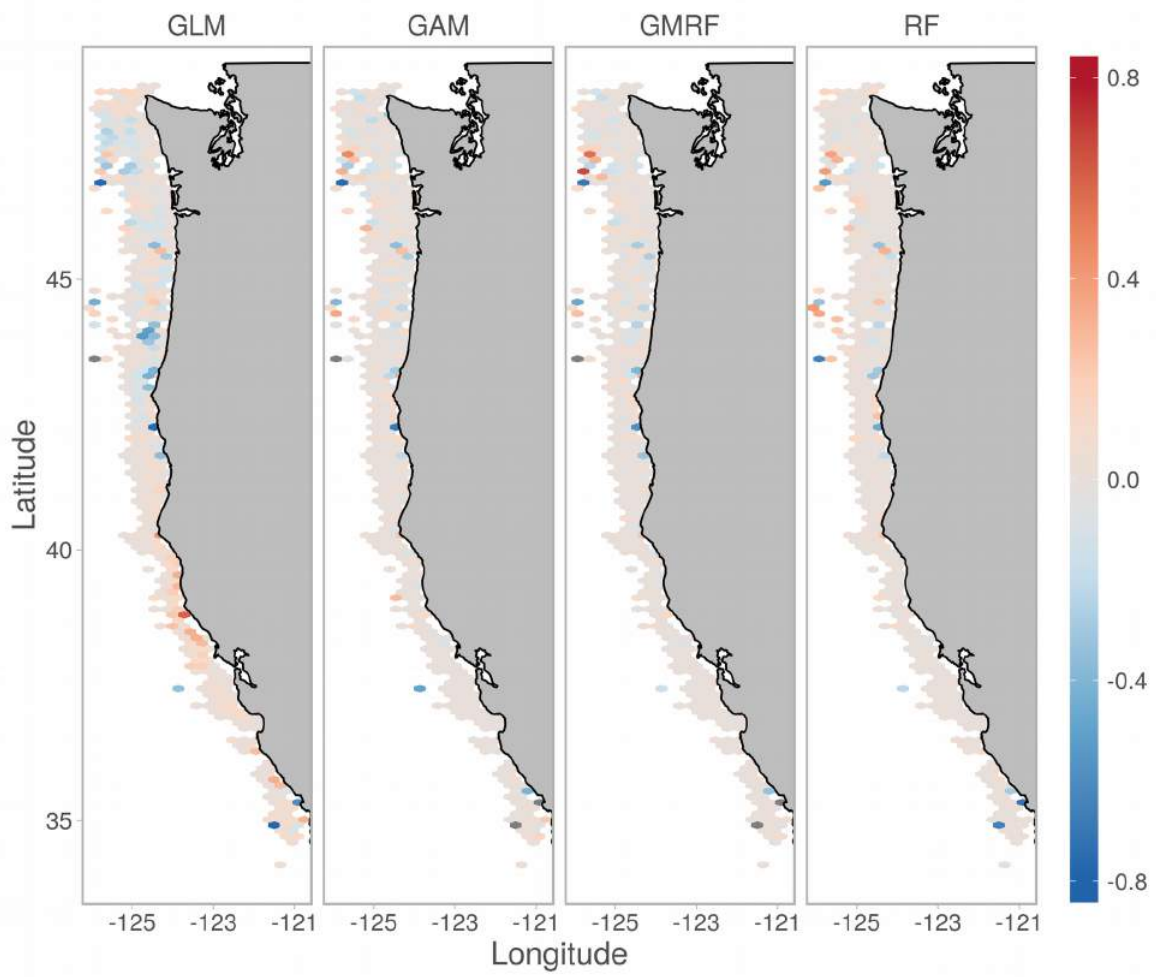


Figure S13. Darkblotched rockfish binomial mean.

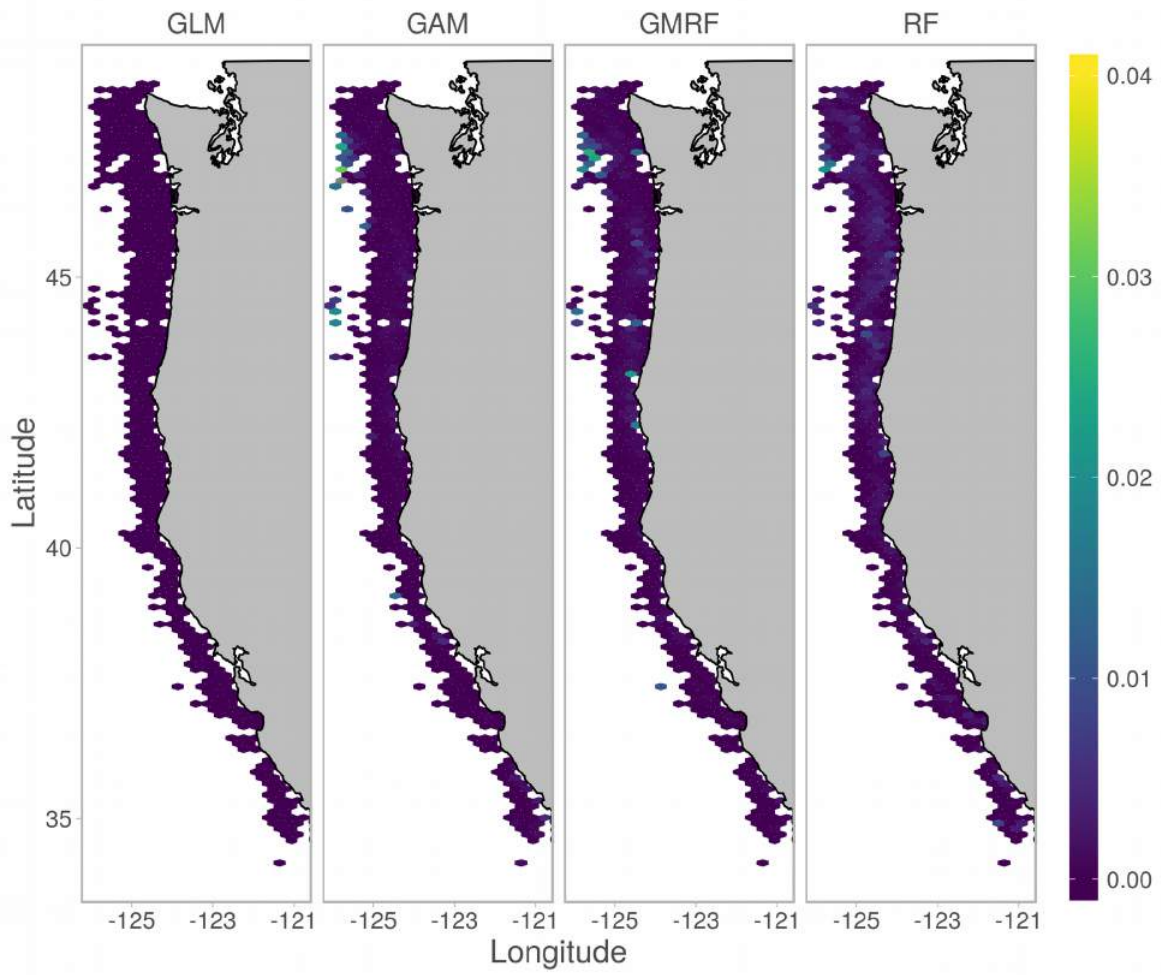


Figure S14. Darkblotched rockfish binomial variance. Predictions from GMRF and RF were more variable than for GLM and GAM.

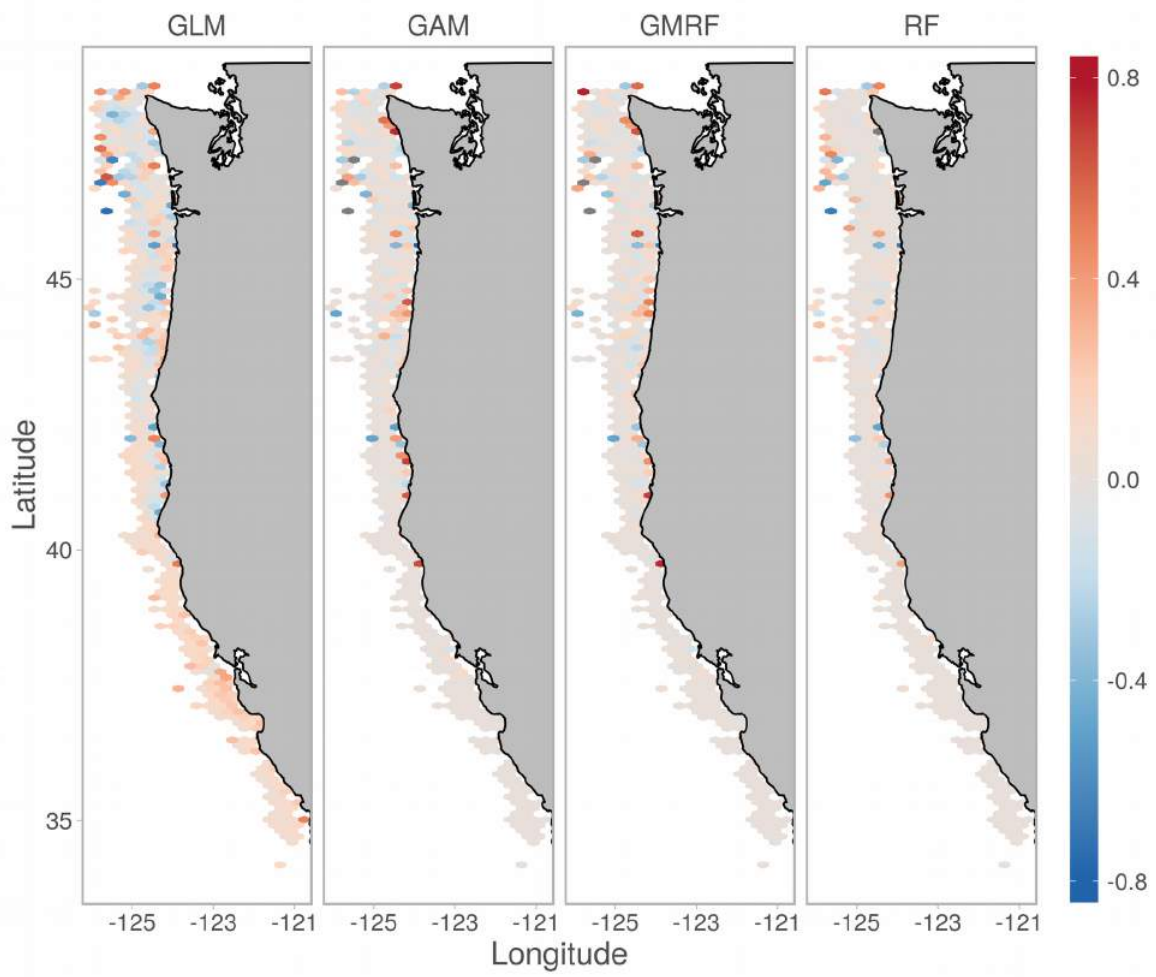


Figure S15. Pacific halibut binomial mean. Residuals were lower for RF than the other three models.

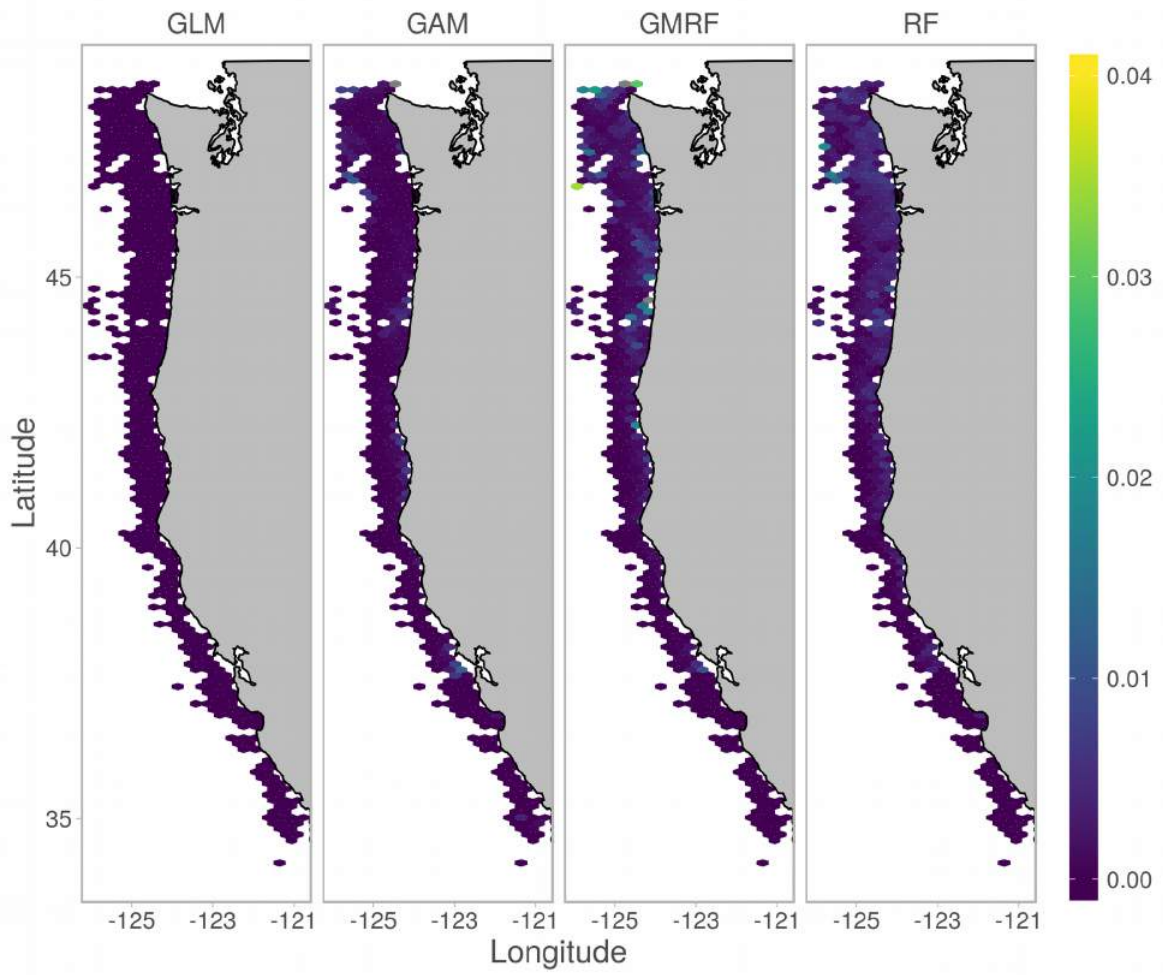


Figure S16. Pacific halibut binomial variance. Predictions from GMRF and RF were more variable than for GLM and GAM.

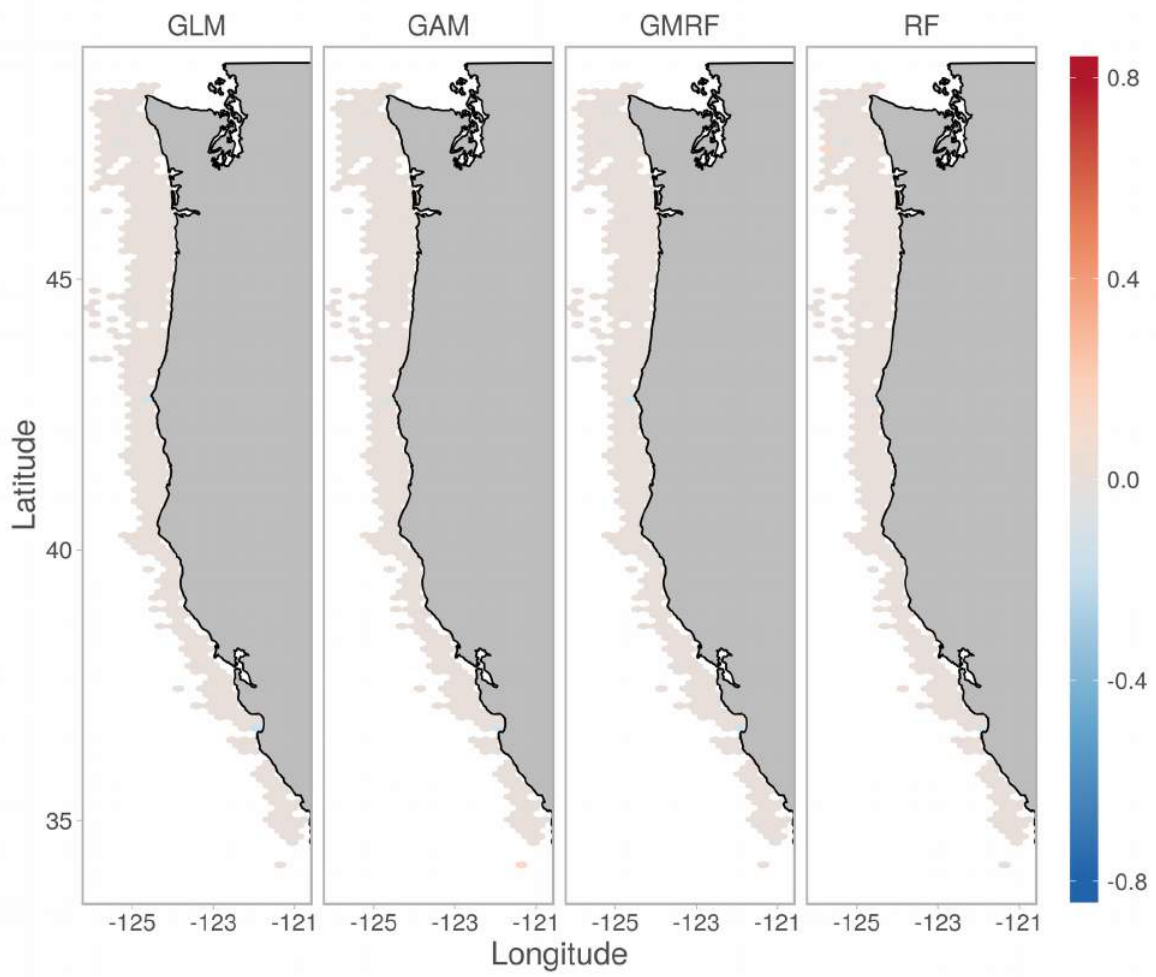


Figure S17. Yelloweye rockfish binomial mean.

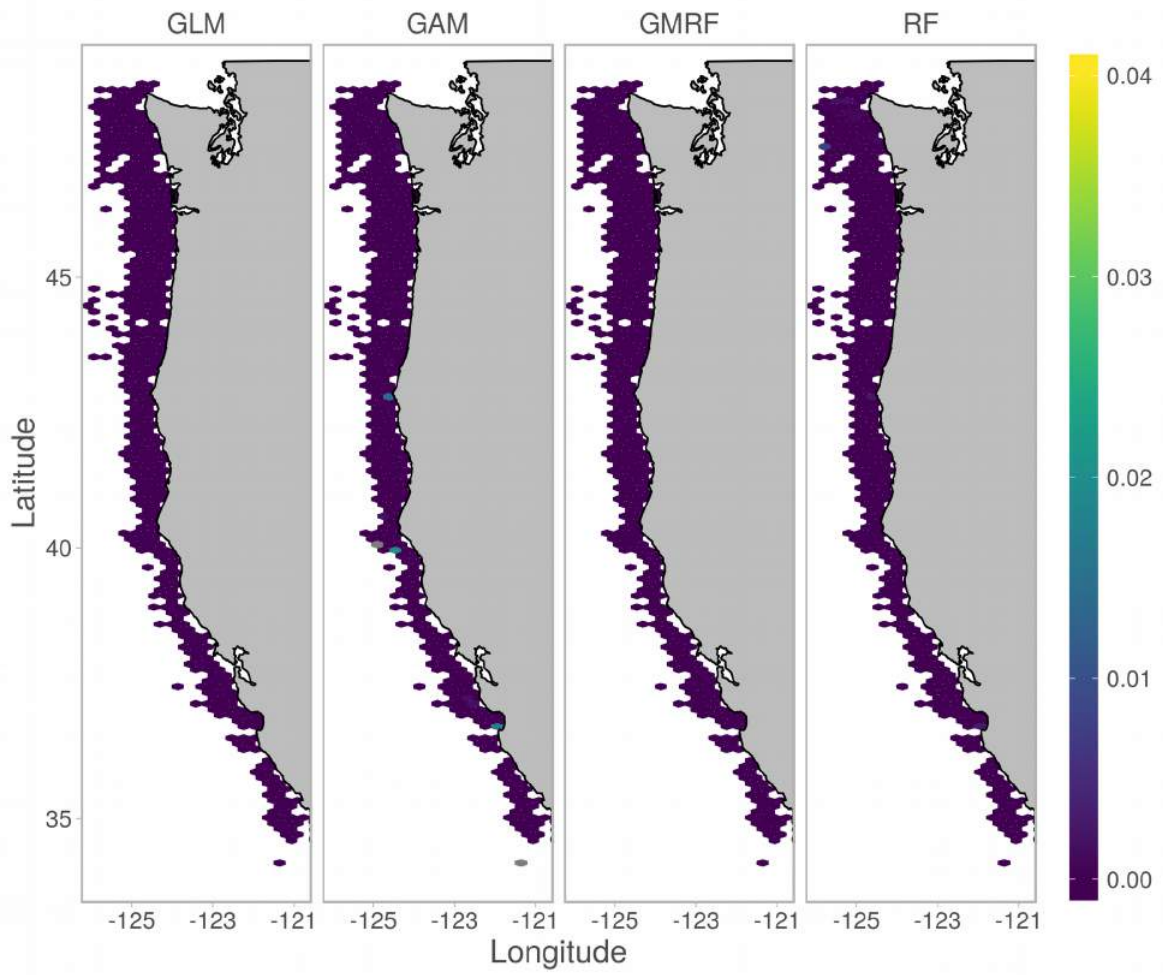


Figure S18. Yelloweye rockfish binomial variance.

Chapter 3

Assessing the response of Cayman Islands Nassau Grouper (*Epinephelus striatus*) spawning aggregations to spatial protections using *in situ* length data

Abstract

Fish species that form large, predictable fish spawning aggregations (FSAs) are especially vulnerable to overexploitation. Despite their vulnerability, quantitative assessments of FSAs are rare. The fate of Nassau Grouper (*Epinephelus striatus*) in the Caribbean is a textbook example, where overfishing has caused dramatic declines in catch and the disappearance of roughly half of the known FSAs. Responding to this risk and fishers' concerns, the Cayman Islands government protected its known and historic Nassau Grouper FSAs in 2003 and implemented a long-term monitoring program to evaluate these protections. To detect changes in size structure following protection, we collected noninvasive length distribution data using diver-operated laser calipers (video camera mounted between parallel lasers calibrated a set distance apart). Combining 15 years of such length data with an estimate of abundance (numbers of mature fish) and life history parameters, we fit a length-based assessment model to calculate recruitment and spawning stock biomass of the Little Cayman FSA through time. While the number of fish has roughly doubled (ca. 3000 to 6000), it took longer for the size structure to recover—only now, after 15 years, has the spawning biomass reached pre-exploitation levels. We also documented a large recruitment spike (7x average, 95% CI: 4.0–12.5) from 2011 spawning as a pulse of small fish in the bimodal length distributions from 2017 and 2018. A similar pulse of small fish was evident on Cayman Brac, although the Cayman Brac fish were 3–5 cm larger than those on Little Cayman. Density-dependent growth can explain 2–3 cm (35–80%) of this size difference, which suggests that there was one synchronous successful recruitment event in 2011 on both islands. Our results bear four noteworthy lessons for managers: i) spatial closures can be effective conservation measures, but expectations of population response timelines should be realistic—the Cayman Islands waited 14 years after protections to see a strong cohort of Nassau Grouper; ii) as populations recover, density-dependent growth may slow the increase in biomass and this effect should be considered; iii) appropriate SPR targets for managing spawning aggregation fisheries may need to be much higher than previous studies recommend (i.e. >0.65 instead of 0.4); iv) population size structure is important to consider

in addition to numbers, and collecting *in situ* length data is an especially effective method for monitoring protected fish spawning aggregations.

3.1 Introduction

Traditional fisheries management based on stock assessments and biological reference points is effective for many fish populations (stocks). Because of this, the majority of assessed stocks are either above sustainable levels or are currently exploited at rates that should allow them to rebuild (Beddington et al., 2007; Worm et al., 2009). On the other hand, overfishing has caused many species to decline to the point where they are threatened or endangered with extinction (Jackson et al., 2001). Not all fish species are equally at risk, however. Vulnerability to overfishing is commonly divided into two components—productivity and susceptibility (Hobday et al., 2011; Stobutzki et al., 2001, 2002; Hordyk and Carruthers, 2018). Species with life history traits associated with low productivity are more vulnerable to overfishing (e.g. long-lived, late maturity, slow growth, low fecundity, high trophic level; Hobday et al., 2011; Patrick et al., 2010). Species that are more susceptible to overfishing are also at higher risk (e.g. easier to catch, exhibit aggregating behavior, more economically desirable, not assessed or well-managed; Patrick et al., 2010). Large-bodied reef fish that form fish spawning aggregations (FSAs), such as grouper (Epinephelidae) and snapper (Lutjanidae), exhibit many of these characteristics. As such, they are particularly vulnerable to overfishing and ought to be harvested only with precautionary, or even “data-less”, management (Sadovy and Domeier, 2005; Johannes, 1998).

Aggregating reef fish are not only easily overfished, they are prone to collapse because they are hyperstable. When large numbers of fish aggregate predictably, fishers’ catch-per-unit-effort (CPUE) can remain high even as abundance declines (Hilborn and Walters, 1992). Thus, using CPUE data as an index of abundance in assessments can be misleading (Rose and Kulka, 1999; Robinson et al., 2015). While fishery-dependent CPUE data have issues relating to hyperstability, fishery-independent data via underwater visual censuses are also difficult to gather effectively (Sadovy and Domeier, 2005). Counts of fish at FSAs can vary for a variety of reasons: visibility and fish behavior can change the probability of detection, the number of fish present can change daily over the spawning season, and the area occupied by the FSA can shift within a day, between

days, and year-to-year (Sadovy de Mitcheson, 2016). Aggregation spawning may also lead to Allee effects, i.e. lower reproductive success at low population sizes, which requires many years of stock–recruit data to detect and complicates assessment modeling (Allee, 1931; Sadovy de Mitcheson and Erisman, 2012; Chen et al., 2002; Liermann and Hilborn, 2001). Furthermore, aggregation fisheries are often small-scale, found in tropical developing countries, and lack basic biological data necessary for classical stock assessments (e.g. stock structure, movement, age-length and length-weight relationships, sex ratios, and fecundity; Sadovy de Mitcheson and Colin, 2012a). Taken together, these factors begin to explain why quantitative assessments of aggregating species are rare, and highlight the urgent need for cost-effective assessment methodologies (Grüss et al., 2014; Sherman et al., 2016).

Spatial closures, or marine protected areas (MPAs), are a complementary fisheries management tool to biological reference points (Beddington et al., 2007). While the wisdom of using MPAs to control fishing mortality in general is debatable (Sala and Giakoumi, 2018b,a; Hilborn, 2018a,b; Pendleton et al., 2018), MPAs are particularly attractive to protect large, transient spawning aggregations because fishing can be extremely intense over very small spatial and temporal scales (e.g. 100s of meters, 1s of days; Russell et al., 2012). Oftentimes, a temporal ban during spawning season may actually be far easier to enforce, since this prevents situations where catch can be claimed legal simply by leaving the spawning grounds. Although many spatiotemporal closures have been implemented to conserve FSAs, in most cases populations have continued to decline or their status is unknown (Table 11.1 in Russell et al., 2012, 2014). This may be due to significant fishing pressure continuing outside spawning season, or to the difficulty of simultaneously achieving the necessary community buy-in, effective enforcement, and long-term monitoring. Well-documented cases of FSA population increases following spatiotemporal protection do exist, but are uncommon (Russ and Alcalá, 2004; Nemeth, 2005a; Luckhurst and Trott, 2009; Hamilton et al., 2011; Sadovy de Mitcheson and Colin, 2012b).

Understanding population dynamics processes is necessary for evaluating population re-

sponses to protection. For example, populations with a long history of exploitation may exhibit changes in growth, age and size at maturity, fecundity, and survival (Hutchings, 2005). Density-dependent growth can slow the increase in biomass of a recovering population as more individuals compete for resources. This is likely not a concern initially for a severely depleted population for two reasons: 1) density is low, and 2) large fish, responsible for more of the density-dependence, likely have been removed by fishing (Lorenzen, 2008). However, density-dependent growth may become important as a recovering population approaches carrying capacity, and this has led some to predict that MPAs may counterintuitively decrease fisheries yield (Gårdmark et al., 2006). Second, population increases are driven by successful recruitment (i.e. offspring reaching maturity and joining the spawning population), which is highly variable. Very few stock-recruitment data exist for tropical reef fish (Szuwalski et al., 2015; Porch et al., 2003), and the recruitment process remains poorly understood even for most well-studied temperate species supporting large-scale fisheries (Myers, 1998; Pepin, 2016). In addition, long-lived species are periodic strategists that can withstand long periods of recruitment failure punctuated by sporadic successes (Winemiller and Rose, 1992). For such species, decades of protection may be necessary before conservation actions yield measurable results (Jennings, 2001; Russ and Alcala, 2004; Porch et al., 2003; Hutchings, 2000).

Managers can use several metrics to assess fish population responses to protection, e.g. numbers, biomass, or size structure of adult spawners. The expected recovery timelines for each of these metrics differ, depending on life history traits, metapopulation structure, and the stochastic success of individual recruitment events (Jennings, 2001). Increases in adult numbers and biomass are fundamental expectations following FSA protections. Any initial (i.e. before the age at maturity) increases in numbers or biomass would be due to decreased fishing mortality on juveniles and already recruited cohorts (Jennings, 2001). Subsequent increases in numbers and biomass require successful recruitment events. Distinguishing between biomass increases attributable to decreased fishing mortality versus recruitment requires size-frequency data collected over multiple years. For

spawning aggregations that still support fisheries, scientists can easily collect length and weight data by sampling catch. For protected FSAs, scientists can use underwater visual censuses, stereo cameras, or laser calipers to obtain length measurements (Colin, 2012a; Heppell et al., 2012). Mean size of fish at FSAs is expected to increase following protections, and most length-based analyses of FSA responses to protections stop there (e.g. Beets and Friedlander, 1999; Nemeth, 2005b; Luckhurst and Trott, 2009). However, length-frequency data collected over many years and across sites contains more information, however, and may allow density-dependent growth (differences by site) or recruitment events (differences by year) to be detected (Heppell et al., 2012).

Spawning potential ratio, or spawning biomass per recruit (SPR), is another commonly used metric of population status and measures the reduction in reproductive potential due to fishing as $SPR = (\text{egg production with fishing}) / (\text{egg production without fishing})$ (Goodyear, 1993; Walters and Martell, 2004). By definition, SPR ranges from 0 to 1, and in the absence of stock–recruitment data many fisheries are managed using SPR between 0.3 and 0.4 as a target reference point (Clark, 1993, 2002; Mace, 1994; Restrepo et al., 1998). However, the appropriate SPR for a given stock depends on its productivity, the slope of the stock–recruit curve at low stock size. Therefore, less productive stocks such as rockfish (*Sebastes* spp.) and sharks (*Carcharhinus* spp.) may require higher SPR in the range 0.5–0.85 (Restrepo et al., 1998; Brooks et al., 2010; Clark, 2002). Hordyk et al. (2015a,b) showed that SPR could be calculated from life history parameters and length-frequency data under the assumptions of knife-edge selectivity and maturity, and Hordyk et al. (2016) extended their work to cases where selectivity is size-dependent. The length-based SPR (LBSPR) assessment model they developed is a promising method for populations with limited monitoring data.

The LBSPR model, however, has a number of limitations that may warrant caution when applying it to aggregating species. First, the LBSPR model and SPR guidelines are derived from Beverton-Holt or Ricker stock–recruit relationships that do not allow for an Allee effect (i.e. depensation, lower recruits per spawner at low stock size; Brooks et al., 2010; Hordyk et al., 2015b).

Spawning aggregation behavior may be an strong Allee effect mechanism, whereby FSAs no longer form at population sizes (or densities) below a threshold and few, if any, recruits are produced (Courchamp et al., 2008; Sadovy de Mitcheson, 2016). Second, recruitment of pelagically-spawning tropical reef fish that form FSAs may be highly variable and driven more by ocean currents than stock size. Third, the LBSPR model assumes the population is in equilibrium and only considers one length distribution at a time (either one year of data, or multiple years pooled). Rudd and Thorson (2018) relaxed this equilibrium assumption in their length-based integrated mixed effects (LIME) model. LIME estimates time-varying recruitment and fishing mortality in a state-space framework and can be run using only length data (as the LBSPR) or include fishery catch and an index of abundance if they exist. Despite their limitations, the LBSPR and LIME models may be well-suited for monitoring protected FSAs because all mature fish gather in high density, which enables the necessary length and maturity data to be efficiently collected.

The decline of Nassau Grouper (*Epinephelus striatus*) is a textbook example of the challenge that aggregating behavior poses to fisheries management. Nassau Grouper are large (mature adults range 50-85 cm), long-lived (at least 29 years) piscivorous reef fish found throughout the Caribbean Sea (Sadovy and Eklund, 1999). They are important predators in coral reef ecosystems, capable of causing trophic cascades and impacting reef health by regulating the biomass of their prey (Mumby et al., 2006; Stallings, 2008). Nassau Grouper form large (tens of thousands) spawning aggregations that are predictable in time and space, which makes them easily overexploited by small-scale fishermen using traps and handlines (Smith, 1972). These aggregations historically supported one of the most important finfish fisheries in the Caribbean (Sala et al., 2001), but intense aggregation fishing has driven striking population declines, leading to a Critically Endangered listing by the IUCN (Sadovy and Eklund, 1999; Sadovy et al., 2018). The United States has prohibited take and possession of Nassau Grouper since 1990 and recently listed the species as Threatened under the Endangered Species Act (NMFS, 2016). Several Caribbean governments, including Mexico, Belize, the Cayman Islands, and the Bahamas, have instituted MPAs or other protections

at known Nassau Grouper FSA sites in response to steep declines in catch. These efforts have been generally successful at reducing fishing mortality at FSA sites, but recovery has been variable and quantitative estimates of population responses—either abundance or size-frequency—are rare (Sadovy de Mitcheson and Colin, 2012*b*).

In the Cayman Islands, a UK Overseas Territory in the Caribbean Sea, Nassau Grouper historically formed five known FSAs (Fig. 3.1). Fishermen have targeted these FSAs with small boats and handlines around the full moons in January and February since the early 1900s (Bush et al., 2006). An additional FSA exists at Pickle Bank, an offshore seamount whose political jurisdiction is unclear due to the overlapping Exclusive Economic Zones of the Cayman Islands and Cuba. Responding to fishermen's concerns over declining numbers and size of Nassau Grouper, the Cayman Islands government restricted fishing these FSAs to residents and hook-and-line gear in 1985. In 1987 the Cayman Islands Department of the Environment (CIDOE) began monitoring catch-per-unit-effort and collecting biological data (length, weight, sex, and age; Bush and Ebanks-Petrie, 1994). This study produced the most complete growth curve and oldest recorded individual for the species (29 years; Bush et al., 2006; Sadovy and Eklund, 1999).

Four of the Cayman FSAs were fished out by 2000, but in 2001 local fishermen discovered a new FSA off the west end of Little Cayman Island (Bush et al., 2006). At the time of its discovery the aggregation was estimated to attract 7,000 fish (Whaylen et al., 2007). Intense fishing by local fishermen removed roughly 4,000 fish in two years (ca. 2,000 in 2001 and 1,934 in 2002; Whaylen et al., 2004). In 2003, the Cayman Islands Marine Conservation Board banned fishing on the aggregation site. Since 2003, the Grouper Moon Project, a collaboration between the CIDOE, Reef Environmental Education Foundation (REEF), and academic scientists, has published several key findings: i) acoustically-tagged adult fish on Little Cayman and Cayman Brac do not cross deep water to other islands, and all tagged fish attend the FSA on their island to spawn (Semmens et al., 2009, 2007); ii) observations of ocean currents suggest that larvae spawned at the Little Cayman FSA may self-recruit to Little Cayman, Cayman Brac, or Grand Cayman (Heppell et al., 2009, 2011;

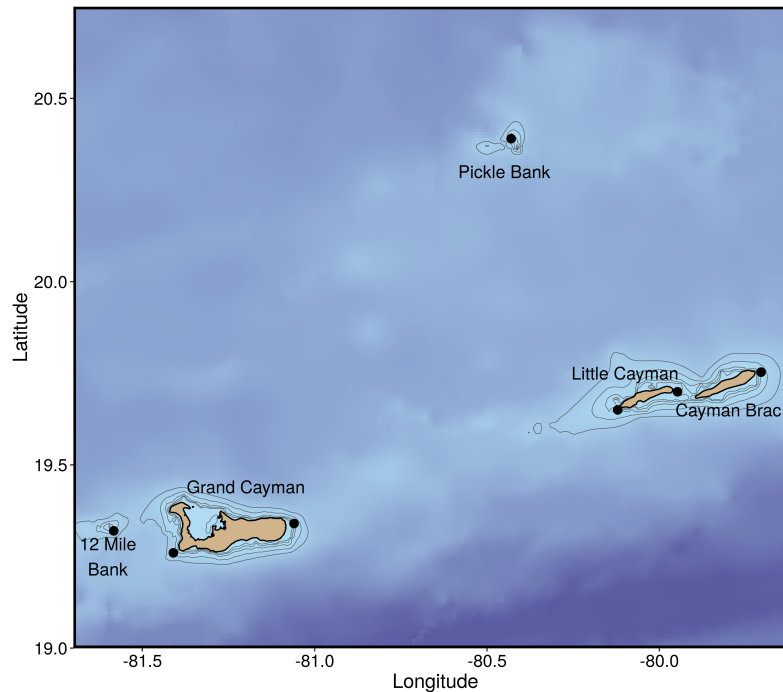


Figure 3.1: Map showing the location of historic and current Nassau Grouper spawning aggregations in the Cayman Islands. Aggregations (black points) are found either at shelf edges near reef promontories (Grand Cayman, Little Cayman, Cayman Brac) or offshore seamounts that rise to within 30 m of the surface (12 Mile Bank, Pickle Bank). The three FSAs on the east ends of Grand Cayman, Little Cayman, and Cayman Brac historically supported the fishery. The FSA off the west end of Little Cayman Island is currently the largest and the main focus of this study. Bathymetry is shown in blue with grey contour lines at 50, 100, 200, 500, and 1000 m. Adult Nassau Grouper apparently do not cross deep water between islands (>200 m).

Colin, 2012*b*; Sadovy de Mitcheson and Colin, 2012*b*); and iii) mark-recapture and length-frequency analysis indicates that numbers have increased at the Little Cayman FSA (Heppell et al., 2012; Semmens et al., 2012; Waterhouse et al., In prep). This evidence motivated continued renewal of the initial FSA fishing bans, and in 2016 protections were strengthened via comprehensive legislation (Cayman Islands Cabinet, 2016).

We present a case study of Nassau Grouper (*Epinephelus striatus*) population responses to 15 years of spatiotemporal spawning aggregation protection in the Cayman Islands. We combine fishery-independent data (15 years of *in situ* length-frequency, 14 year index of abundance) with

fishery-dependent data (age-length and length-weight relationships) into a length-based stock assessment model (Rudd and Thorson, 2018). We specifically address the following:

- i) How have population size structure and biomass changed?
- ii) How do SPR estimates compare across sites and years, and what SPR target might be appropriate?
- iii) What is the timeline of biomass recovery, and has this been affected by density-dependent growth and pulse recruitment?

3.2 Methods

In situ length frequency data

For each year from 2004 to 2018 we collected noninvasive length distribution data from the west end Little Cayman FSA using diver-operated laser calipers (video camera mounted between parallel lasers calibrated a set distance apart, Fig. 3.2), following Heppell et al. (2012). In addition to the aluminum bracket system described in Heppell et al. (2012), we created two new systems that placed two red laser diodes (Bea Lasers 160-5-650, www.bealasers.com) 20 cm apart inside a waterproof acrylic housing, with GoPro Hero™ video cameras attached in front. We aimed to collect 500–1,000 total length measurements per year because simulation studies of length-based assessment methods show a performance plateau above this sample size (Hordyk et al., 2015b; Rudd and Thorson, 2018). The number of dives and days necessary to achieve this sample size varied by year, primarily depending on dive conditions and currents. We were not able to collect large sample sizes at the FSA on the east end of Cayman Brac ($n_{2017} = 107$, $n_{2018} = 125$) because there were fewer and more dispersed fish and because the site typically has challenging boat operation and dive conditions (high seas, strong currents).

We calibrated the laser caliper systems before diving to be within 19.5–20.5 cm at a distance of 10 m. On a given dive, the operator turned on the video camera and lasers, and placed the laser

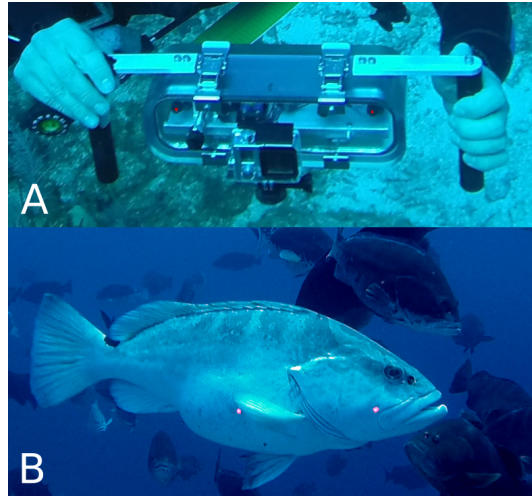


Figure 3.2: Laser caliper system used to measure fish lengths *in situ*. Two parallel laser diodes are placed 20 cm apart inside a custom-machined acrylic housing, with a GoPro Hero™ camera in separate housing mounted in front. A) A diver using the system. B) Example still-frame image with the two laser dots on a fish perpendicular to the camera. The known distance between the laser dots is used as a scale to measure total length.

points on a dive slate held perpendicularly by their dive buddy, while the dive buddy swam away until the laser points could not be seen. The operator then moved to the far end of the aggregation and swam slowly back to the starting point, placing the laser points on fish that were perpendicular to the camera for ~ 3 s per fish.

The first step to obtain length measurements from the video is to capture still frames where the laser points are on a fish, the fish is perpendicular to the camera and fully in view, and the fish is straight (tail not curved). We then opened the still frames in ImageJ software, used the measurement of the laser points on the dive slate to set the scale (pixels cm^{-1}), and measured the total length of the fish.

We estimated the measurement error of the laser caliper method by a similar analysis to Heppell et al. (2012). For two objects of known size (55.72 and 60.96 cm), we replicated the above method at 2 and 4 m distances, and increasing angles offset from perpendicular (0° , 5° , 10° , 15° , 20° , 25° , and 30°). For both distances, the measurement error was 5–7% at angles less than 10° (Fig. 3.3). Beyond 10° , measurement error increased to 10–20%. Although we did not do a formal

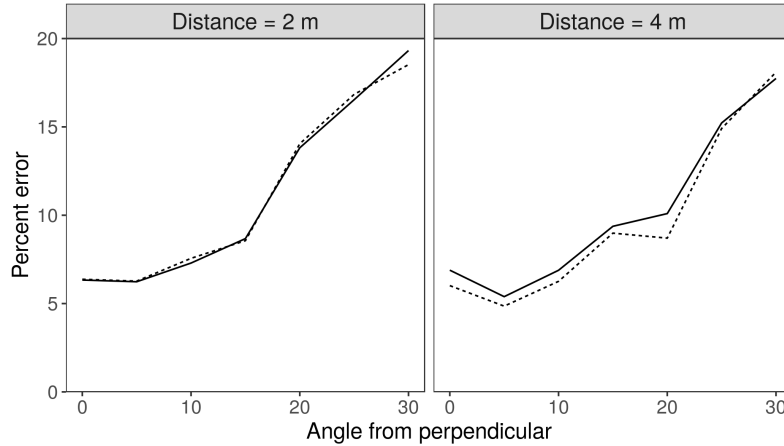


Figure 3.3: Measurement error of the laser caliper system as a function of distance-to-camera and angle offset from perpendicular. We measured two objects of known size typical of Nassau Grouper (55.72 cm, solid lines; 60.96 cm, dashed lines) at 2 and 4 m distances and 0–30° from perpendicular. Measurement error was 5–7% at angles less than 10° and increased rapidly beyond 15°.

test to determine at which angles video analysts rejected images, analysts felt they would begin to reject images at angles $>10^\circ$.

Nassau Grouper at the Little Cayman FSA typically spawn in either January or February, depending on when the full moon falls in the month (e.g. if the full moon is in late January and late February, major spawning is likely to be in January, and vice-versa). When full moons fall in the middle of the month, it is difficult to know whether major spawning will be in January or February. Thus, in some years we collected length data from both major and minor spawning months. We found no differences in length distributions between major and minor spawning months across years, and therefore pooled all data within years in subsequent analyses (Fig. 3.4).

In 2018 we used an alternative method, a stereo camera system (described in Williams et al., 2010), to collect *in situ* length measurements from the east end Cayman Brac FSA. In contrast to the laser calipers, which can only measure one fish at a time and must be diver-operated, stereo systems effectively build a 3-dimensional image from two synchronized cameras and can measure objects anywhere in their field of view. Thus, they can be used remotely (either baited or un-baited; Watson et al., 2005) and may be more efficient for monitoring FSA size structure. In order to confirm that

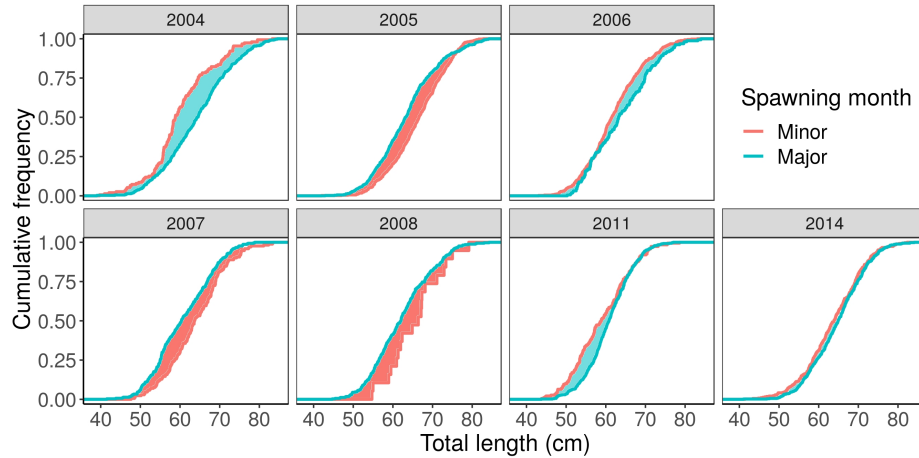


Figure 3.4: Length distributions for major versus minor spawning months. Fish lengths in major spawning months were larger in 4 out of 7 years (blue curve right of red curve; 2004, 2006, 2011, 2014), and smaller in the other 3 years (blue curve left of red curve; 2005, 2007, 2008).

the stereo camera produced comparable length measurements, we attached the laser calipers to the stereo camera for two dives and measured all fish with laser points in the stereo camera images. We found good agreement between the length measurements produced by the two systems (Fig. 3.5). Since they reconstruct 3-dimensional coordinates, stereo cameras also can estimate the distance to objects in images. These estimates confirmed that most of our distances-to-fish when using the laser calipers were between 3–4 m, and all were between 2–5 m.

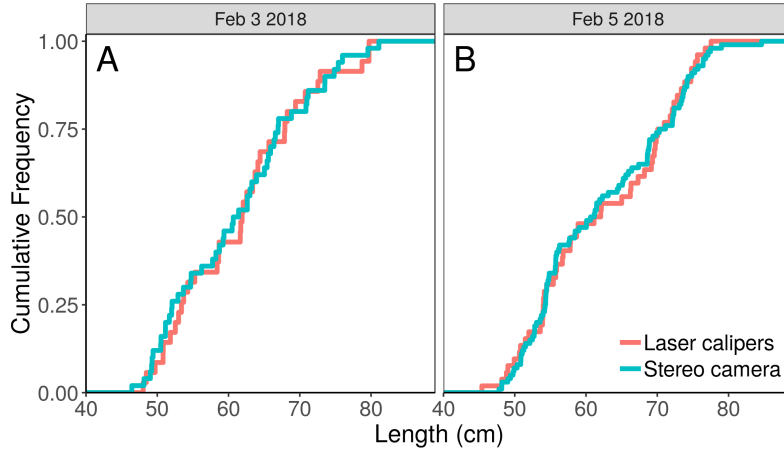


Figure 3.5: Length distributions measured from the stereo camera (blue) and laser calipers (red). On two dives the laser calipers were attached to the stereo camera and all fish with laser points in the stereo camera images were measured.

Fisheries-dependent data

We used biological data collected from the Cayman Islands Nassau Grouper FSA fishery in 1987–1995 before protections (Bush and Ebanks-Petrie, 1994; Bush et al., 2006). CIDOE recorded length, weight, sex, and age of fish caught at the three main historic FSAs on the east ends of Grand Cayman, Cayman Brac, and Little Cayman (Fig. 3.1). Following Bush and Ebanks-Petrie (1994) and Bush et al. (2006), we added one year to otolith ring counts because all fish were caught on FSAs and had "plus" growth. We also included 104 lengths of un-aged fish known to be 1.5 years old from a large recruitment event in 2012 (simulated from $\mathcal{N}(\mu = 18.4, \sigma = 3.4)$; Camp et al., 2013). We fit standard age-length (von Bertalanffy growth, $L[a] = L_{\infty}[1 - e^{-k(a-a_0)}]$) and length-weight ($W[L] = aL^b$) relationships using maximum likelihood estimation.

We estimated natural mortality, $M = 0.262 \text{ yr}^{-1}$ (95% CI: 0.14–0.38), using catch-curve analysis of length data from Pickle Bank, a sporadically exploited, offshore Nassau Grouper FSA (Fig. 3.1). We converted length data to ages using the best fit growth curve ($k = 0.191$, $L_{\infty} = 77.3$, and $a_0 = -0.01$; Fig. 3.6), and then followed the guidance of Smith et al. (2012) to use the Chapman-Robson estimator (Chapman and Robson, 1960), implemented in the 'FSA' R package

(Ogle et al., 2018). This estimate of M depends on the assumption that Pickle Bank is unexploited and will be biased upwards if this is not true, although this assumption is reasonable given the large fish observed on Pickle Bank (Fig. 3.7). The estimate $M = 0.262 \text{ yr}^{-1}$ falls within the range reported by previous catch-curve analysis for Nassau Grouper ($M = 0.17\text{--}0.30 \text{ yr}^{-1}$; Thompson and Munro, 1978) and is well below the estimate from the Pauly (1980) method ($M = 0.46$, using a conservative average annual sea surface temperature for the Cayman Islands, 27°C).

Length-based assessment

Stock assessments typically rely on three types of data to estimate stock status: i) fishery catch, ii) an index of population abundance, and iii) age- or length-composition. Assessment methods using all three data types can be classified as “data-rich”, methods with two data types as “data-moderate”, and methods with only one data type as “data-poor” (Berkson and Thorson, 2015). The Little Cayman FSA falls into the “data-moderate” category, since we have time series of length-frequency (this study) and a fishery-independent index of abundance (Waterhouse et al., In prep), as well as biological data (Sec 3.2). While CIDOIE collected catch and effort data from the FSA fishery before protection, we did not have catch data following the ban on FSA fishing from 2003–2018. Note that fishing Nassau Grouper was still legal after the FSA protections were enacted, but only outside the FSA and spawning season. We used two length-based assessment frameworks to estimate the Little Cayman population response to protection.

First, the length-based spawning potential ratio (LBSPR) model is a data-poor method that uses length-compositions to estimate spawning potential ratio (SPR), a measure of stock status relative to unfished levels (Hordyk et al., 2015*b*). Since the LBSPR model leverages length and maturity data, it is well-suited for assessing FSAs because all large, mature fish gather in high density. The LBSPR model, however, assumes the population is in equilibrium and only considers one length distribution at a time (either one year of data, or multiple years pooled). We fit the LBSPR model to FSA length-frequency data from before and after protections, using the parameters

Table 3.1: Parameters used to fit the LBSPR model.

Parameter	Description	Value	Source
L_∞	von Bertalanffy asymptotic length	77.3 cm	this study (Fig. 3.6)
k	von Bertalanffy growth coefficient	0.191 yr ⁻¹	this study (Fig. 3.6)
M	Natural mortality	0.262 yr ⁻¹	this study
L_{50}	Length at 50% maturity	47.4 cm	Sadovy and Eklund (1999)
L_{95}	Length at 95% maturity	55.7 cm	Sadovy and Eklund (1999)

Table 3.2: Parameters used to fit the LIME model.

Parameter	Description	Value	Source
L_∞	von Bertalanffy asymptotic length	varied	this study (Fig. 3.10)
k	von Bertalanffy growth coefficient	varied	this study, (Fig. 3.10)
M	Natural mortality	varied	this study
L_{50}	Length at 50% maturity	47.4 cm	Sadovy and Eklund (1999)
L_{95}	Length at 95% maturity	55.7 cm	Sadovy and Eklund (1999)
S_{50}	Length at 50% selectivity	47.4 cm	Sadovy and Eklund (1999)
S_{95}	Length at 95% selectivity	55.7 cm	Sadovy and Eklund (1999)
α	Length–weight scalar	3.726e-06	this study
β	Length–weight allometric	3.385	this study
σ_F	Fishing mortality process error	0.3	default
σ_I	Abundance index observation error	0.3	
σ_R	Recruitment process error	1	
CV_L	Growth curve coefficient of variation	0.06–0.08	

in Table 3.1 and the ‘LBSPR’ R package (Hordyk, 2017; Hordyk et al., 2016).

The length-based integrated mixed effects (LIME) model is similar to the LBSPR but has more data requirements and does not assume that the population is in equilibrium (Rudd and Thorson, 2018). LIME estimates time-varying recruitment and fishing mortality in a state-space framework and can be run using only length data (i.e. data-poor) or can include fishery catch and an index of abundance if they exist (i.e. data-moderate or data-rich). We fit the LIME model to 15 years of *in situ* length data and a 14-year index of abundance (numbers of mature fish, Waterhouse et al., In prep) from the Little Cayman FSA, using the parameters in Table 3.2 and the ‘LIME’ R package (Rudd, 2018).

To account for uncertainty in life history parameters (M , k , and L_∞), we fit LIME using 53

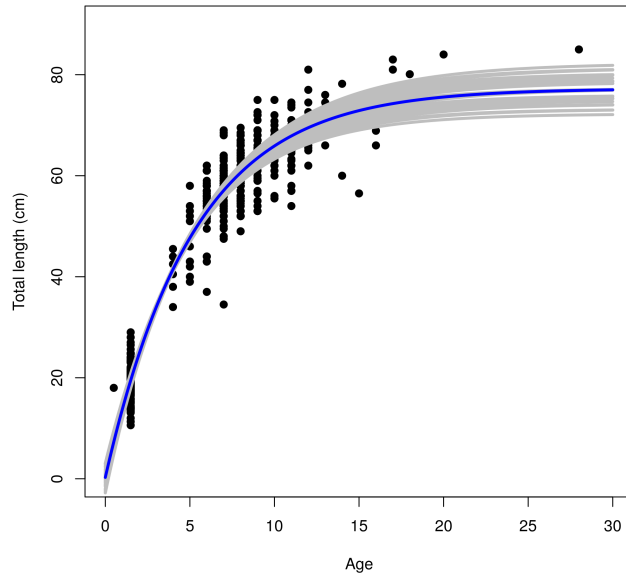


Figure 3.6: Range of growth parameters used to fit the length-based assessment model. Growth curves defined by each parameter set (grey lines) are plotted on top of the data (black points). The maximum likelihood estimates from the best growth curve fit were $k = 0.191$ and $L_{\infty} = 77.3$ (blue).

different parameter sets (Figs. 3.6 and 3.10). The parameter grid was centered on the maximum likelihood estimates (MLE) from the growth curve fit ($k = 0.191$, $L_{\infty} = 77.3$) and estimated $M = 0.262 \text{ yr}^{-1}$ from the catch-curve analysis. Nodes in the grid were generated using the covariance matrix from the R package ‘FishLife’ and a 2-dimensional Gauss-Hermite quadrature rule, level 5, via the R package ‘mvQuad’ (Fig. 3.10 Rudd et al., In prep; Thorson, 2017; Thorson et al., 2017; Weiser, 2016).

Density-dependent growth calculations

The 2017 and 2018 length distributions from both Little Cayman and Cayman Brac were bimodal. The differences in the smaller of the two modes between islands and years could either be explained by differences in growth or age of strong year classes. Under the assumption that the modes represented fish of the same age, we analyzed shifts in the smaller modes to evaluate

whether differences in growth stemming from density-dependence could plausibly explain the observed length distribution differences. For each year and FSA, we generated 10,000 bootstrap samples from the length data and calculated the kernel density modes for each. We calculated the growth increments for each FSA and differences between FSAs in the same year by subtracting the bootstrapped mode lengths.

To estimate density-dependent growth we needed the habitat area (ha) on each island and the biomass (kg) that would affect growth for fish spawned in 2011. For the Little Cayman FSA, we approximated biomass by multiplying the number of spawners by the weight-distribution (observed length-distribution multiplied by the length-weight relationship) for each year, and then took the mean across years 2011-2018. The number of spawners on Cayman Brac is less well-known, so we repeated the above calculation for a range of possible population sizes ($N_{Brac} = 500, 1000, \text{ and } 1500$). We calculated adult habitat area as the geographic area for depths between 5 and 50 m using high-resolution bathymetry (R packages ‘raster’ v2.8-4 and ‘sf’ v0.7-1; Hijmans, 2018; Pebesma, 2018).

Finally, we used the empirical relationship from Lorenzen and Enberg (2002) to estimate the plausible difference in growth due to different observed biomass densities of Nassau Grouper on Little Cayman and Cayman Brac. Density-dependent growth as a result of competition for food is not expected to change the growth rate, k , but is expected to reduce L_∞ according to:

$$L_\infty(B) = L_{\infty_L} - gB,$$

where g , the competition coefficient, accounts for decreases in asymptotic size as biomass density increases (Eq. 1.1 in Lorenzen and Enberg, 2002). $L_\infty(B)$ is the asymptotic length for a given level of biomass density, B , and L_{∞_L} is the limiting asymptotic length as B approaches 0. We then used the empirical relationship $g = 3.3 \bar{B}^{-1}$ to calculate $L_\infty(B)$, where \bar{B} is average biomass density.

3.3 Results

Length distribution analysis

The catch length distributions from the three historic FSAs on the east ends of Little Cayman, Cayman Brac, and Grand Cayman were similar, except that catch lengths from Grand Cayman had a smaller range and were about 3 cm larger on average. (Fig. 3.7). Catches from the recently discovered west end Little Cayman FSA in 2002 had a notably wider range than catches from the historic east end FSA in 1987–1995. This increased range was due to more large individuals present, not fewer small individuals. Pickle Bank had much larger fish—the average was 10 cm larger than the three historic FSAs. Individuals greater than 70 cm were rare at the three historic FSAs, whereas they comprised roughly half of the catch on Pickle Bank.

All years (2002-2018) of length distributions from the recently discovered west end Little Cayman FSA had wider range and larger individuals than catches at the historic east end FSA (1987–1995, Fig. 3.8). This was true both for fisheries catch before protection (2002) and *in situ* laser caliper data after protection (2003–2018). The 2017 and 2018 distributions were bimodal, with a pulse of small fish 40–55 cm not seen in the other 21 years.

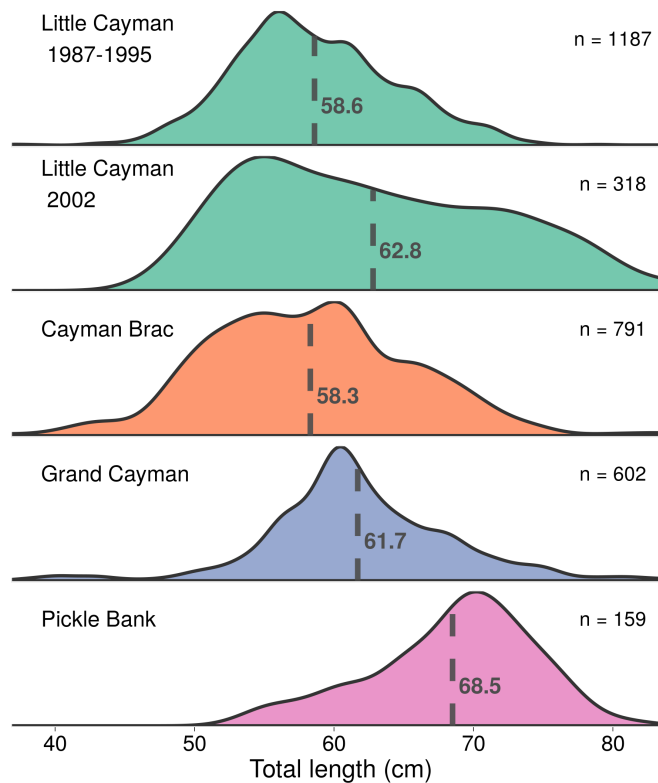


Figure 3.7: Nassau Grouper catch length distributions from four FSA fisheries in the Cayman Islands before protections. We pooled data across years for Little Cayman (1987–1988, 1992–1995), Cayman Brac (1990–1995, 1998, 2000), Grand Cayman (1988–1989, 1993, 1995, 1997), and Pickle Bank (2000). We divided data from Little Cayman into two periods because no fishing occurred for 7 years between 1995 and 2001, and data from 1987–1995 are from the historic east end FSA while data from 2002 are from the current west end FSA. Dashed lines indicate the means by FSA.

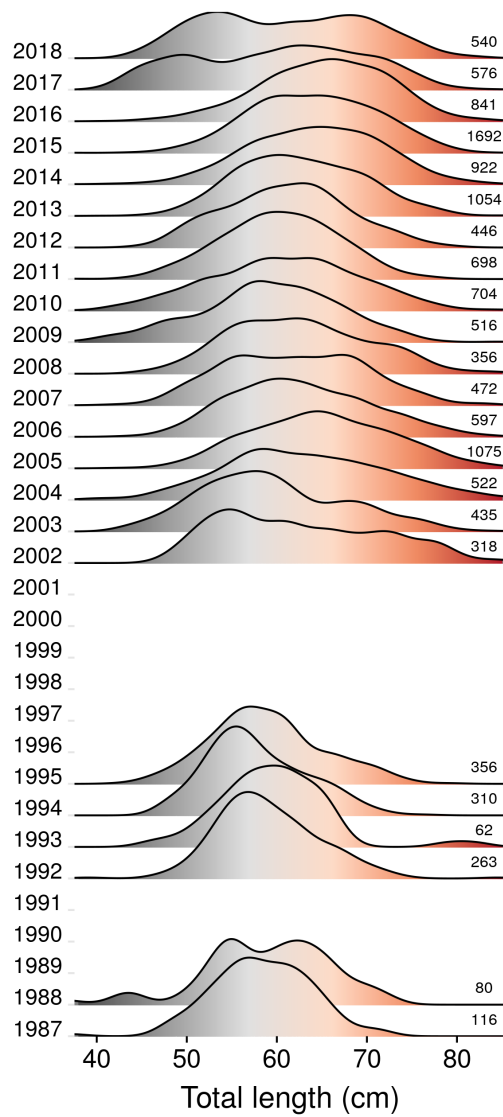


Figure 3.8: Length distributions from the west and east end Little Cayman Nassau Grouper FSAs. Data from 1987–1995 are from fisheries catch at the historic east end FSA. Data from 2002–2018 were collected at the “rediscovered” west end FSA, from fisheries catch before protections (2002) and from laser calipers after protections (2003–2018). Density curves are shaded according to length, with larger fish in red and smaller fish in dark grey. The increase in larger fish following 7 years of no fishing and subsequent protection is shown by more red shading from 2002–2018. The 2017 and 2018 distributions are bimodal, showing a pulse of small fish (dark grey). The sample sizes for each year are displayed at right.

Length-based assessment models

The LBSPR model estimated SPR at the three historic FSAs before protections to range from 0.46 to 0.59 (mean and 95% CI: Little Cayman, 0.46 (0.43–0.50); Cayman Brac, 0.56 (0.49–0.63); Grand Cayman, 0.59 (0.54–0.64); Fig. 3.9). The lightly exploited Pickle Bank FSA had higher SPR, 0.76 (95% CI: 0.62–0.91). SPR for the Little Cayman population in 2002, following several years of no fishing, was estimated to increase from 0.46 to 1.00 (95% CI: 1.00–1.00). Following two years of intense aggregation fishing (2001, 2002) and protection in 2003, the Little Cayman SPR decreased over the next 10 years to 0.63 (95% CI: 0.58–0.66) before increasing to 1.00. SPR for Cayman Brac also dramatically increased following protection, from 0.56 to 1.00.

The data-moderate LIME model, fit to *in situ* length data and an index of abundance, converged for 19 out of 53 growth parameter combinations (Fig. 3.10). Models using slightly lower k and higher L_∞ than the MLE from the fitted growth curve were generally more supported by AIC, and the model with lowest AIC used $k = 0.166$ and $L_\infty = 78.3$ (Fig. 3.10). LIME generally fit the length-frequency data well, including the bimodal distributions in 2017 and 2018 (Fig. 3.11).

The LIME model with lowest AIC estimated a decline in spawning biomass from 2000–2008, driven by both decreasing size and numbers of fish, and then increased by 280% from 2008–2018 (Fig. 3.12). The number of spawners reached a minimum in 2007, increased slightly from 2008–2013, and then increased dramatically from 2015–2018. Mean size went through three periods: decrease 2004–2010, increase 2010–2016, and a steep decrease 2016–2018. A large recruitment pulse was estimated in 2011, 7 times average recruitment (95% CI: 4.0–12.5).

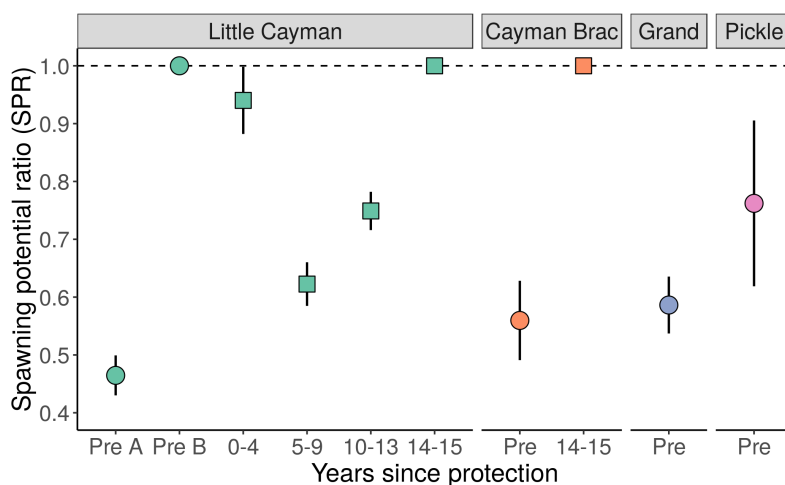


Figure 3.9: Estimated spawning potential ratio (SPR) for Cayman Islands Nassau Grouper spawning aggregations before and after protections implemented in 2003. Pre-protection length data (squares) were collected by sampling fisheries catch on Little Cayman (“Pre A”: 1987–1988 and 1992–1995, “Pre B”: 2002), Cayman Brac (1990–1995, 1998, 2000), Grand Cayman (1988–1989, 1993, 1995, 1997), and Pickle Bank (2000). Data from Little Cayman were divided into two pre-protection periods, “Pre A” and “Pre B”, because no fishing occurred for 7 years between 1995 and 2001, manifested by large differences in size structure (Fig. 3.7). Post-protection length data (circles) were collected from diver-operated laser calipers on Little Cayman (2003–2018, pooled into 5-year bins) and Cayman Brac (2017–2018).

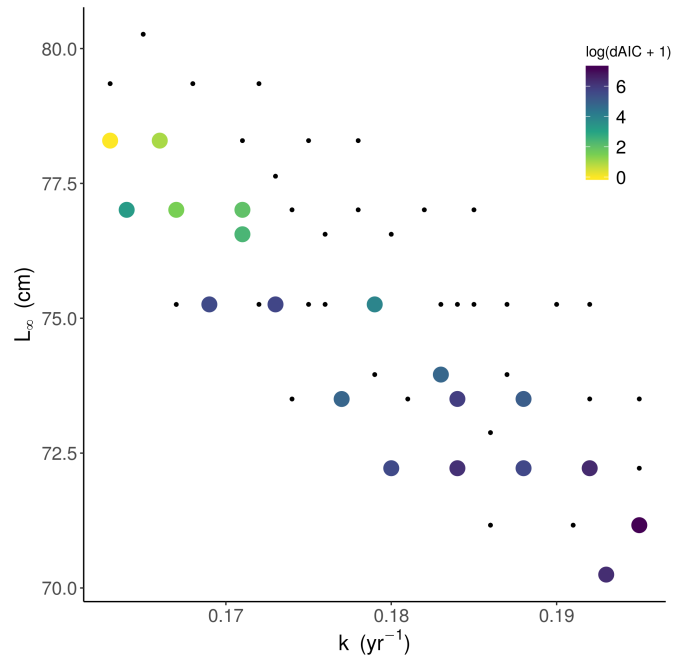


Figure 3.10: Range of von Bertalanffy growth curve parameters, k (growth rate, yr^{-1}) and L_∞ (asymptotic size, cm), used to fit the length-based assessment model. The parameter grid was centered on $k = 0.179$ and $L_\infty = 75.3$. The grid was calculated using the FishLife covariance matrix and a 2-dimensional Gauss-Hermite quadrature rule, level 5 (Rudd et al., In prep). The assessment model converged for 19 parameter combinations (large colored points) and failed to converge for 30 (small black points). The model using $k = 0.166$ and $L_\infty = 78.3$ was most supported by the data (lowest AIC, yellow), and models with high k and low L_∞ were less supported (higher AIC, purple).

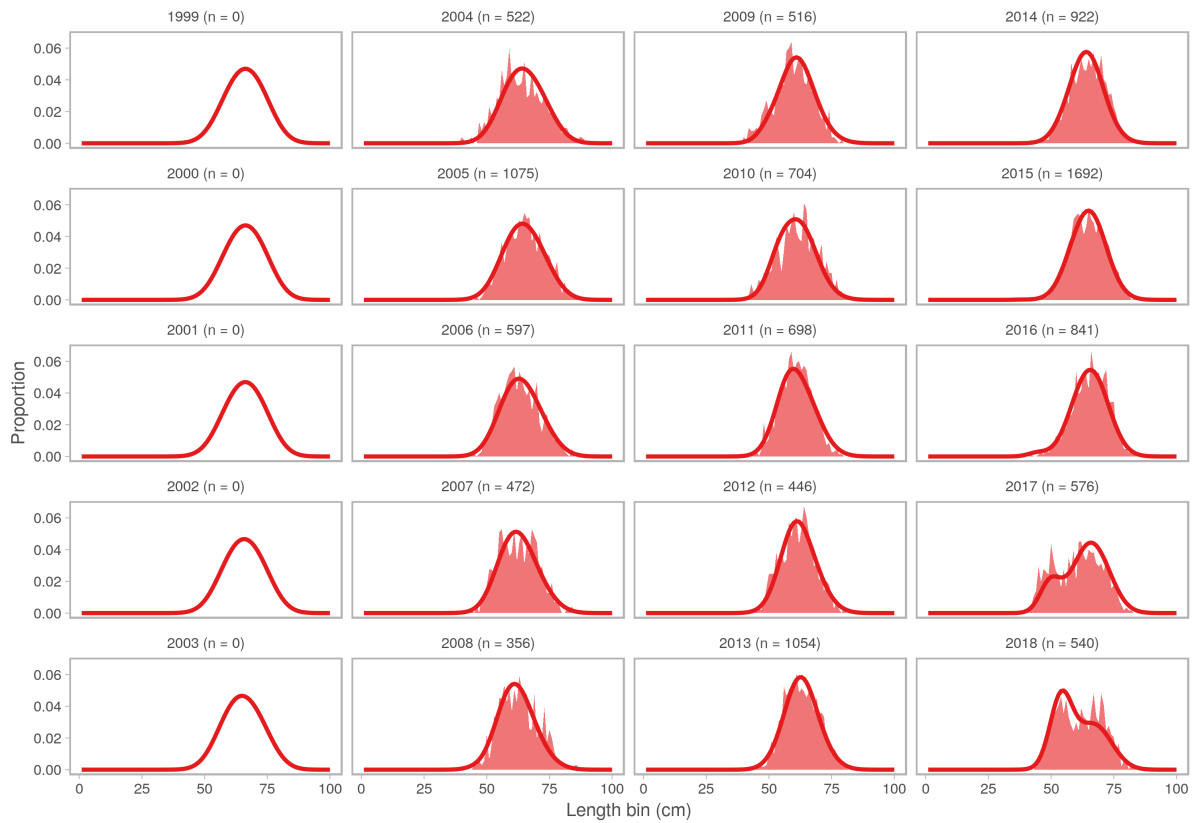


Figure 3.11: Fits to *in situ* Little Cayman length-frequency data from the LIME model with lowest AIC. Histograms show raw length data and curves show LIME model fits. LIME was able to fit the bimodal length distributions in 2017 and 2018. The model was fit starting in 1999, five years before data time series begins.

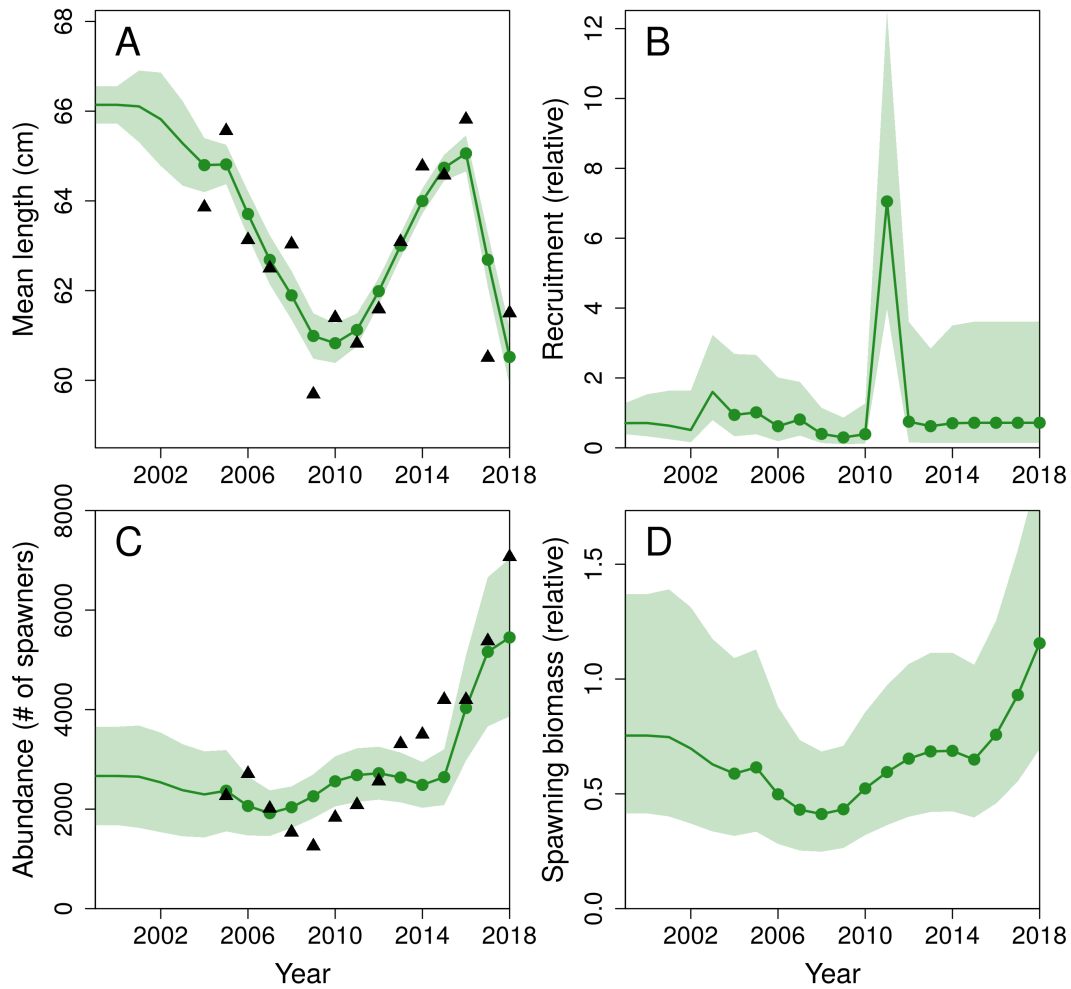


Figure 3.12: Length-based assessment model output for the Nassau Grouper spawning aggregation on Little Cayman Island: A) mean length (cm), B) recruitment (relative), C) abundance (number of spawners), and D) spawning biomass (relative). Black triangles show the input data. Green points, lines, and shading depict the maximum likelihood estimates and 95% confidence intervals. Years with estimates but not data are distinguished by green lines without points (length: 1999–2003, abundance: 1999–2004).

Bimodal length distributions in 2017 and 2018

The 2017 and 2018 length distributions were bimodal from the FSAs on both Little Cayman and Cayman Brac (Fig. 3.13). The modes (local maxima, dashed lines in Fig. 3.13) shifted right from 2017 to 2018 on both islands, as expected if the modes represent growth of a single strong cohort. In both years the modes are larger on Cayman Brac than Little Cayman. The Cayman Brac modes align well with growth curve predictions of age 6 in 2017 (growth curve prediction: 52.8 cm, mode: 53.4 cm) and age 7 in 2018 (growth curve prediction: 57.1 cm, mode: 58.6 cm). The Little Cayman 2017 mode (49.5 cm) lies in between growth curve predictions for ages 5 (47.6 cm) and 6 (52.8 cm), and the Little Cayman 2018 mode aligns with age 6 (52.6 vs. 52.8 cm). Thus, the observed growth increment (2018 mode minus 2017 mode) on Cayman Brac agrees well with the growth curve expectation, while the growth increment on Little Cayman is smaller than expected (Fig. 3.14).

There are two alternate hypotheses for the difference in length modes between the two islands: i) fish on both islands are the same age, which means they grew faster on Cayman Brac, or ii) fish grew at the same rate on both islands, but are one year older on Cayman Brac. Hypothesis (ii) could be tested by aging fish on the two islands, although this is unlikely to happen due to their protected status. Aside from this, hypothesis (ii) is improbable, as it would require large recruitment events in subsequent years that the islands did not share, even though they are only separated by 8 km. On the other hand, several mechanisms could reasonably cause differences in growth rates between the two islands (hypothesis i). One such mechanism could be density-dependent growth, since the density of fish is much (roughly six times) lower on Cayman Brac. Thus, we evaluated how much of the observed length differences could possibly be explained by density-dependent growth.

Little Cayman and Cayman Brac are approximately the same size. We calculated available adult habitat (area covering 5–50 m depth) for Little Cayman as 1,440 ha and for Cayman Brac as 1,689 ha (Fig. 3.15).

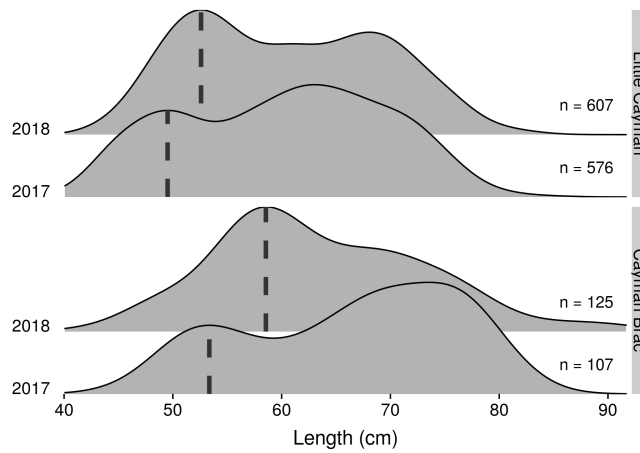


Figure 3.13: Bimodal length distributions from Little Cayman and Cayman Brac in 2017 and 2018. The modes (local maxima, dashed lines) shift right from 2017 to 2018 on both islands. In both years the modes are larger on Cayman Brac than Little Cayman. Predicted lengths from the growth curve are: 47.6 cm at age 5, 52.8 cm at age 6, and 57.1 cm at age 7.

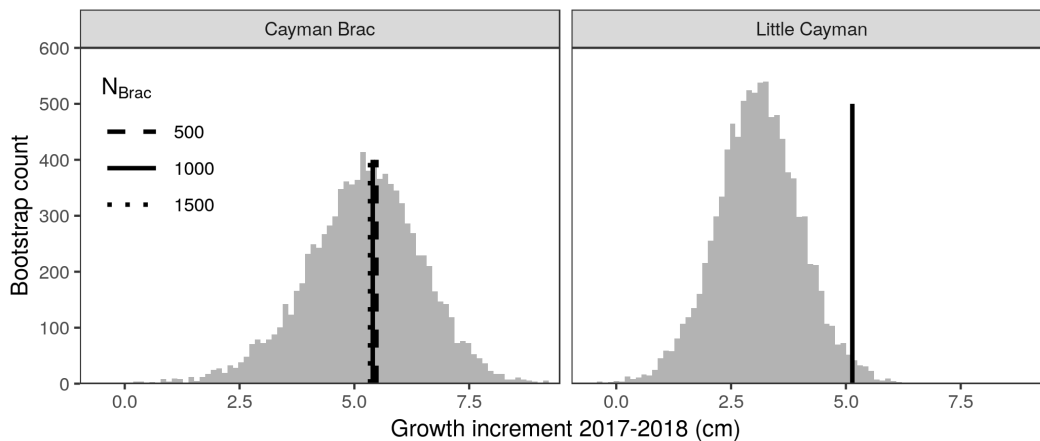


Figure 3.14: Bootstrap distribution of the growth increment of modes from 2017 to 2018. For each island and year, we took 10,000 bootstrap samples from the length data, calculated the kernel density modes, and subtracted the 2017 mode length from 2018. The observed growth increment on Cayman Brac matches the expected growth increment for age 6 to 7 from the growth curve (black lines). The observed growth increment on Little Cayman is smaller than expected (bootstrap samples left of line). Assuming growth is density-dependent, expected growth increments are fairly insensitive to population size (line type).

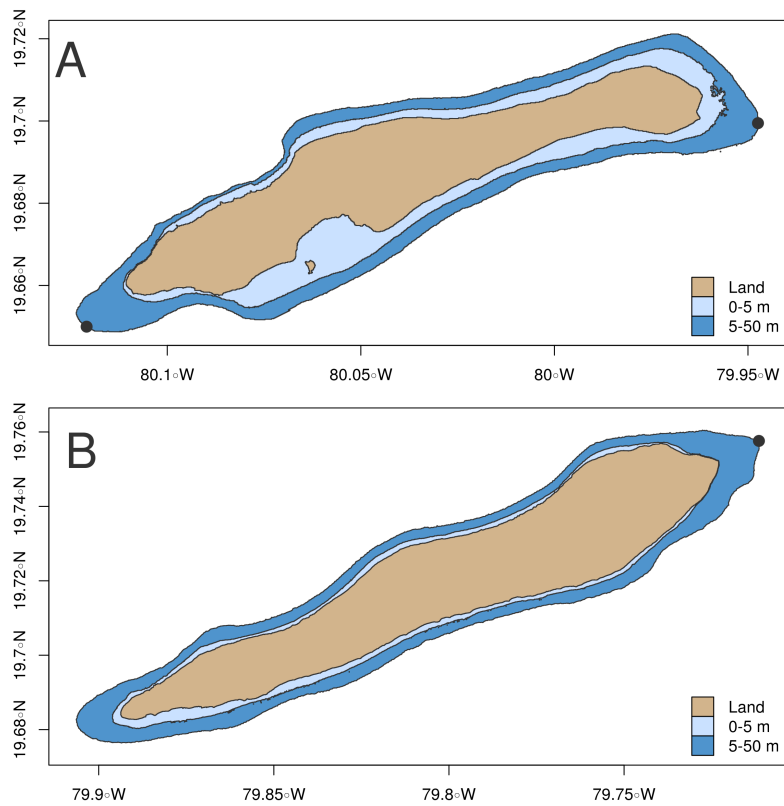


Figure 3.15: Habitat area available to Nassau Grouper on Little Cayman and Cayman Brac. A) Little Cayman has 1,440 ha of adult habitat area (5–50 m depth, dark blue) and 1,315 ha of juvenile habitat area (0–5 m depth, light blue). B) Cayman Brac has 1,689 ha of adult habitat and 572 ha of juvenile habitat. FSA locations are depicted by black points at the west (current) and east (historic) ends of Little Cayman, the east end of Cayman Brac.

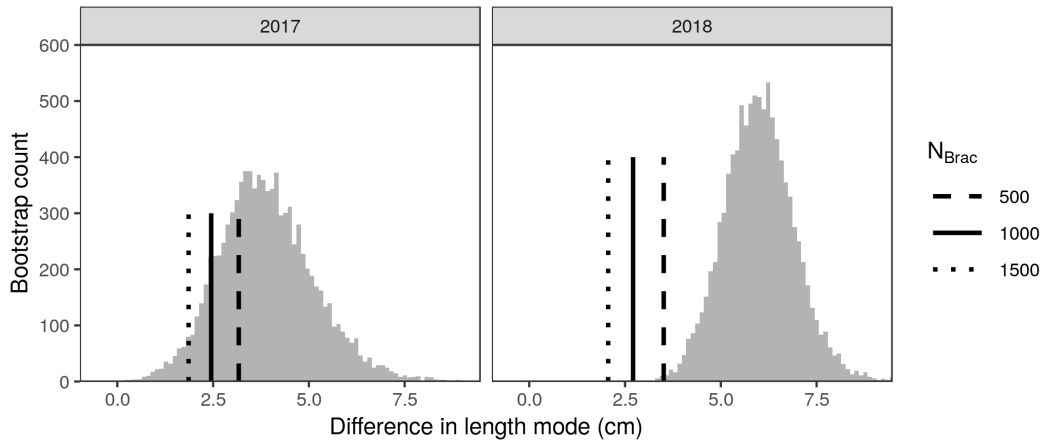


Figure 3.16: Bootstrap distribution of the difference in modes between Little Cayman and Cayman Brac in 2017 and 2018. For each island and year, we took 10,000 bootstrap samples from the length data, calculated the kernel density modes, and subtracted the Little Cayman mode (smaller) from the Cayman Brac mode (larger). Assuming the population size on Cayman Brac is 500–1,500, density-dependent growth can explain 1.9–3.2 cm (black lines, 48–81%) of the observed difference in 2017 (3.9 cm). Density-dependent growth can explain 2.1–3.5 cm (34–59%) of the observed difference in 2018 (6.0 cm).

We estimated that density-dependent growth could explain 1.9–3.2 cm (48–81%) of the observed length mode difference in 2017 (3.9 cm), and 2.1–3.5 cm (34–59%) of the difference in 2018 (6.0 cm, Fig. 3.16). See Section 3.2 for calculation details.

3.4 Discussion

Our results attest to the value of monitoring population size structure in addition to numbers. We demonstrated that collecting *in situ* length data over time is an especially effective method for monitoring protected FSAs, where all mature fish aggregate at high density and can be efficiently measured. Both the laser caliper and stereo camera systems had measurement error rates of 5–7% at angles less than 10° , which was accurate enough to detect strong year classes in bimodal length distributions.

What have we learned about recruitment?

Driven by the bimodal length distributions in 2017 and 2018, the LIME model estimated one year of very strong recruitment (7 times average, 95% CI: 4.0–12.5, Fig. 3.12B) out of 16 years of monitoring. Accordingly, recruitment variability was estimated to be high ($\sigma_r = 0.82$, 95% CI 0.57–1.16). This is not surprising, since Nassau Grouper are periodic strategists (Winemiller and Rose, 1992): long-lived and highly fecund, capable of withstanding years of recruitment failure sporadically punctuated by large successful spawning events. Given the dramatic decline of Nassau Grouper throughout the Caribbean, it is possible that external recruitment (i.e. from other FSAs) is more sporadic now than in the past. When FSAs were far greater in size and number, the probability of a population receiving larvae from a different FSA was likely higher, and therefore recruitment less variable. Now, with fewer active FSAs, the remaining FSAs may be more dependent on self-recruitment. More reliance on self-recruitment, however, implies a tighter stock–recruitment relationship (Strathmann et al., 2002). Contrary to this expectation, we observed high recruitment variability for the Little Cayman FSA that had no correlation with spawning stock biomass. This is important information for management as it implies long recovery timelines should be expected. We found that spawning biomass took 14 years to recover from two years of intense FSA fishing (Fig. 3.12d).

Length-frequency analysis showed that the big successful recruitment event occurred in 2011, synchronously on Little Cayman and Cayman Brac. This is supported by observations of numerous 1.5 year old juveniles on Little Cayman in July 2012 (Camp et al., 2013; Semmens et al., 2013). Nearly zero juveniles were sighted in all years 2004–2017 except for 2011 (Semmens et al., 2013). It is reasonable that Little Cayman and Cayman Brac would show strong recruitment in the same year because they are only separated by 8 km, and late-stage larvae are easily capable of swimming this distance against currents (Leis, 2015).

An obvious question is: What was special about conditions in 2011? Like many reef fish, Nassau Grouper are benthic but spawn pelagically, and successful recruitment may largely depend

on favorable currents bringing larvae close to suitable reef habitat. The prevailing current around the Cayman Islands flows east-northeast to west-southwest, but the mean current is weak and looping eddies that retain water for months are common (Richardson, 2005). Thus, the possibility exists for self-recruitment within the Caymans (Colin, 2012*b*; Heppell et al., 2011, 2009; Colin et al., 1987). Future work could model larval dispersal from Little Cayman using archived remote sensing data and compare 2011 against low recruitment years. Alternatively, strong recruitment in 2011 could have been related to abundant prey or fewer predators at critical space and time scales for larval survival (e.g. Cushing's match-mismatch hypothesis; Cushing, 1990). It is also possible for physical forcing to positively affect larval dispersal and survival simultaneously (Checkley Jr et al., 1988). While intriguing, these possibilities would be difficult to test in hindsight.

Nassau Grouper at different locations throughout the Caribbean appear to spawn during months when average temperature is around 26 °C (Table 2 in Tucker et al., 1993). Sea surface temperature off Little Cayman was indeed relatively cold in 2011, around 26 °C (Fig. 3.17). However, temperatures were also cold in 2005, 2006, and 2009, and no large recruitment events were observed in these years. Future work could investigate a possible temperature effect on recruitment, which may be acting as a proxy for effects related to currents, prey, or predators.

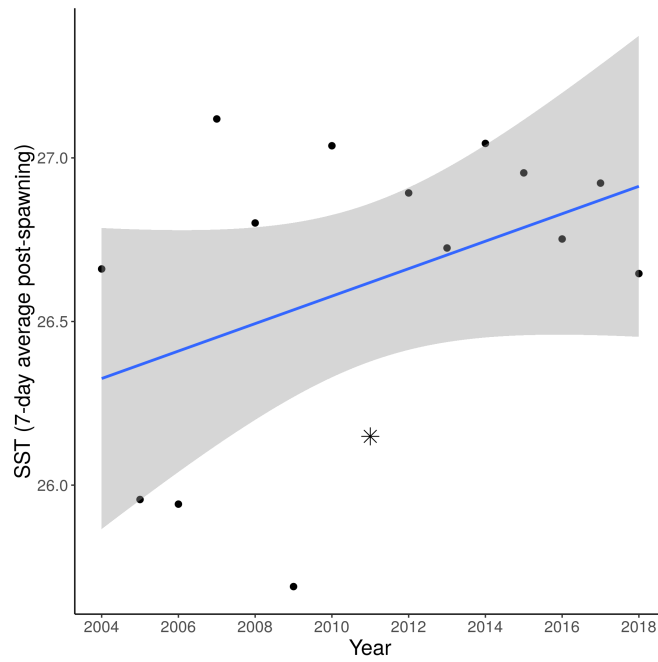


Figure 3.17: Sea surface temperature surrounding Little Cayman after spawning events from 2004–2018, 7-day average. For each year, peak spawning dates were recorded by divers from CIDOE and REEF. Temperature was averaged for the 7 days following each spawning date over latitude 19.6–19.8 °N and longitude 80.15–79.70 °W. Temperature data were downloaded from <https://podaac.jpl.nasa.gov/dataset/MUR-JPL-L4-GLOB-v4.1>.

Aggregation fisheries status and management

The LBSPR model estimated SPR at the three historic FSAs to range from 0.46 to 0.59, and all of these populations soon declined to levels not worth fishing. The Grand Cayman FSA, with an estimated SPR of 0.59 (95% CI: 0.54–0.64) from pooled 1988–1997 data, has shown no sign of recovery despite 15 years of protection. In addition, only two years of intense aggregation fishing (2001, 2002) caused the Little Cayman SPR to decrease from 1.00 to 0.63. These observations suggest that $SPR < 0.6$ would be an unsustainable reference point for managing the Nassau Grouper spawning aggregation fishery. Many studies repeat the advice of Clark (2002, 1993) and Mace (1994), which recommend $SPR = 0.4$ as a risk-adverse reference point in cases where the stock–recruit relationship is not estimable (e.g. Hordyk et al., 2015b; Rudd and Thorson, 2018). Brooks et al. (2010) and Clark (2002), however, demonstrated that the appropriate SPR depends on the slope of the stock–recruit curve at low stock size, and that for less resilient species (i.e. lower stock–recruit steepness) SPR in the range 0.6–0.86 could be warranted. The appropriate SPR for Nassau Grouper may also lie in this range, well above the oft-cited 0.4 value.

We would expect the sustainable SPR to be higher than 0.4 for Nassau Grouper because the species' life history does not follow the assumptions underlying the typical SPR reference point guidelines. First, the SPR guidelines are derived from Beverton-Holt or Ricker stock–recruit relationships that do not admit the possibility of an Allee effect (i.e. depensation, lower recruits per spawner at low stock size; Brooks et al., 2010). The spawning aggregation behavior of Nassau Grouper may well be a strong Allee effect mechanism, whereby FSAs no longer form at population sizes (or densities) below a threshold and few, if any, recruits are produced (Courchamp et al., 2008; Sadovy de Mitcheson, 2016). If such a threshold exists, Nassau Grouper stock sizes need to be kept above it. Second, Nassau Grouper exhibit highly variable recruitment. As a pelagically-spawning tropical reef fish, Nassau Grouper recruitment may be driven by variable larval dispersal and only weakly related to stock size. The SPR guidelines were derived based on stock–recruit curves for temperate species, as assessments and stock–recruit data do not exist for most tropical species. In

addition, stock assessments assume that stock structure and connectivity are known, but the degree to which FSAs are connected by larval dispersal within the Cayman Islands and throughout the Caribbean is poorly understood for Nassau Grouper. All of these demonstrate the danger of blindly applying recommendations from well-studied, temperate fish species to poorly-studied, tropical species, either based on theoretical or meta-analysis studies. They also highlight the need for fisheries assessment and management tools to be adapted for aggregating species' life history (e.g. depensation, variable recruitment weakly related to stock size, and metapopulation stock structure; Sadovy de Mitcheson, 2016).

The Cayman Islands government should be commended for acting quickly to protect the Little Cayman FSA. Roughly two-thirds of the population was harvested in the two years before protection, but the remaining population never stopped forming a spawning aggregation. It will likely take longer for Nassau Grouper to recover at historic FSA sites elsewhere where aggregating behavior ceased. The recovery of these historic sites may depend on getting a pulse of larvae from a healthy FSA—it is possible this occurred on Cayman Brac in 2011.

Ecological impacts of recovering Nassau Grouper

The biomass density of Nassau Grouper increased five-fold from 2008 to 2018 (4 to 22 kg ha⁻¹). Nassau Grouper growth may be slower on Little Cayman than Cayman Brac due to density-dependent effects. In the small modes of the 2017 and 2018 bimodal length distributions, the Cayman Brac fish were 3–5 cm larger than those on Little Cayman, and it is reasonable to assume that these represent fish of the same age. Density-dependent growth could possibly explain 2–3 cm (35–80%) of this size difference. As populations recover, density-dependent growth may slow the increase in biomass and this effect should be considered in assessment models and management. For example, the equation for density-dependent growth in Lorenzen and Enberg (2002) could easily be added to the LIME assessment model.

Nevertheless, density-dependence is only one of many possible mechanisms underlying

the difference in growth rates between Little Cayman and Cayman Brac. Instead of intraspecific competition, Nassau Grouper may have less access to food on Little Cayman because interspecific competition is higher or the system is less productive as a whole. Prey may be harder to capture on Little Cayman, requiring Nassau Grouper to allocate more energy to active metabolism and less to growth. Water temperature may be slightly warmer or colder on one island compared to the other, pushing Little Cayman Nassau Grouper away from their growth optimum. Nassau Grouper on Little Cayman may have matured earlier than their counterparts on Cayman Brac, which would result in an energy reallocation from somatic growth to reproductive growth. Of these alternative explanations, we can at least rule out different ages at maturity because the 2011 cohort was absent from the 2015 length distribution on Little Cayman. Still, there are many conceivable mechanisms behind the difference in growth rates, and future work could test for these possibilities.

Nassau Grouper are dominant predators in reef ecosystems, and the substantial increase in Nassau Grouper—especially large Nassau Grouper—on Little Cayman is likely to affect other species as well. The Exuma Cays Land and Sea Park (ECLSP), Bahamas, is another rare location in the Caribbean with high Nassau Grouper density. At ECLSP, Nassau Grouper populations increased in response to protection and this was associated with reduced densities of smaller grouper such as coney and graysby (Chiappone and Sealey, 2000). Mumby et al. (2006) demonstrated that Nassau Grouper caused a trophic cascade in the ECLSP, whereby only large parrotfish escape predation, and these provide disproportionate grazing control of macroalgae. Another potential ecosystem benefit of increasing Nassau Grouper predation is the control of invasive lionfish (Mumby et al., 2011; but see Hackerott et al., 2013).

Future work and outlook for the species

Several important questions remain whose answers would inform Nassau Grouper management in the Cayman Islands and aid recovery efforts Caribbean-wide.

- i) How connected are FSAs via larval dispersal? Relatedly, how important is self-recruitment

to sustaining FSAs, and does this vary amongst FSAs? Currents and reef topography vary substantially throughout the Caribbean, ranging from small isolated islands (e.g. Little Cayman) and offshore seamounts (e.g. Pickle Bank) to larger islands (e.g. Cuba) and wide shelf platforms (e.g. Bahamas). A key difference is that on the larger islands and shelves, adult Nassau Grouper can migrate long distances and access multiple FSAs (Bolden, 2000; Sadovy de Mitcheson et al., 2008), whereas on smaller islands and atolls only one FSA typically forms (e.g. Glover's Reef, Starr et al., 2007; Little Cayman, Semmens et al., 2007; Cayman Brac, Semmens et al., 2009). Physical processes leading to local retention of larvae and self-recruitment in one location may differ from other locations. In addition, the relative significance of self-recruitment is dependent on population size. For FSAs where local retention of larvae occurs, self-recruitment will appear increasingly important as the population size increases because external recruits will comprise a shrinking proportion of total recruitment (Strathmann et al., 2002). The Little Cayman Nassau Grouper FSA, therefore, should appear more reliant on self-recruitment now than in the past when it was smaller. Conversely, if the Little Cayman FSA supplies demographically-relevant levels of larvae to populations elsewhere, the importance of self-recruitment at those sites would be expected to decrease. Given currents in the region and probable dispersal distances of tens to hundreds of kilometers, transport of Little Cayman larvae only seems likely within the Cayman Islands and to southern Cuba (Cowen, 2006; Richardson, 2005; Jackson et al., 2014; Cowen et al., 2000).

ii) What is the carrying capacity for Nassau Grouper on Caribbean reefs, and how much larger can the Little Cayman FSA grow? Although appropriate management action for declining FSAs has long been fairly obvious (e.g. protect FSAs from fishing; Sadovy and Domeier, 2005), it is less clear how to manage an increasing FSA such as Little Cayman. The current biomass density on Little Cayman is approximately 22 kg ha^{-1} ($220 \text{ g } 100 \text{ m}^{-2}$) and should increase substantially as the 2011 year class grows. It is unclear how this density estimate compares with historic levels or recent estimates from other locations based on visual transects outside spawning season (Mumby et al., 2011; Chiappone and Sealey, 2000; Tupper and Rudd, 2002), and the few documented reports

of FSA size (Sala et al., 2001). While we know—based on imprecise diver counts—that many FSA sizes have dramatically declined (e.g. Smith, 1972; Sala et al., 2001), we often do not know the catchment area or size structure to estimate biomass density. More accurate and comparable population assessments would be helpful.

iii) Are large spawning aggregations necessary for successful reproduction, or will Nassau Grouper spawn in smaller social groups (Colin, 1992)? In other words, does an Allee effect exist, and if so, how strong is it? This is a critical question, as it determines the species' ability to recover at the many FSA sites where aggregations have disappeared. Increases have been seen at FSAs with very low numbers of Nassau Grouper (e.g. from 30 to 214 individuals over 8 years, Bernard et al., 2016), although spawning has not been documented and it is unclear if the increase is due to adult migration or recruitment. Nassau Grouper have been directly observed to spawn at FSAs numbering approximately 100 and 500 individuals (Colin, 1992).

iv) What is the contribution of FSAs at natural refuges? FSA sites that are more remote and have rough sea conditions are less susceptible to fishing and may harbor healthy populations that can replenish depleted stocks elsewhere, even without protections (Thompson and Munro, 1978). For example, the Nassau Grouper population on Pickle Bank appeared healthy when sampled in 2000 (SPR = 0.76, 95% CI 0.62–0.91), even though jurisdiction of Pickle Bank is disputed and protection is unlikely.

The FSA on Little Cayman is the largest currently documented for the species. Although they remain to be formally assessed, sizable Nassau Grouper populations exist elsewhere. FSA protections are increasingly common, and Nassau Grouper recovery Caribbean-wide depends on population responses to these protections. In the Cayman Islands, scientific monitoring following temporary FSA protections bolstered the necessary political will to expand and make these protections permanent. We found that time series of *in situ* length data is an especially effective method for assessing protected FSAs, and was even able to detect recruitment of strong year classes and differences in growth between FSAs. The methods demonstrated here are useful for assessing FSAs

and lend themselves to efforts aimed at managing sustainable reef fisheries.

Acknowledgements

We thank the hard-working CIDOE staff who have provided years of field support: Bradley Johnson, Ivan Montieth, Keith Neale, Robert Walton, James Gibb, Cody Panton, Kevin Jackson, and Chris Dixon. Many REEF staff and volunteer divers helped collect laser caliper video, including Leslie Whaylen, Steve Gittings, Hal Peterson, Todd Bohannon, Cody Panton, Tammi Warrender, and Josh Stewart. Peter Hillenbrand (Southern Cross Club), Jason Belport (Little Cayman Beach Resort), and Cayman Airways generously provided accommodations and logistical support. BCS received support from the Cooperative Institute for Marine Ecosystems and Climate (CIMEC) and the National Science Foundation Graduate Research Fellowship under Grant No. DGE-1144086. ICD was funded by the Scripps Institution of Oceanography Director's Office in support of the 2017 Scripps Undergraduate Research Fellowship (SURF) REU program (NSF-OCE 1659793).

This chapter, in part, is currently in preparation for submission for publication and is printed here with the permission of co-authors Scott A. Heppell, Lynn Waterhouse, India C. Dove, Christy V. Pattengill-Semmens, Croy M. McCoy, Phillippe G. Bush, Gina Ebanks-Petrie, and Brice X. Semmens. The dissertation author was the primary investigator and author of this paper.

References

- Allee, W. C. 1931. Animal aggregations: a study in general sociology. University of Chicago Press, Chicago.
- Beddington, J. R., D. J. Agnew, and C. W. Clark. 2007. Current Problems in the Management of Marine Fisheries. *Science*, **316**:1713–1716.
- Beets, J. and A. Friedlander. 1999. Evaluation of a conservation strategy: a spawning aggregation closure for red hind, *Epinephelus guttatus*, in the U.S. Virgin Islands. *Environmental Biology of Fishes*, **55**:91–98.
- Berkson, J. and J. T. Thorson. 2015. The determination of data-poor catch limits in the United States: is there a better way? *ICES Journal of Marine Science*, **72**:237–242.

- Bernard, A. M., K. A. Feldheim, R. Nemeth, E. Kadison, J. Blondeau, B. X. Semmens, and M. S. Shivji. 2016. The ups and downs of coral reef fishes: the genetic characteristics of a formerly severely overfished but currently recovering Nassau grouper fish spawning aggregation. *Coral Reefs*, **35**:273–284.
- Bolden, S. K. 2000. Long-distance movement of a Nassau grouper (*Epinephelus striatus*) to a spawning aggregation in the central Bahamas. *Fishery Bulletin*, **98**:642. 642.
- Brooks, E. N., J. E. Powers, and E. Cortés. 2010. Analytical reference points for age-structured models: application to data-poor fisheries. *ICES Journal of Marine Science*, **67**:165–175.
- Bush, P. and G. Ebanks-Petrie. 1994. The Cayman Islands Nassau Grouper study - a progress report. In *Proceedings of the 43rd Annual Gulf and Caribbean Fisheries Institute*, pages 387–388. Charleston, South Carolina, USA.
- Bush, P. G., E. D. Lane, G. C. Ebanks-Petrie, K. Luke, B. Johnson, C. McCoy, J. Bothwell, and E. Parsons. 2006. The Nassau Grouper spawning aggregation fishery of the Cayman Islands – An historical and management perspective. In *Proceedings of the 57th Annual Gulf and Caribbean Fisheries Institute*, pages 515–524. St. Petersburg, Florida, USA.
- Camp, E. F., K. E. Lohr, S. C. Barry, P. G. Bush, C. A. Jacoby, and C. Manfrino. 2013. Microhabitat associations of late juvenile Nassau Grouper (*Epinephelus Striatus*) off Little Cayman, BWI. *Bulletin of Marine Science*, **89**:571–581.
- Cayman Islands Cabinet. 2016. The National Conservation (General) Regulations, 2016. <http://www.gov.ky/portal/pls/portal/docs/1/12326595.PDF>.
- Chapman, D. and D. Robson. 1960. The analysis of a catch curve. *Biometrics*, **16**:354–368.
- Checkley Jr, D. M., S. Raman, G. L. Maillet, and K. M. Mason. 1988. Winter storm effects on the spawning and larval drift of a pelagic fish. *Nature*, **335**:346–348.
- Chen, D. G., J. R. Irvine, and A. J. Cass. 2002. Incorporating Allee effects in fish stock-recruitment models and applications for determining reference points. *Canadian Journal of Fisheries and Aquatic Sciences*, **59**:242–249.
- Chiappone, M. and K. M. S. Sealey. 2000. Marine reserve design criteria and measures of success: lessons learned from the Exuma Cays Land and Sea Park, Bahamas. *Bulletin of Marine Science*, **66**:691–705.
- Clark, W. G. 1993. The effect of recruitment variability on the choice of a target level of spawning biomass per recruit. In *Proceedings of the international symposium on management strategies for exploited fish populations*, pages 233–246. University of Alaska Fairbanks.
- Clark, W. G. 2002. $F_{35\%}$ revisited ten years later. *North American Journal of Fisheries Management*, **22**:251–257.

- Colin, P. L. 1992. Reproduction of the Nassau grouper, *Epinephelus striatus* (Pisces: Serranidae) and its relationship to environmental conditions. *Environmental Biology of Fishes*, **34**:357–377.
- Colin, P. L. 2012a. Studying and Monitoring Aggregating Species. In Y. Sadovy de Mitcheson and P. L. Colin, editors, *Reef Fish Spawning Aggregations: Biology, Research and Management*, pages 285–329. Springer Netherlands, Dordrecht.
- Colin, P. L. 2012b. Timing and Location of Aggregation and Spawning in Reef Fishes. In Y. Sadovy de Mitcheson and P. L. Colin, editors, *Reef Fish Spawning Aggregations: Biology, Research and Management*, pages 117–158. Springer Netherlands, Dordrecht.
- Colin, P. L., D. Y. Shapiro, and D. Weiler. 1987. Aspects of the reproduction of two groupers, *Epinephelus guttatus* and *E. striatus* in the West Indies. *Bulletin of Marine Science*, **40**:220–230.
- Courchamp, F., L. Berec, and J. Gascoigne. 2008. *Allee Effects in Ecology and Conservation*. Oxford University Press.
- Cowen, R. K. 2006. Scaling of Connectivity in Marine Populations. *Science*, **311**:522–527.
- Cowen, R. K., K. M. M. Lwiza, S. Sponaugle, C. B. Paris, and D. B. Olson. 2000. Connectivity of marine populations: Open or closed? *Science*, **287**:857–859.
- Cushing, D. 1990. Plankton Production and Year-class Strength in Fish Populations: an Update of the Match/Mismatch Hypothesis. *Advances in Marine Biology*, **26**:249–293.
- Goodyear, C. P. 1993. Spawning stock biomass per recruit in fisheries management: foundation and current use. In S. J. Smith, J. J. Hunt, and D. Rivard, editors, *Risk evaluation and biological reference points for fisheries management*, pages 67–81. Number 120 in Canadian Special Publication of Fisheries and Aquatic Sciences, National Research Council, Ottawa. OCLC: 833202625.
- Grüss, A., D. M. Kaplan, and J. Robinson. 2014. Evaluation of the effectiveness of marine reserves for transient spawning aggregations in data-limited situations. *ICES Journal of Marine Science*, **71**:435–449.
- Gårdmark, A., N. Jonzén, and M. Mangel. 2006. Density-dependent body growth reduces the potential of marine reserves to enhance yields. *Journal of Applied Ecology*, **43**:61–69.
- Hackerott, S., A. Valdivia, S. J. Green, I. M. Côté, C. E. Cox, L. Akins, C. A. Layman, W. F. Precht, and J. F. Bruno. 2013. Native Predators Do Not Influence Invasion Success of Pacific Lionfish on Caribbean Reefs. *PLOS ONE*, **8**:e68259.
- Hamilton, R. J., T. Potuku, and J. R. Montambault. 2011. Community-based conservation results in the recovery of reef fish spawning aggregations in the Coral Triangle. *Biological Conservation*, **144**:1850–1858.

- Heppell, S., B. X. Semmens, C. V. Pattengill-Semmens, P. G. Bush, B. C. Johnson, C. M. McCoy, J. Gibb, and S. S. Heppell. 2011. Oceanographic patterns associated with Nassau grouper aggregation spawn timing: Shifts in surface currents on the nights of peak spawning. In *Proceedings of the 63rd Gulf and Caribbean Fisheries Institute*, pages 152–154. San Juan, Puerto Rico.
- Heppell, S. A., B. X. Semmens, S. K. Archer, C. V. Pattengill-Semmens, P. G. Bush, C. M. McCoy, S. S. Heppell, and B. C. Johnson. 2012. Documenting recovery of a spawning aggregation through size frequency analysis from underwater laser calipers measurements. *Biological Conservation*, **155**:119–127.
- Heppell, S. A., B. X. Semmens, C. V. Pattengill-Semmens, P. G. Bush, B. C. Johnson, C. M. McCoy, C. Paris, J. Gibb, and S. S. Heppell. 2009. Tracking potential larval dispersal patterns from Nassau grouper aggregation sites: Evidence for local retention and the "importance of place". In *Proceedings of the 61st Gulf and Caribbean Fisheries Institute*, pages 325–327. Gosier, Guadeloupe, French West Indies.
- Hijmans, R. J. 2018. raster: Geographic Data Analysis and Modeling. v2.8-4. <https://CRAN.R-project.org/package=raster>.
- Hilborn, R. 2018*a*. Are MPAs effective? *ICES Journal of Marine Science*, **75**:1160–1162.
- Hilborn, R. 2018*b*. Counterpoint to Sala and Giakoumi. *ICES Journal of Marine Science*, **75**:1169–1170.
- Hilborn, R. and C. J. Walters. 1992. *Quantitative fisheries stock assessment*. Springer Science & Business Media.
- Hobday, A. J., A. D. M. Smith, I. C. Stobutzki, C. Bulman, R. Daley, J. M. Dambacher, R. A. Deng, J. Dowdney, M. Fuller, D. Furlani, S. P. Griffiths, D. Johnson, R. Kenyon, I. A. Knuckey, S. D. Ling, R. Pitcher, K. J. Sainsbury, M. Sporcic, T. Smith, C. Turnbull, T. I. Walker, S. E. Wayte, H. Webb, A. Williams, B. S. Wise, and S. Zhou. 2011. Ecological risk assessment for the effects of fishing. *Fisheries Research*, **108**:372–384.
- Hordyk, A. 2017. LBSPR: Length-Based Spawning Potential Ratio. v0.1.2. <https://CRAN.R-project.org/package=LBSPR>.
- Hordyk, A., K. Ono, K. Sainsbury, N. Loneragan, and J. Prince. 2015*a*. Some explorations of the life history ratios to describe length composition, spawning-per-recruit, and the spawning potential ratio. *ICES Journal of Marine Science*, **72**:204–216.
- Hordyk, A., K. Ono, S. Valencia, N. Loneragan, and J. Prince. 2015*b*. A novel length-based empirical estimation method of spawning potential ratio (SPR), and tests of its performance, for small-scale, data-poor fisheries. *ICES Journal of Marine Science*, **72**:217–231.
- Hordyk, A. R. and T. R. Carruthers. 2018. A quantitative evaluation of a qualitative risk assessment framework: Examining the assumptions and predictions of the Productivity Susceptibility Analysis (PSA). *PLOS ONE*, **13**:e0198298.

- Hordyk, A. R., K. Ono, J. D. Prince, and C. J. Walters. 2016. A simple length-structured model based on life history ratios and incorporating size-dependent selectivity: application to spawning potential ratios for data-poor stocks. *Canadian Journal of Fisheries and Aquatic Sciences*, **73**:1787–1799.
- Hutchings, J. A. 2000. Collapse and recovery of marine fishes. *Nature*, **406**:882–885.
- Hutchings, J. A. 2005. Life history consequences of overexploitation to population recovery in Northwest Atlantic cod (*Gadus morhua*). *Canadian Journal of Fisheries and Aquatic Sciences*, **62**:824–832.
- Jackson, A. M., B. X. Semmens, Y. Sadovy de Mitcheson, R. S. Nemeth, S. A. Heppell, P. G. Bush, A. Aguilar-Perera, J. A. B. Claydon, M. C. Calosso, K. S. Sealey, M. T. Schärer, and G. Bernardi. 2014. Population structure and phylogeography in Nassau Grouper (*Epinephelus striatus*), a mass-aggregating marine fish. *PLoS ONE*, **9**:e97508.
- Jackson, J. B. C., M. X. Kirby, W. H. Berger, K. A. Bjorndal, L. W. Botsford, B. J. Bourque, R. H. Bradbury, R. Cooke, J. Erlandson, J. A. Estes, T. P. Hughes, S. Kidwell, C. B. Lange, H. S. Lenihan, J. M. Pandolfi, C. H. Peterson, R. S. Steneck, M. J. Tegner, and R. R. Warner. 2001. Historical Overfishing and the Recent Collapse of Coastal Ecosystems. *Science*, **293**:629–637.
- Jennings, S. 2001. Patterns and prediction of population recovery in marine reserves. *Reviews in Fish Biology and Fisheries*, **10**:209–231.
- Johannes, R. E. 1998. The case for data-less marine resource management: examples from tropical nearshore finfisheries. *Trends in Ecology & Evolution*, **13**:243–246.
- Leis, J. M. 2015. Is dispersal of larval reef fishes passive? In C. Mora, editor, *Ecology of Fishes on Coral Reefs*, pages 223–226. Cambridge University Press, Cambridge.
- Liermann and Hilborn. 2001. Depensation: evidence, models and implications. *Fish and Fisheries*, **2**:33–58.
- Lorenzen, K. 2008. Fish population regulation beyond "stock and recruitment": the role of density-dependent growth in the recruited stock. *Bulletin of Marine Science*, **83**:16.
- Lorenzen, K. and K. Enberg. 2002. Density-dependent growth as a key mechanism in the regulation of fish populations: evidence from among-population comparisons. *Proceedings of the Royal Society of London B: Biological Sciences*, **269**:49–54.
- Luckhurst, B. E. and T. M. Trott. 2009. Seasonally-Closed Spawning Aggregation Sites for Red Hind (*Epinephelus guttatus*): Bermuda's Experience over 30 years (1974 – 2003). page 6.
- Mace, P. M. 1994. Relationships between common biological reference points used as thresholds and targets of fisheries management strategies. *Canadian Journal of Fisheries and Aquatic Sciences*, **51**:110–122.

- Mumby, P. J., C. P. Dahlgren, A. R. Harborne, C. V. Kappel, F. Micheli, D. R. Brumbaugh, K. E. Holmes, J. M. Mendes, K. Broad, J. N. Sanchirico, K. Buch, S. Box, R. W. Stoffle, and A. B. Gill. 2006. Fishing, Trophic Cascades, and the Process of Grazing on Coral Reefs. *Science*, **311**:98–101.
- Mumby, P. J., A. R. Harborne, and D. R. Brumbaugh. 2011. Grouper as a Natural Biocontrol of Invasive Lionfish. *PLOS ONE*, **6**:e21510.
- Myers, R. A. 1998. When do environment-recruitment correlations work? *Reviews in Fish Biology and Fisheries*, **8**:285–305.
- Nemeth, R. 2005a. Population characteristics of a recovering US Virgin Islands red hind spawning aggregation following protection. *Marine Ecology Progress Series*, **286**:81–97.
- Nemeth, R. S. 2005b. Population characteristics of a recovering US Virgin Islands red hind spawning aggregation following protection. *Marine Ecology Progress Series*, **286**:81–97.
- NMFS. 2016. Endangered and Threatened Wildlife and Plants: Final Listing Determination on the Proposal To List the Nassau Grouper as Threatened Under the Endangered Species Act. Technical Report 50 CFR Part 223, U.S. Dept. Commerce, National Oceanic and Atmospheric Administration, National Marine Fisheries Service.
- Ogle, D. H., P. Wheeler, and A. Dinno. 2018. FSA: Fisheries Stock Analysis. <https://github.com/droglenc/FSA>. R package version 0.8.22.
- Patrick, W. S., P. Spencer, J. Link, J. Cope, J. Field, D. Kobayashi, P. Lawson, T. Gedamke, E. Cortés, O. Ormseth, K. Bigelow, and W. Overholtz. 2010. Using productivity and susceptibility indices to assess the vulnerability of United States fish stocks to overfishing. *Fishery Bulletin*, **108**:305–322.
- Pauly, D. 1980. On the interrelationships between natural mortality, growth parameters, and mean environmental temperature in 175 fish stocks. *ICES Journal of Marine Science*, **39**:175–192.
- Pebesma, E. 2018. Simple Features for R: Standardized Support for Spatial Vector Data. **10**:439–446.
- Pendleton, L. H., G. N. Ahmadi, H. I. Browman, R. H. Thurstan, D. M. Kaplan, and V. Bartolino. 2018. Debating the effectiveness of marine protected areas. *ICES Journal of Marine Science*, **75**:1156–1159.
- Pepin, P. 2016. Reconsidering the impossible—linking environmental drivers to growth, mortality, and recruitment of fish. *Canadian Journal of Fisheries and Aquatic Sciences*, **73**:205–215.
- Porch, C. E., A.-M. Eklund, and G. P. Scott. 2003. An assessment of rebuilding times for goliath grouper. Technical Report SEDAR6-RW-3, U.S. Department of Commerce, National Marine Fisheries Service, Southeast Fisheries Science Center, 75 Virginia Beach Drive, Miami, FL 33149.

- Restrepo, V. R., G. G. Thompson, P. M. Mace, W. L. Gabriel, L. L. Low, A. D. MacCall, R. D. Methot, J. E. Powers, B. L. Taylor, P. R. Wade, and J. F. Witzig. 1998. Technical guidance on the use of precautionary approaches to implementing National Standard 1 of the Magnuson-Stevens Fishery Conservation and Management Act. Technical report.
- Richardson, P. L. 2005. Caribbean Current and eddies as observed by surface drifters. *Deep Sea Research Part II: Topical Studies in Oceanography*, **52**:429–463.
- Robinson, J., N. A. J. Graham, J. E. Cinner, G. R. Almany, and P. Waldie. 2015. Fish and fisher behaviour influence the vulnerability of groupers (*Epinephelidae*) to fishing at a multispecies spawning aggregation site. *Coral Reefs*, **34**:371–382.
- Rose, G. A. and D. W. Kulka. 1999. Hyperaggregation of fish and fisheries: how catch-per-unit-effort increased as the northern cod (*Gadus morhua*) declined. **56**:10.
- Rudd, M. B. 2018. Length-based integrated mixed effects model. v2.0.7. <https://github.com/merrillrudd/LIME>.
- Rudd, M. B. and J. T. Thorson. 2018. Accounting for variable recruitment and fishing mortality in length-based stock assessments for data-limited fisheries. *Canadian Journal of Fisheries and Aquatic Sciences*, **75**:1019–1035.
- Rudd, M. B., J. T. Thorson, and S. R. Sagarese. In prep. Ensemble models for data-poor assessment: the value of life-history information. page 39.
- Russ, G. R. and A. C. Alcala. 2004. Marine reserves: long-term protection is required for full recovery of predatory fish populations. *Oecologia*, **138**:622–627.
- Russell, M. W., Y. S. de Mitcheson, B. E. Erisman, R. J. Hamilton, B. E. Luckhurst, and R. S. Nemeth. 2014. Status Report World's Fish Aggregations 2014. page 13.
- Russell, M. W., B. E. Luckhurst, and K. C. Lindeman. 2012. Management of Spawning Aggregations. In Y. Sadovy de Mitcheson and P. L. Colin, editors, *Reef Fish Spawning Aggregations: Biology, Research and Management*, pages 371–404. Springer Netherlands, Dordrecht.
- Sadovy, Y., A. Aguilar-Perera, and E. Sosa-Cordero. 2018. *Epinephelus striatus*. The IUCN Red List of Threatened Species 2018: e.T7862A46909843. <http://dx.doi.org/10.2305/IUCN.UK.2018-2.RLTS.T7862A46909843.en>.
- Sadovy, Y. and M. Domeier. 2005. Are aggregation-fisheries sustainable? Reef fish fisheries as a case study. *Coral Reefs*, **24**:254–262.
- Sadovy, Y. and A.-M. Eklund. 1999. Synopsis of Biological Data on the Nassau Grouper, *Epinephelus striatus* (Bloch, 1792), and the Jewfish, *E. itajara* (Lichtenstein, 1822). Technical Report NOAA Technical Report NMFS 146. A Technical Report of the Fishery Bulletin. FAO Fisheries Synopsis 157., U.S. Department of Commerce.

- Sadovy de Mitcheson, Y. 2016. Mainstreaming fish spawning aggregations into fishery management calls for a precautionary approach. *BioScience*, **66**:295–306.
- Sadovy de Mitcheson, Y. and P. L. Colin, editors. 2012*a*. Reef Fish Spawning Aggregations: Biology, Research and Management. Springer Netherlands, Dordrecht.
- Sadovy de Mitcheson, Y. and P. L. Colin. 2012*b*. Species Case Studies. In Y. Sadovy de Mitcheson and P. L. Colin, editors, Reef Fish Spawning Aggregations: Biology, Research and Management, pages 405–565. Springer Netherlands, Dordrecht.
- Sadovy de Mitcheson, Y., A. Cornish, M. Domeier, P. L. Colin, M. Russell, and K. C. Lindeman. 2008. A global baseline for spawning aggregations of reef fishes. *Conservation Biology*, **22**:1233–1244.
- Sadovy de Mitcheson, Y. and B. Erisman. 2012. Fishery and Biological Implications of Fishing Spawning Aggregations, and the Social and Economic Importance of Aggregating Fishes. In Y. Sadovy de Mitcheson and P. L. Colin, editors, Reef Fish Spawning Aggregations: Biology, Research and Management, pages 225–284. Springer Netherlands, Dordrecht.
- Sala, E., E. Ballesteros, and R. M. Starr. 2001. Rapid decline of Nassau Grouper spawning aggregations in Belize: Fishery management and conservation needs. *Fisheries*, **26**:23–30.
- Sala, E. and S. Giakoumi. 2018*a*. Counterpoint to Hilborn. *ICES Journal of Marine Science*, **75**:1163–1164.
- Sala, E. and S. Giakoumi. 2018*b*. No-take marine reserves are the most effective protected areas in the ocean. *ICES Journal of Marine Science*, **75**:1166–1168.
- Semmens, B., S. Heppell, P. Bush, C. Pattengill-Semmens, C. McCoy, and B. Johnson. 2013. Evidence of episodic mass recruitment of Nassau Grouper in the Cayman Islands. In Proceedings of the 65th Gulf and Caribbean Fisheries Institute, page 199. Santa Marta, Columbia.
- Semmens, B. X., P. Bush, S. Heppell, B. Johnson, C. McCoy, C. Pattengill-Semmens, and S. S. Heppell. 2009. The spatial ecology of a remnant Nassau Grouper stock on Cayman Brac, Cayman Islands. In Proceedings of the 61st Gulf and Caribbean Fisheries Institute. Gosier, Guadeloupe, French West Indies.
- Semmens, B. X., P. Bush, S. Heppell, C. Pattengill-Semmens, C. McCoy, and B. Johnson. 2012. An in situ visual mark-recapture method to assess the abundance of spawners at an aggregation site. In Proceedings of the 64th Gulf and Caribbean Fisheries Institute, pages 224–226. Puerto Morelos, Mexico.
- Semmens, B. X., K. E. Luke, P. G. Bush, C. Pattengill-Semmens, B. Johnson, C. McCoy, and S. Heppell. 2007. Investigating the reproductive migration and spatial ecology of Nassau Grouper (*Epinephelus striatus*) on Little Cayman Island using acoustic tags – An Overview. In Proceedings of the 58th Annual Gulf and Caribbean Fisheries Institute, pages 199–206. San Andres, Columbia.

- Sherman, K., C. Dahlgren, J. Stevens, and C. Tyler. 2016. Integrating population biology into conservation management for endangered Nassau grouper *Epinephelus striatus*. *Marine Ecology Progress Series*, **554**:263–280.
- Smith, C. L. 1972. A spawning aggregation of Nassau Grouper, *Epinephelus striatus* (Bloch). *Transactions of the American Fisheries Society*, **101**:257–261.
- Smith, M. W., A. Y. Then, C. Wor, G. Ralph, K. H. Pollock, and J. M. Hoenig. 2012. Recommendations for catch-curve analysis. *North American Journal of Fisheries Management*, **32**:956–967.
- Stallings, C. D. 2008. Indirect Effects of an Exploited Predator on Recruitment of Coral-Reef Fishes. *Ecology*, **89**:2090–2095.
- Starr, R., E. Sala, E. Ballesteros, and M. Zabala. 2007. Spatial dynamics of the Nassau grouper *Epinephelus striatus* in a Caribbean atoll. *Marine Ecology Progress Series*, **343**:239–249.
- Stobutzki, I., M. Miller, and D. Brewer. 2001. Sustainability of fishery bycatch: a process for assessing highly diverse and numerous bycatch. *Environmental Conservation*, **28**:167–181.
- Stobutzki, I. C., M. J. Miller, D. S. Heales, and D. T. Brewer. 2002. Sustainability of elasmobranchs caught as bycatch in a tropical prawn (shrimp) trawl fishery. *Fishery Bulletin*, **100**:800–821.
- Strathmann, R. R., T. P. Hughes, A. M. Kuris, K. C. Lindeman, S. G. Morgan, J. M. Pandolfi, and R. R. Warner. 2002. Evolution of local recruitment and its consequences for marine populations. *Bulletin of Marine Science*, **70**:20.
- Szuwalski, C. S., K. A. Vert-Pre, A. E. Punt, T. A. Branch, and R. Hilborn. 2015. Examining common assumptions about recruitment: a meta-analysis of recruitment dynamics for worldwide marine fisheries. *Fish and Fisheries*, **16**:633–648.
- Thompson, R. and J. L. Munro. 1978. Aspects of the biology and ecology of Caribbean reef fishes: Serranidae (hinds and groupers). *Journal of Fish Biology*, **12**:115–146.
- Thorson, J. T. 2017. FishLife: Estimate fish traits for all marine fish species globally. v1.0.2. <https://github.com/James-Thorson/FishLife>.
- Thorson, J. T., S. B. Munch, J. M. Cope, and J. Gao. 2017. Predicting life history parameters for all fishes worldwide. *Ecological Applications*, **27**:2262–2276.
- Tucker, J., P. G. Bush, and S. T. Slaybaugh. 1993. Reproductive patterns of Cayman Islands Nassau Grouper (*Epinephelus striatus*) populations. *Bulletin of Marine Science*, **52**:961–969.
- Tupper, M. and M. A. Rudd. 2002. Species-specific impacts of a small marine reserve on reef fish production and fishing productivity in the Turks and Caicos Islands. *Environmental Conservation*, **29**:484–492.

- Walters, C. J. and S. J. D. Martell. 2004. Fisheries ecology and management. Princeton University Press.
- Waterhouse, L., S. Heppell, C. V. Pattengill-Semmens, C. M. McCoy, B. Johnson, and B. X. Semmens. In prep. Monitoring recovery of a heavily exploited aggregating species: Nassau Grouper (*Epinephelus striatus*) in the Cayman Islands.
- Watson, D. L., E. S. Harvey, M. J. Anderson, and G. A. Kendrick. 2005. A comparison of temperate reef fish assemblages recorded by three underwater stereo-video techniques. *Marine Biology*, **148**:415–425.
- Weiser, C. 2016. mvQuad: Methods for multivariate quadrature. v1.0-6. <https://CRAN.R-project.org/package=mvQuad>.
- Whaylen, L., P. Bush, B. Johnson, K. E. Luke, C. Mccoy, B. Semmens, and M. Boardman. 2007. Aggregation dynamics and lessons learned from five years of monitoring at a Nassau grouper (*Epinephelus striatus*) spawning aggregation in Little Cayman, Cayman Islands, BWI. In Proceedings of the 59th Annual Gulf and Caribbean Fisheries Institute, pages 479–488. Belize City, Belize.
- Whaylen, L., C. V. Pattengill-Semmens, B. X. Semmens, P. G. Bush, and M. R. Boardman. 2004. Observations of a Nassau grouper, *Epinephelus striatus*, Spawning Aggregation Site in Little Cayman, Cayman Islands, Including Multi-Species Spawning Information. *Environmental Biology of Fishes*, **70**:305–313.
- Williams, K., C. N. Rooper, and R. Towler. 2010. Use of stereo camera systems for assessment of rockfish abundance in untrawlable areas and for recording pollock behavior during midwater trawls. *Fishery Bulletin*, **108**:352–362.
- Winemiller, K. O. and K. A. Rose. 1992. Patterns of Life-History Diversification in North American Fishes: implications for Population Regulation. *Canadian Journal of Fisheries and Aquatic Sciences*, **49**:2196–2218.
- Worm, B., R. Hilborn, J. K. Baum, T. A. Branch, J. S. Collie, C. Costello, M. J. Fogarty, E. A. Fulton, J. A. Hutchings, S. Jennings, O. P. Jensen, H. K. Lotze, P. M. Mace, T. R. McClanahan, C. Minto, S. R. Palumbi, A. M. Parma, D. Ricard, A. A. Rosenberg, R. Watson, and D. Zeller. 2009. Rebuilding global fisheries. *Science*, **325**:578–585.

Chapter 4

3-dimensional advection, diffusion, and mortality of eggs and larvae dispersing from a Nassau Grouper (*Epinephelus striatus*) spawning aggregation observed with a novel plankton imaging system

Abstract

Fisheries biologists' quest to disentangle the roles of fishing from the environment often centers on understanding recruitment, as it largely determines fluctuation in adult abundance. Recruitment variability is driven by physical-biological processes that mediate the survival and dispersal of egg and larval stages. In addition, the degree of self-recruitment and population connectivity via larval dispersal is important to the population dynamics and spatial management of fish with limited adult movement, e.g. tropical reef fish. For all of these reasons, understanding the fate of eggs and larvae is a critical part of efforts to characterize population processes. Satellite-tracked drifter releases and physical-biological models are frequently applied to study dispersal, but their assumptions often go untested without direct field data of egg and larvae distributions. In this study, we demonstrated the ability of a novel in situ plankton imaging system to observe the 3D positions of individual eggs and larvae around drogued drifters. The egg and larvae images were of sufficient resolution to clearly distinguish development stages. We then used these fine-scale spatiotemporal data to statistically fit parameters of a 3-dimensional diffusion-mortality model for two cohorts of Nassau Grouper eggs as they dispersed following spawning in 2017. Finally, we used our estimates of diffusivity and mortality to predict the spread of eggs and larvae around previous years' drifter tracks in order to evaluate the possibility of self-recruitment. Our results confirm that drogued drifters track eggs at least until hatching (23–26 hours), and suggest self-recruitment as a possible mechanistic explanation for the strong 2011 year class of Nassau Grouper on Little Cayman Island.

4.1 Introduction

Recruitment, i.e. survival from the egg stage to adult stage and entering the fishery, is highly variable in most marine fish and thought to be the principal driver of natural variability in adult abundance (Miller and Kendall, 2009; Hjort, 1914; Leggett and DeBlois, 1994). This is the case because, for fish that spawn in the water column, mortality is generally highest during the egg stage and decreases as larvae grow and develop (Bailey and Houde, 1989; Peterson and Wroblewski, 1984; Fuiman et al., 2015). Thus, small changes in mortality rates at these stages can have disproportionate impacts on the adult population size. Understanding the mechanisms that drive variability in recruitment is, therefore, important to explaining and predicting past and future changes in adult numbers. Fisheries scientists have long known that differences in egg and larval survival are key to recruitment variability (Hjort, 1914). Although many researchers have since refined and expanded on Hjort's hypotheses (Houde, 2008), evidence has mounted that mortality of the early life history stages largely dictates recruitment variability and deserves research into its causal mechanisms (Cushing, 1975).

Three important processes govern successful recruitment: larvae must eat enough prey, avoid predation, and disperse to suitable habitat (Bailey and Houde, 1989). Disentangling the relative importance of these processes is difficult because of the interactions between feeding, growth, capability development, and mortality (Leggett and DeBlois, 1994). Still, Bailey and Houde (1989) concluded that predation was likely more important than starvation, and perhaps especially so in tropical reef systems (Johannes, 1978). Much less is known about tropical reef fish recruitment and its causal mechanisms than for temperate fish. For example, there are very few stock assessments or stock–recruitment relationships for tropical reef fish (Szuwalski et al., 2015), and recruitment hypotheses based on temperate ecosystems simply may not apply to the tropics (e.g. timing of spring bloom and the match-mismatch hypothesis; Cushing, 1990). In addition to predation, dispersal is considered to be particularly important to reef fish recruitment. Until the late 1990s, larval dispersal was assumed to be long-range and determined by mean surface currents (e.g. Roberts, 1997). This

paradigm has been convincingly overturned, however, by many studies demonstrating that reef fish recruitment is often local (Jones et al., 1999; Cowen et al., 2000; Cowen, 2006; Swearer et al., 1999; Thorrold et al., 2001; Jones, 2015; Jones et al., 2005). Work in the last decade has progressed to explain mechanisms allowing self-recruitment, e.g. how reef fish can detect, orient to, and capably swim towards home reefs (Gerlach et al., 2007; Leis et al., 2013; Leis, 2015; Staaterman et al., 2012; Irisson et al., 2015; Atema et al., 2015; Kingsford et al., 2002). The next step in the progression is to record the variability in physical and biological conditions and how they relate to recruitment in the tropical reef fish, with the ultimate aim of predicting future recruitment in order to inform appropriate management.

Dispersal, connectivity, and the degree of self-recruitment of fish populations are hugely important to population dynamics and management (Strathmann et al., 2002; Fogarty and Botsford, 2007; Cowen and Sponaugle, 2009). First, connectivity determines the appropriate scale of management. If self-recruitment dominates, then the population size and growth rate are relatively insensitive to the periodic arrival of external recruits. This simplifies management, as local protections will directly benefit local populations. If dispersal dominates, local actions have less effect and population-scale impacts of fishing depend on the connectivity between locations. Second, connectivity matters in the design and evaluation of marine reserves (Jennings, 2001). For example, to determine if a reserve benefits a fishery, it is necessary to measure the extent of larval exchange from the reserve to fished areas (Fogarty and Botsford, 2007).

Yet, it is difficult to directly estimate diffusion or mortality of fish eggs in the open ocean—the entire egg distribution must be sampled, and physical transport must be accounted for (Helbig and Pepin, 1998; Davis et al., 1991; McGurk, 1989; Gawarkiewicz et al., 2007). Researchers have used many methods to quantify dispersal, reviewed by (Cowen and Sponaugle, 2009) and (Jones, 2015): drogued drifters (either long-range, satellite-tracked; Richardson (2005); or cheaper, short-range GPS-tracked; Méndez-Jiménez et al. (2015); Johnson et al. (2003)), otolith microchemistry (Thorrold et al., 2001), biophysical models (Miller, 2007; Cowen, 2006), and genetics (Taylor, 2003;

Jackson et al., 2014). Drifters are a particularly attractive option to approximate the dispersal of eggs and larvae for reef fish that form large fish spawning aggregations (FSAs), where all of the annual reproductive output may be released over a few days and from a well-defined spatial location that is consistent across years (Méndez-Jiménez et al., 2015; Colin, 2012, 1992; Heppell et al., 2009, 2011; Cimino et al., 2018). The simplest biophysical models of dispersal are advection-diffusion-mortality models, which typically assume constant diffusivity in each direction and do not include larval behavior, mesoscale physical features, or complex coastlines (McGurk, 1989; Hill, 1991; Largier, 2003; Roberts, 1997; Siegel et al., 2003; Hill, 1990). In the last two decades, individual-based coupled physical-biological models have included increasing realism, although they are often not informed by direct field data (Miller, 2007; Cowen and Sponaugle, 2009; Gawarkiewicz et al., 2007). Implicit in the use of drifters and biophysical models are that the eggs and larvae actually remain with the drifters and simulated particles. This assumption of these commonly applied tools is rarely tested using field observations of egg and larval concentrations. Models have taught us much about fish egg and larval transport, but they are infrequently validated by in situ (Gawarkiewicz et al., 2007).

The ultimate goal of this work is to understand the role of physical-biological processes in determining recruitment and connectivity of tropical reef fish populations. In this study, we demonstrate the ability of a novel in situ towed plankton imaging system to observe the 3D positions of individual eggs and larvae. We then use this fine-scale spatiotemporal data to statistically fit parameters of a 3-dimensional diffusion-mortality model of Nassau Grouper eggs as they dispersed from their origin following spawning in 2017. Finally, we use our estimates of diffusivity and mortality to predict the spread of eggs and larvae around previous years' drifter tracks in order to evaluate the possibility of self-recruitment. Our results confirm that drogued drifters track eggs at least until hatching (23–26 hours), and suggest self-recruitment as a possible mechanistic explanation for a previously observed strong year class of Nassau Grouper (Stock et al., in prep).

4.2 Methods

Study species: Nassau Grouper

Nassau Grouper are ecologically, economically, and culturally important predatory reef fish in the Caribbean (Sadovy and Eklund, 1999; Mumby, 2006; Stallings, 2008). They form large (hundreds to tens of thousands), transient (6–8 days) fish spawning aggregations (FSAs) that are highly predictable, typically following one or two full moons per year at a given location (Whaylen et al., 2007; Smith, 1972; Whaylen et al., 2004; Sadovy and Eklund, 1999). The 2–4 days over which spawning occurs at these FSAs likely represents the total annual reproduction for the species (Whaylen et al., 2007). FSAs are targeted by fishermen and easy to overharvest even with simple fishing methods such as small skiffs and handlines (Smith, 1972; Sala et al., 2001). Heavy fishing of these FSAs is a difficult management problem because population declines are often masked by stable catch-per-unit-effort trends (i.e. hyperstability, Hilborn and Walters, 1992). As a result, Nassau Grouper have dramatically declined throughout their range and are currently listed as Critically Endangered by the IUCN and Threatened under the United States' Endangered Species Act (Sadovy and Eklund, 1999; NMFS, 2016; Sadovy et al., 2018). Several nations have instituted protections for the species, but populations have failed to recover in many places (Sadovy de Mitcheson and Colin, 2012). Recovery hinges upon successful spawning and recruitment, yet little is known about the necessary conditions for this to occur or what happens to the eggs and larvae after spawning.

Nassau Grouper early life history has been described by lab-reared collections of eggs at FSAs or induced ovulation of captured females. Eggs are transparent, spherical, 0.86–1.02 mm in diameter, neutrally buoyant at 32‰ salinity, and typically contain a single oil globule (Tucker et al., 1991; Powell and Tucker, 1992; Waterhouse et al., in prep). Time to hatching is temperature-dependent and takes roughly 24–27 hours at 26 °C (Powell and Tucker, 1992; Watanabe et al., 1995; Colin et al., 1987). Recently hatched larvae are unpigmented and slightly curved around

their yolk-sac and (Powell and Tucker, 1992). At 3–4 days post hatch (dph), larvae begin feeding and gain pigmentation in the eyes and caudal peduncle. By 5–7 dph, larvae exhaust their yolk and oil reserves and will starve if unfed (Watanabe et al., 1995; Waterhouse et al., in prep^b). Larval swimming speed and endurance greatly increases after notochord flexion (Clark et al., 2005; Leis et al., 2009), which occurs around 5–6.5 mm and 16–20 dph in Nassau Grouper (Powell and Tucker, 1992). The few measurements of swimming speed for postflexion Serranidae and Epinephelidae larvae indicate that they can swim 25–35 cm s⁻¹ at settlement stage (Fisher et al., 2005; Leis et al., 2009). Larvae transition from pelagic to juvenile habitat around 35–45 dph and 20–27 mm length, with settlement possibly aided by onshore water movement during flood tides and storms (Colin et al., 1997; Shenker et al., 1993). Nassau Grouper sexually mature and recruit to the spawning population between 4–7 years old (Sadovy and Eklund, 1999).

The Nassau Grouper FSA off the west end of Little Cayman Island is the largest quantitatively assessed FSA for the species (Sadovy et al., 2018). The population declined to roughly 1,500 individuals following heavy fishing in 2001–2001, but has since recovered in both numbers and size structure. By the time of this study in 2016–2017, the FSA comprised 4,200–5,400 fish (Waterhouse et al., in prep^a). Acoustic tagging studies have found that adult Nassau Grouper on Little Cayman and a neighboring island, Cayman Brac, remain on the island on which they are tagged and do not cross the deep water between them (Semmens et al., 2007, 2009). Thus, the observed population increase has been driven by recruitment and not by immigration of adults. A length-based stock assessment found that recruitment has been highly variable with one particularly strong year class spawned in 2011 that joined the FSA in 2017 (Stock et al., in prep). Although undocumented, the possibility of Nassau Grouper larvae settling near the FSA where they were spawned (i.e. self-recruitment) has long been hypothesized based on general circulation patterns and observations of satellite-tracked drifters, both in the Cayman Islands and elsewhere (Colin et al., 1987, 1997; Heppell et al., 2009, 2011).

Study location

Nassau Grouper aggregate to spawn at the southwestern tip of the Little Cayman shelf (Figs. 4.1, 4.2). The shelf slopes very gradually to 30 m depth and then abruptly drops to over 500 m (Kobara and Heyman, 2008). The benthic habitat is composed of alternating sand valleys and ridges of hard and soft corals and sponges (Whaylen et al., 2004). During the day, Nassau Grouper form a band along the shelf edge, with some individuals scattered nearby on the bottom. Spawning begins shortly after sunset and lasts about one hour. Small groups of 10–15 individuals rapidly ascend and release gametes between 20–30 m, then return to the bottom (Sadovy and Eklund, 1999). Prevailing winds and currents are westward, and the FSA site is on the leeward side of the island. Currents at the FSA site are complex, vary vertically, and range from slack to 3 knots (Whaylen et al., 2004).

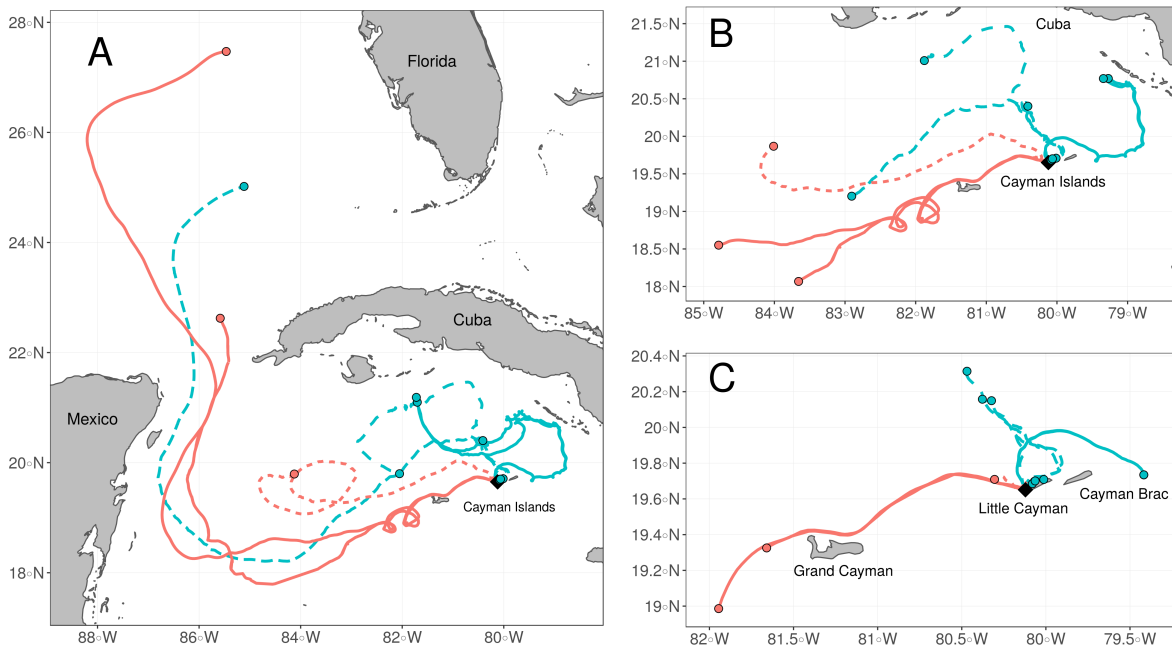


Figure 4.1: Satellite-tracked drifters released from the Little Cayman FSA (black diamond) on nights of spawning in 2016 (red) and 2017 (blue). Subsequent nights of spawning in a given year are distinguished by line type (2 in 2016, 4 in 2017). A) After 40 days, roughly the end of the larval duration period, three drifters had entered the Gulf of Mexico while the other ten remained in the northwest Caribbean. B) After 20 days, when larvae complete flexion, the two drifters released on Feb 14, 2017 were within 15–20 km of the Cuban archipelago Jardines de la Reina (top-right, blue solid lines). C) After 4 days, at first feeding, there was substantial variability in drifter location between and within years (west, north, east, and grounded on Little Cayman). All releases were standard Surface Velocity Program (SVP) drifters drogued at 15 m depth.

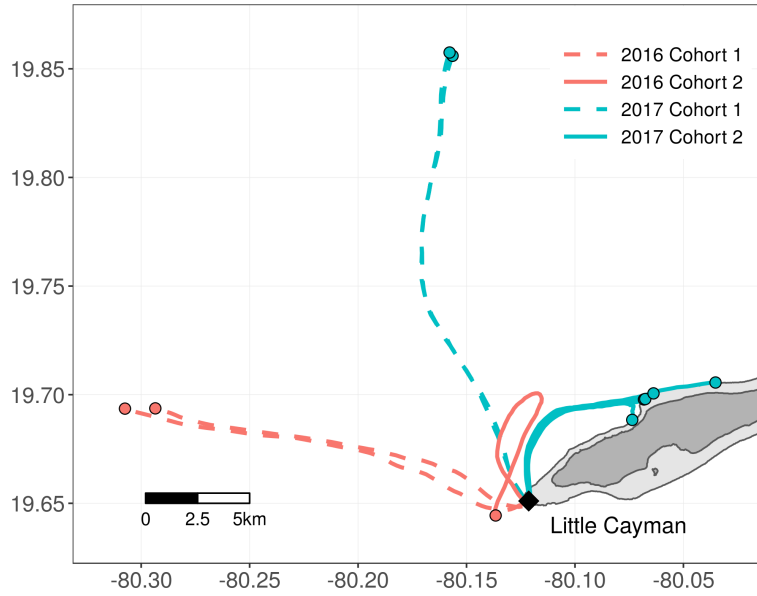


Figure 4.2: 20-hour drifter tracks from sampled spawning nights: Feb 25, 2016 (dashed red), Feb 26, 2016 (solid red), Feb 14, 2017 (dashed blue), and Feb 15, 2017 (solid blue). All five drifters released on Feb 15, 2017 grounded on the north side of Little Cayman Island within 20 hours. Light grey indicates the Little Cayman shelf (0–30 m depth).

Drifter deployments

On four nights of spawning in 2016 (Feb 25, 26) and 2017 (Feb 14, 15), we released standard drogued surface velocity program (SVP) drifters to track currents at 15 m depth (Pacific Gyre, Inc. and Global Drifter Program). On Feb 14, 2017, two drifters were released near the end of the evening’s spawning. On Feb 15, 2017, we released five drifters staggered throughout the hour of spawning. Divers signaled to the boat when and where spawning was occurring by sending a float to the surface. The drifters served as visual references for sampling, and we affixed strobes (ACR Firefly PRO SOLAS) to the drifter floats to enable visual tracking at night.

Plankton imaging systems

We sampled the concentration of eggs around the drifters with two different in situ towed plankton imaging systems in 2016 and 2017, both based on the Scripps Plankton Camera (SPC;

Jaffe, 2016; Roberts et al., 2014). The SPC uses darkfield illumination and is composed of two coupled pressure housings. One holds a telecentric imaging lens, camera, computer, and interface electronics. The second holds a set of high intensity LED strobes and illumination optics. The onboard computer controls image acquisition, processing, and storage. Raw images are segmented into regions of interest (ROIs) in real-time, and only these ROIs are saved. Hereafter, ROIs will be referred to as images. Because these ROIs were saved but not collated or summarized in real-time, we attempted to survey the egg patch by towing the imaging systems along alternating 1–2 km transects perpendicular and parallel to the drifter trajectories. In both years we used the Cayman Islands Department of the Environment R/V Seakeeper (46 foot Newton) to tow the imaging systems.

In 2016 we used the ‘NetCam’, consisting of a plankton net (0.5 m diameter, 500 μm mesh) with two SPCs attached on the cod end (Fig. 4.3a; Jaffe, 2016). The two SPCs each imaged 17.3 mL per frame and captured 8 frames s^{-1} . Assuming the plankton net filtration efficiency was close to 100% (UNESCO, 1968), we calculated that the net concentrated plankton in the images by a factor of 30.9 by taking the ratio of the mouth area to the cod end area (i.e., $25^2/4.5^2 = 30.9$). The overall sampling rate was 8.55 L s^{-1} . The effective pixel size was 13.8 μm , constant throughout the field of view because the SPCs are telecentric. The NetCam was deployed with a fixed amount of line, allowing for only crude depth control by varying the towing speed. To account for the effect of tow speed on volume filtered per second, we divided by the real-time flow rate (Valeport Model 106 Current Meter) when calculating organism densities. We towed the NetCam around drifters released during spawning on Feb 25, 2016 for 4 hours. We cut sampling short as sea conditions worsened.

In 2017 we used a next-generation SPC microscope with much larger imaging volume, 627 mL, but lower resolution, 22.6 μm pixels. The frame rate was 7 s^{-1} , for a volume sampling rate of 4.4 L s^{-1} . We removed the plankton net and attached the SPC to an undulating towed vehicle (AcrobatTM, Sea Sciences, Inc.) and CTD (SBE 49, Sea-Bird Scientific), hereafter the ‘TowCam’, to better sample the vertical distribution of Nassau Grouper eggs through time (Fig. 4.3b). We

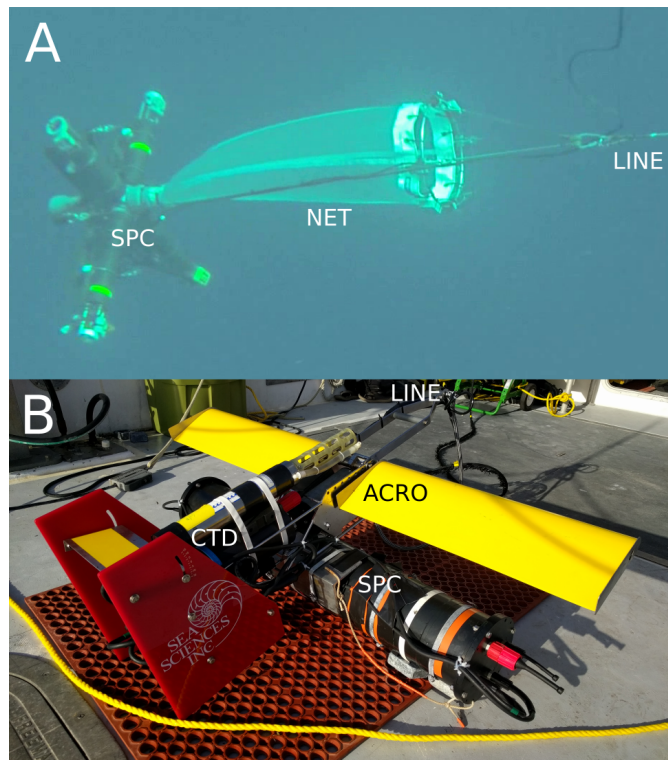


Figure 4.3: In situ plankton imaging systems used to measure Nassau Grouper egg concentration. A) In 2016, the ‘NetCam’ featured two Scripps Plankton Camera (SPC) microscopes in a cross pattern, each with 17.3 mL imaging volumes at the center of the cross. We attached a plankton net (NET) to concentrate plankton in the microscope images. Photo courtesy of Tammi Warrender. B) In 2017, the ‘TowCam’ used a next-generation SPC microscope with larger imaging volume and lower resolution. We attached the SPC to an undulating towed vehicle (ACRO, Acrobat™, Sea Sciences, Inc.) and CTD to measure egg concentration, temperature, and salinity in three dimensions.

towed the TowCam at 4–5 knots because vertical control was best at that speed. On Feb 14, 2017 we undulated the TowCam between 5–30 m depth for the first 6 hours at roughly 3 cycles km^{-1} , and switched to 1–30 m undulations after 6 hours. Vertical sampling on Feb 15, 2017 was complicated by the drifters initially moving north and remaining over the shelf (Figs. 4.2 and 4.13). To avoid hitting the reef (20–30 m depth), we undulated the TowCam at 2–10 m until the drifters moved off the shelf (hours 0–1.5), and then switched to the intended tow profile (5–30 m initially, then 2–30 at 7 hours). Around 14.5 hours when three of the drifters grounded on the reef, we shifted to sampling along the shelf edge at 3–15 m depths. The two remaining drifters became widely separated, and we sampled around the drifter that entered Bloody Bay during hours 30–36 post-spawning (Fig. 4.13).

Plankton sample collection

To groundtruth the in situ microscope images, we collected plankton samples using a variety of methods. While sampling with the NetCam on Feb 25, 2016, we towed a plankton net (30 cm diameter, 333 μm mesh) obliquely for 5 minutes starting at 17 m depth, centered on the drifters, at 2 and 3 hours post spawning. We sampled around the drifter released the subsequent night of spawning, Feb 26, 2016, with a bongo net (66 cm diameter, 200 μm mesh) approximately 20 and 40 hours after spawning. On nights of TowCam sampling in 2017, divers collected Nassau Grouper eggs by hand-towing a plankton net through the spawn cloud. These eggs were raised to hatch in aquaria at ambient temperature in filtered seawater to generate an image sequence of egg development. Finally, divers collected eggs from individual Nassau Grouper spawning bursts roughly 15–20 seconds after gamete release using plastic zipper bags in 2014, 2016, and 2017.

All plankton samples were split, half preserved in 2–5% formalin for visual analysis and half in 95% ethanol for genetic analysis. We sorted fish eggs in formalin-preserved samples, took photos under a dissecting microscope (Zeiss Stemi 2000-C, Cannon EOS Rebel T3), and measured egg diameters using ImageJ (Schneider et al., 2012), using a stage calibration slide to set the scale. We selected eight individual eggs from the ethanol-preserved samples covering a range of diameters

(0.56–1.00 mm) and identified them to species using DNA barcoding following the methods in Harada et al. (2015).

Image classification

The NetCam deployment on 2016 produced 49,904 images, which we manually classified using a custom MATLAB graphical user interface. The TowCam deployments in 2017 generated many more images (238,184), so we manually classified a subset and then trained a machine learning algorithm to predict plankton classes for the remaining images. We manually verified all of the algorithm-classified fish egg images and estimated the false positive rate. To estimate the false negative rate (i.e. true fish eggs missed by the algorithm), we manually identified fish eggs in a random sample of 20,000 images. The false negative rate is then the number of false negatives (i.e. images identified as fish eggs manually but not by the algorithm) divided by the number of true positives (total images identified as fish eggs manually). Since yolk-sac larvae were rare in the image dataset, we manually identified all images in the sampling period with possible yolk-sac larvae, hours 30–36 after spawning on Feb 15, 2017.

3-dimensional advection-diffusion-mortality model

We estimated horizontal diffusivity and mortality by fitting the Nassau Grouper egg concentration data ($\text{counts s}^{-1} = \text{counts [4.4L]}^{-1}$) from the two 2017 cohorts to a simple 3-dimensional model of advection, diffusion, and mortality. We did not fit the model to the NetCam data from 2016 because sampling was only conducted for 4 hours.

Assuming that the drifters captured the horizontal advection and there was no vertical current shear, we subtracted the locations of the drifter centroid from the egg concentration locations and removed advective terms. We assumed continuity (i.e. seawater was incompressible), constant mortality in space and time, and separability of vertical and horizontal diffusion (i.e. vertical diffusion did not vary horizontally, and horizontal diffusion did not vary vertically). These assump-

tions allowed us to model the egg concentration at depth z and time t , $C(z,t)$, independently from mortality, μ , and the concentration in horizontal space, $C(x,y,t)$, and then multiply the results to get the concentration at any point in 3-dimensional space and time:

$$C(x,y,z,t) = C(z,t) \times C(x,y,t)$$

Vertical diffusion

To model vertical diffusion, we used a particle-tracking (random-walk) model based on Tanaka and Franks (2008). The vertical diffusivity, $K_z(z)$, is a function of wind speed, U , and decays exponentially with depth, z :

$$K_z(z) = [K_1 + K_2 U^2] e^{-z/z_{MLD}}$$

where K_1 is the background diffusivity at the surface, K_2 scales the effect of wind speed on mixing, and z_{MLD} is the mixed layer (i.e. pycnocline) depth. This formulation is appropriate when there is weak vertical stratification (i.e. buoyancy frequency is \sim constant), as in the surface mixed layer. The wind speed and vertical stratification were relatively constant and weak during our experiment ($U = 2.2 \text{ m s}^{-1}$, Fig. 4.9). Therefore we reduced Eq. 1 to:

$$K_z = K_0 e^{-z/z_{MLD}},$$

which reduced the number of parameters by one. Ordinarily the initial condition does not matter much because the vertical distribution rapidly reaches equilibrium (in a few hours). However, a substantial portion of our observations came before equilibrium. We set the initial particle distribution for both cohorts as $\mathcal{N}(\mu = 26.4, \sigma = 3)$ to match the observed egg distribution of cohort 1 in the first hour, because we were unable to sample cohort 2 below 10 m. We simulated 10,000

particles, updating depths at time steps, $\Delta t = 10$ s, according to:

$$z_{n+1} = z_n + \frac{\partial K_z(z_n)}{\partial z} \Delta t + R \left[\frac{2K_z(z_n + \frac{1}{2} \frac{\partial K_z}{\partial z} \Delta t)}{r} \right]^{1/2} + w_s \Delta t$$

where R is a random process with mean zero and variance r , and w_s is the egg floating speed. Following Tanaka and Franks (2008) and Ross and Sharples (2004), we used $r = 1/3$, $R \sim \text{Unif}(-1, 1)$, and a reflecting boundary condition at the surface (i.e. a particle that diffuses a distance z above 0 m is placed at z m).

We used a floating speed of $w_s = -0.00169 \text{ ms}^{-1}$ based on Eq. 1 in Sundby (1983), average seawater properties measured during the experiment at 15 m depth, and egg salinity at neutral buoyancy of 32‰ (Tucker et al., 1991). This floating speed is close to the $w_s = -0.00183 \text{ ms}^{-1}$ value cited for the congeneric *E. fulva* (Colin, 1992). Following Sundby (1983), we gave the particles a range of floating speeds to account for individual egg differences in density and diameter, $w_s \sim \mathcal{N}(-0.000169, \sigma_w)$.

The unknown parameters in the above vertical diffusion model were diffusivity at the surface (K_0), pycnocline depth (z_{MLD}), and standard deviation of egg floating speed (σ_w). For each cohort in 2017, we ran the particle-tracking model over combinations of the parameters ranging from: K_0 (0.01–0.08), z_{MLD} (60–100), and σ_w (0.00015–0.00045). We took the 2D kernel density estimate of the particle distributions to be $\hat{C}(z, t)$, the predicted egg concentration at depth z and time t . We fit negative binomial generalized linear models (GLMs) of $\hat{C}(z, t)$ to the observed egg data, $Y_i \sim \text{NB}(\mu = e^{\alpha + \beta \hat{C}(z_i, t_i)})$, and selected the best model based on AIC. We used a negative binomial distribution because the egg counts showed evidence of overdispersion (positive slope in Ord plots, Fig. 4.4; Ord, 1967), and the negative binomial was supported by AIC over other possible distributions for count data (Table 4.1).

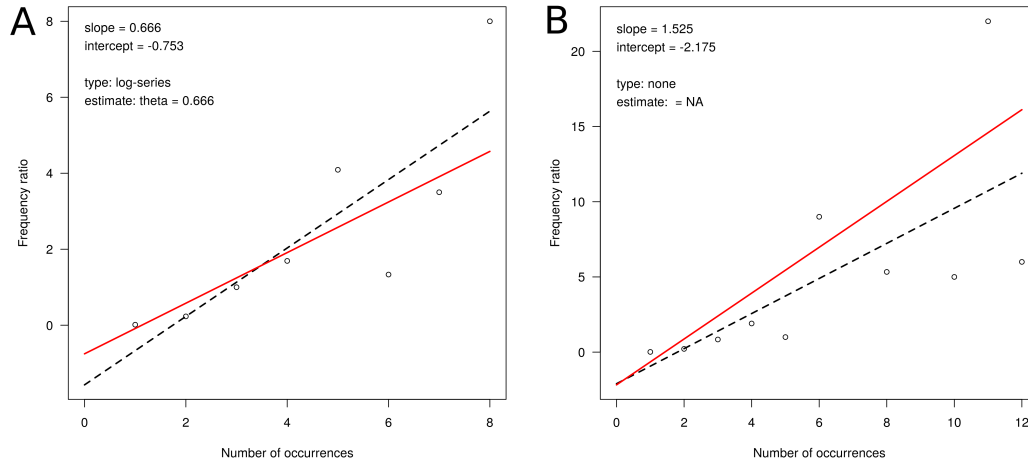


Figure 4.4: Ord plots of egg count data from cohorts 1 (A) and 2 (B). Positive slopes indicate overdispersion and that the negative binomial distribution is appropriate, while a horizontal line would indicate a Poisson.

Table 4.1: AIC table for considered distributions for the egg count data. The negative binomial distribution had the lowest AIC for both cohort 1 (AIC_1) and cohort 2 (AIC_2), indicating that overdispersion was more important than zero-inflation.

Model	AIC_1	ΔAIC_1	AIC_2	ΔAIC_2	df
Poisson	8061.761	328.1	9889.557	975.4	4
Zero-inflated Poisson	7780.313	46.7	9000.516	86.4	5
Negative Binomial	7733.615	0.0	8914.134	0.0	5
Zero-inflated Negative Binomial	7735.630	2.0	8916.129	2.0	6

Horizontal diffusion and mortality

We allowed for anisotropic horizontal diffusivity, i.e. $K_x \neq K_y$, and assumed that diffusivity was constant in each direction following Fick's Law, where the diffusive flux, J_x , is proportional to the concentration gradient, $J_x = K_x \frac{\partial C}{\partial x}$ (Okubo and Levin, 2010). Alternative models of diffusion may be more appropriate in general, but assuming Fickian diffusion was justifiable here because the size of the egg patch varied much less than one order of magnitude over the course of our observations (i.e. 500–1500 m; Okubo and Levin, 2010). Assuming an instantaneous point release at 19:00 local time, the horizontal egg concentration, $C(x, y, t)$, is given by McGurk (1989) and Hill (1991):

$$C(x, y, t) = \frac{1}{4\pi t \sqrt{K_x K_y}} e^{\left(-\frac{x^2}{4K_x t} - \frac{y^2}{4K_y t} - \mu t\right)}$$

However, instead of assuming eggs are evenly distributed throughout a water column of thickness H as in McGurk (1989), we multiply the horizontal concentration, $C(x, y, t)$, by the vertical concentration, $C(z, t)$, to get the egg concentration at any given x , y , z , and t , $C(x, y, z, t)$. We then fit the egg count data for observation i , $Y(x_i, y_i, z_i, t_i)$, with a negative binomial GLM using $C(x, y, z, t)$ as the expected mean:

$$Y(x_i, y_i, z_i, t_i) \sim \text{NB} \left(\mu = e^{\beta C(x_i, y_i, z_i, t_i)} \right)$$

We fit the model using maximum likelihood via the 'bbmle' package in R (v1.0.20; Bolker, 2017), and calculated confidence intervals for the parameters K_x , K_y , and μ using likelihood profiles. In addition to the model described above, we fit all nested submodels and evaluated the importance of including each parameter using AIC.

4.3 Results

Drifter trajectories

Drifters released from the Little Cayman FSA on nights of spawning exhibited substantial variability, both between years and nights within a given year (Figs. 4.1, 4.2). On one night in 2016 the drifters moved swiftly west, coming close to Grand Cayman around 3 days after spawning (Fig. 4.1c) before entering the Yucatan Current (Fig. 4.1a). On the following spawning night in 2016 the lone released drifter made a slow loop to the north, returned within 2 km of the FSA 20 hours after spawning (Fig. 4.2), and was still within 20 km of the FSA after 4 days (Fig. 4.1c).

The two drifters released on Feb 14, 2017 moved north and then east, coming within 15–20 km of the Cuban archipelago Jardines de la Reina after 20 days, when larvae complete flexion and become increasingly capable swimmers (Fig. 4.1b). All five drifters from Feb 15, 2017 grounded on the north side of Little Cayman within 20 hours (Figs. 4.2 and 4.13). Three of these had grounded by 15 hours on the protrusion marking the east end of Bloody Bay, while one continued east and the other entered Bloody Bay to the south (Figs. 4.2 and 4.13).

Lab-reared eggs

Of the eggs collected from spawning on Feb 14–15, 2017 and raised in aquaria, roughly 50% hatched between 23–26 hours post fertilization (hpf) and all eggs hatched by 28 hpf (Fig. 4.5).

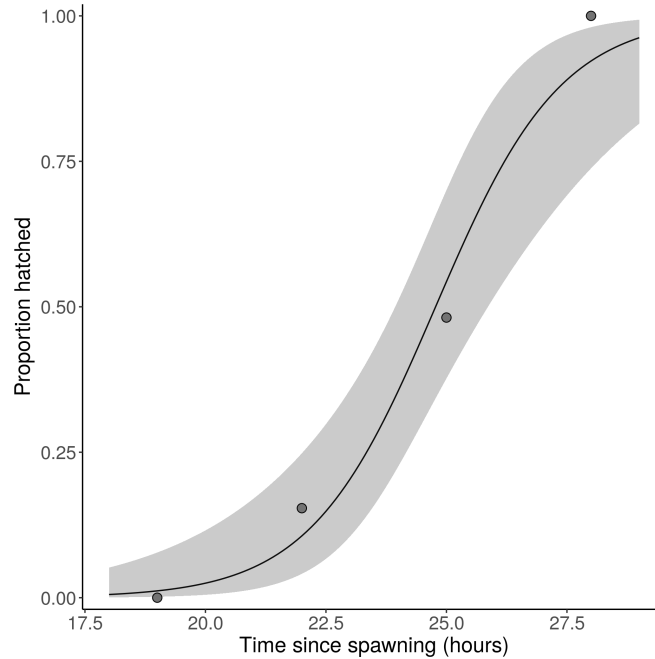


Figure 4.5: Hatching time of lab-reared Nassau Grouper eggs collected from spawning on Feb 14–15, 2017.

In situ microscope images

Of the 49,904 NetCam images from Feb 25, 2016, we manually identified 1,331 as fish eggs. Of the 238,184 TowCam images from Feb 14–15, 2017, the algorithm predicted 3,153 fish eggs. Manual verification identified 414 of these as false positives, which amounts to a false positive rate of 13.1%. Two of the images contained two overlapping eggs. Thus, the total count of fish eggs from 2017 sampling was 2,741. The false negative test detected one missed fish egg out of 195 true positives in 20,000 images, for a false negative rate of 0.51%. Manual identification of the images from cohort 2 in hours 30–36 revealed 47 yolk-sac larvae (Fig. 4.7n–r).

All methods indicated that egg diameter between 0.87–1.20 mm was a reliable metric to classify in situ fish egg images as Nassau Grouper eggs (Fig. 4.6). Of the 2,741 total fish egg images in 2017, 2,264 (82.6 %) were between 0.87–1.20 mm and classified as Nassau Grouper. None of the 89 fish eggs detected in sampling 30–36 hours post-spawning were 0.87–1.20 mm, when all Nassau Grouper eggs should have hatched into yolk-sac larvae.

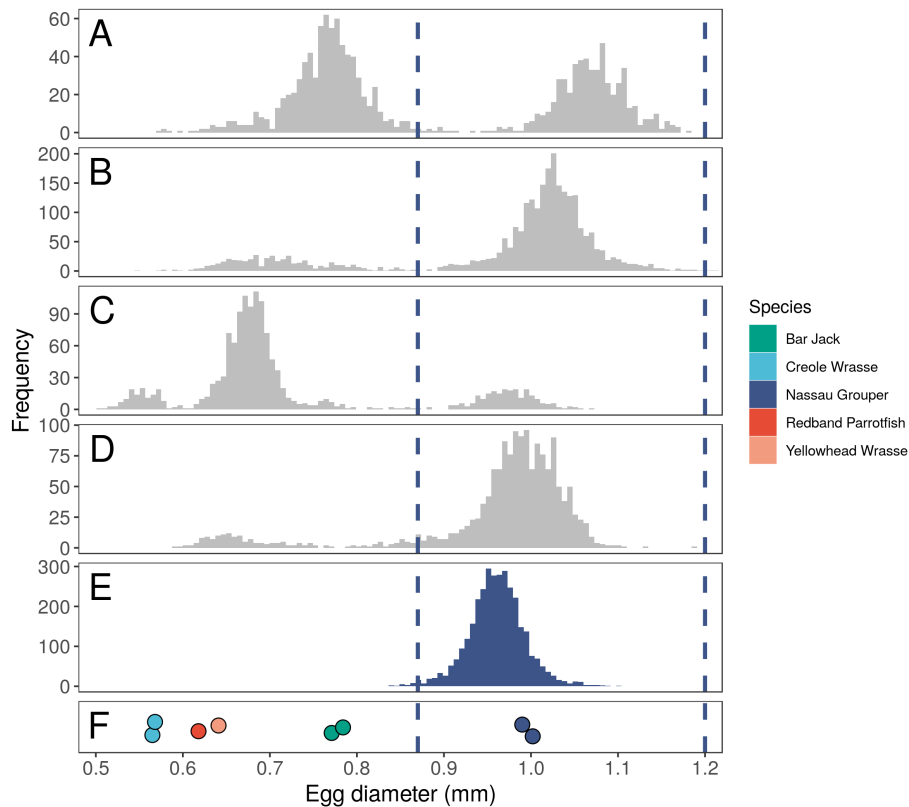


Figure 4.6: Diameters of fish eggs sampled near drifters using different methods: A) in situ NetCam images taken 1–5 hours after spawning on Feb 25, 2016 ($n = 1331$, 42% NG); B) in situ TowCam images taken 0–36 hours after spawning Feb 14–16, 2017 ($n = 2741$, 83% NG); C) plankton tows taken 3 and 4 hours after spawning Feb 25, 2016 ($n = 1386$, 17% NG); D) bongo net tows taken 20 and 40 hours after spawning Feb 26, 2016 ($n = 1604$, 88% NG); E) diver-collected samples of Nassau Grouper spawning bursts taken 10–30 seconds after spawning 2014–2017 ($n = 3317$, 99% NG); F) Eggs from C) identified to species using DNA barcoding ($n = 8$, 25% NG). Eggs of unknown species are shown in grey (A–D); eggs of known species are shown in color (E, F). All methods indicated that egg diameter between 0.87–1.2 mm (vertical dashed lines) was a reliable metric to classify fish egg microscope images as Nassau Grouper (= NG) eggs.

TowCam images were of sufficient resolution to distinguish Nassau Grouper egg and larval development stages (Fig. 4.7), following Kimmel et al. (1995). Egg and larval development in situ aligned well with the sequence of images of lab-reared eggs and larvae.

Of the 2,264 Nassau Grouper egg images, 10 (0.4%) showed possible predation by pelagic invertebrate zooplankton. Of these, 2 were of medusae, 1 was a polychaete, and 7 were radiolaria, likely spinose planktonic foraminifera (Fig. 4.8).

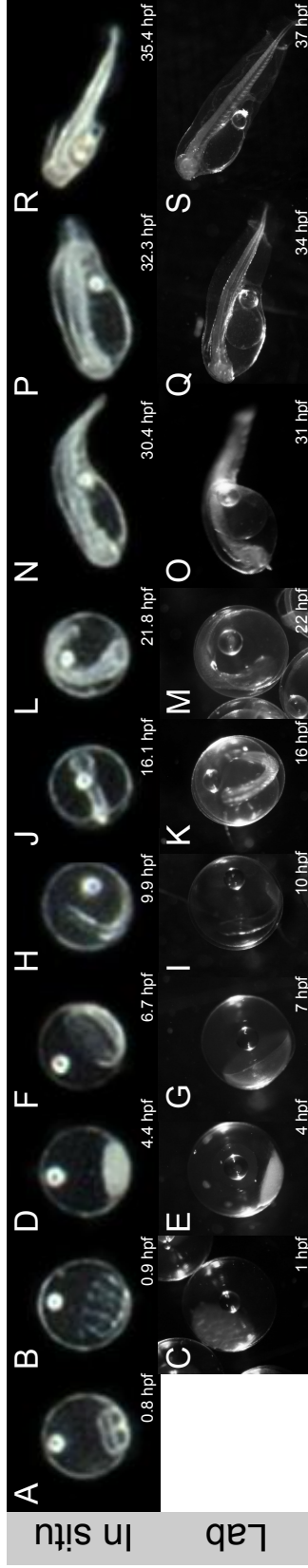


Figure 4.7: Image sequences showing Nassau Grouper egg and larvae development over 1–37 hours post fertilization (hpf). Top: In situ TowCam images taken around drifters following the egg patch from Feb 15, 2017. Bottom: Light microscope images of lab-reared eggs and larvae collected from the same spawn cloud of Feb 15, 2017. A) Early cleavage period, 4-cell stage (< 1 hpf). B–C) Late cleavage period, regular rows of blastomeres (1 hpf). D–E) Blastula period, yolk cell bulging (4 hpf). F–G) Early gastrula period, blastoderm is an inverted cup rising from animal pole to vegetal pole (7 hpf). H–I) Late gastrula period, rudimentary notochord visible (10 hpf). J–K) Segmentation period (16 hpf). L–M) Near hatching (22 hpf). N–O) Early yolk-sac larvae, notochord curved (31 hpf). P–Q) Early yolk-sac larvae, notochord straightening (32.3–34 hpf). R–S) Yolk-sac larvae, notochord straight and yolk reduced in size (35.5–37 hpf). Pixels in TowCam images are 22.6 μm .

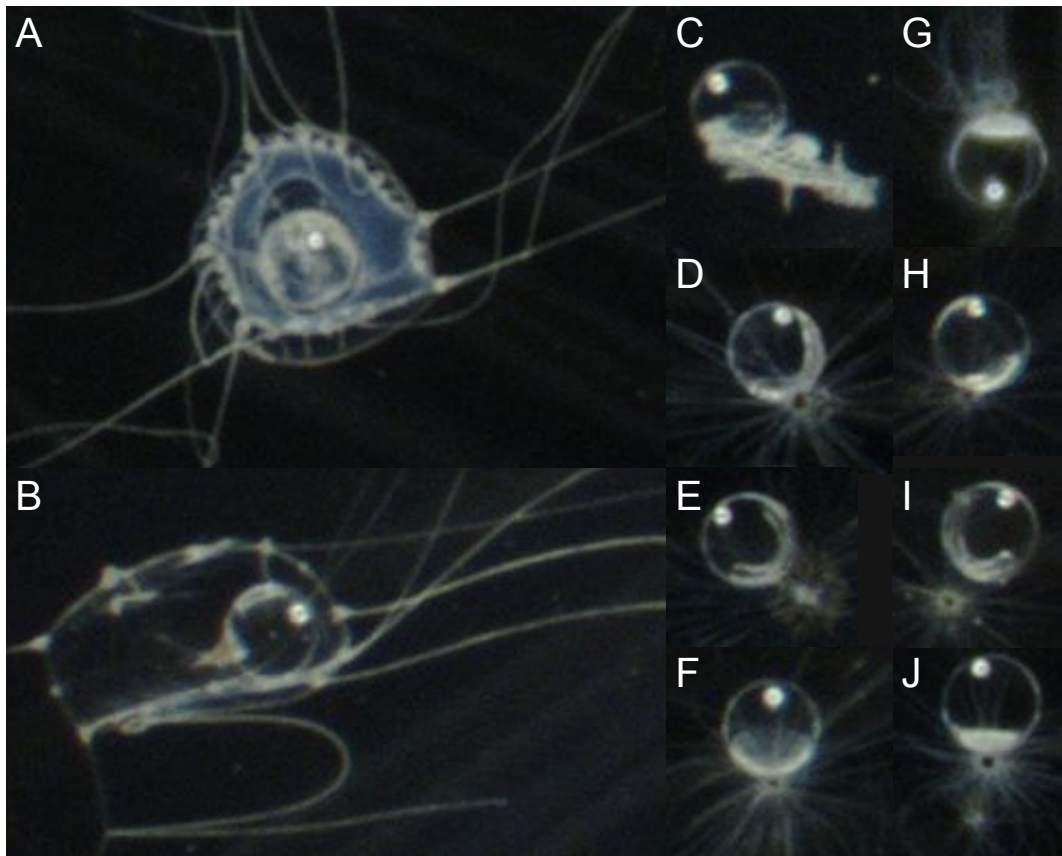


Figure 4.8: In situ microscope images of possible predation on Nassau Grouper eggs by pelagic invertebrate zooplankton. A, B) Medusae. C) Polychaete. D–J) Rhizaria, likely spinose planktonic foraminifera. Pixels in TowCam images are 22.6 μm and eggs are ~ 0.95 mm in diameter (Fig. 4.6e).

Cohort #1: Feb 14, 2017

The two drifters released at the Little Cayman FSA during spawning on Feb 14, 2017 traveled 18.3 km NNE during the 14.5 hours of sampling (average velocity 0.35 m s^{-1} , Fig. 4.2). The initial (first hour) vertical distribution of Nassau Grouper eggs was approximately normal with mean depth 26.4 m (standard deviation 2.7 m). The upper 30 m of the water column was weakly stratified ($\Delta\rho = 0.2 \text{ kg m}^{-3}$) with no pycnocline throughout sampling (Fig. 4.9).

The best fit (lowest AIC) model of vertical diffusion produced reasonable predictions of relative egg concentration and used $K_0 = 0.05 \text{ m}^2 \text{ s}^{-1}$, $z_{MLD} = 60 \text{ m}$, and $\sigma_w = 0.00045 \text{ m s}^{-1}$ (Fig. 4.10). The model predicted that eggs spawned at 26.4 m were spread throughout 0–30 m depths 1–3 hours after spawning, and accumulated in the upper 5 m beyond 3 hours after spawning.

Horizontal diffusion was clearly noticeable in the egg distribution over the 14.5 hours of sampling, as the egg patch increased in horizontal extent and the concentration at the center of the patch decreased through time (Fig. 4.11).

The horizontal diffusivity and mortality parameters were estimable in the 3D diffusion-mortality model and nested submodels (Table 4.2). The full model clearly fit the best (100% Akaike weight), and estimated horizontal diffusivity to be $K_x = 14900$ (95% CI: 12000–19000) $\text{m}^2 \text{ h}^{-1} = 4.1$ (95% CI: 3.3–5.3) $\text{m}^2 \text{ s}^{-1}$ in the x-direction and $K_y = 49100$ (95% CI: 40800–60500) $\text{m}^2 \text{ h}^{-1} = 13.6$ (95% CI: 11.3–16.8) $\text{m}^2 \text{ s}^{-1}$ in the y-direction. Instantaneous mortality was estimated as 0.172 h^{-1} , which implies that daily mortality was $1 - e^{-0.172 \times 24} = 0.984 \text{ d}^{-1}$ and 1.6% of the eggs survive to hatching at 24 hours. Estimating isotropic vs. anisotropic horizontal diffusion (i.e. $K_x = K_y$ vs. $K_x \neq K_y$) did not affect the mortality estimates (e.g., compare Models 1 vs. 2 and 3 vs. 5 in Table 4.2). However, including or excluding vertical or (especially) horizontal diffusion did impact the mortality estimates. The 3D diffusion-mortality model fit the observed data well and explained 24.2% of the deviance (Fig. 4.12).

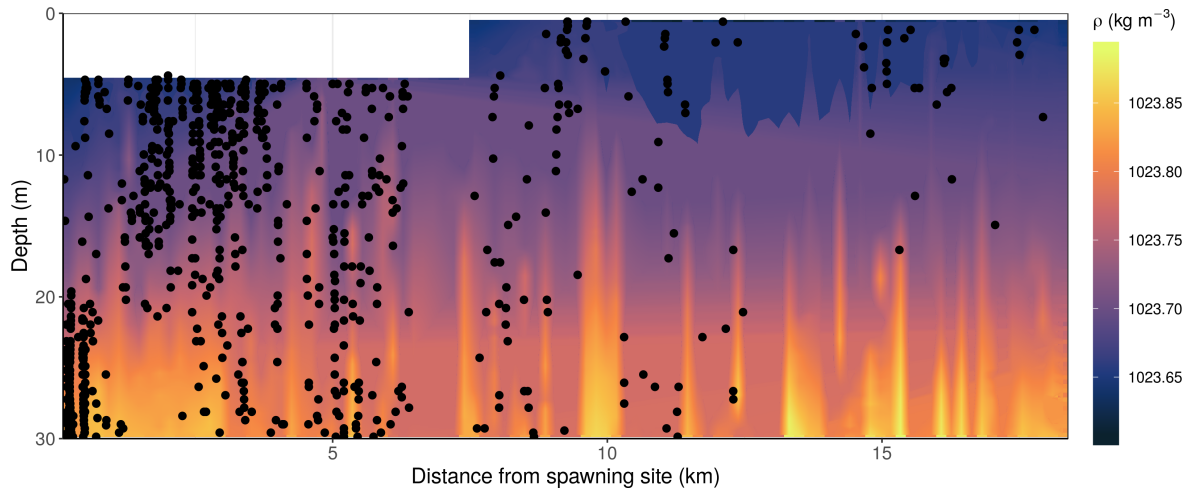


Figure 4.9: Vertical density profile and distribution of Nassau Grouper eggs along the track of the drifter centroid (blue dashed line in Fig. 4.2) following spawning for cohort 1 (Feb 14, 2017). Depths 0–5 m were not sampled for the first 6 hours. The upper 30 m of the water column was weakly stratified with no clear pycnocline. The drifters traveled 18.3 km from the FSA over 14.5 hours of sampling.

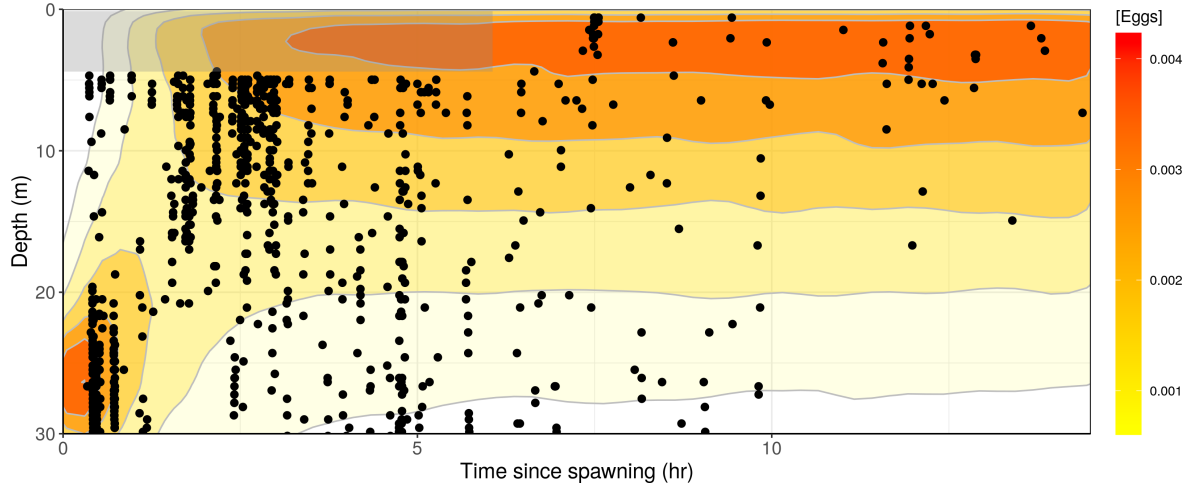


Figure 4.10: Best fit vertical diffusion model for Nassau Grouper eggs following spawning for cohort 1 (Feb 14, 2017). Predicted relative concentration is shown in color and contour lines. Black points indicate the time and depth of TowCam microscope images classified as Nassau Grouper eggs. The initial particle distribution was input as $\mathcal{N}(\mu = 26.4, \sigma = 3)$ to match the observed egg distribution in the first hour. Parameter values were $K_0 = 0.05 \text{ m}^2 \text{ s}^{-1}$, $z_{MLD} = 60 \text{ m}$, and $\sigma_w = 0.00045 \text{ m s}^{-1}$. Grey transparency shows depth-times that were not sampled (0–5 m in hours 0–6).

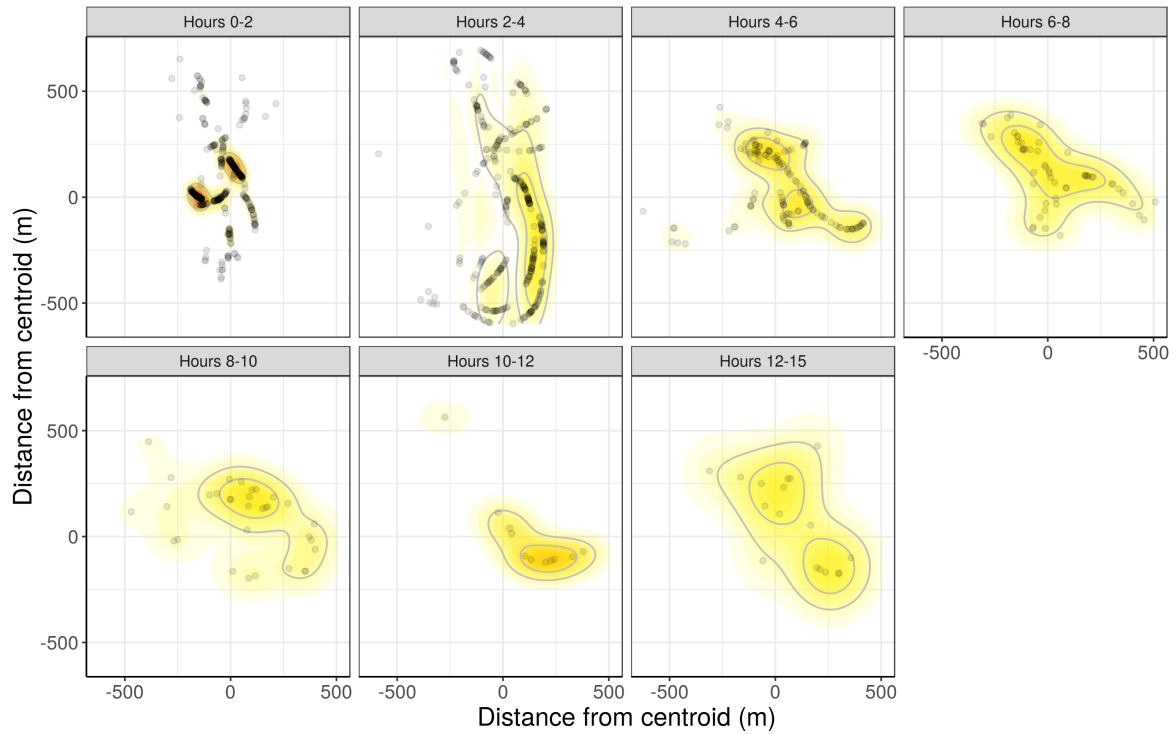


Figure 4.11: Horizontal diffusion of Nassau Grouper eggs in the 15 hours following cohort 1 spawning (Feb 14, 2017). Points are north-south (x-y) distances of individual Nassau Grouper eggs from the egg centroid (weighted average). Color and contour lines indicate 2D kernel density estimate of egg concentration within 2-hour time intervals.

Table 4.2: 3D diffusion-mortality model results for cohort 1 (Feb 14, 2017). Model 1 had the lowest AIC, and included anisotropic horizontal diffusivity ($K_x \neq K_y$), vertical diffusivity (K_z), and mortality (μ). Model parameters were estimated using maximum likelihood and non-symmetric 95%CI were calculated using likelihood profiles ('mle2' package in R).

Model	Δ AIC	Weight	K_x ($\text{m}^2 \text{hr}^{-1}$)	K_y ($\text{m}^2 \text{hr}^{-1}$)	μ (hr^{-1})
1) $K_x + K_y + K_z + \mu$	0.0	1	14900 (12000–19000)	49100 (40800–60500)	0.172 (0.148–0.197)
2) $K_x + K_z + \mu$	39.2	0	39400 (33900–46400)		0.166 (0.142–0.191)
3) $K_x + K_y + \mu$	143.2	0	14500 (11700–18600)	47000 (39200–57700)	0.171 (0.145–0.197)
5) $K_x + \mu$	180.6	0	38100 (32800–44800)		0.164 (0.139–0.191)
4) $K_x + K_y + K_z$	231.1	0	21300 (16400–29700)	89700 (68600–126000)	
8) $K_x + K_z$	256.9	0	65300 (53900–80800)		
6) $K_z + \mu$	333.7	0			0.359 (0.334–0.385)
7) $K_x + K_y$	352.7	0	21000 (16100–29100)	79900 (62300–108000)	
9) K_x	376.4	0	60300 (50200–73900)		
11) μ	549.7	0			0.348 (0.322–0.375)
10) K_z	1402.6	0			

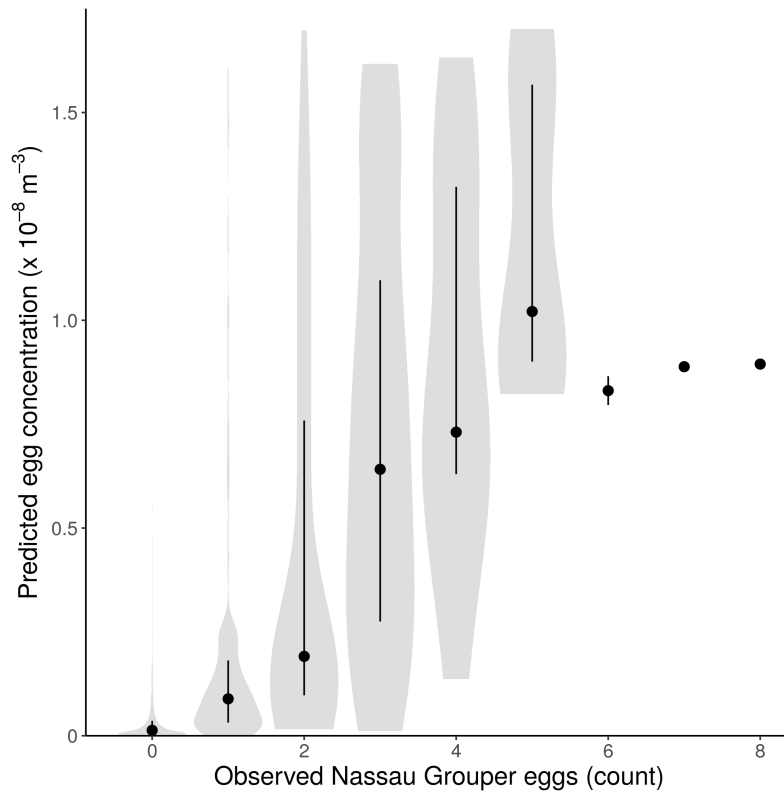


Figure 4.12: Predicted egg concentrations from the best fit 3D diffusion-mortality model versus observed Nassau Grouper egg counts (s^{-1} for cohort 1 (Feb 14, 2017)). Violin plots show the distribution of predicted egg concentrations ($\hat{C}(x, y, z, t)$), points show the median, and lines show the interquartile range (25%–75%). The diffusion-mortality model predictions explained 24.2% of the observed deviance in a generalized linear model, $Y \sim \text{NB}(\mu = e^{\alpha + \beta \hat{C}(x, y, z, t)})$.

Cohort #2: Feb 15, 2017

Unlike previous drifter releases at the Little Cayman FSA, the five drifters released during spawning on Feb 15, 2017 (cohort 2) all grounded on the Little Cayman shelf within 20 hours (Fig. 4.2). Three of the drifters grounded on a protrusion of the shelf on the northeast side of Bloody Bay, one drifter continued approximately 5 km east along the north edge of the shelf before grounding, and the other drifter entered Bloody Bay before eventually grounding (Fig. 4.13). As was the case during the previous evening, the upper 30 m of the water column was weakly stratified at the FSA (0.15 psu difference between 30 m and the surface), but became more well-mixed as the drifters turned east and hit the Little Cayman shelf (Fig. 4.14). The water column east of Bloody Bay was weakly stratified in a manner similar to the area near the FSA.

Just as with cohort 1, the horizontal diffusion of the cohort 2 egg patch was clearly noticeable over the 20 hours of sampling (Fig. 4.15). The horizontal extent of the egg patch increased from hours 0–5 to the hours 5–10, but did not change much from hours 5–10 to 10–15. The egg patch greatly increased in size when it hit the Little Cayman shelf around 15 hours after spawning (Fig. 4.15).

The best fit vertical diffusion model used $K_0 = 0.08 \text{ m}^2 \text{ s}^{-1}$, $z_{MLD} = 100 \text{ m}$, and $\sigma_w = 0.00035 \text{ m s}^{-1}$. The model predictions were similar to those for cohort 1; the eggs spread throughout 0–30 m depth shortly (1 hour) after spawning and then reached an equilibrium distribution with highest concentrations just below the surface (2–3 m depth), decreasing with depth (Fig. 4.16). Vertical diffusivity, K_0 , was estimated slightly higher than for cohort 1, which meant the eggs reached the surface slightly earlier.

Since the horizontal diffusivity appeared to abruptly increase when the drifters hit the shelf at 15 hours (Figs. 4.15, 4.13), we only fit the diffusion-mortality models to the first 15 hours of data. The model with lowest AIC was Model 8, which included isotropic horizontal diffusivity ($K_x = K_y$) and vertical diffusivity (K_z), but not mortality (μ , Table 4.3). Unlike for cohort 1, however, there was no clear best model and Models 4, 2, and 1 received non-trivial Akaike weights (20.1%, 19.5%,

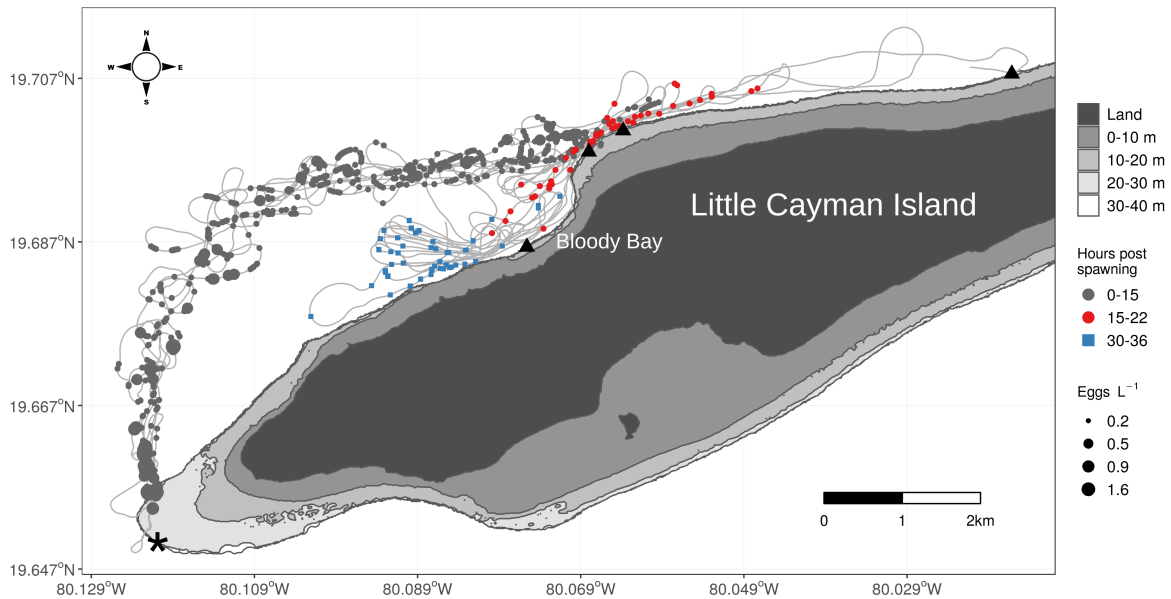


Figure 4.13: Drifter grounding locations (triangles) and horizontal distribution of Nassau Grouper eggs and yolk-sac larvae following cohort 2 spawning (Feb 15, 2017). The starting point for eggs and drifters was the FSA off the west end of Little Cayman, marked by *. Nassau Grouper egg counts (s^{-1} , circles) were converted to concentration (eggs L^{-1} , circle size) based on the TowCam imaging volume and frame rate. Circle color highlights the increased horizontal spread of eggs observed after (hours 15–22, red) versus before (hours 0–15, grey) the drifters grounded (Fig. 4.15). Locations of yolk-sac larvae 30–36 hours post-spawning are shown as blue squares. Sampling tracks are shown as light grey lines.

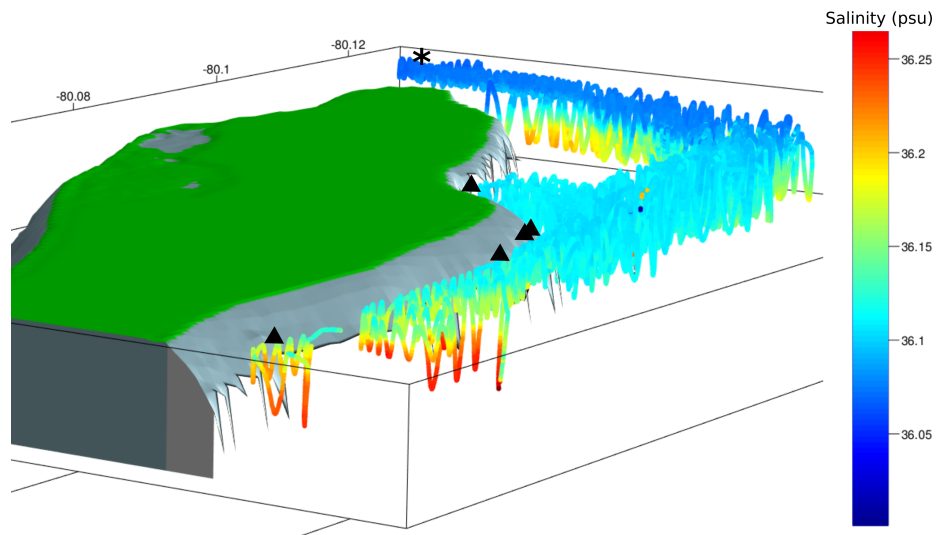


Figure 4.14: Vertical salinity profile around drifters released during spawning of cohort 2 (Feb 15, 2017). The upper 30 m of the water column was initially weakly stratified at the FSA (*) and became more well-mixed as the drifters neared the Little Cayman shelf. Triangles show approximate drifter grounding locations.

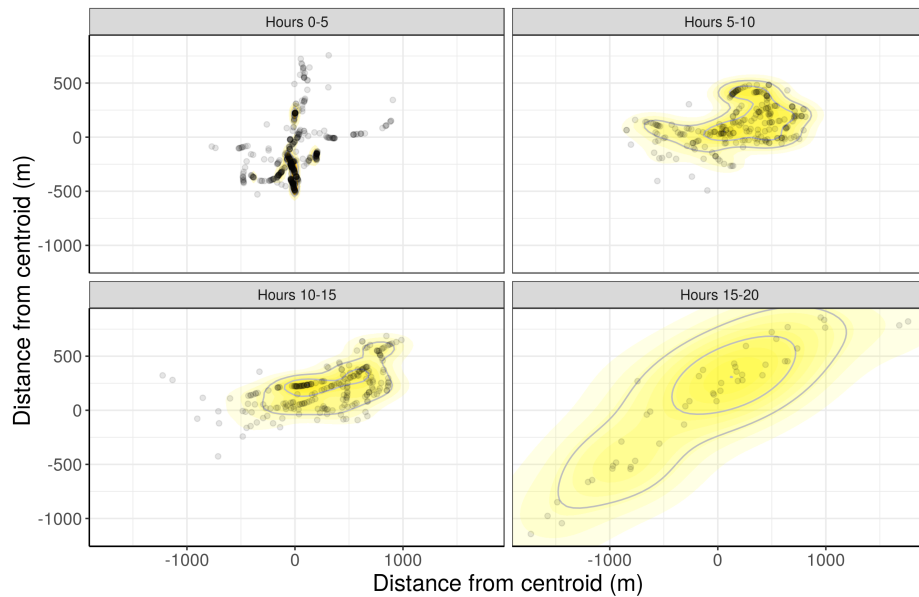


Figure 4.15: Horizontal diffusion of Nassau Grouper eggs in the 20 hours following spawning on Feb 15, 2017 (cohort 2). Points are north-south (x-y) distances of individual Nassau Grouper eggs from the egg centroid (weighted average). Color and contour lines indicate 2D kernel density estimate of egg concentration within 5-hour time intervals.

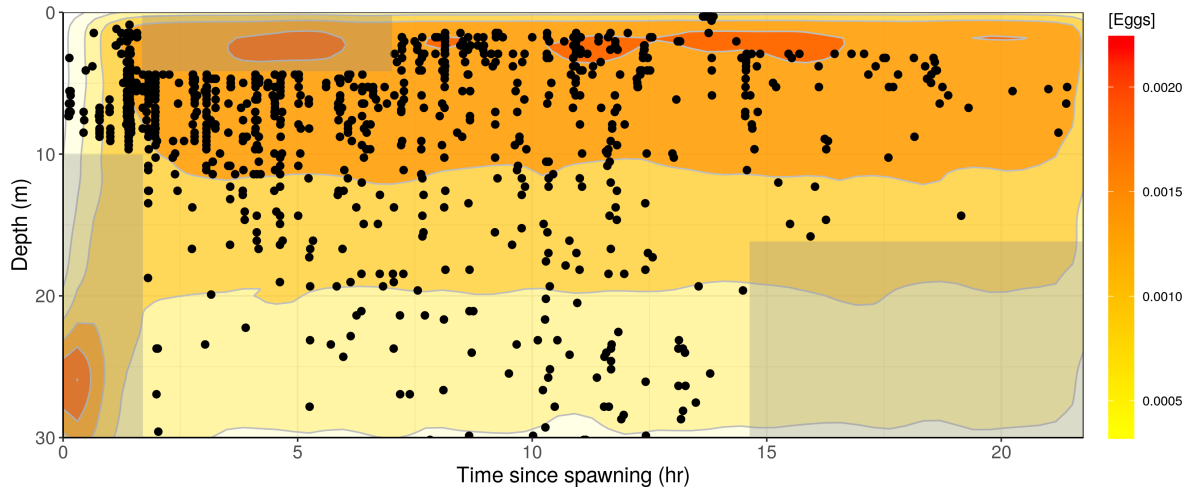


Figure 4.16: Best fit vertical diffusion model for Nassau Grouper eggs following spawning on Feb 15, 2017 (cohort 2). Predicted relative egg concentration is shown as color and contour lines. Black points indicate the time and depth of TowCam microscope images classified as Nassau Grouper eggs. Grey transparency shows depth-times that were not sampled (10–30 m in hours 0–1.5, 0–5 m in hours 1.5–7, and 15–30 m after hour 14.5). The initial particle distribution was input as $\mathcal{N}(\mu = 26.4, \sigma = 3)$ to match the observed initial egg distribution of cohort 1. The model predicted that eggs spread throughout 0–30 m depths 1–3 hours after spawning, and accumulated in the upper 5 m beyond 3 hours after spawning.

and 7.4% respectively). Horizontal diffusivity estimates were higher than for cohort 1, and this was consistent across models (Model 8: $K_x = K_y = 60\,500\text{ m}^2\text{ h}^{-1}$; Model 4: $K_x = 65\,400\text{ m}^2\text{ h}^{-1}$, $K_y = 60\,100\text{ m}^2\text{ h}^{-1}$). Mortality was only estimable by Models 6 and 11, which did not include horizontal diffusion and were not supported by AIC. Nevertheless, the instantaneous mortality estimates of 0.144 and 0.122 h^{-1} imply 3.2 and 5.3% daily survival. The best model (#8) appeared to fit the observed data well but only explained 11.1% of the deviance (Fig. 4.17).

Table 4.3: 3D diffusion-mortality model results for cohort 2 (Feb 15, 2017). Model 8 had the lowest AIC but models 4, 2, and 1 received non-trivial Akaike weights (20.1%, 19.5%, and 7.4% respectively). Mortality was only estimable by models 6 and 11, which did not include horizontal diffusion and were not supported by AIC. Model parameters were estimated using maximum likelihood and non-symmetric 95%CI were calculated using likelihood profiles ('mle2' package in R).

Model	ΔAIC	Weight	K_x ($\text{m}^2 \text{hr}^{-1}$)	K_y ($\text{m}^2 \text{hr}^{-1}$)	μ (hr^{-1})
8) $K_x + K_z$	0.0	0.530	60500 (50600–73700)		
4) $K_x + K_y + K_z$	1.9	0.201	65400 (38800–188000)	60100 (50000–73700)	
2) $K_x + K_z + \mu$	2.0	0.195	60500 (50600–73700)		0 (NA)
1) $K_x + K_y + K_z + \mu$	3.9	0.074	65400 (38900–189000)	60100 (50000–73700)	0 (NA)
6) $K_z + \mu$	169.3	0.000			0.144 (0.126–0.163)
9) K_x	197.0	0.000	48000 (41000–56900)		
7) $K_x + K_y$	197.3	0.000	71600 (40500–276000)	46600 (39700–55400)	
5) $K_x + \mu$	199.0	0.000	48000 (41000–56900)		0 (NA)
3) $K_x + K_y + \mu$	199.3	0.000	71500 (40400–273000)	46600 (39700–55400)	0 (NA)
11) μ	341.1	0.000			0.122 (0.103–0.141)
10) K_z	407.7	0.000			

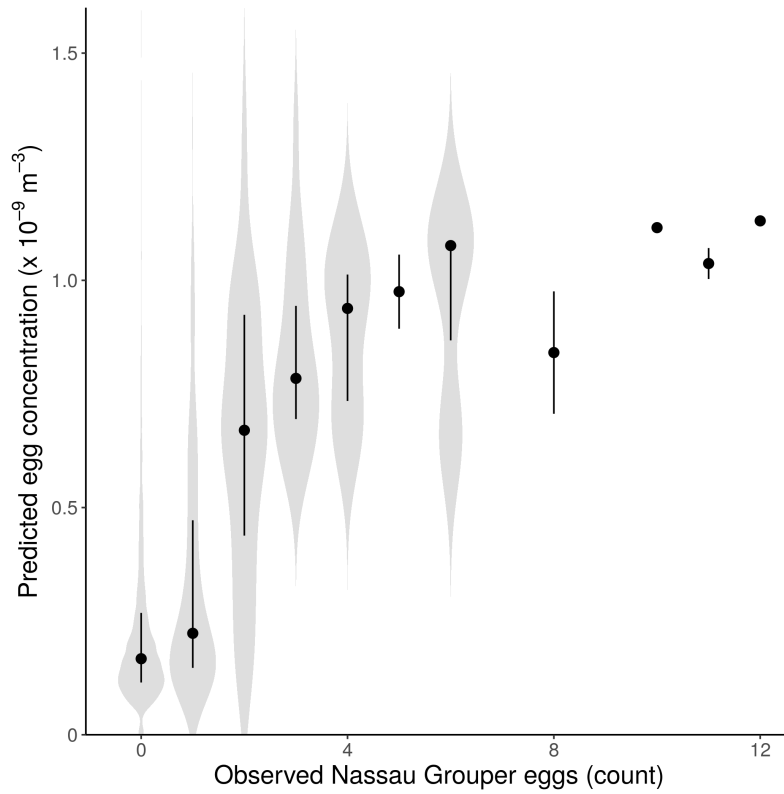


Figure 4.17: Predicted egg concentrations from the best fit diffusion-mortality model versus observed Nassau Grouper egg counts (s^{-1}) for cohort 2 (Feb 15, 2017). The best fit model (#8) did not include anisotropic diffusion or mortality. Violin plots show the distribution of predicted egg concentrations ($\hat{C}(x, y, z, t)$), points show the median, and lines show the interquartile range (25%–75%). The diffusion-mortality model predictions explained 11.1% of the observed deviance in a generalized linear model, $Y \sim \text{NB}(\mu = e^{\alpha + \beta \hat{C}(x, y, z, t)})$.

4.4 Discussion

This study demonstrates how technological advances can further our understanding of the physical-biological processes that determine recruitment and connectivity of tropical reef fish populations. We developed a novel in situ towed plankton imaging system and demonstrated its ability to observe 3-dimensional positions of individual zooplankton, fish eggs, and larvae (Figs. 4.7 and 4.8). We measured the 3D concentration of two cohorts of Nassau Grouper eggs for over 15 hours as they dispersed from the Little Cayman FSA (Figs. 4.9, 4.11, and 4.13). Drifters tracking the second cohort ran aground on the island and we followed this cohort beyond hatching, observing yolk-sac larvae 31–35 hours after spawning (Figs. 4.13 and 4.7). Our plankton imaging system had sufficient resolution to document egg development through the cleavage, blastula, gastrula, and segmentation periods (Fig. 4.7). We generated sufficient fine-scale egg position data to estimate diffusivity and mortality simultaneously using a 3D diffusion-mortality model (Tables 4.2 and 4.3).

We are not aware of any studies of egg and larval dispersal that have fit an advection-diffusion-mortality model to 3-dimensional data. Our unique dataset allowed us to evaluate the effect of commonly-made simplifying assumptions. For example, over the time and space scales considered here, it was not important to consider anisotropic horizontal diffusivity (i.e. estimate $K_x \neq K_y$ separately instead of assuming $K_x = K_y$); the mortality estimates were nearly identical (e.g. models 1 vs. 2 and 3 vs. 5 in Table 4.2). Neglecting the vertical egg distribution (i.e. assuming eggs are distributed evenly in the water column and only considering K_x , K_y , and μ) only slightly changed the mortality rate estimates, from 0.172 h^{-1} to 0.166 h^{-1} (models 1 vs. 3 in Table 4.2); this small difference is well within the 95% confidence intervals. There was a much larger effect of neglecting horizontal diffusion (i.e. including only K_z and μ , models 6 and 11 in Table 4.2). Similarly, we can evaluate the effect of excluding mortality on the estimates of horizontal diffusivity (models 1 vs. 4 in Table 4.2). As expected, the model that does not include mortality compensates by substantially increasing diffusivity, 43% in the x-direction and 83% in the y-direction. In contrast to cohort 1, we were not able to simultaneously estimate diffusivity and mortality for cohort 2 (Table 4.3), when our

sampling was complicated by the egg patch staying over and returning to the shelf (Figs. 4.13 and 4.16). This suggests that either i) the simple diffusion-mortality model centered on drifter tracks less adequately describes the more complex nearshore physical oceanography, or ii) the model was adequate but simply not estimable without observations over the full depth range of the eggs. Taken together, these results illustrate the importance of considering dispersal as a problem in three dimensions, even if one is primarily interested in mortality or diffusion in one dimension.

Field estimates of fish egg mortality are wildly variable, and we are not aware of any for tropical reef fish. Bunn et al. (2000) report 48 instantaneous daily mortality rates, all from temperate species, that range from 0.02–3.64 d^{-1} (mean 0.516). Our estimated daily mortality rate for cohort 1, 0.984 d^{-1} , is both well above this average and well within this range. Pepin (1991) showed that fish egg mortality increases substantially with increasing temperature across 18 species, although all species considered that spawn in waters above 20 °C were clupeoids. The expected daily mortality at 27 °C, the temperature observed during TowCam sampling, using Eqn. 9 in Pepin (1991) is $0.03e^{0.18 \times 27} = 3.87 \text{ d}^{-1}$. Thus, our estimate of Nassau Grouper egg mortality is within the reported range for pelagic fish eggs, above the average for temperate species, but below the expectation taking temperature into account.

The horizontal diffusivities estimated here (4–13 $\text{m}^2 \text{ s}^{-1}$) are within the range predicted by Okubo (1971) given the observed patch size ($3\sqrt{2\sigma_X\sigma_Y} = 300\text{--}1500 \text{ m}$), albeit towards the upper end. For comparison, McGurk (1989) and Davis et al. (1991) estimated slightly lower horizontal diffusivities (1–5.5 $\text{m}^2 \text{ s}^{-1}$) at slightly larger spatial scales (ca. 10 km) using advection-diffusion-mortality models applied to fish larvae. The higher horizontal diffusivity observed in our study may be the result of vertical current shear, especially during the initial dispersal when the egg patch is near, or over, the Little Cayman shelf.

The biological parameter estimates from the vertical diffusion model, egg floating speed (w_s) and its standard deviation (σ_w), should apply to future studies considering the diffusion of fish eggs from FSAs at other locations, or different years at this location. In contrast, estimates of the

physical parameters (vertical diffusivity, horizontal diffusivity, pycnocline depth) and mortality may not represent average values or be broadly applicable. Notably, the diffusivity estimates presented here are likely lower than Nassau Grouper eggs typically encounter in the waters surrounding Little Cayman. The wind speed (2 m s^{-1}) and sea state ($< 0.5 \text{ m}$, Beaufort 2) were anomalously calm during the TowCam deployment on Feb 14–15, 2017. Conditions during Nassau Grouper spawning off Little Cayman are generally between Beaufort 3–5, as in the NetCam deployment on Feb 25, 2016. At higher wind speeds, and therefore higher vertical diffusivity, the Tanaka and Franks (2008) model predicts eggs would be less accumulated at the surface and more evenly distributed with depth. The horizontal diffusion model did not include a direct effect of wind speed, but horizontal diffusivity is also expected to be higher in rougher seas. We note, however, that recruitment of long-lived reef fish such as Nassau Grouper can be highly variable and occur in sporadic pulses (Stock et al., in prep). With this in mind, the notion of an ‘average recruitment event’ may make little sense, and it may be more relevant to characterize the variability of the physical-biological processes governing recruitment. This may be true more generally, beyond long-lived tropical reef fish. For example, McGurk (1989) found 3–6-fold differences in horizontal diffusivity and 8-fold differences in mortality between two cohorts of Pacific herring larvae.

With the above caveats in mind, we can use the estimated horizontal diffusivities and mortality rate to predict the spread of eggs and yolk-sac larvae around drifters released in previous or future years from the Little Cayman FSA. This is a useful exercise because releasing drifters is inexpensive and takes little time, and can therefore be done much more frequently than following the patch of spawned eggs for 24 hours. One year of interest is 2011, when an extremely strong year class was spawned ($7\times$ average; Stock et al., in prep), and we do not know if the fish that recruited to the Little Cayman FSA were spawned on Little Cayman (i.e. self-recruited). However, we released drifters on the two nights of observed spawning in 2011, Feb 24–25, and they remained within 20 km of the FSA during the first 4–5 days. We calculated that there were roughly 4.2 (3.4–5.2) billion eggs spawned by the Little Cayman FSA in 2011, assuming a sex ratio of 1:1

and multiplying numbers-at-length (Waterhouse et al., in *prepa*; Stock et al., in *prep*) by fecundity-at-length (Carter et al., 1994). We then used the diffusivity and mortality estimates from cohort 1 in 2017 to calculate the expected concentration of larvae around the drifters. Note that using the diffusivities and mortality estimated from 2017 is conservative for three reasons: sea state was calmer in 2017 than 2011, the 2017 diffusivity estimates were from shorter time and length scales (diffusivity increases with scale; Okubo, 1971), and the 2017 mortality estimate was from the egg stage (mortality decreases with development and size; Bailey and Houde, 1989). The results showed that by Feb 29 (5 days after spawning on Feb 24, 4 days after spawning on Feb 25), non-trivial concentrations of passive larvae would be dispersed to Little Cayman reefs (Fig. 4.18). Recognizing that we made many oversimplifications in this calculation, these results nonetheless provide a compelling mechanistic explanation for the strong 2011 year class on Little Cayman: favorable currents that allowed for self-recruitment.

Beyond the diffusion-mortality model, the observation that all five drifters released during spawning on Feb 15, 2017 grounded on the reef is noteworthy. The current paradigm of reef fish recruitment does not make a clear prediction of the fate of pelagic eggs immediately returning to the reef before hatching. Instead, it seeks to explain the more typical observation whereby eggs are spawned pelagically, larvae move offshore and develop away from the reef, and then return after a significant duration (e.g. 35–45 days for Nassau Grouper). The most commonly cited hypothesis for the evolutionary motivation underlying this behavior is that predation on eggs would be extremely high on coral reefs and lower offshore (Johannes, 1978). This is consistent with several common characteristics of reef fish eggs that minimize predation: eggs are transparent, develop rapidly, and are spawned at sunset. We would therefore expect cohort 2 to have experienced very high predation, especially as vulnerable eggs and yolk-sac larvae. On the other hand, we would also expect more abundant food near the reef and no loss due to advection (Strathmann et al., 2002). It will be interesting to see whether a strong year class from 2017 spawning recruits to the Little Cayman FSA.

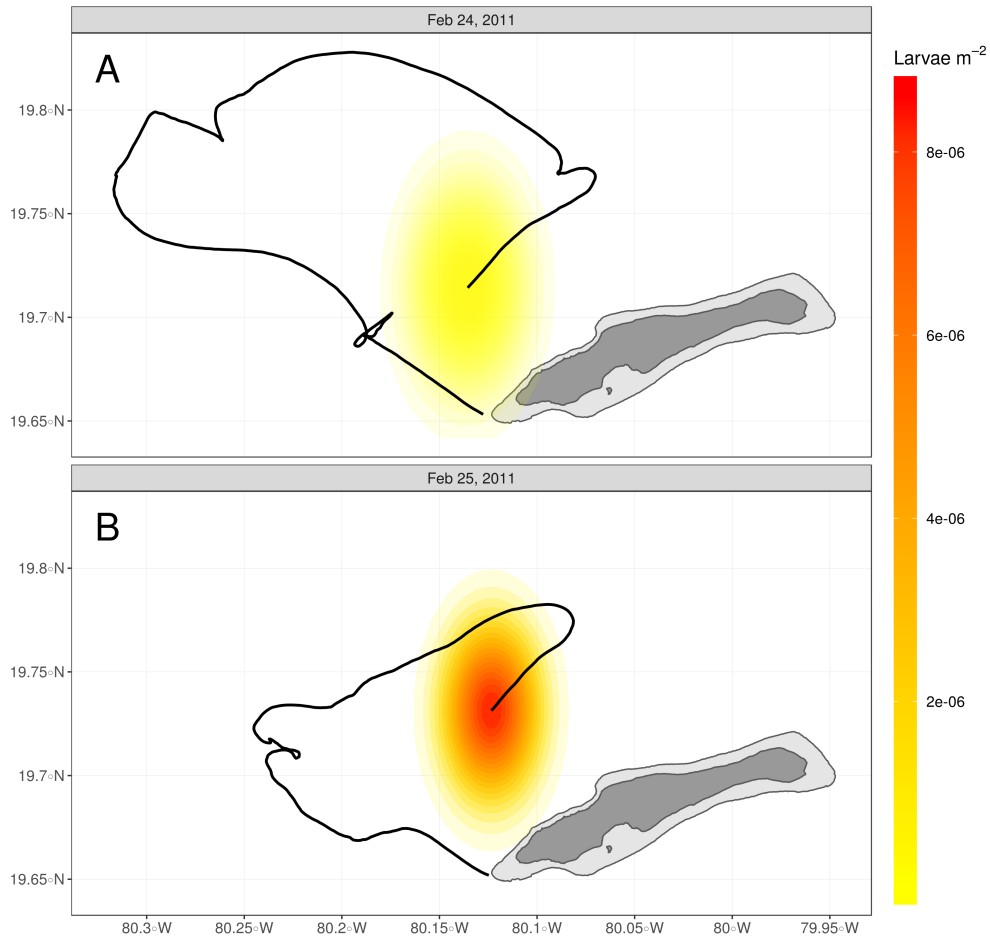


Figure 4.18: Estimated dispersal of larvae from the Little Cayman FSA on Feb 29, 2011 around drifters released during spawning on Feb 24 (A) and Feb 25 (B). The predicted concentration is lower and more diffuse in A) than B) because 5 days have elapsed after Feb 24 spawning (A) while 4 days have elapsed after Feb 25 spawning (B), and the assumed mortality rate implies 1.6% survival per day.

In this study we found that currents on subsequent spawning nights were quite variable (Figs. 4.1, 4.2). The fact that Nassau Grouper choose to spawn on multiple nights in an environment where this behavior enhances the spread of siblings is consistent with the hypothesis that there is some selection for dispersal (i.e. spread of siblings; Strathmann, 1974). If habitat patches exhibit temporal variation in quality, dispersal should reduce variation and increase average fitness over several generations. If we consider human-induced fishing mortality on FSAs (which can be extremely high and variable) as an important component of habitat quality, then a mix of dispersal and self-recruitment is likely advantageous for Nassau Grouper in the current era of high human impact. As the Little Cayman FSA is the largest known remaining FSA for the species (Sadovy et al., 2018), this is good news because it allows for the possibility that larvae from Little Cayman may replenish other FSAs while still motivating local protection.

The diffusion model used here could be improved upon in at least two ways. First, parameterizing horizontal diffusivity by latitude, K_y , and longitude, K_x , is somewhat arbitrary. Decomposing horizontal diffusivity into along (parallel to) drifter track versus across (orthogonal to) drifter track components would more consistent with physics because i) along-track diffusivity should be greater than across-track diffusivity due to shear diffusion (Strathmann, 1974; Okubo and Levin, 2010), and ii) if the drifter track curves—as on Feb 15, 2017—the along- and across-drifter directions change (Fig. 4.13). Second, alternative models of diffusion where the apparent diffusivity, A , increases as a function of length scale, ℓ , are more generally appropriate than the Fickian diffusion equation used here ($A = K$ independent of ℓ ; Okubo and Levin, 2010). Future work could consider the diffusion models $A = 0.204P\ell$ (Joseph and Sendner, 1958), or $A = 0.266\gamma\ell^{4/3}$ (Ozmidov, 1958), especially if considering longer time periods and therefore larger spatial scales.

The images of possible predation on Nassau Grouper eggs by pelagic invertebrate zooplankton are intriguing. Pelagic coelenterates (medusae, ctenophores, and siphonophores) can certainly have high predation rates on fish eggs and larvae (Purcell and Arai, 2001). Planktonic fish eggs and young larvae are ideal prey because they are small, passive (i.e. unable to escape predation attempts),

nutrient-rich, and often occur in high densities (Peterson and Wroblewski, 1984; Bailey and Houde, 1989; Purcell and Arai, 2001; Fuiman et al., 2015). For these reasons they may be targeted and consumed in large quantities, especially by cruising predators that can occur at high densities (e.g. scyphomedusae; Purcell and Arai, 2001). Because Nassau Grouper spawn at sunset, contact and cruising predators may be more important than visual predators (Bailey and Houde, 1989). Seven of the ten predation images are likely pelagic foraminifera. It is possible that foraminifera are significant predators of Nassau Grouper eggs; they grow largest in the tropics, can consume prey 2–3 times their size, and spinose species in particular prefer zooplankton to phytoplankton prey (Schiebel and Hemleben, 2017). Omnivory and symbiosis allows pelagic foraminifera to persist in oligotrophic environments and then bloom when prey becomes abundant—as would be the case in a high density patch of Nassau Grouper eggs (Schiebel and Hemleben, 2017). While siphonophores were abundant in the TowCam images, there were no images of them preying on fish eggs. This is unsurprising since they are ambush predators more likely to attack mobile fish larvae than passive eggs (Purcell, 1981). Still, they may be important predators of Nassau Grouper larvae in a high density patch once they hatch. While these observations are interesting, a much larger sample size would be necessary to quantify the degree of invertebrate predation and its impact on Nassau Grouper egg mortality.

Inference at both fine and large spatiotemporal scales was limited by sampling constraints. While we obtained fine-scale 3D position data (i.e. latitude, longitude, depth, and time of individual eggs), the high proportion of zeros and low counts limited our ability to analyze fine-scale spatiotemporal patterns such as patchiness. At larger space and time scales, the area and density of observations were constrained by having one research vessel traveling at 4–5 knots. Both of these considerations will be important if we hope to observe Nassau Grouper larval distributions further in time to critical biological timepoints, e.g. first-feeding at 3–5 days, flexion at 14–20 days, and settlement at 35–45 days. The patch should progressively increase in size and decrease in concentration, complicating observation. Attaching a plankton net to concentrate organisms in

the images (as in the NetCam, Fig. 4.3a) is one possibility to increase sampling volume, but this decreases vertical control.

The in situ plankton imaging systems used here demonstrated promising capabilities. We envision that future technological improvements enabling higher spatiotemporal sampling resolution and better characterization of physical variables (e.g., currents) could shed light on important physical-biological processes affecting recruitment from FSAs: i) annual variation in diffusivity and mortality parameters. How applicable are the estimates presented here in past and future years? ii) in situ variability in egg and larvae development, growth, and mortality. How do these compare to estimates made in the lab? For example, lab studies often use antibiotics and filtered seawater (no bacteria, parasites, predators, etc.), iii) spatiotemporal overlap with predator and prey distributions, iv) spatial variability or density-dependence in mortality, v) spatiotemporal distribution of larger predators, and vi) separation of mortality due to predation, starvation, and transport (Hjort, 1914; Bailey and Houde, 1989).

Acknowledgements

We thank the dedicated staff of the Cayman Islands Department of the Environment who facilitated the use of R/V Seakeeper: Gina Ebanks-Petrie, Tim Austin, Ivan Montieth, Keith Neale, Robert Walton, Chris Dixon, and Kevin Jackson. The REEF Grouper Moon Project, Peter Hillenbrand (Southern Cross Club), Little Cayman Beach Resort, and Cayman Airways provided travel funds and logistical support. Eggs were reared in the wet lab at the Central Caribbean Marine Institute. The NetCam deployment was funded by NSF INSPIRE Grant No. 1344291. The TowCam deployment was funded by the UC San Diego Frontiers of Innovation Scholars Program (FISP). Tammi Warrender contributed the photo of the NetCam. Jaffe Lab members Paul Roberts and Devin Ratelle built the NetCam and TowCam. Paul Roberts, Devin Ratelle, Steve Gittings, and Lynn Waterhouse assisted with the NetCam deployment. Chris Casagrande of Sea Sciences, Inc. provided training on the AcrobatTM and assisted with the TowCam deployment. Lauren Arnold

helped sort plankton samples, funded by the UC Office of the President through the UC-HBCU Oceans as a Bridge Program. Paul Roberts, Eric Orenstein, and Kevin Le helped classify plankton images. Dave Checkley advised on ichthyoplankton sampling and analysis. Peter Franks advised on the advection-diffusion-mortality model. Ron Burton and Alice Harada contributed reagents and assisted with the DNA barcoding. Mark Ohman, Linsey Sala, and Tristan Biard helped identify zooplankton images. The Global Drifter Program donated five SVP drifters. BCS received support from the Cooperative Institute for Marine Ecosystems and Climate (CIMEC) and the National Science Foundation Graduate Research Fellowship under Grant No. DGE-1144086.

This chapter, in full, is currently in preparation for submission for publication and is printed here with the permission of co-authors Andrew D. Mullen, Jules S. Jaffe, Allison Candelmo, Scott A. Heppell, Christy V. Pattengill-Semmens, Croy M. McCoy, Bradley Johnson, and Brice X. Semmens. The dissertation author was the primary investigator and author of this paper.

References

- Atema, J., G. Gerlach, and C. B. Paris. 2015. Sensory biology and navigation behavior of reef fish larvae. In C. Mora, editor, *Ecology of Fishes on Coral Reefs*, pages 3–15. Cambridge University Press, Cambridge.
- Bailey, K. and E. Houde. 1989. Predation on Eggs and Larvae of Marine Fishes and the Recruitment Problem. *Advances in Marine Biology*, **25**:1–83.
- Bolker, B. 2017. *bbmle: Tools for General Maximum Likelihood Estimation*. <https://CRAN.R-project.org/package=bbmle>.
- Bunn, N. A., C. J. Fox, and T. Webb. 2000. A literature review of studies on fish egg mortality: Implications for the estimation of spawning stock biomass by the annual egg production method. Technical Report 111, Centre for Environment, Fisheries, and Aquaculture Science, Lowestoft.
- Carter, J., G. J. Marrow, and V. Pryor. 1994. Aspects of the ecology and reproduction of Nassau Grouper (*Epinephelus striatus*) off the coast of Belize, Central America. In *Proceedings of the 43rd Annual Gulf and Caribbean Fisheries Institute*, pages 65–111. Charleston, South Carolina, USA.
- Cimino, M., P. Colin, T. Schramek, S. Lindfield, M. Domeier, and E. Terrill. 2018. Oceanographic, acoustic, and remote approaches reveal the spatio-temporal dynamics of blackfin snapper at an aggregation site in Palau. *Marine Ecology Progress Series*, **601**:185–201.

- Clark, D., J. Leis, A. Hay, and T. Trnski. 2005. Swimming ontogeny of larvae of four temperate marine fishes. *Marine Ecology Progress Series*, **292**:287–300.
- Colin, L., W. A. Laroche, and B. Brothers. 1997. Ingress and settlement in the Nassau Grouper, *Epinephelus striatus* (Pisces: Serranidae), with relationship to spawning occurrence. *Bulletin of Marine Science*, **60**:656–667.
- Colin, P. L. 1992. Reproduction of the Nassau grouper, *Epinephelus striatus* (Pisces: Serranidae) and its relationship to environmental conditions. *Environmental Biology of Fishes*, **34**:357–377.
- Colin, P. L. 2012. Timing and Location of Aggregation and Spawning in Reef Fishes. In Y. Sadovy de Mitcheson and P. L. Colin, editors, *Reef Fish Spawning Aggregations: Biology, Research and Management*, pages 117–158. Springer Netherlands, Dordrecht.
- Colin, P. L., D. Y. Shapiro, and D. Weiler. 1987. Aspects of the reproduction of two groupers, *Epinephelus guttatus* and *E. striatus* in the West Indies. *Bulletin of Marine Science*, **40**:220–230.
- Cowen, R. K. 2006. Scaling of Connectivity in Marine Populations. *Science*, **311**:522–527.
- Cowen, R. K., K. M. M. Lwiza, S. Sponaugle, C. B. Paris, and D. B. Olson. 2000. Connectivity of marine populations: Open or closed? *Science*, **287**:857–859.
- Cowen, R. K. and S. Sponaugle. 2009. Larval dispersal and marine population connectivity. *Annual Review of Marine Science*, **1**:443–466.
- Cushing, D. 1975. *Marine ecology and fisheries*. Cambridge University Press, Cambridge, UK.
- Cushing, D. 1990. Plankton Production and Year-class Strength in Fish Populations: an Update of the Match/Mismatch Hypothesis. *Advances in Marine Biology*, **26**:249–293.
- Davis, T., V. Lyne, and G. Jenkins. 1991. Advection, dispersion and mortality of a patch of southern bluefin tuna larvae *Thunnus maccoyii* in the East Indian Ocean. *Marine Ecology Progress Series*, **73**:33–45.
- Fisher, R., J. M. Leis, D. L. Clark, and S. K. Wilson. 2005. Critical swimming speeds of late-stage coral reef fish larvae: variation within species, among species and between locations. *Marine Biology*, **147**:1201–1212.
- Fogarty, M. and L. Botsford. 2007. Population connectivity and spatial management of marine fisheries. *Oceanography*, **20**:112–123.
- Fuiman, L. A., T. L. Connelly, S. K. Lowerre-Barbieri, and J. W. McClelland. 2015. Egg boons: central components of marine fatty acid food webs. *Ecology*, **96**:362–372.
- Gawarkiewicz, G., S. Monismith, and J. Largier. 2007. Observing larval transport processes affecting population connectivity: progress and challenges. *Oceanography*, **20**:40–53.

- Gerlach, G., J. Atema, M. J. Kingsford, K. P. Black, and V. Miller-Sims. 2007. Smelling home can prevent dispersal of reef fish larvae. *Proceedings of the National Academy of Sciences*, **104**:858–863.
- Harada, A. E., E. A. Lindgren, M. C. Hermsmeier, P. A. Rogowski, E. Terrill, and R. S. Burton. 2015. Monitoring spawning activity in a southern California marine protected area using molecular identification of fish eggs. *PLOS ONE*, **10**:e0134647.
- Helbig, J. A. and P. Pepin. 1998. Partitioning the influence of physical processes on the estimation of ichthyoplankton mortality rates. I. Theory. **55**:17.
- Heppell, S., B. X. Semmens, C. V. Pattengill-Semmens, P. G. Bush, B. C. Johnson, C. M. McCoy, J. Gibb, and S. S. Heppell. 2011. Oceanographic patterns associated with Nassau grouper aggregation spawn timing: Shifts in surface currents on the nights of peak spawning. In *Proceedings of the 63rd Gulf and Caribbean Fisheries Institute*, pages 152–154. San Juan, Puerto Rico.
- Heppell, S. A., B. X. Semmens, C. V. Pattengill-Semmens, P. G. Bush, B. C. Johnson, C. M. McCoy, C. Paris, J. Gibb, and S. S. Heppell. 2009. Tracking potential larval dispersal patterns from Nassau grouper aggregation sites: Evidence for local retention and the "importance of place". In *Proceedings of the 61st Gulf and Caribbean Fisheries Institute*, pages 325–327. Gosier, Guadeloupe, French West Indies.
- Hilborn, R. and C. J. Walters. 1992. *Quantitative fisheries stock assessment*. Springer Science & Business Media.
- Hill, A. 1990. Pelagic dispersal of Norway lobster *Nephrops norvegicus* larvae examined using an advection-diffusion-mortality model. *Marine Ecology Progress Series*, **64**:217–226.
- Hill, A. 1991. Advection-diffusion-mortality solutions for investigating pelagic larval dispersal. *Marine Ecology Progress Series*, **70**:117–128.
- Hjort, J. 1914. Fluctuations in the great fisheries of Northern Europe viewed in the light of biological research. *Rapports et Procès-Verbaux des Réunions du Conseil Permanent International Pour L'Exploration de la Mer*, **20**:1 – 228.
- Houde, E. D. 2008. Emerging from Hjort's Shadow. *Journal of Northwest Atlantic Fishery Science*, **41**:53–70.
- Irisson, J.-O., C. B. Paris, J. M. Leis, and M. N. Yerman. 2015. With a Little Help from My Friends: Group Orientation by Larvae of a Coral Reef Fish. *PLOS ONE*, **10**:e0144060.
- Jackson, A. M., B. X. Semmens, Y. Sadovy de Mitcheson, R. S. Nemeth, S. A. Heppell, P. G. Bush, A. Aguilar-Perera, J. A. B. Claydon, M. C. Calosso, K. S. Sealey, M. T. Schärer, and G. Bernardi. 2014. Population structure and phylogeography in Nassau Grouper (*Epinephelus striatus*), a mass-aggregating marine fish. *PLoS ONE*, **9**:e97508.
- Jaffe, J. S. 2016. To sea and to see: That is the answer. *Methods in Oceanography*, **15-16**:3–20.

- Jennings, S. 2001. Patterns and prediction of population recovery in marine reserves. *Reviews in Fish Biology and Fisheries*, pages 209–231.
- Johannes, R. E. 1978. Reproductive strategies of coastal marine fishes in the tropics. *Environmental Biology of Fishes*, **3**:65–84.
- Johnson, D., R. Stocker, R. Head, J. Imberger, and C. Pattiaratchi. 2003. A compact, low-cost GPS drifter for use in the oceanic nearshore zone, lakes, and estuaries. *Journal of Atmospheric and Oceanic Technology*, **20**:1880–1884.
- Jones, G. P. 2015. Mission impossible: unlocking the secrets of coral reef fish dispersal. In C. Mora, editor, *Ecology of Fishes on Coral Reefs*, pages 16–27. Cambridge University Press, Cambridge.
- Jones, G. P., M. J. Milicich, M. J. Emslie, and C. Lunow. 1999. Self-recruitment in a coral reef fish population. **402**:3.
- Jones, G. P., S. Planes, and S. R. Thorrold. 2005. Coral Reef Fish Larvae Settle Close to Home. *Current Biology*, **15**:1314–1318.
- Joseph, J. and H. Sendner. 1958. Über die horizontale diffusion im meere. *Deutsche Hydrografische Zeitschrift*, **11**:49–77.
- Kimmel, C. B., W. W. Ballard, S. R. Kimmel, B. Ullmann, and T. F. Schilling. 1995. Stages of embryonic development of the zebrafish. *Developmental Dynamics*, **203**:253–310.
- Kingsford, M. J., J. M. Leis, A. Shanks, K. C. Lindeman, and S. G. Morgan. 2002. Sensory environments, larval abilities and local self-recruitment. *Bulletin of Marine Science*, **70**:309–340.
- Kobara, S. and W. D. Heyman. 2008. Geomorphometric Patterns of Nassau Grouper (*Epinephelus striatus*) Spawning Aggregation Sites in the Cayman Islands. *Marine Geodesy*, **31**:231–245.
- Largier, J. L. 2003. Considerations in Estimating Larval Dispersal Distances from Oceanographic Data. *Ecological Applications*, **13**:S71–S89.
- Leggett, W. C. and E. Deblois. 1994. Recruitment in marine fishes: Is it regulated by starvation and predation in the egg and larval stages? *Netherlands Journal of Sea Research*, **32**:119–134.
- Leis, J., A. Hay, and G. Howarth. 2009. Ontogeny of in situ behaviours relevant to dispersal and population connectivity in larvae of coral-reef fishes. *Marine Ecology Progress Series*, **379**:163–179.
- Leis, J. M. 2015. Is dispersal of larval reef fishes passive? In C. Mora, editor, *Ecology of Fishes on Coral Reefs*, pages 223–226. Cambridge University Press, Cambridge.
- Leis, J. M., J. E. Caselle, I. R. Bradbury, T. Kristiansen, J. K. Llopiz, M. J. Miller, M. I. O’Connor, C. B. Paris, A. L. Shanks, S. M. Sogard, S. E. Swearer, E. A. Trembl, R. D. Vetter, and R. R. Warner. 2013. Does fish larval dispersal differ between high and low latitudes? *Proceedings of the Royal Society B: Biological Sciences*, **280**:20130327–20130327.

- McGurk, M. 1989. Advection, diffusion and mortality of Pacific herring larvae *Clupea harengus pallasii* in Bamfield Inlet, British Columbia. *Marine Ecology Progress Series*, **51**:1–18.
- Miller, B. and A. W. Kendall. 2009. *Early life history of marine fishes*. University of California Press, Berkeley.
- Miller, T. 2007. Contribution of individual-based coupled physical–biological models to understanding recruitment in marine fish populations. *Marine Ecology Progress Series*, **347**:127–138.
- Mumby, P. J. 2006. Fishing, Trophic Cascades, and the Process of Grazing on Coral Reefs. *Science*, **311**:98–101.
- Méndez-Jiménez, A., W. D. Heyman, and S. F. DiMarco. 2015. Surface drifter movement indicates onshore egg transport from a reef fish spawning aggregation. *Physical Geography*, **36**:353–366.
- NMFS. 2016. *Endangered and Threatened Wildlife and Plants: Final Listing Determination on the Proposal To List the Nassau Grouper as Threatened Under the Endangered Species Act*. Technical Report 50 CFR Part 223, U.S. Dept. Commerce, National Oceanic and Atmospheric Administration, National Marine Fisheries Service.
- Okubo, A. 1971. Oceanic diffusion diagrams. *Deep Sea Research and Oceanographic Abstracts*, **18**:789–802.
- Okubo, A. and S. A. Levin. 2010. *Diffusion and ecological problems: modern perspectives*. Springer, New York. OCLC: 825558450.
- Ord, J. K. 1967. Graphical methods for a class of discrete distributions. *Journal of the Royal Statistical Society. Series A (General)*, **130**:232–238.
- Ozmidov, R. V. 1958. On the calculation of horizontal turbulent diffusion of the pollutant patches in the sea. *Dokl. Akad. Nauk SSSR*, **120**:761–763.
- Pepin, P. 1991. Effect of temperature and size on development, mortality, and survival rates of the pelagic early life history stages of marine fish. *Canadian Journal of Fisheries and Aquatic Sciences*, **48**:503–518.
- Peterson, I. and J. S. Wroblewski. 1984. Mortality Rate of Fishes in the Pelagic Ecosystem. *Canadian Journal of Fisheries and Aquatic Sciences*, **41**:1117–1120.
- Powell, A. B. and J. W. Tucker. 1992. Egg and larval development of laboratory-reared Nassau Grouper, *Epinephelus striatus* (Pisces, Serranidae). *Bulletin of Marine Science*, **50**:171–185.
- Purcell, J. E. 1981. Feeding ecology of *Rhizophysa eysenhardti*, a siphonophore predator of fish larvae. *Limnology and Oceanography*, **26**:424–432.
- Purcell, J. E. and M. N. Arai. 2001. Interactions of pelagic cnidarians and ctenophores with fish: a review. In J. E. Purcell, W. M. Graham, and H. J. Dumont, editors, *Jellyfish Blooms: Ecological and Societal Importance*, pages 27–44. Springer Netherlands, Dordrecht.

- Richardson, P. 2005. Caribbean Current and eddies as observed by surface drifters. *Deep Sea Research Part II: Topical Studies in Oceanography*, **52**:429–463.
- Roberts, C. M. 1997. Connectivity and Management of Caribbean Coral Reefs. *Science*, **278**:1454–1457.
- Roberts, P. L., J. S. Jaffe, E. C. Orenstein, B. Laxton, P. J. Franks, C. Briseno, M. L. Carter, and M. Hilbern. 2014. Pier recognition: An in situ plankton web camera. In *Ocean Optics XXII*. Portland, ME, USA.
- Ross, O. N. and J. Sharples. 2004. Recipe for 1-D Lagrangian particle tracking models in space-varying diffusivity: Recipe for Lagrangian models. *Limnology and Oceanography: Methods*, **2**:289–302.
- Sadovy, Y., A. Aguilar-Perera, and E. Sosa-Cordero. 2018. *Epinephelus striatus*. The IUCN Red List of Threatened Species 2018: e.T7862A46909843. <http://dx.doi.org/10.2305/IUCN.UK.2018-2.RLTS.T7862A46909843.en>.
- Sadovy, Y. and A.-M. Eklund. 1999. Synopsis of Biological Data on the Nassau Grouper, *Epinephelus striatus* (Bloch, 1792), and the Jewfish, *E. itajara* (Lichtenstein, 1822). Technical Report NOAA Technical Report NMFS 146. A Technical Report of the Fishery Bulletin. FAO Fisheries Synopsis 157., U.S. Department of Commerce.
- Sadovy de Mitcheson, Y. and P. L. Colin. 2012. Species Case Studies. In Y. Sadovy de Mitcheson and P. L. Colin, editors, *Reef Fish Spawning Aggregations: Biology, Research and Management*, pages 405–565. Springer Netherlands, Dordrecht.
- Sala, E., E. Ballesteros, and R. M. Starr. 2001. Rapid Decline of Nassau Grouper Spawning Aggregations in Belize: Fishery Management and Conservation Needs. *Fisheries*, **26**:23–30.
- Schiebel, R. and C. Hemleben. 2017. *Planktic Foraminifers in the Modern Ocean*. Springer Berlin Heidelberg, Berlin, Heidelberg.
- Schneider, C. A., W. S. Rasband, and K. W. Eliceiri. 2012. NIH Image to ImageJ: 25 years of image analysis. *Nature Methods*, **9**:671–675.
- Semmens, B. X., P. Bush, S. Heppell, B. Johnson, C. McCoy, C. Pattengill-Semmens, and S. S. Heppell. 2009. The spatial ecology of a remnant Nassau Grouper stock on Cayman Brac, Cayman Islands. In *Proceedings of the 61st Gulf and Caribbean Fisheries Institute*. Gosier, Guadeloupe, French West Indies.
- Semmens, B. X., K. E. Luke, P. G. Bush, C. Pattengill-Semmens, B. Johnson, C. McCoy, and S. Heppell. 2007. Investigating the reproductive migration and spatial ecology of Nassau Grouper (*Epinephelus striatus*) on Little Cayman Island using acoustic tags – An Overview. In *Proceedings of the 58th Annual Gulf and Caribbean Fisheries Institute*, pages 199–206. San Andres, Columbia.

- Shenker, J., E. Maddox, E. Wishinski, A. Pearl, S. Thorrold, and N. Smith. 1993. Onshore transport of settlement-stage Nassau grouper *Epinephelus striatus* and other fishes in Exuma Sound, Bahamas. *Marine Ecology Progress Series*, **98**:31–43.
- Siegel, D., B. Kinlan, B. Gaylord, and S. Gaines. 2003. Lagrangian descriptions of marine larval dispersion. *Marine Ecology Progress Series*, **260**:83–96.
- Smith, C. L. 1972. A spawning aggregation of Nassau Grouper, *Epinephelus striatus* (Bloch). *Transactions of the American Fisheries Society*, **101**:257–261.
- Staaterman, E., C. B. Paris, and J. Helgers. 2012. Orientation behavior in fish larvae: A missing piece to Hjort's critical period hypothesis. *Journal of Theoretical Biology*, **304**:188–196.
- Stallings, C. D. 2008. Indirect Effects of an Exploited Predator on Recruitment of Coral-Reef Fishes. *Ecology*, **89**:2090–2095.
- Stock, B. C., S. A. Heppell, L. Waterhouse, I. Dove, C. V. Pattengill-Semmens, C. M. McCoy, P. G. Bush, G. Ebanks-Petrie, and B. X. Semmens. in prep. Assessing the response of Cayman Islands Nassau Grouper (*Epinephelus striatus*) spawning aggregations to spatial protections using *in situ* length data.
- Strathmann, R. 1974. The spread of sibling larvae of sedentary marine invertebrates. *The American Naturalist*, **108**:29–44.
- Strathmann, R. R., T. P. Hughes, A. M. Kuris, K. C. Lindeman, S. G. Morgan, J. M. Pandolfi, and R. R. Warner. 2002. Evolution of local recruitment and its consequences for marine populations. *Bulletin of Marine Science*, **70**:20.
- Sundby, S. 1983. A one-dimensional model for the vertical distribution of pelagic fish eggs in the mixed layer. *Deep Sea Research Part A. Oceanographic Research Papers*, **30**:645–661.
- Swearer, S. E., J. E. Caselle, D. W. Lea, and R. R. Warner. 1999. Larval retention and recruitment in an island population of a coral-reef fish. *Nature*, **402**:799–802.
- Szuwalski, C. S., K. A. Vert-Pre, A. E. Punt, T. A. Branch, and R. Hilborn. 2015. Examining common assumptions about recruitment: a meta-analysis of recruitment dynamics for worldwide marine fisheries. *Fish and Fisheries*, **16**:633–648.
- Tanaka, Y. and P. J. S. Franks. 2008. Vertical distributions of Japanese sardine (*Sardinops melanostictus*) eggs: comparison of observations and a wind-forced Lagrangian mixing model. *Fisheries Oceanography*, **17**:89–100.
- Taylor, M. S. 2003. Genetic Evidence for Local Retention of Pelagic Larvae in a Caribbean Reef Fish. *Science*, **299**:107–109.
- Thorrold, S. R., C. Latkoczy, P. K. Swart, and C. M. Jones. 2001. Natal homing in a marine fish metapopulation. *Science*, **291**:297–299.

- Tucker, J. W., J. E. Parsons, G. C. Ebanks, and P. G. Bush. 1991. Induced Spawning of Nassau Grouper *Epinephelus striatus*. *Journal of the World Aquaculture Society*, **22**:187–191.
- UNESCO. 1968. Zooplankton sampling: review papers of the proceedings of the symposium on the hydrodynamics of zooplankton sampling, volume 2 of *Monographs on Oceanographic Methodology*. Paris.
- Watanabe, W. O., C.-S. Lee, S. C. Ellis, and E. P. Ellis. 1995. Hatchery study of the effects of temperature on eggs and yolk sac larvae of the Nassau grouper *Epinephelus striatus*. *Aquaculture*, **136**:141–147.
- Waterhouse, L., S. Heppell, C. V. Pattengill-Semmens, C. M. McCoy, B. Johnson, and B. X. Semmens. in prepa. Monitoring recovery of a heavily exploited aggregating species: Nassau Grouper (*Epinephelus striatus*) in the Cayman Islands.
- Waterhouse, L., J. D. Stewart, B. C. Stock, B. Johnson, C. M. McCoy, A. Candelmo, C. V. Pattengill-Semmens, S. A. Heppell, and B. X. Semmens. in prepb. Survival of groupers in warmer waters: Variability in egg fertilization rates, morphometrics, and survival in Nassau Grouper (*Epinephelus striatus*) and Tiger Grouper (*Mycteroperca tigris*).
- Whaylen, L., P. Bush, B. Johnson, K. E. Luke, C. McCoy, B. Semmens, and M. Boardman. 2007. Aggregation dynamics and lessons learned from five years of monitoring at a Nassau grouper (*Epinephelus striatus*) spawning aggregation in Little Cayman, Cayman Islands, BWI. In *Proceedings of the 59th Annual Gulf and Caribbean Fisheries Institute*, pages 479–488. Belize City, Belize.
- Whaylen, L., C. V. Pattengill-Semmens, B. X. Semmens, P. G. Bush, and M. R. Boardman. 2004. Observations of a Nassau grouper, *Epinephelus striatus*, Spawning Aggregation Site in Little Cayman, Cayman Islands, Including Multi-Species Spawning Information. *Environmental Biology of Fishes*, **70**:305–313.